UNIVERSITAT POLITÈCNICA DE VALÈNCIA

INSTITUTO INTERUNIVERSITARIO DE INVESTIGACIÓN DE RECONOCIMIENTO MOLECULAR Y DESARROLLO TECNOLÓGICO

Preclinical evaluation of senescence-based strategies to improve cancer therapy

PhD. THESIS

Submitted by

Alejandra Estepa Fernández

PhD. Supervisors:

Prof. Ramón Martínez Máñez

Dra. María del Mar Orzáez Calatayud

Prof. Félix Sancenón Galarza

Valencia, June 2022

RAMÓN MARTÍNEZ MÁÑEZ, PhD in Chemistry and Professor at the *Universitat Politècnica de València*, MARÍA DEL MAR ORZÁEZ CALATAYUD, PhD in Biology at the *Universitat de València*, and FÉLIX SANCENÓN GALARZA, PhD in Chemistry and Professor at the *Universitat Politècnica de València*.

CERTIFY:

That the work ***"Preclinical evaluation of senescence-based strategies to improve cancer therapy"*** has been developed by Alejandra Estepa Fernández under their supervision in the Instituto Interuniversitario de Investigación de Reconocimiento Molecular y Desarrollo Tecnológico (IDM) of the *Universitat Politècnica de València*, forming part of the Unidad Mixta UPV-CIPF de Investigación en Mecanismos de Enfermedades y Nanomedicina, as a Thesis Project in order to obtain the degree of PhD in Biotechnology at the *Universitat Politècnica de València.*

Valencia, June 30th 2022

Prof. Ramón Martínez Máñez — Director

Dra. Mar Orzáez Calatayud — Directora

Prof. Félix Sancenón Galarza — Director

A mi familia

“Para ser grande, sé entero: nada
tuyo exageres o excluyas.
Sé todo en cada cosa. Pon cuanto eres
en lo mínimo que hagas, …”

Fernando Pessoa

Agradecimientos

Acknowlegements

La verdad es que llevaba varios días (más bien semanas, para qué vamos a engañarnos) aplazando el momento de escribir estos agradecimientos, ya que no sabía cómo reflejar todo el cariño y agradecimiento que tengo para todos los que, de algún modo, han colaborado en que esta tesis se hiciera realidad.

En primer lugar, gracias a mis directores de tesis: Ramón, Félix y Mar. Gracias, Ramón, por darme la oportunidad de realizar esta tesis. Gracias por tu supervisión y por las oportunidades que me has proporcionado. Gracias por tu exigencia (también por los momentos de agobio) y por darme la libertad que ha permitido que aprendiera tanto por el camino. Gracias también por las palabras de ánimo, que son tan necesarias cuando no ves la luz al final del túnel en el que a veces se convierte la tesis. A Félix, gracias por tu supervisión, por ser tan eficiente y por hacer que la burocracia sea mucho más sencilla. Mar, gracias tener la puerta de tu despacho siempre abierta cuando lo he necesitado. Gracias por tu guía y tus consejos (profesionales y personales) durante esta etapa.

Gracias también a mis compañeras de etapa, las principesas. Gracias a mi mamá pato Irene por darme las primeras pinceladas del mundo de la senescencia, ¡ha resultado ser apasionante! Gracias Alba por tu ayuda sobre todo durante la última etapa de mi tesis. Gracias por tu eficiencia, disponibilidad (incluso un viernes a las 9 de la noche) y tus consejos. Gracias a Elena, Blanca y Javi por los momentos y ánimos compartidos. ¡Ánimo, que ya queda menos! También gracias a Juanjo. Ha sido muy gratificante ser la directora de tu TFM y ver tu evolución a doctorando; confío que tu gran entusiasmo y motivación siempre te acompañen. No puedo olvidarme de las nuevas incorporaciones, David, te dejo en buenas manos.

Ara, has sido mi hermana de tesis, ¡qué alegría ha sido haber compartido todo este camino contigo! Gracias por ayudarme tanto experimental como personalmente en esta

tesis. Gracias por estar siempre disponible (fines de semana incluidos) para ayudarme cuando la tesis me superaba. Gracias por las risas, por los fines de semana de fiesta y todos los planes. Todo lo que te pueda decir se queda corto frente al gran apoyo que has sido. Espero haberte devuelto al menos una pequeña parte (lo he intentado).

Gema, has sido otro de mis pilares fundamentales durante la tesis. Eres el claro ejemplo de que las primeras impresiones no reflejan la realidad. Gracias por tu inconformismo y por tu amistad estos años. Como bien me dijiste hace unos días, lo mejor de esta etapa, sin duda, ha sido saber que iba a trabajar todos los días con mis amigas.

Gracias a las chicas del (ya antiguo) I12: Ally, Estefi, Paula, Paula Carrascosa, Danya, Laura, Carmen y Mónica Sancho. Gracias por el buen ambiente que se creó en el lab, guardo muy buen recuerdo de esa etapa en la que todas estabais por ahí. Por todas las risas y buenos momentos, las discusiones filosóficas en las comidas, las locuras de las Paulas, los *brigadeiros* de Danya, etc… Carmen, coincidimos al principio de mi tesis y fuiste un torbellino con tu entusiasmo. Aprendí muchísimas cosas de ti. Ally, ¡qué gran mérito tienes! Tu experiencia vale oro, no veas lo que me acordé de ti cuando tuve que pelearme con el HPLC y el sintetizador de péptidos. Mónica, muchas gracias por tu orientación y por tu disponibilidad a compartir tus conocimientos. ¡Eres una gran fuente de sabiduría! Estefi, no eres consciente de lo que me han ayudado tu pensamiento crítico y tus consejos durante esta etapa. Has sido como una hermana mayor, siempre has sabido qué hacer en cada situación. Por no hablar de todos tus "qué bien se está" en los momentos compartidos fuera del lab. Gracias también por participar en la revisión de esta tesis.

Si el CIPF ha sido una casa para mi durante mi tesis es gracias a todas las personas que forman parte de él. Gracias, Pilar, por tu alegría, optimismo y eficiencia. Gracias a Alfredo, al personal de informática (Vicente, Lucas y Joshland), mantenimiento, administración, recepción y limpieza y esterilización, por solucionarme (muchas veces sin tener que hacerlo) cualquier problema que haya podido tener. Mención especial al personal de cafetería (Javi, Mónica, Emilio), como bien dicen vuestras camisetas (we feed

science) alimentáis la ciencia, ¡cómo echaré de menos vuestra comida y simpatía! Gracias también al personal de los servicios científicos del CIPF: microscopía, histología, animalario y citometría. Alberto, gracias por tu asesoramiento científico y por tu amistad. ¡Qué bien lo hemos pasado en las tardes de juegos de mesa y las barbacoas en tu azotea! Gracias, Alicia, por tu buena disposición y disponibilidad siempre. Gracias, Mario, por tener tanta paciencia conmigo en mi aprendizaje en el mundo de la histología. Gracias a todo el personal del animalario, Viviana, Nerea y Amparo, por ser tan grandes profesionales, por vuestra buena disposición, paciencia para enseñarme y por encontrar un hueco para ayudarme en lo que hiciera falta (pese a todo el trabajo que teníais). Gracias, Nerea, por dejar todo lo que estabas haciendo y entrar corriendo al animalario a intentar reanimar al pobre ratón que no supe pinchar. Mil gracias, Viviana, por tu guía, por tu paciencia y, sobre todo, por ayudarme a superar mis miedos cuando pensaba que el mundo de la experimentación animal no era para mí.

Gracias a los más de 250 ratones que han hecho posible esta tesis.

También quiero agradecer a todas las personas que aún no he nombrado y con las que he compartido mi día a día en el CIPF: Mari Paz, Carmen, Marcos, Angy, Ana, Carlos, Magda, Laura… ¡Ojalá haber podido volver a las mesas de boda para comer al sol y a los almuerzos de cumpleaños después del COVID! No me olvido de las nuevas incorporaciones: Mili, Iván, ... Gracias especialmente a Mari Paz, por su ayuda en la corrección ortográfica y la búsqueda de errores en esta tesis.

Gracias también a mis compañeros de etapa en el laboratorio de química incluyendo tanto a todos los integrantes del 2.6 pasados y presentes: Eva Garrido, Paula, Andrea E, Bea de Luis, Toni, Lorena, Andy, Borja, Iris, Sara Rojas, Serena, Amelia, Lorena, Santi, Elisa, Bea Lozano, Marcia, Giovanni, Guille, Javi Hicke…Y también a las chicas de La Fe: Marina, Isa, Alba y Nieves. Probablemente todos me habéis ayudado de algún modo en algún momento de la tesis o en las semanas de síntesis, cuando andaba tan perdida por el laboratorio de química. Mención especial a mis "*partners*" químicos: gracias, Angy, María,

Xente y Juan Fran por vuestra buena predisposición para ayudar, vuestro tiempo y vuestra paciencia. Gracias también a Elena Aznar, Vicente y Andrea Bernardos por su labor más *senior* en el grupo. Gracias a la parte más administrativa del grupo, que también ha tenido un papel fundamental para realizar esta tesis. Eva Brun y Tania, gracias por vuestra eficiencia y buena predisposición. También gracias a Marta, Pablo, Arantxa y Enrique.

Gracias a Dani por la oportunidad de realizar mi estancia internacional en tu grupo; ha sido una experiencia totalmente enriquecedora profesional y personalmente. Thanks also to Dr. Ljiljana Fruk for allowing me to temporarily be part of her group. Also, I want to thank Daniel Muñoz-Espin lab members: Drew, Cristina, Estela, David, Samir, Hui-Ling, Mary, Chandan… and Fruk-lab members: Andrea, Badri, Leander, Chris, Swetha, ... I have felt really welcomed from everyone, you are so nice! I have very good memories of the meals in the sofas of the medical school and of the lab meetings with breakfast! Thanks specially to Drew for sharing your messy desk and ideas with me. It has been so refreshing to meet you, you are so enthusiastic! Also, thanks to Andrea and Samir for their availability to evaluate of this thesis.

No quiero olvidarme de agradecer a varias personas que (aunque probablemente no la leerán) también han tenido un papel importante para que decidiera tomar este camino y realizar esta tesis. Gracias en primer lugar a Antonio Giménez; fuiste una fuente de inspiración con el cariño y el entusiasmo que le ponías a la docencia de la biología. Gracias también a Emilio; tuviste una paciencia infinita conmigo en mi primer contacto con el laboratorio, los cultivos celulares, las contaminaciones, los Western y las qPCR. Os recuerdo a ambos con mucho cariño.

Gracias a mis amigos de siempre, volver a casa, hacer planes con vosotros y ponernos al día ha sido una de las mejores vías de recarga de energía de esta etapa.

Agradecimientos

Gracias a mi familia, mis padres y mi hermano, Alberto. Gracias papá y mamá por vuestro apoyo incondicional, por vuestro esfuerzo para darme la mejor educación y vida posibles, por despertar en mí el gusanillo de la curiosidad desde pequeña, por no ponerme límites y por todos los valores que me habéis inculcado. Alberto, gracias por estar siempre para apoyarme a pesar de que esta tesis nos separó de nuestras cenas románticas (¡espero que podamos recuperarlas pronto!). A mis abuelos, que me ven con tanto cariño y me hacen ser consciente constantemente de la felicidad de las pequeñas cosas. Y, por último, a Álvaro, gracias por elegirme como compañera de vida, gracias por tu amor incondicional, tu apoyo y comprensión durante esta etapa.

Un trocito de esta tesis es también vuestra. Os quiero mucho,

Alejandra

Resumen

Esta tesis doctoral titulada "*Evaluación preclínica de estrategias basadas en la senescencia para mejorar la terapia contra el cáncer*" se centra en explotar la senescencia como opción terapéutica en los tratamientos contra el cáncer mediante el diseño, la síntesis y la evaluación *in vitro* e *in vivo* de varios nanodispositivos y profármacos, así como la identificación de un nuevo fármaco senolítico.

En la introducción se incluye una descripción general de los diferentes conceptos relacionados con la senescencia celular, así como del papel que juegan las células senescentes a nivel fisiológico y patológico. También se abordan la posibilidad de desarrollar nuevas terapias para el tratamiento del cáncer utilizando la senescencia celular y su papel en la metástasis. Además, se incluyen conceptos básicos de nanotecnología, nanomedicina, nanopartículas de sílice mesoporosa (MSNs) y puertas moleculares. Finalmente, se detallan las interacciones de las nanopartículas con los sistemas biológicos, los nanosistemas descritos en la literatura en relación con la senescencia celular, así como las posibilidades de translación a la práctica clínica de estos nanosistemas.

A continuación, se presentan los objetivos generales de esta tesis doctoral y los objetivos específicos que se abordan en los diferentes capítulos experimentales.

En el primer capítulo experimental evaluamos el efecto negativo de la senescencia endotelial en el contexto tumoral y la consecuencia de su eliminación mediante el uso del senolítico navitoclax. Comprobamos que el tratamiento sistémico con palbociclib en un modelo ortotópico de cáncer de mama en ratones induce senescencia en las células endoteliales vasculares, generando un endotelio alterado funcionalmente que favorece la migración de células cancerosas. La recuperación de la funcionalidad endotelial se consiguió con una estrategia terapéutica que, tras la inducción de senescencia con palbociclib, consigue la eliminación de las células senescentes (senólisis) con una nanopartícula (NP(nav)-Gal). Este nanodispositivo senolítico se basa en MSNs cargadas

con navitoclax y funcionalizadas con un hexa-galacto-oligosacárido (galactán) que se hidroliza en presencia de la enzima lisosomal β-galactosidasa, la cual presenta mayor actividad en las células senescentes. En el modelo preclínico, el tratamiento combinado de palbociclib con NP(nav)-Gal disminuyó la senescencia endotelial en venas, así como los nódulos metastásicos en los pulmones.

Teniendo en cuenta los resultados obtenidos en el primer capítulo, el capítulo dos describe una estrategia terapéutica en dos pasos similar a la anterior para cáncer de mama triple negativo (TNBC). En este caso se emplea un modelo de ratón implantado con xenoinjertos humanos de este tipo de cáncer para evaluar el efecto de la terapia combinada de palbociclib y navitoclax. Para superar los efectos secundarios del tratamiento con navitoclax (principalmente trombocitopenia), evaluamos el efecto del profármaco nav-Gal, sintetizado mediante la conjugación de galactosa con navitoclax. La senescencia inducida por la terapia (TIS) con palbociclib, seguida de una terapia adyuvante con navitoclax o nav-Gal, provoca la eliminación sinérgica de las células senescentes tumorales y la reducción del crecimiento tumoral y de la metástasis pulmonar en el modelo utilizado de ratones con xenoinjertos de cáncer de mama humano agresivo (hTNBC).

El capítulo tres se centra en el diseño y el desarrollo de un nuevo sistema de comunicación de nanopartículas por estigmergía para mejorar la terapia tumoral en el cáncer de mama. La comunicación de nanopartículas por estigmergía consiste en un sistema secuencial de dos nanopartículas en la que la primera modifica el entorno permitiendo que la segunda nanopartícula pueda actuar. Para ello, nos basamos de nuevo en una terapia en dos pasos, siendo el primer paso la inducción de senescencia con palbociclib en las células tumores y el segundo su posterior eliminación con navitoclax. Con este objetivo, se prepararon dos nanodispositivos basados en MSNs con puertas moleculares. El primer nanodispositivo (NP(palbo)PEG-MUC1) se cargó con palbociclib y se funcionalizó, mediante enlaces disulfuro, con un poli(etilenglicol) unido a un aptámero

dirigido a la proteína de superficie MUC1, frecuentemente sobreexpresada en las células tumorales de mama. El segundo nanodispositivo fue la nanopartícula senolítica NP(nav)-Gal ya descrita en el tercer capítulo. Cuando ambos conjuntos de nanopartículas se administraron secuencialmente se consiguió un efecto aumentado, retrasando el crecimiento tumoral y reduciendo las metástasis en pulmón en el modelo descrito previamente de ratones con xenoinjerto hTNBC.

En el cuarto capítulo identificamos un nuevo agente senolítico (H14) que puede eliminar a las células tumorales senescentes de melanoma con una eficacia y seguridad óptima *in vivo*. Para ello, se realizó un cribado de una biblioteca combinatoria de hexapéptidos de D-aminoácidos en células senescentes de melanoma SK-Mel-103, en las que la inducción de la senescencia se había producido mediante el tratamiento con palbociclib. El tratamiento combinado de palbociclib y el hexapéptido H14 logró una mejora en la eliminación de células tumorales senescentes *in vivo*, así como en la reducción del crecimiento tumoral, alcanzando efectos similares al tratamiento combinado de palbociclib con navitoclax.

Finalmente, se presentan las principales conclusiones derivadas del trabajo experimental presentado, así como las conclusiones generales derivadas de esta tesis doctoral. Esperamos que los resultados obtenidos en esta tesis doctoral abran nuevas oportunidades de investigación, e inspiren el desarrollo de estrategias avanzadas con nanodispositivos inteligentes y profármacos, para su aplicación en el campo de la senescencia celular, en otras áreas biomédicas o en tecnologías de detección y comunicación, para resolver las necesidades del paciente.

Resum

Aquesta tesi doctoral titulada "*Avaluació preclínica d'estratègies basades en la senescencia per millorar la teràpia contra el càncer*" se centra a explotar la senescència com a opció terapèutica en els tractaments contra el càncer mitjançant el disseny, la síntesi i l'avaluació *in vitro* i *in vivo* de diferents nanodispositius i profàrmacs, així com la identificació d'un fàrmac senolític nou per millorar la teràpia contra el càncer.

A la introducció s'inclou una descripció general dels diferents conceptes relacionats amb la senescència cel·lular, així com el paper que juguen les cèl·lules senescents a nivell fisiològic i patològic. També s'aborda la possibilitat de desenvolupar noves teràpies per al tractament del càncer utilitzant la senescència cel·lular i el paper que té la senescència cel·lular en la metàstasi. Més endavant, s'hi inclouen conceptes bàsics de nanotecnologia, nanomedicina, nanopartícules de sílice mesoporosa (MSNs) i portes moleculars. Finalment, s'aborden les interaccions de les nanopartícules amb els sistemes biològics, els nanosistemes descrits a la literatura en relació amb la senescència cel·lular, així com les possibilitats de translació a la pràctica clínica d'aquests nanosistemes.

A continuació, se presenta els objectius generals d'aquesta tesi doctoral i els objectius específics que s'aborden als diferents capítols experimentals.

Al primer capítol experimental se avaluem l'efecte de la senescència endotelial en el context tumoral. Més senolítics Comprovem que el tractament sistèmic amb palbociclib en un model ortotòpic de càncer de mama en ratolins indueix la senescència a les cèl·lules endotelials vasculars generant un endoteli alterat funcionalment que afavoreix la migració de cèl·lules de canceroses. La recuperació de la funcionalitat endotelial es va aconseguir amb una estratègia terapèutica en dos etapes que va combinar la inducció de senescència amb palbociclib seguida de l'eliminació de les cèl·lules senescents (senòlisi) amb una nanopartícula carregada amb navitoclax (NP(nav)-Gal). Aquest nanodispositiu senolític es basa en MSNs carregades amb navitoclax i funcionalitzades amb un hexa-galactooligosacàrid (galactan) que s'hidrolitza en presència de l'enzim lisosomal β-

galactosidasa, que presenta més activitat en les cèl·lules senescents. En el model preclínic, el tractament combinat de palbociclib amb NP(nav)-Gal va disminuir la senescència endotelial en venes així com els nòduls metastàsics als pulmons.

Segons els resultats obtinguts al primer capítol, el capítol dos descriu una estratègia terapèutica similar de dos etapes per a pacients amb càncer de mama triple negatiu (TNBC). En aquest cas s´utilitza un model de ratolí implantat amb xenoempelts humans per avaluar l'efecte de la teràpia combinada de palbociclib més navitoclax. Per superar els efectes secundaris del tractament amb navitoclax (principalment trombocitopènia), avaluem l'efecte del profàrmac nav-Gal, sintetitzat mitjançant la conjugació de galacotsa i navitoclax. La senescència induïda per la teràpia (TIS) amb palbociclib seguida d'una teràpia adjuvant amb navitoclax o nav-Gal provoca l'eliminació sinèrgica de les cèl·lules senescents tumorals i la reducció del creixement tumoral i de la metàstasi pulmonar en un model de ratolins amb xenoempelts de càncer de mama humà agressiu (hTNBC).

El tercer capítol se centra en el disseny i desenvolupament d'un nou sistema de comunicació de nanopartícules mitjançant estigmèrgia per millorar la teràpia tumoral en càncer de mama. La comunicació de nanopartícules per estigmergia consisteix en un sistema seqüencial de dues nanopartícules on la primera modifica l'entorn permetent que la segona nanopartícula pugui actuar. Per això, ens basem de nou en una teràpia en dos passos, sent el primer pas la inducció de senescència amb palbociclib i el segon la posterior eliminació de les cèl·lules senescents tumorals amb navitoclax. Amb aquest objectiu, es van preparar dos nanodispositius basats en MSNs amb portes moleculars. El primer nanodispositiu (NP(palbo)PEG-MUC1) es va carregar amb palbociclib i es va funcionalitzar, mitjançant un enllaç disulfur, amb un poli(etilenglicol) unit a un aptàmer dirigit a la proteïna de superfície MUC1, sobreexpressada a les cèl·lules tumorals de mama. El segon nanodispositiu va ser el senolític NP(nav)-Gal ja descrit al tercer capítol. Quan els dos conjunts de nanopartícules es van administrar seqüencialment es va

aconseguir un efecte sinèrgic, endarrerint el creixement tumoral i reduint les metàstasis de pulmó en el model descrit prèviament de ratolins amb xenoempelt hTNBC.

Al quart capítol, identifiquem un nou agent senilític (H14) que pot eliminar les cèl·lules tumorals senescents de melanoma amb una eficàcia i seguretat òptima *in vivo*. Per fer-ho, es va realitzar un garbellat d'una biblioteca combinatòria d'hexapèptids de D-aminoàcids en cèl·lules senescents de melanoma SK-Mel-103 on la inducció de la senescència s'havia produït mitjançant el tractament amb palbociclib. El tractament combinat de palbociclib i l'hexapeptid H14 va aconseguir una millora en l'eliminació de cèl·lules tumorals senescents, així com en la reducció del creixement tumoral, assolint efectes similars al tractament combinat de palbociclib amb navitoclax.

Finalment, es presenten les conclusions principals derivades del treball experimental presentat, així com les conclusions generals derivades d'aquesta tesi doctoral. Esperem que els resultats obtinguts en aquesta tesi doctoral obrin noves oportunitats de recerca i inspirin el desenvolupament d'estratègies avançades amb nanodispositius intel·ligents i profàrmacs per a la seva aplicació al camp de la senescència cel·lular o en altres àrees biomèdiques diferents com la nanomedicina o les tecnologies de detecció i comunicació per resoldre les necessitats del pacient.

Abstract

This PhD thesis entitled "*Preclinical evaluation of senescence-based strategies to improve cancer therapy*" focuses on exploiting senescence as a therapeutic option in cancer treatments through the design, synthesis, *in vitro* and *in vivo* evaluation of several nanodevices and prodrugs as well as the identification of a novel senolytic drug.

The introduction includes an overview of the different concepts related to cellular senescence and the role that senescent cells play at physiological and pathological levels. The possibility of developing new therapies for cancer treatment using cellular senescence and its role in metastasis is also addressed. Later, basic concepts on nanotechnology, nanomedicine, mesoporous silica nanoparticles (MSNs), and molecular gates are included. Finally, challenges related to the interactions of nanoparticles with biological systems, nanosystems described in literature related to cellular senescence, as well as the possibilities of translation of these nanosystems to the clinical practice are described.

Next, the general objectives of this PhD thesis and the specific objectives that are addressed in the different experimental chapters.

In the first experimental chapter, we evaluate the negative effect of endothelial senescence in the tumor context and the consequence of its elimination through the use of the senolytic navitoclax. We found that systemic treatment with palbociclib in an orthotopic mice model of breast cancer induces senescence in vascular endothelial cells, generating an altered endothelium that favors cancer cells migration. Recovery of endothelial functionality was achieved, after palbociclib-senescence induction, by removal of senescent cells (senolysis) with navitoclax-loaded nanoparticles (NP(nav)-Gal). This senolytic nanodevice is based on MSNs loaded with navitoclax and functionalized with a hexa-galacto-oligosaccharide (galactan) that is hydrolyzed in the presence of the lysosomal enzyme β-galactosidase, which is overexpressed in senescent cells. In a

preclinical model, the combined treatment of palbociclib with NP(nav)-Gal decreased endothelial senescence in veins as well as in metastatic nodules in the lungs.

Based on the results obtained in the first chapter, chapter two describes a similar one-two punch therapeutic strategy for triple-negative breast cancer patients. In this case, a human xenograft mice model was employed to evaluate the effect of combined therapy of palbociclib plus navitoclax. In order to overcome the side effects of navitoclax treatment (mainly thrombocytopenia), we evaluated the effect of the prodrug nav-Gal, synthetized by the galactose-conjugation of navitoclax. Palbociclib therapy-induced senescence (TIS) followed by adjuvant therapy with navitoclax or nav-Gal caused a synergistic elimination of senescent tumor cells and reduction of tumor growth and lung metastasis in a xenograft mice model of aggressive human TNBC (hTNBC).

Chapter three focuses on the design and development of a new stigmergy nanoparticle communication system to improve tumor therapy in breast cancer. The communication of nanoparticles by stigmergy consists of a sequential system of two nanoparticles in which the first modifies the environment allowing the second nanoparticle to act. To do this, we again rely on a two-step therapy. The first step is the induction of senescence with palbociclib, and the second is the subsequent elimination of senescent tumor cells with navitoclax. For this purpose, two nanodevices based on gated MSNs were prepared. The first nanodevice (NP(palbo)PEG-MUC1) was loaded with palbociclib and functionalized, through disulfide bonds, with a poly(ethylene glycol) that binds to an aptamer cap that targets the MUC1 surface protein, which is overexpressed in breast tumor cells. The second nanodevice was the senolytic NP(nav)-Gal already described in the third chapter. A synergistic effect was achieved when both nanoparticles were sequentially administered, delaying tumor growth and reducing metastases in a xenograft hTNBC mice model.

In the fourth chapter, we identify a novel senolytic agent (H14) that can target malignant tumoral melanoma senescent cells with optimal *in vivo* efficacy and safety. To

do so, a combinatorial library of D-amino acid hexapeptides was screened in senescent SK-Mel-103 melanoma cells in which the induction of senescence was achieved by treatment with palbociclib. The combined therapy of palbociclib and H14-hexapeptide improved the elimination of senescent tumor cells and reduced tumor growth, reaching effects similar to the combined treatment of palbociclib with navitoclax.

Finally, the main conclusions derived from the presented experimental work, as well as the general conclusions of this Ph.D. thesis, are addressed. Future breakthroughs in the field of cellular senescence treatment are expected. We hope that the results achieved in this PhD thesis will open new research opportunities and inspire the development of advanced strategies with smart nanodevices and prodrugs for their application in the field of cellular senescence and other different biomedical areas and in sensing and communication technologies to solve patient needs.

Publications

Results of this PhD thesis and other contributions have resulted in the following scientific publications.

- **Alejandra Estepa-Fernández,** María Alfonso, Ángela Morellá-Aucejo, Alba García-Fernández, Araceli Lérida-Viso, Beatriz Lozano-Torres, Irene Galiana, Paula Mª Soriano-Teruel, Félix Sancenón, Mar Orzáez, Ramón Martínez-Máñez. Senolysis reduces senescence in veins and cancer cell migration. *Advanced Therapeutics*. Volume 4 (10) 2100149 (2021)
- Beatriz Lozano-Torres, **Alejandra Estepa-Fernández**, Miguel Rovira, Mar Orzáez, Manuel Serrano, Ramón Martínez-Máñez & Félix Sancenón. The chemistry of senescence*. Nature Reviews Chemistry*. Volume 3, pages 426–441 (2019)
- Araceli Lérida-Viso; **Alejandra Estepa Fernández**; Ángela Morellá-Aucejo; Beatriz Lozano-Torres; María Alfonso; Juan F. Blandez; Viviana Bisbal; Pilar Sepúlveda; Mar Orzáez; Ramón Martínez-Máñez. Pharamacological senolysis reduces doxorubicin-induced cardiotoxicity and improves cardiac function in mice. *Submitted.*
- **Alejandra Estepa-Fernández**, Alba García-Fernández, Araceli Lérida-Viso, Juan F. Blandez, Irene Galiana, Félix Sancenón-Galarza, Mar Orzáez, Ramón Martínez-Máñez. Combination of palbociclib with navitoclax based-therapies shows *in vivo* antitumoral activity in triple-negative breast cancer. *Submitted.*
- **Alejandra Estepa-Fernández**, Alba García-Fernández, Araceli Lérida-Viso, Ángela Morellá-Aucejo, Juan José Esteve-Moreno, Juan F. Blandez, María Alfonso, Vicente Candela-Noguera, Gema Vivo-Llorca, Félix Sancenón-Galarza, Mar Orzáez, Ramón Martínez-Máñez. Engineering nanoparticle communication in living systems by stigmergy: an application to enhance antitumor therapy in triple-negative breast cancer. *Submitted.*

- **Alejandra Estepa-Fernández***, Irene Galiana*, Araceli Lérida-Viso, Alicia Belén García-Jareño, Alba García-Fernández, Félix Sancenón-Galarza, Mar Orzáez, Ramón Martínez-Máñez. Identification of a novel senolytic hexapeptide for malignant melanoma. *Submitted*. *Both authors have contributed equally.
- Araceli Lérida-Viso*, **Alejandra Estepa-Fernández***, Alba García-Fernández, Vicente Marti-Centelles, Ramón Martínez-Máñez. Biosafety features of mesoporous silica nanoparticles towards clinical translation. *Both authors have contributed equally. *Submitted.*

Abbreviations and Acronyms

α-Fuc	α-L-fucosidase
α-tub	α-tubulin
AKT	Protein kinase B
AMP	Adenosine monophosphate
APTES	(3-Aminopropyl)triethoxysilane
ATCC	American Type Culture Collection
ATP	Adenosine triphosphate
B2MG	Beta-2 microglobulin
Bad	Bcl-2 antagonist of cell death
Bak	Bcl-2 associated killer protein
Bax	Bcl-2 associated X protein
Bcls	B-cell lymphoma proteins
Bcl-2	B-cell lymphoma 2
Bcl-w	Bcl-2-like protein 2
Bcl-xL	B-cell lymphoma-extra large
BC	Breast cancer
BCA	Bicinchoninic acid
BSA	Bovine serum albumin
BET	Brunauer–Emmett–Teller
BJH	Barret-Joyner-Halenda
BRAF	v-raf murine sarcoma viral oncogene homolog B1
C	Control
C-dots	Cornell dots
C_{12}FDG	5-dodecanoylaminofluorescein di-β-D-galactopyranoside
CD4	Cluster of Differentiation 4
CD9	Cluster of Differentiation 9. Tetraspanin
CD20	Cluster of Differentiation 20
CD68	Cluster of Differentiation 68
CD86	Cluster of Differentiation 86
CDC7	Cell Division Cycle 7

CDK	Cyclin-dependent kinases
CDK4/6	Cyclin-dependent kinases 4 and 6
CM	Conditioned media
cRGDY	Cyclic arginine–glycine–aspartic acid peptide
CSNRs	Core–shell spiky nanorods
CTAB	Cetyltrimethylammonium bromide
Cu_xCo_yS	Chiral nanoparticles
Cy5	Cyanine 5
Cy5.5	Cyanine 5.5
Cyt	Cytokines
DAPI	4′,6-diamidino-2-phenylindole
DDR	DNA-damage response
DLS	Dynamic light scattering
DMEM	Dulbecco's Modified Eagle Medium
DMF	Dimethylformamide
DMSO	Dimethyl sulfoxide
DNA	Deoxyribonucleic acid
DTT	Dithiothreitol
E2F	Transcription factor E2F
ECGS	Endothelial cell growth supplement from bovine neural tissue
ECL	Electroluminiscence
EDTA	Ethylenediamine tetraacetic acid
EGTA	Ethyleneglycol tetraacetic acid
EMT	Epithelial mesenchymal transition
EPR	Enhanced and permeability retention effect
ER	Estrogen receptor
FBS	Fetal bovine serum
FDA	Food and Drug Administration
FITC	Fluorescein Isothiocyanate
FOXO	Forkhead box protein O

G1	Cell growth phase 1 of the cell cycle
G2	Cell growth phase 2 of the cell cycle
GADPH	Glyceraldehyde 3-phosphate dehydrogenase
GF	Growth factors
GSH	Glutathione
H3K9me3	Trimethylation of lysine 9 at histone 3
H8	Hexapeptide 8
H14	Hexapeptide 14
HAT	Histone acetyltransferase
HDAC	Histone deacetylase
HDF	Human dermal fibroblasts
HEPES	N-2-Hydroxyethylpiperazine-N'-2-Ethanesulfonic Acid
HER2	Human epidermal growth factor receptor 2
HIF-1α	Hypoxia-inducible factor 1
HPLC	High-performance liquid chromatography
HR	Hormone receptor
HSP-90	Heat shock protein 90
hTNB	human Triple Negative Breast Cancer
HUVEC	Human Umbilical Vein Endothelial Cells
IC50	Half maximal inhibitory concentration
ICG	Indocyanine Green
ICP-MS	Inductively coupled plasma mass spectroscopy
IFNγ	Interferon γ
IgG	Immunoglobulin G
Il1a	Interleukin 1 alpha
IL-6	Interleukin 6
i.p.	Intraperitoneal administration
i.v.	Intravenous administration
IVIS	*In vivo* imaging system
Ki67	Marker of proliferation Ki-67

MAD	Mother against decapentaplegic
MCM-41	Mobil Composition of Matter No. 4
MDA-MB-231	M.D. Anderson - Metastatic Breast 231 cell line
MEK	Mitogen-activated protein kinase kinase
MMP	Matrix-remodelling proteins
MMP3	Matrix-remodelling protein 3
MPTMS	(3-mercaptopropyl)trimethoxysilane
MS	Mass Spectrometry
MSNs	Mesoporous silica nanoparticles
MtMP	Mitochondrial membrane potential
mTOR	Mammalian target of rapamycin
MUC1	Mucin 1
NADH	Nicotinamide adenine dinucleotide
nanoMIPs	Molecularly imprinted polymer nanoparticles
Nav	Navitoclax
Nav-Gal	Galacto-conjugated navitoclax
NB	Nile Blue
NHS	N-hydroxysuccinimide
NIR	Near-infrared (NIR) light
NOTA	1,4,7-triazacyclononane-N, N’, N''-triacetic acid
NPs	Nanoparticles
OCT	Optimal cutting temperature
o.g.	Oral gavage
OIS	Oncogene-induced senescence
ORR	Objective response rate
OS	Overall survival
P	Palbociclib
p16	Cyclin-dependent kinase inhibitor 2A
p21	Cyclin-dependent kinase inhibitor 1A
p53	Tumor protein p53

PAGE	Polyacrylamide gel electrophoresis
Palbo	Palbociclib
PARPi	Poly(ADP-ribose) polymerase 1 inhibitor
PBS	Phosphate buffer saline
PD1	Programmed cell death protein 1
PDGF-AA	Platelet derived growth factor AA
PEG	Poly(ethylene glycol)
PET	Polyethylene terephthalate
PFA	Paraformaldehyde
PFS	Progression-free survival
PI	Propidium iodide
PI3K	Phosphatidylinositol-3-kinase
PKC	Protein kinase C
PR	Progesterone receptor
pRb	Phosphorylated retinoblastoma protein
PROTAC	Proteolysis-targeting chimera
PSMA	Prostate-specific membrane antigen
PTFE	Polytetrafluoroethylene
PXRD	Powder X-ray diffraction
QTOF	Quadrupole Time-of-Flight Mass Spectrometry
R	Chemical radical
Rb	Retinoblastoma protein
RES	Reticuloendothelial system
RhB	Rhodamine B
RIPA	Radioimmunoprecipitation assay
RNA	Ribonucleic acid
ROS	Reactive oxygen species
S	DNA synthesis phase of the cell cycle
SA-β-Gal	Senescence-associated β-galactosidase
saf	Safranine O

SAHF	Senescence-associated heterochromatic foci
SAMP8	Senescence-accelerated mouse model
SASP	Senescence-associated secretory phenotype
SCAPS	Senescent-cell anti-apoptotic pathways
SD	Standard deviation
SDS	Sodium dodecyl sulphate
SEM	Standard error of the mean
Ser	Serine
SMAD	Suppresor of mother against decapentaplegic
TBS	Tris-hydroxymethyl-aminomethane
TEM	Transmission electron microscopy
TEM-EDX	TEM coupled with energy-dispersive X-ray spectroscopy
TEOS	Tetraethyl orthosilicate
TGA	Thermogravimetric analysis
TGFβ	Transforming growth factor β
Thr	Threonine
TIS	Therapy-induced senescence
TME	Tumor microenvironment
TMRE	Tetramethylrhodamine ethyl ester
TNBC	Triple negative breast cancer
TNFα	Tumor necrosis factor α
TPP	Triphenylphosphonium
TUNEL	Terminal deoxynucleotidyl transferase biotin-dUTP nick end labeling
UAuTE NPs	Gold tetrahedron nanoparticles
UV-Vis	Ultraviolet-visible
VCAM1	Vascular cell adhesion molecule 1
WGA	Wheat germ agglutinin
X-gal	5-Bromo-4-chloro-3-indolyl β-D-galactopyranoside
Zvad	Pan-caspase inhibitor Z-VAD-FMK

General index

Table of contents

General introduction

1. Cellular senescence

Senescence is a cellular state characterized by a highly stable cell cycle arrest associated with specific phenotypic changes.(López-Otín et al., 2013) The senescence concept emerged in 1961 when Hayflick and Moorhead found that serial cell cultures of human fetal fibroblasts lose their proliferative potential after a limited number of passages.(Hayflick and Moorhead, 1961) This type of senescence is known today as "replicative senescence" and is triggered by telomeres shortening or damage, which promotes the activation of DNA-damage checkpoint responses (DDR). (Harley, Futcher and Greider, 1990; Yu et al., 1990; Olovnikov, 1996; Bodnar et al., 1998; Takai, Smogorzewska and De Lange, 2003)

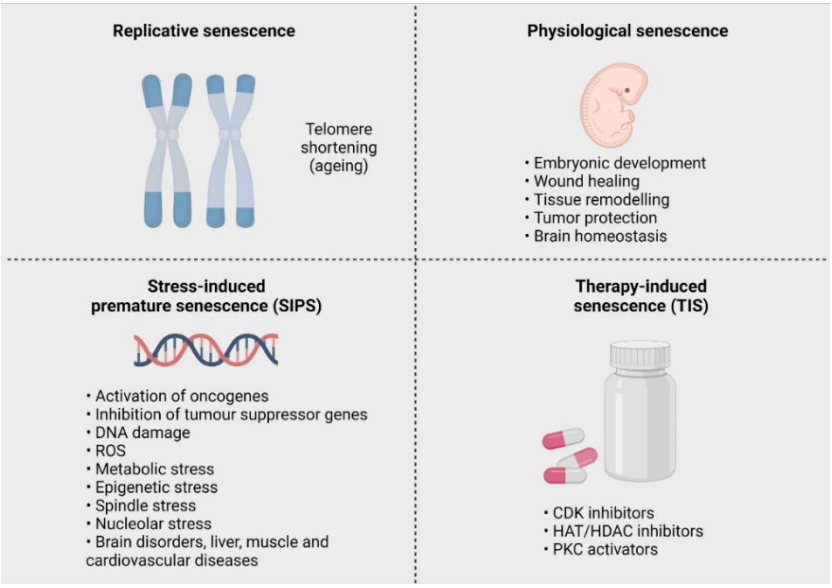

Figure 1 | Types of cellular senescence. Senescence occurs naturally and, depending on how it is triggered, can be classified as replicative senescence, physiological senescence, stress-induced premature senescence (SIPS), or therapy-induced senescence (TIS). CDK, cyclin-dependent kinases; HAT, histone acetyltransferase; HDAC, histone deacetylase; PKC, protein kinase C; ROS, reactive oxygen species. Adapted from Lozano-Torres et al., 2019.

Introduction

Nowadays, many factors (Figure 1) have been found to trigger “stress-induced premature senescence" (also called “premature senescence” or “oncogene-induced senescence” (OIS)), such as high-fat diet, oncogene activation, radiotherapy, and chemotherapy (known as “therapy-induced senescence”(TIS)), reactive oxygen species (ROS), metabolic and epigenetic changes and mitochondrial dysfunction.(Han, Williams and Cadenas, 2001; Collado, Blasco and Serrano, 2007; Jun and Lau, 2010; Barnes, 2015; Bielak-Zmijewska, Mosieniak and Sikora, 2018) In all these cases, senescence induction is considered a way to protect the body from damaged or stressed cells that are unable to engage apoptosis.

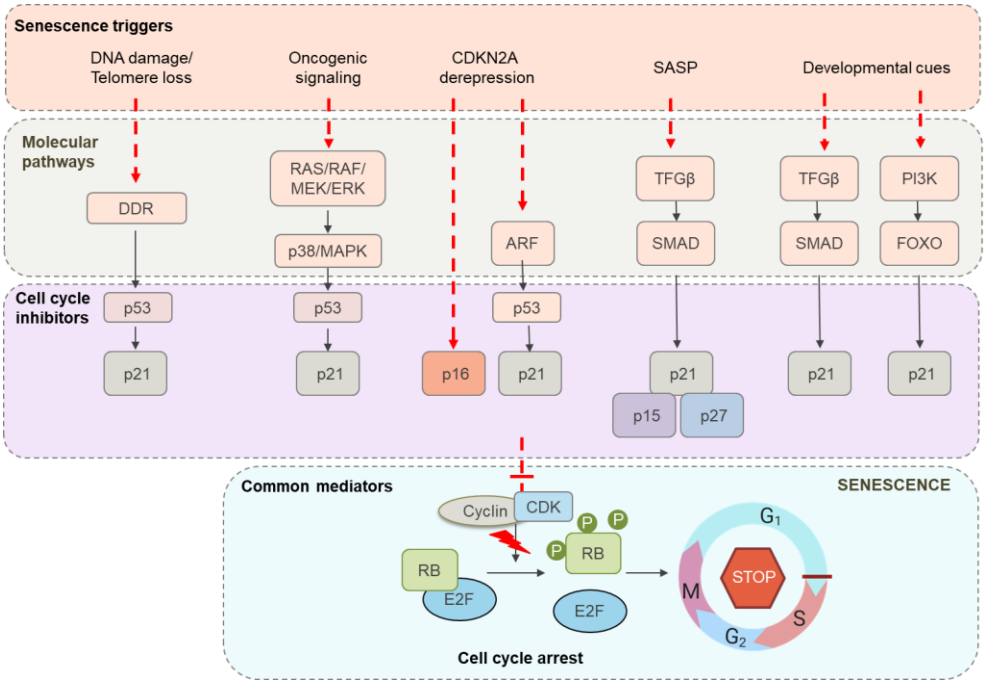

Figure 2 | Molecular pathways involved in senescence. Several senescence triggers can affect signaling pathways converging in the overexpression of cell cycle inhibitors, such as $p21_{CIP1}$ and $p16_{Ink4a}$. These proteins stop cyclin-dependent kinases (CDK)–cyclin complexes from phosphorylating the retinoblastoma protein (Rb). Consequently, the transcription factor E2F, which is usually responsible for the expression of the genes needed for cell cycle progression, is sequestered by Rb, and the cell cycle is arrested. DDR, DNA-damage response; FOXO, forkhead box protein O; PI3K, phosphatidylinositol-3-kinase; ROS, reactive oxygen species; SASP, senescence-associated secretory phenotype; SMAD (Suppressor of Mothers against Decapentaplegic), MAD

(mother against decapentaplegic); TGFβ, transforming growth factor β. Adapted from Lozano-Torres et al., 2019

The induction of cellular senescence is controlled by different signaling pathways that stably block cell proliferation and are conserved across vertebrates.(Alimonti *et al.*, 2010; Collado and Serrano, 2010; Muñoz-Espín and Serrano, 2014) Depending on the senescence-inducing stimuli, different molecular pathways which converge in the activation of cyclin-dependent kinase (CDKs) inhibitors (e.g., $p16_{INK4A}$, $p15_{INK4B}$, $p21_{CIP1,}$ and $p27_{KIP1}$) (Figure 2).(Campisi and d'Adda di Fagagna, 2007; Muñoz-Espín and Serrano, 2014) When CDKs are inhibited, the phosphorylation of retinoblastoma protein (Rb) does not occur.(Chicas *et al.*, 2010) Consequently, the transcription factor E2F (that controls the expression of the genes needed for cell cycle progression) remains sequestered by Rb protein, inhibiting the expression of cell cycle progression genes, therefore, inducing cell cycle arrest in the G1 phase.(Peeper *et al.*, 1993; Bloom and Cross, 2007; Vicencio *et al.*, 2008; Malumbres and Barbacid, 2009; Goel *et al.*, 2018)

1.1. Hallmarks of senescent cells

Senescence is considered a dynamic, multi-step process during which the properties of senescent cells constantly evolve and diversify depending on the context.(Van Deursen, 2014) In addition to proliferation arrest, one of the most obvious phenotypic characteristics of senescent cells *in vitro* is the morphological change.(Hernandez-Segura, Nehme and Demaria, 2018) Senescent cells *in vitro* have an irregular shape with a flattened appearance and enlarged nuclei.(Campisi and d'Adda di Fagagna, 2007) Typically, senescent cells also have enlarged lysosomes and increased Golgi apparatus, nucleolar size, and cytoplasmic granularities with many lipids droplets.(Kuilman *et al.*, 2010; Salama *et al.*, 2014; Frescas *et al.*, 2017; Hernandez-Segura, Nehme and Demaria, 2018) It is important to note that *in vivo* senescent cells tend to maintain the morphology established by tissue architecture.(Muñoz-Espín and Serrano, 2014)

Introduction

One of the most widely used markers to detect senescent cells is the enzyme β-galactosidase (SA-β-Gal), which is overexpressed in the lysosomes of senescent cells.(Dimri *et al.*, 1995; Biran *et al.*, 2017) The major drawback of using SA-β-Gal for the detection of senescence cells *in vitro* is that SA-β-Gal activity increases not only in senescent cells but also in confluent quiescent cultured cells or under serum starvation, leading to the detection of false positives.(Yang and Hu, 2005) Apart from SA-β-Gal, the overexpression of other lysosomal hydrolases, such as α-L-fucosidase (α-Fuc), has also been used to detect senescent cells.(Knaś *et al.*, 2012; Hildebrand *et al.*, 2013)

As senescent cells are growth-arrested, genes responsible for cell proliferation (e.g. p53, $p16_{INK4A}$ or $p21_{CIP1}$) are suitable markers to identify senescent cells.(Takahashi, Ohtani and Hara, 2007; Burd *et al.*, 2013; Baker *et al.*, 2016; Hernandez-Segura *et al.*, 2017) The absence of the Ki67 proliferative marker and the hypophosphorylation of Rb protein in the tumors are also an indicative of senescence.(Gerdes *et al.*, 1984; Chicas *et al.*, 2010; Muñoz-Espín *et al.*, 2018; Alessio *et al.*, 2021)

Another well-known characteristic of senescent cells is their resistance to apoptosis.(Wang, 1995; Hampel *et al.*, 2004; Marcotte, Lacelle and Wang, 2004; Ryu, Oh and Park, 2007; Sanders *et al.*, 2013; Childs *et al.*, 2014; Zhu *et al.*, 2015) The survival of senescent cells depends on the expression of anti-apoptotic B-cell lymphoma proteins (Bcls), such as Bcl-xL, Bcl-2 or Bcl-W. The overexpression of antiapoptotic Bcls preserves outer mitochondrial membrane integrity and prevents cell death by apoptosis.(Childs *et al.*, 2014)

Although senescent cells remain viable, they present alterations in their metabolic activity.(Wiley and Campisi, 2021) Mitochondria from senescent cells have an impaired electron transport chain, resulting in altered membrane potential, elevated intracellular levels of ROS, decreased cytosolic NAD+/NADH ratios and increased AMP/ATP ratios.(Lee *et al.*, 1999; Passos *et al.*, 2007, 2010; Wiley *et al.*, 2016) In addition, lysosomes of senescent cells can become permeable, acidifying the cytosol and disrupting some forms

of autophagy.(Young *et al.*, 2009; Kwon *et al.*, 2017) This can lead to the accumulation of transition metals inside senescent cells.(Killilea *et al.*, 2003; Masaldan *et al.*, 2018) Senescent cells are also characterized by the presence of lipofuscin granules and non-degradable aggregates of oxidized proteins, lipids, and oligosaccharides that accumulate progressively in the lysosomes.(Katz *et al.*, 1984; Georgakopoulou *et al.*, 2012; Evangelou *et al.*, 2017) Considering that senescence is a complex and variable phenomenon, it is possible that those metabolic alterations may be present in some, but not all, forms of senescence.

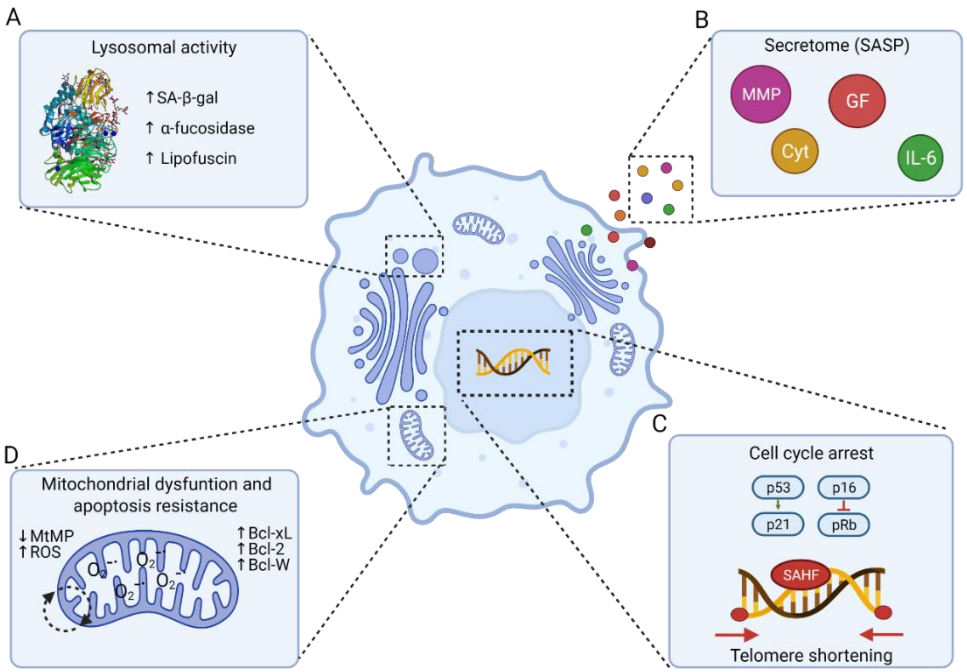

Figure 3 | Features of cellular senescence. (A) Increased lysosomal mass leads to an increased SA-β-gal and α-fucosidase activity and lipofuscin accumulation. (B) The senescence-associated secretory phenotype, SASP, is a dynamic and complex secretome that can comprise extracellular matrix-remodeling proteins (MMP), cytokines (Cyt) (e.g., IL-6), growth factors (GF), among others. (C) Senescence induction stimuli (e.g., telomere shortening or DNA damage) lead to cell cycle arrest regulated through the p53/p21 and p16/Rb pathways. Also, senescence-associated heterochromatic foci (SAHF) can limit proliferation-promoting genes. (D) Apoptosis resistance and mitochondrial dysfunction are common hallmarks of cellular senescence. ROS production is

increased along with reduced mitochondrial membrane potential (MtMP). Also, antiapoptotic Bcls (Bcl-xL, Bcl-2, and Bcl-W) are overexpressed in senescent cells. Adapted from Morsli *et al*., 2022.

Moreover, senescent cells undergo dramatic gene expression changes along with chromatin remodeling. A peculiar foci of condensed nuclear chromatin enriched for histone modifications, including lysine9-trimethylated histone H3, called senescence-associated heterochromatic foci (SAHF), can be observed in some senescent cell types.(Narita *et al.*, 2003; Chandra *et al.*, 2015) Other genetic and epigenetic alterations present in senescent cells are changes or shortening of telomere length, phosphorylation of the histone H2AX, and loss of lamin B1.(Freund *et al.*, 2012; Chandra *et al.*, 2015)

Finally, all senescent cells develop a complex, multi-component senescent-associated secretory phenotype (SASP). The SASP acts as a non-autonomous cell mechanism changing the surrounding tissue microenvironment and altering the behavior of neighboring cells.(Birch and Gil, 2020) The SASP is highly dynamic, variable, and plastic; its characteristics depend on the cell type and senescence inducer and can change over time.(Coppé *et al.*, 2008; Basisty *et al.*, 2020) It is formed by a complex mixture of extracellular factors such as inflammatory mediators (IL-6, MMP3), growth factors, bioactive lipids, detached cell surface molecules, or extracellular matrix components.(Krizhanovsky *et al.*, 2008; Coppé *et al.*, 2010; Acosta *et al.*, 2013; Demaria *et al.*, 2014; Yun, Davaapil and Brockes, 2015; Ritschka *et al.*, 2017; Saleh *et al.*, 2018)

It is important to consider that some of the aforementioned senescence-associated features can be present in other cellular states and conditions (Hernandez-Segura, Nehme and Demaria, 2018). Likewise, these widely used senescence markers are neither invariable nor universal. Thus, multiple markers are required to assess the presence of senescent cells *in vitro* or in tissues *in vivo* (Figure 3).(Gorgoulis *et al.*, 2019; González-Gualda *et al.*, 2021)

1.2. Senescence in physiology and pathology

Initially, senescence was considered a tissue culture artifact. However, several studies have shown that senescence plays complex biological roles in the organism contributing to different physiological and pathological processes.(Hanahan and Weinberg, 2011; Burton and Krizhanovsky, 2014) The main biological role of cellular senescence is to prevent the proliferation of potentially dysfunctional, damaged, or stressed cells.(Collado, Blasco and Serrano, 2007; Muñoz-Espín and Serrano, 2014; Kang *et al.*, 2015; Childs *et al.*, 2017; Maciejowski and De Lange, 2017; Faget, Ren and Stewart, 2019) Possibly, senescence evolved as a protective mechanism to maintain tissue homeostasis and complement programmed cell death.(Hanahan, 2022)

Regarding its beneficial effects, senescence plays key physiological roles during embryonic development.(Muñoz-Espín *et al.*, 2013; Storer *et al.*, 2013), wound healing (Ramakrishna *et al.*, 2012; Demaria *et al.*, 2014), tissue remodeling (Yun, Davaapil and Brockes, 2015) or tumorigenesis.(Collado, Blasco and Serrano, 2007; Hanahan and Weinberg, 2011; Kang *et al.*, 2015; Childs *et al.*, 2017; Maciejowski and De Lange, 2017; Faget, Ren and Stewart, 2019; Hanahan, 2022) To point out some examples, programmed cellular senescence contributes to the formation of the mesonephros, the closing of the neural tube, and the proper development of the endolymphatic sac of the inner ear.(Muñoz-Espín *et al.*, 2013; Storer *et al.*, 2013) In adult organisms, physiological senescence also occurs in the maturation process of placental syncytiotrophoblasts or megakaryocytes.(Besancenot *et al.*, 2010; Chuprin *et al.*, 2013) During wound healing, senescent fibroblasts and endothelial cells secrete the SASP component platelet derived growth factor AA (PDGF-AA), which promotes myofibroblast differentiation and facilitates optimal wound closure.(Demaria et al., 2014) The role of senescence in tumorigenesis will be discussed in more detail below.

Senescent cells can modify the tissue environment and affect tissue regenerative capacities in either a positive or negative way through the SASP. The secretome of senescent cells alerts the immune system by inducing the recruitment of inflammatory cells (e.g., natural killer cells, macrophages, neutrophils, lymphocytes) to the damaged area, which eventually eliminate senescent cells.(Kang *et al.*, 2011; Di Mitri and Alimonti, 2016; Sagiv *et al.*, 2016) However, excessive secretion of SASP factors leads to chronic inflammation (also called inflammaging), tissue aging, and dysfunction.(Freund *et al.*, 2010; Salminen, Kauppinen and Kaarniranta, 2012; Tchkonia *et al.*, 2013) An example of the double-face of senescence occurs in the placenta. As mentioned before, senescence in the placenta is a physiological process (Sultana *et al.*, 2018), whereas aberrant senescence could lead to adverse pregnancy events like preeclampsia or spontaneous preterm birth.(Cox and Redman, 2017; Cindrova-Davies *et al.*, 2018)

There is also a close relationship between senescence and aging. In fact, senescence considered one of the key aging hallmarks. The accumulation of senescent cells in multiple tissues increases with aging (Muñoz-Espín and Serrano, 2014; Hudgins *et al.*, 2018), supporting the hypothesis that senescence itself can drive aging.(Hayflick and Moorhead, 1961; Hayflick, 1965; Campisi *et al.*, 2011; López-Otín *et al.*, 2013) In the aging process senescent cells tend to accumulate in the tissue, a result of a defective elimination by the also aged immune system. Indeed, senescent cells have been detected in several age-related diseases like atherosclerosis, osteoporosis, pulmonary and liver fibrosis, cardiac and brain disorders, and kidney disease.(Jimenez *et al.*, 2005; Yang and Fogo, 2010; Muñoz-Espín and Serrano, 2014; Chandrasekaran, Idelchik and Melendez, 2017; Farr *et al.*, 2017; Schafer *et al.*, 2017; Sun *et al.*, 2017; Baker and Petersen, 2018; Wandrer *et al.*, 2018; Hernandez-Segura, Nehme and Demaria, 2018; Khosla, Farr and Kirkland, 2018; McHugh and Gil, 2018) Additionally, some authors have highlighted the role of senescent cells in the severity of COVID-19 infection.(De Biasi *et al.*, 2020; Nehme *et al.*, 2020; Lee *et al.*, 2021)

1.3. Role of senescence in tumorigenesis

Senescence is considered one of the hallmarks of cancer.(Hanahan and Weinberg, 2011; Hanahan, 2022) However, the role of senescence in tumorigenesis is complex. Traditionally, cellular senescence has been seen as a strong barrier against tumorigenesis due to the activation of an irreversible proliferation arrest that limits tumor growth.(Sager, 1991; Campisi, 2001; Collado and Serrano, 2010) Additionally, the induction of senescence in tumors can be considered an opportunity to alert the immune system (due to the SASP) of the presence of premalignant or malignant cells and promote their elimination.(Braig *et al.*, 2005; Chen *et al.*, 2005; Collado *et al.*, 2005; Michaloglou *et al.*, 2005)

Some chemotherapeutic drugs as well as the radiation treatments induce senescence in cancer cells. This type of senescence is called therapy-induced senescence (TIS). Based on these observations, during the last years several pro-senescence therapies have evolved, such as telomerase inhibitors (Zhou *et al.*, 2006; Marconett *et al.*, 2011; Huang *et al.*, 2012; Müller *et al.*, 2012; Zhao and Wink, 2013), DNA-damaging agents (Robles and Adami, 1998; Wang *et al.*, 1998; B D Chang *et al.*, 1999; Hirose, Berger and Pieper, 2001; Han *et al.*, 2002; te Poele *et al.*, 2002; Mansilla, Piña and Portugal, 2003; Coppé *et al.*, 2008), tumor suppressor gene activators (Efeyan *et al.*, 2007; Ling *et al.*, 2014) or CDK4/6 inhibitors.(Finn *et al.*, 2009; Sutherland and Musgrove, 2009; Leontieva and Blagosklonny, 2013) The importance of pro-senescence therapies will be further discussed below.

However, the induction of senescent cells in tumors is a double-edged sword in the fight against tumorigenesis.(Ohtani *et al.*, 2012) Despite its beneficial role in limiting tumor cell proliferation, accumulation of senescent tumor cells can promote inflammation, angiogenesis, or even cause cancer recurrence by facilitating senescence escape or invasiveness.(Demaria *et al.*, 2017; Saleh *et al.*, 2018) SASP factors are the main responsibles for the dual impact of senescent cells in the surrounding tissue and microenvironment, acting in a non-autonomous way. As mentioned before, this secretory

phenotype can either attract cells from the immune system to the tumor, promoting tissue regeneration, or promote chronic inflammation that will trigger tissue dysfunction and unfavorable outcomes.(Rao and Jackson, 2016) In this regard, the combination of pro-senescent therapies with senolytics (drugs that specifically eliminate senescent cells) is an effective approach to reduce the pro-tumorigenic effects induced by senescent cells (Figure 4). The promising therapeutic benefits of senolytic approaches will be further discussed below.

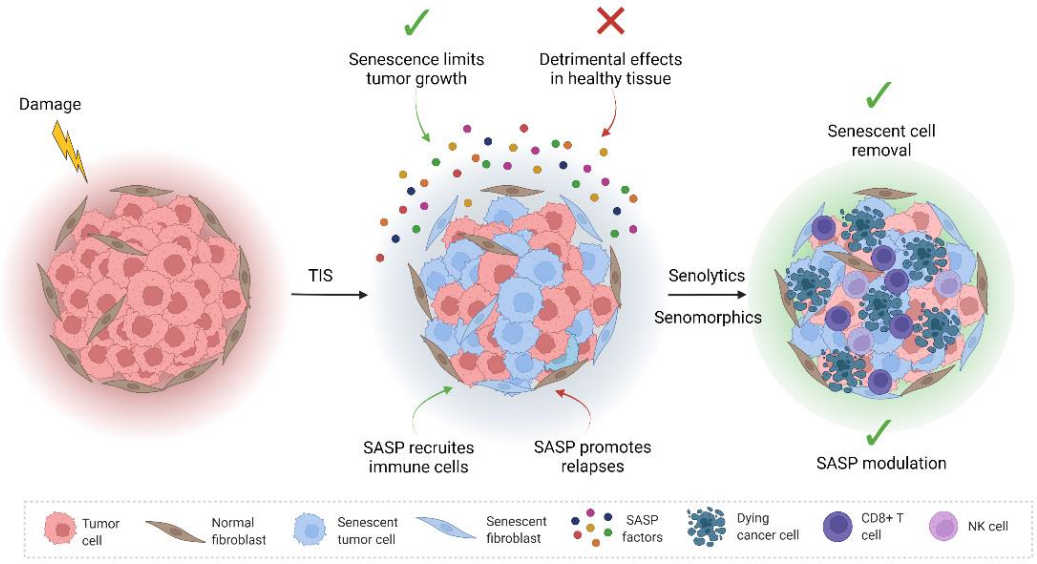

Figure 4 | Senotherapy on cancer. Therapy-induced senescence (TIS) can positively and negatively impact cancer therapy. The use of senolytic drugs to specifically kill senescent cells and senomorphics to modulate the SASP can contribute to the success of the therapy while reducing the secondary effects. SASP: Senescence-Associated Secretory Phenotype. Adapted from Senolytics in Disease, Ageing, and Longevity, 2019.

1.3.1. Role of senescence in promoting metastasis

In recent years, several studies have highlighted the negative role of TIS tumor cells Despite this role, senescence has always been considered a permanent and irreversible cell cycle arrest. Recent studies have suggested that, under certain conditions, senescent

tumor cells induced by TIS can escape from this condition and re-enter the cell cycle, thus acquiring an aggressive character.(Roberson *et al.*, 2005; Saleh *et al.*, 2019; Saleh, Tyutyunyk-Massey and Gewirtz, 2019; Triana-Martínez, Loza and Domínguez, 2020; Yu *et al.*, 2020) As aforementioned, key signaling drive of the senescence program are $p16^{INK4a}$, $p21^{CIP1,}$ and p53, as well as trimethylation of lysine 9 at histone H3 (H3K9me3). These components are also critical regulators of stem-cell functions (which are collectively termed 'stemness').(Elmore *et al.*, 2005) Milanovic and coworkers, using p53-regulable models of acute lymphoblastic leukemia and acute myeloid leukemia, found that tumor cells that scape from senescence re-entered the cell cycle with strongly enhanced tumor initiation potential.(Milanovic *et al.*, 2018) This data, along with other recent works, indicate that senescent cancer cells may be one form of dormant tumor cells that survive therapy because they become apoptosis-resistant and contribute to tumor recurrence.(Guan *et al.*, 2017; Milanovic, Yu and Schmitt, 2018; Saleh *et al.*, 2019; Saleh, Tyutyunyk-Massey and Gewirtz, 2019)

Therapy can induce senescence not only in tumor cells but also in their neighbor stroma cells and even in distant tissues.(Schosserer, Grillari and Breitenbach, 2017) The tumor microenvironment (TME) includes various cell types (endothelial cells, fibroblasts, immune cells, *etc*.) and extra-cellular components (cytokines, growth factors, hormones, extracellular matrix, *etc*.) that surround tumor cells and are maintained by a vascular network.(Wu and Dai, 2017) Cells in the tumor microenvironment can become senescent due to pro-senescence therapies and additionally, in a paracrine way as a consequence of the SASP from neighboring senescent tumor cells.Thus, tumor senescent cells can induce a so-called 'bystander' senescence effect through SASP factors.(Di *et al.*, 2008; Nelson *et al.*, 2012; Sapega *et al.*, 2018) SASP of senescent stromal cells enhances inflammatory responses, stimulates the growth of nearby malignant cells, and promotes metastasis.(Krtolica *et al.*, 2001; Collado *et al.*, 2005; Y. H. Kim *et al.*, 2017) Moreover, the SASP has been shown to contribute to the epithelial-mesenchymal transition (EMT), a phenomenon by which tumor cells gain migratory and invasive properties.(Parrinello *et*

al., 2005) Guan and coworkers (Guan *et al.*, 2017) demonstrated that prolonged CDK4/6 inhibitor treatment induces senescence in stromal fibroblasts, which adopt a robust SASP, suppressing the antitumor immune response and promoting tumor growth in a melanoma mice model. Furthermore, systemic administration of common chemotherapeutic drugs like doxorubicin, paclitaxel, cisplatin, or temozolomide induces cellular senescence in mice in different organs such as skin, lung, and liver.(Demaria *et al.*, 2017)

The induction of senescence in endothelial cells after therapy has also been studied. The endothelium is a thin mono-cellular layer that covers the inner surface of blood vessels.(Lüscher and Barton, 1997) It is involved in nutrient transport, in inflammatory and immune processes by regulating proliferation and cell migration, as well as in adherence and leukocytes activation.(Butler, Kobayashi and Rafii, 2010; El Assar *et al.*, 2012; Al-Soudi, Kaaij and Tas, 2017) Likewise, it is a barrier against cancer relapse and metastasis.(Kumar *et al.*, 2009; Reymond, D'Água and Ridley, 2013) A compromised endothelium facilitates the pass of circulating cancer cells to the tissues favoring metastases in other organs.(Shenoy and Lu, 2016) Endothelium senescence alters its cytoskeleton and increases endothelium permeability, facilitating transendothelial migration, promoting neutrophil infiltration, tumor cell adhesion, and metastasis.(Wieland *et al.*, 2017) The SASP from endothelial cells that experience TIS promotes the aggressive behavior of cancer cells.(Hwang *et al.*, 2020) Moreover, palbociclib-induced senescent cancer cells can alter and remodel the surrounding vasculature through the induction of a pro-angiogenic SASP, which might also impact cancer cells migration.(Ruscetti *et al.*, 2020) The role of endothelial senescence in the tumor context will be discussed in Chapter 1.

Besides, the presence of long-term TIS cells in the tumors can intensify many side effects of cancer therapy, such as fatigue, bone marrow suppression, bone loss, cardiac dysfunction, a physical decline in treated patients, and tumor relapse. (Shao *et al.*, 2014; Demaria *et al.*, 2017; Yao *et al.*, 2020) In summary, SASP from TIS cells can remodel the surrounding microenvironment leading to a tumor-permissive inflammatory

environment, cancer relapse, and therapeutic resistance.(Coppé *et al.*, 2008; Burton and Stolzing, 2018; Faget, Ren and Stewart, 2019).

1.4. Pro-senescence therapies

Many commonly used cancer treatments induce cellular senescence in either malignant or nonmalignant cells or tissues. Pro-senescence therapies that are actually used in the clinical context can be categorized into four families: chemotherapy, radiotherapy, immunotherapy, and CDK4/6 inhibitors.(Wang, Kohli and Demaria, 2020; Wyld *et al.*, 2020)

1.4.1. Chemotherapy

Chemotherapy can cause cell death resulting in tumor regression, or induce cellular senescence leading to tumor growth arrest. Moderate chemotherapy doses are more likely to cause senescence, and higher doses more likely to cause cell death by apoptosis.(Roninson, 2003) Chemotherapeutic drugs generate DNA damage which can eventually activate a non-lethal DDR response, triggering senescence.(Van Deursen, 2014) Some of the DNA-damaging agents are commonly used in clinics and induce senescence *in vivo* are doxorubicin (Chang *et al.*, 1999), etoposide (te Poele *et al.*, 2002), cisplatin (Wang *et al.*, 1998), bleomycin o temozolomide. (Hirose, Berger and Pieper, 2001).

1.4.2. Radiotherapy

The mechanism of action of radiotherapy relays on the generation of direct DNA damage, activating DDR response and increasing ROS in the treated area. Due to its lack of specificity, radiotherapy can be used to treat several tumors, including lymphoma, soft tissue sarcomas, central nervous system tumors, and a wide range of carcinomas (lung, prostate, skin, breast, head and neck, bladder).(Baskar *et al.*, 2012) Numerous studies have demonstrated that ionizing radiation induces SA-β-gal and other senescence

markers in breast, colon carcinoma, neuroblastoma, and fibrosarcoma cell lines. (Bey Dih Chang *et al.*, 1999; Jones *et al.*, 2005; Zhang *et al.*, 2020)

Because radiation therapy is locally derived to the tumor site, damage to non-cancerous areas of tissues is less likely to occur. Besides, it is important to highlight that the therapeutic effect of radiotherapy does not only result in a local effect due to the proliferation inhibition of irradiated cancer cells, but also to a distant effect due to the potentiation of an adaptive immune response mediated by CD86+ cytotoxic T lymphocytes.(Rodriguez-Ruiz *et al.*, 2019) This effect is commonly known as abscopal response (Mole, 1953) and can cause the regression of distant metastatic lesions.(Reynders *et al.*, 2015; Abuodeh, Venkat and Kim, 2016; Poleszczuk *et al.*, 2016; Siva *et al.*, 2016; Cong *et al.*, 2017) Recently, senescence has been involved in abscopal response. Tesei *et al.* (Tesei *et al.*, 2021) demonstrated that irradiated A549 lung cancer cells became senescent and secreted extracellular vesicles as part of their SASP, which can induce senescence on distant not irradiated metastatic cells, stopping its proliferation.

1.4.3. Immunotherapy

The appearance of senescence after immunotherapy has not been explored as deeply as in chemotherapy or radiotherapy. However, we already know that some immunotherapeutic drugs induce senescence, such as rituximab, a CD20 targeting antibody used to treat leukemia and lymphoma.(Däbritz et al., 2016) Along the same line of evidence, IFNγ and TNFα, two cytokines highly secreted by CD4+ T-helper cells after cell immunotherapy (Shimabukuro-Vornhagen et al., 2018), induce senescence in different murine and human cancers.(Braumüller *et al.*, 2013)

1.4.4. CDK4/6 Inhibitors

Cyclin-dependent kinases (CDK) have a critical role in regulating the cell cycle. Specifically, the CDK4/6 complex acts as a checkpoint during the cell cycle transition from cell growth (G1) to the DNA synthesis (S) phase. Its deregulation or overexpression induces abnormal cell proliferation and cancer development.(Malumbres and Barbacid, 2009) The catalytic subunit CDK4/6 interacts with the regulatory subunit cyclin D.(Asghar *et al.*, 2015) The Ser/Thr-kinase component of the complex CDK4/6-cyclin D phosphorylates and inhibits retinoblastoma (Rb) protein. Phosphorylation of Rb protein allows dissociation of the transcription factor E2F from the Rb/E2F complex and the subsequent transcription of the E2F gene, which is in charge of the progression through the G1 phase.(Yu, Geng and Sicinski, 2001; Toogood *et al.*, 2005; Yu *et al.*, 2006; Rivadeneira *et al.*, 2010; Goel *et al.*, 2018) Targeted inhibition of CDKs to avoid cell cycle progression is a critical therapeutic target to limit tumor proliferation.

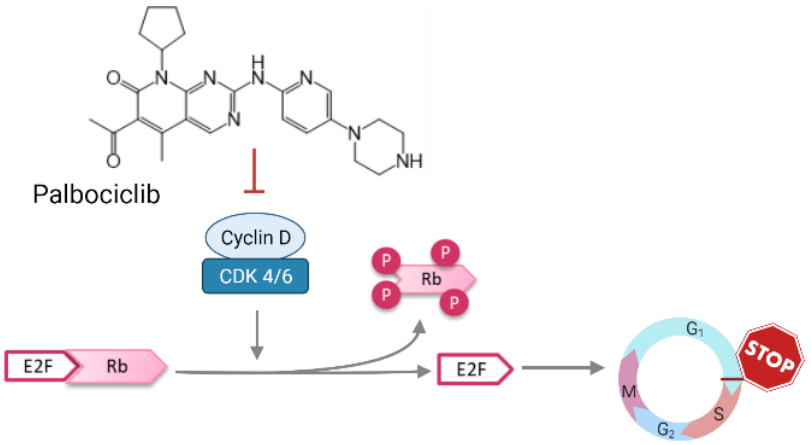

Figure 5 | Mechanism of action of palbociclib. In the cell cycle phase G1, cells must pass a checkpoint to complete the cycle and divide. The complex of kinases CDK4/CDK6, together with cyclin D, carries out the phosphorylation of retinoblastoma protein (Rb), which allows the cell to pass this checkpoint and start dividing. Palbociclib inhibits the action of CDK4/6 so that the CDK4/6 – cyclin D complex cannot perform its phosphorylation function, and the cell cannot continue the cycle.

CDK4/6 inhibitors imitate the mechanism of action of its natural inhibitor, p16, (Coppé *et al.*, 2011) and cause cellular senescence.(Leontieva and Blagosklonny, 2013) Recently, three pharmacological CDK4/6 inhibitors (palbociclib, ribociclib, and abemaciclib) have been developed and approved by the FDA based on PALOMA, MONARCH, and MONALEESA randomized clinical trials.(Beaver *et al.*, 2015; Finn *et al.*, 2015; Turner *et al.*, 2015, 2018; Cristofanilli *et al.*, 2016; Hortobagyi *et al.*, 2016; Walker *et al.*, 2016; Sledge *et al.*, 2017; Cardoso *et al.*, 2020) Palbociclib induces cellular senescence (its mechanism of action is described in Figure 5) in breast and gastric cancer, melanoma, liposarcoma, and hepatocellular carcinoma. On the other hand, other CDK4/6 inhibitors such as ribociclib and abemaciclib also induce cellular senescence in several tumors. For example ribociclib induces senescence in neuroblastoma cells (Rader *et al.*, 2013) and Ewing sarcoma cells (Coppé *et al.*, 2011), and abemaciclib in numerous breast cancer cells.(Goel *et al.*, 2016, 2017; Gong *et al.*, 2017; Torres-Guzmán *et al.*, 2017)

Palbociclib is currently approved by the FDA in combination with letrozole for hormone receptor-positive (HR+)/human epidermal growth factor receptor 2 negative (HER2−) postmenopausal women with metastatic breast cancer or fulvestrant in women with breast cancer that have progressed after endocrine therapy.(Fry *et al.*, 2004; Finn *et al.*, 2009, 2015, 2016; Beaver *et al.*, 2015; Walker *et al.*, 2016; Pernas *et al.*, 2018) In 2017, ribociclib also received approval in combination with an aromatase inhibitor to treat HR+HER2− metastatic breast cancer patients. The same year, abemaciclib was approved in combination with fulvestrant to treat HR+HER2− advanced breast cancer patients who failed to respond to endocrine therapy.(Fry *et al.*, 2004; Rader *et al.*, 2013)

The use of CDK4/6 inhibitors in the treatment of advanced breast cancer benefits for the progression-free survival (PFS), objective response rate (ORR), overall survival (OS), and quality of life of patients.(Gao *et al.*, 2020) Following this success, a robust program of clinical research was developed to incorporate CDK4/6 inhibitors for the treatment of

HER2+ and triple-negative breast cancer and other cancer types.(Sobhani *et al.*, 2019; Gil-Gil *et al.*, 2021)

The three CDK4/6 inhibitors have different toxicity profiles, dosing schedules, pharmacokinetics, and potencies. In this thesis, we will focus on palbociclib. Palbociclib (IBRANCE; PD0332991; Pfizer; $C_{24}H_{29}N_7O_2$) is an orally available drug with a low enzymatic IC50 of 11 nM for CDK4 and 15 nM for CDK6. In monotherapy, the main dose-limiting toxicities were neutropenia and leukopenia.(Sobhani *et al.*, 2019; McCartney *et al.*, 2020) In Chapter 3, a nanoparticle-based strategy to overcome palbociclib-induced senescence side effects will be described.

1.5. Senotherapies

Senotherapies are drugs aimed to limit the deleterious effects of senescent cells by eliminating senescent cells (senolytics), inhibiting the SASP (senomorphics), or inhibiting senescence before it happens (senoblockers). In this thesis, we will focus on senolytics.

1.5.1. Senolytics

Senolytics are pharmacological agents that selectively induce apoptosis in senescent cells. Senolysis is an efficient strategy to protect from the negative side effects of senescent cell accumulation in the body.(Zhu *et al.*, 2015; Soto-Gamez and Demaria, 2017) In fact, senolysis treatment improves the symptoms of aging-related disorders in mice models of arteriosclerosis, osteoarthritis, cataracts, cardiac hypertrophy, renal dysfunction, lipodystrophy, and sarcopenia.(Baker *et al.*, 2011, 2016; Xu *et al.*, 2015; Hashimoto *et al.*, 2016; Y. Zhao *et al.*, 2018) Besides, senolytic drugs have demonstrated to extend both health and life span in naturally aged and progeroid syndrome mice.(Xu *et al.*, 2018; Yousefzadeh *et al.*, 2018)

Over the last few years, several senolytic drugs have been identified including small molecules, peptides, or antibodies. Senolytic discovery was initially driven by the

hypothesis that if senescent cells were resistant to apoptosis, they might rely on pro-survival pathways to resist against pro-apoptotic factors.(Zhu *et al.*, 2015) Using bioinformatics and siRNA technology, different senescent-cell anti-apoptotic pathways (SCAPs), upregulated in senescent cells, were identified as putative senolytic targets. They include interrelated B-cell lymphoma family proteins, p53/p21 transcription factors, hipoxia-inducible factor 1 (HIF-1α), heat-shock protein HSP-90 and phosphatidylinositol-4,5-bisphosphate 3-kinase/protein Kinase B (PI3K/AKT).(Zhu *et al.*, 2015; Fuhrmann-Stroissnigg *et al.*, 2017) Based on this knowledge, different senolytic drugs have been identified evaluating drugs already known to target these SCAPS, such as dasatinib and quercetin, Bcl-2 family inhibitors, fisetin, or HSP90 inhibitors.(Zhu *et al.*, 2015, 2017; Chang *et al.*, 2016; Fuhrmann-Stroissnigg, Niedernhofer and Robbins, 2018) Moreover, screening of drug libraries have led to the identification of novel senolytics as in the case of cardiac glycosides.(Triana-Martínez *et al.*, 2019; Guerrero, Herranz, *et al.*, 2020)

Despite all current knowledge, the FDA has not yet approved any senolytic drug for a senolytic application (dasatinib and quercetin are approved for other uses). This is probably due to the novelty, as well as to some toxicity issues derived from their use. However, some of these drugs, such as dasatinib plus quercetin, fisetin, and navitoclax, are already in early phase clinical trials for diabetic and chronic kidney disease (NCT02848131; NCT03325322), Alzheimer's disease (NCT04785300), osteoporosis (NCT04313634; NCT04313634), osteoarthritis (NCT04210986) and COVID-19 (NCT04771611; NCT04476953; NCT04537299).(Hickson *et al.*, 2019; Justice *et al.*, 2019; Kirkland and Tchkonia, 2020; Verdoorn *et al.*, 2021; Morsli, Doherty and Muñoz-Espín, 2022)

To date, there is no universal senolytic drug capable of effectively eliminating all types of senescent cells nor a specific one able to selectively kill one senescent cell type over another. Finding a selective method to remove a specific senescent cell type could

be a therapy of great potential for precision cancer treatment. In the Chapter 4 of this thesis, the discovery of a novel senolytic for malignant melanoma is described.

1.5.1.1 Navitoclax

Among all the different senolytic drugs, our studies are mainly focused in the use of navitoclax (ABT-263; nav). Navitoclax is a specific inhibitor of the anti-apoptotic proteins Bcl-2, Bcl-xL, and Bcl-W, and also known to be a BH3 mimetic drug that binds to BH3 biding domain of Bcl-2, Bcl-xL and Bcl-W anti-apoptotic members, causing the displacement of the pro-apoptotic proteins Bak and Bax and their oligomerization in the outer mitochondria membrane.(Zhu *et al.*, 2016) This results in the permeabilization of the outer membrane, and the cytochrome C release to the cytosol, ultimately leading to caspase activation and cell death (Figure 6).

Navitoclax reduces cancer relapses (Syahidah *et al.*, 2021) and delays the onset of several aging associated-diseased such as atherosclerosis, neurodegenerative diseases, or hematopoietic system aging.(Chang *et al.*, 2016; Demaria *et al.*, 2017; Kim *et al.*, 2017; Bussian *et al.*, 2018) In aged mice, navitoclax treatment rejuvenated senescent bone marrow hematopoietic stem cells, senescent muscle stem cells and attenuated the osteoclastogenic support capacity of bone marrow stromal cells.(Kim *et al.*, 2017) In a senescent mice model, caused by whole body sub-lethal irradiation, oral administration of navitoclax reduced the senescent cells burden, suppressed the expression of SASP factors in lungs (such as p16, Il1a or TNFα), and also decreased the premature aging of the hematopoietic system caused by irradiation.(Chang *et al.*, 2016; Kim *et al.*, 2017) In a mice model of atherosclerosis, navitoclax treatment reduced atherosclerosis onset showing a diminished plaque burden, number, and size.(Childs *et al.*, 2016) Also, in osteoarthritic mice, navitoclax reduces the symptoms in later-stage disease by creating a prochondrogenic environment.(Jeon *et al.*, 2017)

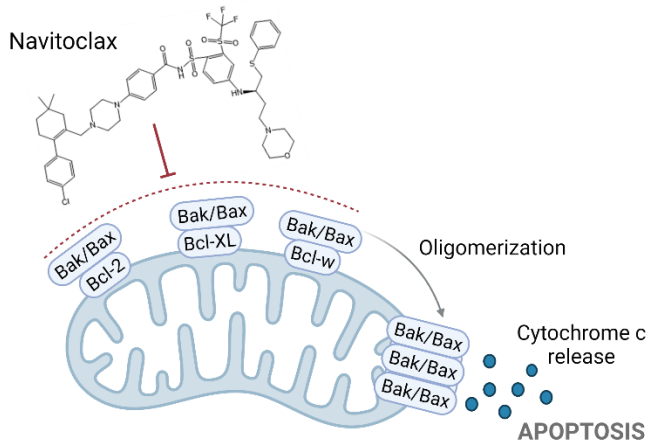

Figure 6 | Navitoclax induces apoptosis. The antiapoptotic members (i.e., Bcl-2, Bcl-W, and Bcl-xL) recruit and inactivate the proapoptotic proteins (i.e., Bax and Bak). Navitoclax, a BH3 mimetic, binds to the BH3 biding domain of Bcl-2, Bcl-xL and Bcl-W, causing the release of the pro-apoptotic proteins Bak and Bax and their oligomerization in the outer mitochondria membrane. This results in the permeabilization of the outer membrane, and the cytochrome C release to the cytosol, ultimately leading to cell death.

Despite its good efficacy in preclinical trials, navitoclax secondary effects have limited its translation to clinical practice. The most relevant negative side-effect is thrombocytopenia as a consequence of the dependence that platelets have on Bcl-xL for their survival.(Kaefer *et al.*, 2014; Kile, 2014; Cang *et al.*, 2015; Chang *et al.*, 2016) To overcome navitoclax toxicity, a second generation of senolytics has been recently reported. A nanotechnological-based strategy (NP(nav)-Gal) to specifically deliver navitoclax in senescent cells with high specificity decreases platelet toxicity.(Muñoz-Espín *et al.*, 2018; Galiana *et al.*, 2020; Estepa-Fernández *et al.*, 2021) The Bcl-xL proteolysis-targeting chimera (PROTAC) PZ15227 (PZ), has shown limited platelet toxicity because it recruits a specific E3 ubiquitin ligase, cereblon, that is poorly expressed in platelets.(He *et al.*, 2020) Additionally, several prodrugs that release the active component in response to lysosomal β-galactosidase activity in senescent cells have been reported, such as the galactose-modified navitoclax (nav-Gal) (González-Gualda *et al.*, 2020), galactose-modified duocarmycin (Guerrero, Guiho, *et al.*, 2020) or gemcitabine-derivative SSK1.(Cai

et al., 2020) In this thesis, we will focus on the NP(nav)-Gal nanoparticles and on the nav-Gal prodrug.

1.5.1.2 The prodrug nav-Gal

Nav-Gal is a prodrug that results from the conjugation of navitoclax with acetylated galactose. Nav-Gal can preferentially be activated by the high activity of lysosomal β-galactosidase in senescent cells. The nav-Gal pro-drug has been effective in reducing tumor size in *in vivo* models of lung adenocarcinoma and in non-small-cell lung cancer in combination with senescence-inducing therapies. Moreover, it has been demonstrated a clear reduction of the hematological toxicity.(González-Gualda *et al.*, 2020) In this work, we address the study of the nav-Gal anti-tumoral activity in triple-negative breast cancer (Chapter 2).

1.6. A one-two punch therapy strategy for cancer treatment

A novel approach for cancer therapy based on the combination of senescence-inducing therapies and senotherapies is illustrated in Figure 4. This one-two punch strategy for cancer therapy has already shown potential as an antitumor strategy *in vivo*.(Muñoz-Espín *et al.*, 2018; Fleury *et al.*, 2019; Triana-Martínez *et al.*, 2019; Galiana *et al.*, 2020; Saleh *et al.*, 2020; Shahbandi *et al.*, 2020; Estepa-Fernández *et al.*, 2021) The first punch is the treatment of the tumor with cancer therapies at a clinical dose that will eliminate tumor cells and at the same time induces senescence in both normal and tumor cells. The second punch will be the selective clearance of senescent cells using a senotherapeutic. Not only does the strategy cause a synergistic effect by limiting tumor growth and simultaneously preventing tumor relapse, metastasis, and development of resistance to treatment, but it also mitigates TIS side effects in normal tissue and helps to restore tissue homeostasis.

Dorr et al (Dörr et al., 2013) reported for the first time the one-two punch approach to selectively eliminate chemotherapy-induced senescent lymphoma cells in mice by using a metabolic senolytic (bafilomycin A) to block glucose utilization or autophagy. Later, other authors have reported that genetic and pharmacological clearance of TIS cells are effective in the treatment of many cancer types in mouse models. For example, the combination of the CDC7 inhibitor and AZD8055 (mTOR inhibitor) results in the growth inhibition of liver cancer.(Wang et al., 2019) The combination of olaparib, a poly(ADP-ribose) polymerase 1 inhibitor (PARPi), and navitoclax reduces tumor growth in ovarian and breast cancer mice xenografts.(Fleury et al., 2019) Combination of TIS plus cardiac glycosides also reduces tumor size *in vivo*.(Triana-Martínez et al., 2019) Our group has demonstrated that the combination of palbociclib plus navitoclax-based therapies is effective in reducing tumor growth *in vivo* and the associated side effects in melanoma and in breast cancer tumors.(Muñoz-Espín et al., 2018; Galiana et al., 2020; González-Gualda et al., 2020; Estepa-Fernández et al., 2021) A more detailed explanation about the effect of this combination will be provided during the development of this thesis.

Additionally, it is important to highlight that several phase 1 and phase 2 clinical trials combining senescence-inducing chemotherapy with navitoclax are ongoing or completed (Table 1), including combination with cisplatin (NCT00878449), etoposide (NCT00878449), or osimertinib (NCT02520778) in lung cancer patients, and dabrafenib or trametinib for patients with metastatic melanoma (NCT01989585). Navitoclax is also combined with gemcitabine (NCT00887757), paclitaxel (NCT00891605), docetaxel (NCT00888108), irinotecan (NCT01009073), erlotinib (NCT01009073), sorafenib (NCT02143401) or trametinib (NCT02079740) in advanced solid tumors.(Paez-Ribes *et al.*, 2019) The fact that there are so many clinical trials currently in development demonstrates the interest of this new strategy for the treatment of cancer.

Table 1 | Clinical trials that are ongoing or have been conducted combining navitoclax with chemotherapy

TREATMENT		CONDITION	PHASE	IDENTIFIER	STATUS
Navitoclax	Cisplatin	Small Cell Lung Cancer	Phase 1	NCT00878449	Completed
	Etoposide	Small Cell Lung Cancer	Phase 1	NCT00878449	Completed
	Osimertinib	Advanced or Metastatic Non-small Cell Lung Cancer	Phase 1	NCT02520778	Active, not recruiting
	Dabrafenib	BRAF Mutant Melanoma	Phase 1/2	NCT01989585	Active, not recruiting
	Trametinib	BRAF Mutant Melanoma	Phase 1/2	NCT01989585	Active, not recruiting
	Gemcitabine	Advanced Solid Tumours	Phase 1	NCT00887757	Completed
	Paclitaxel	Advanced Solid Tumours	Phase 1	NCT00891605	Completed
	Docetaxel	Advanced Solid Tumours	Phase 1	NCT00888108	Completed
	Irinotecan	Advanced Solid Tumours	Phase 1	NCT01009073	Completed
	Erlotinib	Advanced Solid Tumours	Phase 1	NCT01009073	Completed
	Sorafenib	Relapsed or Refractory Solid Tumors	Phase 1	NCT02143401	Active, not recruiting
	Trametinib	Advanced or Metastatic Solid Tumors	Phase 1/2	NCT02079740	Recruiting

2. Nanotechnology and nanomedicine

Nanotechnology is a multidisciplinary area of research that deals with the understanding and manipulation of matter at the nanoscale, with dimensions ranging from one to a few hundred nanometers. Nanomaterials exploit the specific properties that arise from their small-size and are not observed in their bulk counterparts.(Khan *et al.*, 2016) For example, some nanomaterials are stronger or have different magnetic properties than other forms or sizes of the same material. Others are better at conducting heat or electricity, becoming more chemically reactive, reflecting light better, or changing color as their size or structure is altered. The development of these new properties has resulted in applications in fields as diverse as electronics, energy, food science, environmental science, chemistry, biotechnology, and medicine, among others.

Regarding nanomedicine, its major focus of research is the development of drug delivery systems that deliver drugs precisely where they are needed while reducing side effects from therapy.(Farokhzad and Langer, 2009) Another key point of nanomedicine applications is to develop diagnostic tools for the early diagnosis of the disease, in which synthesized nanoparticles are sensitive and specific sensors that allow the recognition of particular biomolecules.(Navya, Kaphle and Daima, 2018) Nanomedicine also has an important role in regenerative medicine, in designing grafts and scaffolds that have resulted in new systems with significantly enhanced cellular and tissue regenerative properties.(Chaudhury *et al.*, 2014)

An example to highlight the current use of nanomedicines is their use as vaccines. Nanomedicine has had a huge impact in managing the COVID-19 pandemic for these last two years. Due to their properties, nanoparticles are ideal for the delivery of antigen, adjuvants, and mimics of viral structures. Thus, it is not surprising that the first developed COVID-19 vaccines were made by mRNA delivered via lipid nanoparticles.(Chung *et al.*, 2020; Kulkarni *et al.*, 2020; Shin *et al.*, 2020; Anselmo *et al.*, 2021)

The continuous advances in the nanomedicine field have meant that more than 30 nanomedicines have been approved by the FDA, and over 100 are currently in clinical trials (Saha *et al.*, 2020; Anselmo *et al.*, 2021), although many clinical problems remain unsolved and more research is needed before they can be used more widely in patient care.

Several nanoparticles have been described to date as drug delivery systems, including organic ones such as liposomes, dendrimers, polymers, and micelles, and inorganic ones such as gold nanoparticles and silica-based nanoparticles.(Peer *et al.*, 2007; Choi and Han, 2018) In this thesis, we will focus on mesoporous silica nanoparticles.

2.1. Mesoporous silica nanoparticles

Mesoporous silica nanoparticles (MSNs) (Figure 7) have been receiving growing attention since the first report of their synthesis back in the early 1990s (Yanagisawa *et al.*, 1990) and their first application in drug delivery in 2001.(Vallet-Regi *et al.*, 2001) Among the advantages of mesoporous silica materials are their large surface areas (ca. 500-1000 m^2/g), and adjustable pore size (from 2-30 nm) with high pore volume (ca. 1 cm^3/g) that allows high loading capacity, their tunable morphology, and how easy it is to modify their surface.(Aznar *et al.*, 2016; Manzano and Vallet-Regí, 2020; Yang *et al.*, 2020) In addition to their chemical properties, their biocompatibility makes it a very suitable material for many biomedical applications.(Li, Zhang and Feng, 2019; Gisbert-Garzarán, Lozano and Vallet-Regí, 2020; Yang *et al.*, 2020; Yuan, Ellis and Davis, 2020)

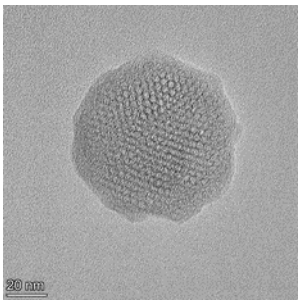

Figure 7 | Transmission electronic microscope (TEM) image of a mesoporous silica nanoparticle.

2.2. Synthesis of mesoporous silica nanoparticles

Although many reaction pathways might be used, the synthesis of mesoporous silica materials is generally based on sol-gel reactions. This involves the conversion of monomers in solution (sol) into an integrated solid network (gel).(Stöber, Fink and Bohn, 1968) To synthesize MSNs (Figure 8), the condensation of a silica precursor (tetraethyl orthosilicate, sodium silicate, or tetramethylammonium silicate) in the presence of cationic surfactants (such as cetyl trimethyl ammonium bromide) under basic conditions is necessary.(Croissant *et al.*, 2018) The surfactant molecules form supermicelles

(supramolecular self-assemblies of individual micelles) act as a template directing the condensation of the silica precursors. Then, silica precursors hydrolyze, forming silanol groups that are polymerized by condensation, yielding the final network of siloxane bonds (Si-O-Si) with a characteristic porous structure.(Frickenstein *et al.*, 2021) The nature and concentration of the surfactant and the silica precursor, as well as the temperature, pH, ionic force, and time, determine the porous structure and the morphology of the final mesoporous silica material.(Raman, Anderson and Brinker, 1996)

In this thesis, we employed mesoporous silica nanoparticles with a hexagonal arrangement of the mesopores (MCM-41). These nanoparticles have a size of ca. 100 nm and present cylindrical unidirectional channels with a diameter of ca. 2.5 nm. For this material, a typical synthetic procedure involves the addition of tetraethyl orthosilicate (TEOS) (silica precursor) over a cetyl trimethyl ammonium bromide (CTAB) micellar solution at 80 °C and at basic pH (adjusted with NaOH). The mixture is stirred for 2 hours, and then the solid is collected through filtration.

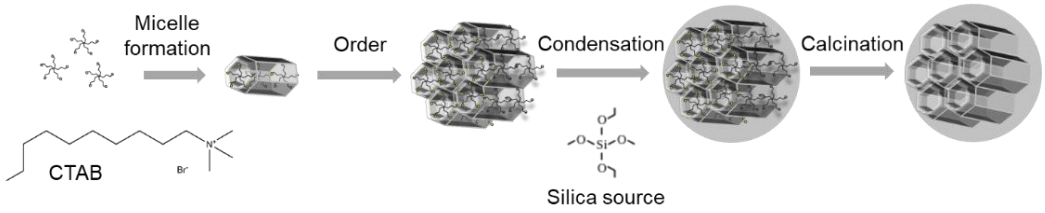

Figure 8 | Schematic representation of the synthesis of the mesoporous silica nanoparticles. First, a super-micellar template is formed in basic water solution. Next, the inorganic siliceous precursor tetraethylorthosilicate hydrolyses and condensates around the template. The final mesoporous inorganic MCM-41 scaffold, which presents cylindrical unidirectional empty channels arranged in a hexagonal distribution, is obtained by removing the surfactant template by calcination. CTAB: cetyl trimethyl ammonium bromide. *Adapted from Hoffmann et al. Angew. Chem. Int. Ed. 2006, 45, 3216.*

2.3. Functionalization of mesoporous silica nanoparticles

One of the most outstanding characteristics of MSNs is that they can be functionalized on their surface with functional groups, which introduces additional versatility to the nanoparticles. In the process of functionalizing mesoporous silica supports, organic groups are incorporated onto the surface or the interior of the support, yielding hybrid organic-inorganic materials. These hybrid materials made by inorganic scaffolds combined with functional organic moieties anchored to their surface are very attractive in a wide range of applications. Incorporating these organic molecules modifies specific surface properties such reactivity, hydrophilicity, hydrophobicity, bonding with other molecules, and stabilization of final materials against hydrolysis or chemical attack. For example, MSNs that are functionalized with polyethylene glycol (PEG) increased their circulation time *in vivo* and decreased their immunogenicity without compromising their activity.(Savoca *et al.*, 1979; Suk *et al.*, 2016) In Chapter 3, a novel MSNs system functionalized with PEG will be described.

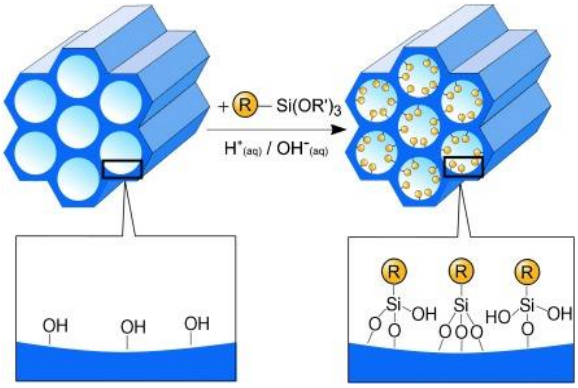

Figure 9 | Scheme of the grafting procedure for functionalizing mesoporous silica materials with organotryalkoxysilanes of the type $(R'O)_3$-Si-R. R= organic functional group. *Reprinted from Hoffmann et al. Angew. Chem. Int. Ed. 2006, 45, 3216. Copyright © 2006 Wiley-VCH*

In general, two main protocols are used to functionalize: (i) grafting, which is the post-synthetic modification of the surface of the inorganic silica material; and (ii) co-condensation, which is the simultaneous condensation of silica and organosilica

precursors.(Hoffmann *et al.*, 2006) In this thesis, we used the grafting protocol to functionalize the surface of MSNs. Briefly, in the grafting procedure, the surface of silica nanoparticles is modified due to the high presence of silanol groups (Si-OH) that act as reactive points to covalently anchor organosilanes containing the desired organic groups on the external surface of the inorganic scaffold. The most used organosilanes are trialkosyxilanes derivatives with $(R'O)_3$-Si-R structure (where R is an organic group) (Figure 9).(Stein, Melde and Schroden, 2000; Hoffmann *et al.*, 2006)

2.4. Stimuli-response gate materials

The functionalization of inorganic materials with organic molecules enhances the properties of the hybrid materials, thus enabling the development of novel advanced systems.(Stein, Melde and Schroden, 2000; Hoffmann *et al.*, 2006) In this scenario, the design of stimuli-responsive gated materials offers an appealing approach with potential applications in various scientific fields, such as the controlled release of chemical species and the design of (bio)chemical sensors.

Gated materials release the cargo loaded in their porous support in response to a selected stimulus.(Lu and Willner, 2015; Y. Zhang et al., 2016; T. Zhao et al., 2018; Manzano and Vallet-Regí, 2019) These materials are composed of two subunits: (i) the inorganic porous scaffold loaded with a cargo (e.g. drugs, dyes, fluorophores, etc.) and (ii) (bio)molecules or supramolecular ensembles attached to the external surface acting as gatekeepers (also known as molecular gates or nanovalves).(Aznar *et al.*, 2016; García-Fernández *et al.*, 2020) These gatekeepers are responsible for keeping the cargo enclosed in the porous support that, in response to external stimuli, will change their dimensions, shapes, or configuration in order to allow cargo release in a controlled manner (Figure 10). A large variety of supramolecular structures, organic molecules, polymers, peptides, aptamers, or enzymes have been used as gatekeepers.(Aznar *et al.*, 2009; Coll *et al.*, 2011; Llopis-Lorente *et al.*, 2017; Wen *et al.*, 2017) Several stimuli have been used to trigger the release of guest molecules from gated materials (Aznar *et al.*, 2016; García-Fernández *et*

al., 2020), including pH (Bernardos *et al.*, 2008; Cauda, Argyo and Bein, 2010), redox potential (Liu *et al.*, 2008; Giménez *et al.*, 2015), target molecules (Zhao *et al.*, 2009; Choi *et al.*, 2011), light (Lin *et al.*, 2010), temperature (Chen *et al.*, 2011), and magnetic fields. (Bringas *et al.*, 2012)

Gated MSNs have been used satisfactorily in *in vivo* models, improving the solubility of encapsulated drugs and reducing undesired side effects.(L. Zhang *et al.*, 2016; Hu *et al.*, 2017; Muñoz-Espín *et al.*, 2018; Yin *et al.*, 2018; Castillo and Vallet-Regí, 2019; Pu *et al.*, 2019)

An example of an endogenous stimulus employed in this thesis to open gated-MSNs is redox potential. The presence of reducing agents inside the cell allows the controlled release of molecules at the intracellular level and this has been used in cancer and other diseases. In the case of cancer, the differences in concentration in glutathione (GSH) between extracellular (approx. 2-10 µM) and intracellular (approx. 2-10 mM) cell compartments or between tumor tissues and healthy tissues allow the reduction and consequent breaking of disulfide bonds in gated materials, releasing the entrapped cargo. A mesoporous material containing a redox-active PEG gate able to open in tumor cells is described in Chapter 3.

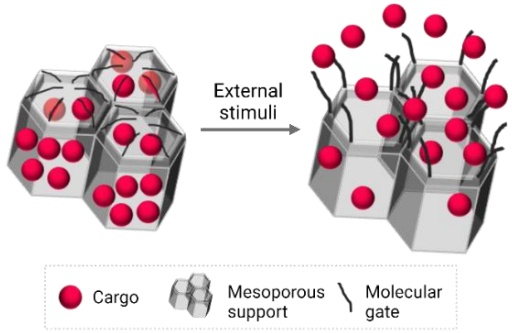

Figure 10 | Scheme of mesoporous nanoparticle functionalized with a molecular gate that opens in response to an external stimulus releasing its cargo.

In another example of a gated material with a controlled cargo release used in this thesis, a hexa-galactooligosaccharide (galactan polymer) is attached to the surface of MSNs. As described above, senescent cells overexpressed the SA-β-Gal enzyme that broke the gatekeeper, achieving the release and accumulation of the cargo in the desired senescent target. This system will be described in more detail in Chapter 1 and Chapter 3.

2.5. Targeting and cellular uptake of mesoporous silica nanoparticles

Nanoparticles administered to the body are internalized by many cell types, including tumor and non-tumor cells (endothelial, fibroblast, and immune system cells).(Radu *et al.*, 2004; Slowing, Trewyn and Lin, 2006, 2007) Several factors contribute to the cellular uptake process, including the cell membrane properties and the unique characteristics of the designed nanoparticles. In addition, the interaction with the cell membrane determines the cellular distribution of nanoparticles, their accumulation in intracellular compartments, their retention in the target area, and, therefore, their efficacy.(Adjei, Sharma and Labhasetwar, 2014; Krpetić *et al.*, 2014) By passive and/or active targeting, nanoparticles can reach damaged cells or tissues specifically.(Danhier, Feron and Préat, 2010; Grandhi and Rege, 2014)

2.5.1. Passive targeting: EPR effect in tumors

When nanoparticles are administered to tumor-bearing mice, they passively accumulate in the tumor due to the enhanced permeability and retention (EPR) effect (Figure 11). The EPR effect was described firstly by Matsumura and Maeda in 1986 (Matsumura and Maeda, 1986) and it is a consequence of the aberrant lymphatic system and tumor vasculature that allow the release of macromolecules and nanoparticles from the blood circulation to tumor tissues.(Croissant *et al.*, 2016; Li *et al.*, 2018; Zhou *et al.*, 2018) Although there is some heterogeneity in different tumors, the EPR effect generally occurs more in large tumors than in smaller ones (Fang, Islam and Maeda, 2020), probably because small tumors do not need vascularization.

2.5.2. Active targeting

In active targeting, functionalizing the surface of nanodevices with specific targeting molecules allows them to target specific cell types without affecting normal tissues. To achieve this, nanoparticles are coated with targeting ligands that bind the appropriate receptors that are overexpressed in the target cells. The most commonly used targeting molecules to functionalize the surface of the nanoparticles are antibodies, microRNA, aptamers, peptides, and proteins.(Grandhi and Rege, 2014) In this thesis, a mesoporous material functionalized with a MUC1-biding aptamer able to specifically target triple-negative breast cancer tumor cells is described in Chapter 3.

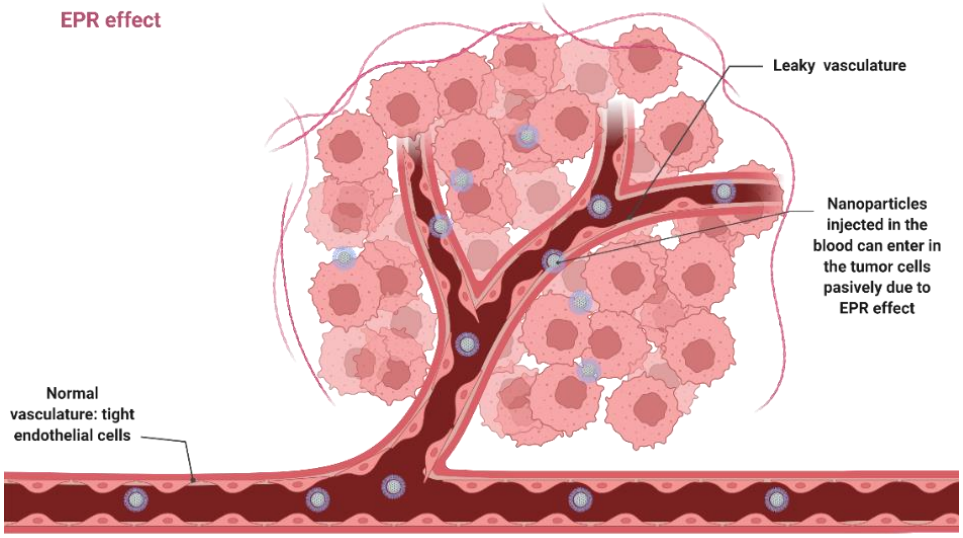

Figure 11 | Scheme of enhanced permeability and retention (EPR) effect of nanoparticles in tumors. The new tumor vessels usually have abnormal architecture and lack effective lymphatic drainage, thereby allowing macromolecules or nanoparticles to be retained in the tumor. The tight vascular endothelial cells in the normal vasculatures form a barrier to prevent macromolecules from extravasation. Nanoparticles designed with a suitable size can penetrate tumor tissue preferably without compromising normal tissue (passive tumor targeting).

2.6. Biodistribution, degradation, and excretion of MSNs

Depending on the routes of administration, absorption and distribution of MSNs in the body vary widely, being the main target organs the liver, lungs, kidneys, and spleen.(Chen *et al.*, 2013; Wu and Tang, 2018) Elimination of the MSNs takes place through urine and feces.(Rojas *et al.*, 2015)

In general, when nanoparticles are administered into the body, a systemic distribution is observed through the bloodstream (Figure 12). Proteins from plasma and intracellular fluid are adsorbed onto the surface of the nanoparticles forming a protein corona.(Lazarovits *et al.*, 2015) The presence of the protein corona is responsible for the quick opsonization of the nanoparticles by immune cells that form part of the reticuloendothelial system (RES), such as monocytes, platelets, leukocytes, and dendritic cells. This is the reason why nanoparticles accumulate mainly in tissues with resident phagocytes: Kupffer cells in the liver, alveolar macrophages in the lung, macrophages and B cells in the spleen, or dendritic cells in the lymph nodes.(Dobrovolskaia *et al.*, 2008)

It is important to note that size, shape, and surface modification of MSNs change the *in vivo* biodistribution of the nanoparticles.(He *et al.*, 2011; Huang *et al.*, 2011; Westmeier, Stauber and Docter, 2016; Dogra *et al.*, 2018) In general, nanoparticles of smaller sizes have a longer blood-circulation lifetime, possibly resulting from the slower capture by various organs such as the liver and the spleen.(He *et al.*, 2011) When nanoparticles are coated with PEG groups, they can escape from phagocytosis, having a longer blood-circulation lifetime, avoiding being captured to a large extent by the spleen, liver, and lungs.(He *et al.*, 2011; Yu *et al.*, 2016; Rascol *et al.*, 2017) This also causes a smaller amount of degradation products to be excreted in the urine.

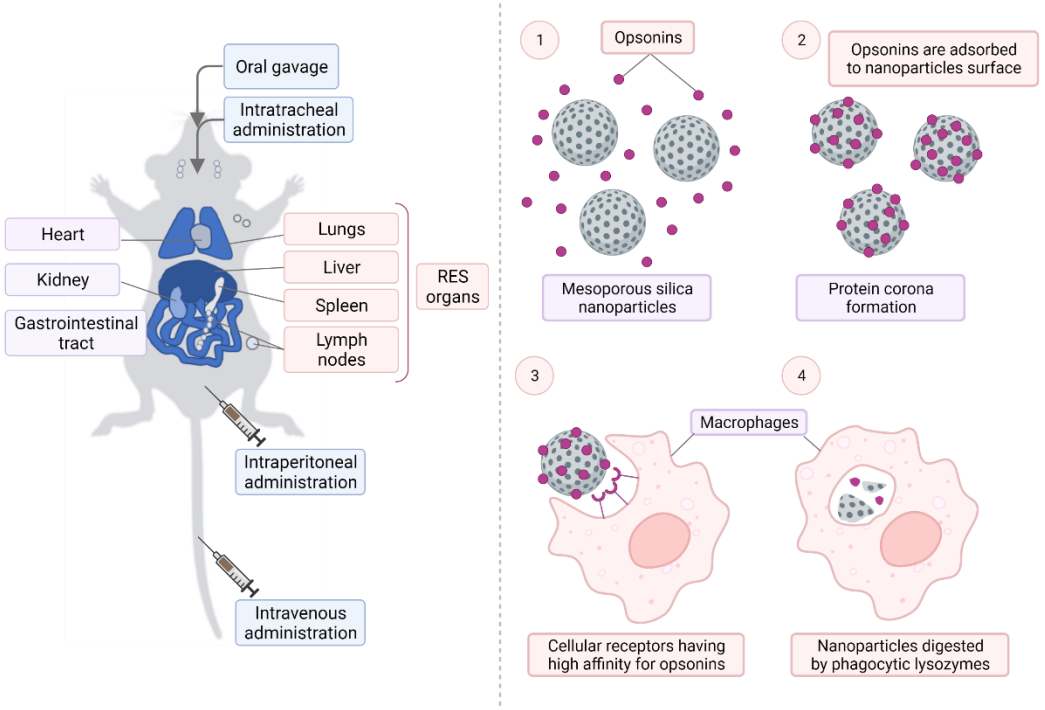

Figure 12 | Scheme of the most common ways of nanoparticle administration in mice models: intravenous administration, intraperitoneal administration, and oral gavage. Reticuloendothelial system (RES) organs such as lung, liver, spleen, and lymph nodes are also indicated in the scheme. When nanoparticles are administered to the body enter the bloodstream (1), opsonins and other plasma proteins present in the blood are adsorbed to the surface of the nanoparticles forming protein corona (2). The RES phagocyte cells circulating in the bloodstream, such as macrophages, have cellular receptors with high affinity for opsonins (3). This causes internalization and digestion of the nanoparticles by phagocytic lysozymes present in the macrophage (4).

As an example of biodistribution, Laprise-Pelletier *et al.* (Laprise-Pelletier *et al.*, 2015) demonstrated that MSNs administrated intravenously reached the liver and spleen a few minutes after injection, followed by progressive elimination over time with a half-life of 14.8 h and 12.9 h for liver and spleen, respectively.

Regarding degradation and excretion, it has been widely described that nanoparticles smaller than 6 nm are directly removed through the kidneys by renal clearance.(Longmire, Choyke and Kobayashi, 2008) In contrast, nanoparticles higher than 6 nm in size circulate

in the blood, reach the target tissue, and are captured by the reticuloendothelial system followed by renal and hepatobiliary excretion.(Ehlerding, Chen and Cai, 2015; Yu and Zheng, 2015) Nanoparticles that can be degraded into small fragments or constitutes, such as MSNs, are processed by the RES or in the diseased target (like tumors) and then return to blood circulation to finally be removed by the renal excretion or hepatobiliary system. In the case of MSNs, the renal clearance is accepted as the main excretion system, followed in a lower proportion by the hepatobiliary system.(Ehlerding, Chen and Cai, 2015; Croissant, Fatieiev and Khashab, 2017) This process, again, is highly dependent on the physicochemical properties of the nanoparticles, such as particle size, porosity, surface functionalization, and nanoparticle charge.

2.7. Nanodevices targeting senescent cells

Several nanotechnological-based strategies to specifically deliver senolytic drugs into senescent cells have been developed in the last years (Figure 13).(Morsli, Doherty and Muñoz-Espín, 2022) These nanodevices are based on MSNs, porous $CaCO_3$ nanoparticles, molecularly imprinted polymer nanoparticles (nanoMIPs), gold nanoparticles, and core–shell spiky nanorods (CSNRs) chiral nanoparticles.

In 2012, our group developed the first described nanodevice to release its cargo in senescent cells selectively.(Agostini *et al.*, 2012) MSNs (ca. 100nm) were loaded with rhodamine B (RhB) and capped with galactooligosaccharides. The enzymatic hydrolysis of the capping galacto-oligosaccharide by SA-β-Gal allowed the selective release of the cargo. A similar system but capped with lactose was previously reported in 2009.(Bernardos *et al.*, 2009) Based on the same strategy, in 2018, our group developed MSNs capped with a hexa-galacto-oligosaccharide (galactan)(NP-Gal).(Muñoz-Espín *et al.*, 2018). These nanoparticles were loaded not only with the dyes RhB or Indocyanine Green (ICG) but also with cytotoxic (doxorubicin) and senolytic drugs (navitoclax). NP-Gal has been tested in a model of pulmonary fibrosis (Muñoz-Espín *et al.*, 2018) and for the treatment of several cancer mice models upon chemotherapy-induced

senescence.(Muñoz-Espín *et al.*, 2018; Galiana *et al.*, 2020; Estepa-Fernández *et al.*, 2021) Moreover, we have found that the encapsulation of doxorubicin and navitoclax reduced their toxicity: cardiotoxicity in the case of doxorubicin and thrombocytopenia in the case of navitoclax.(Muñoz-Espín *et al.*, 2018; Galiana *et al.*, 2020)

Detection and elimination of senescent cells has also been achieved with porous calcium carbonate nanoparticles ($CaCO_3$, ca. 130 nm size) loaded with the senomorphic drug rapamycin (an mTOR inhibitor that prevents senescence by affecting the p53/p21 pathway).(Thapa *et al.*, 2017) Taking advantage of the overexpression of the CD-9 receptor (a cell surface glycoprotein) in senescent cells, porous calcium carbonate nanoparticles were functionalized onto the external surface with a lactose-PEG derivative and an anti-CD-9 antibody.(Nguyen *et al.*, 2017) CD9-mAb-coated nanoparticles targeted senescent cells and displayed a senomorphic effect due to the rapamycin release, inducing a marked reduction of SA-β-Gal levels, p53/p21, CD-9 expression, and decreased SASP factors. More recently, CD9 antibodies have been conjugated to hyaluronic acid-coated MSNs to target senescent cells and deliver rosuvastatin in response to the hyaluronidase present in atherosclerotic plaques (termed CD9-HMSN@RSV).(Pham *et al.*, 2021) CD9-HMSN@RSV shows senolytic efficacy *in vivo,* clearing senescent cells and reducing atherosclerotic pathology.

Another nanodevice for targeting senescent cells, based on the overexpression in senescent cells of the membrane protein β2 microglobulin (B2MG), has been developed using molecularly imprinted nanoparticles (nanoMIPs).(Ekpenyong-Akiba *et al.*, 2019) It has been reported that B2MG is overexpressed in senescent bladder cancer cells, fibrosarcoma cells (HT1080), and human diploid fibroblasts (HDF).(Althubiti *et al.*, 2014) NanoMIPs preferentially accumulate in the external membrane of senescent bladder cells. Also, nanoMIPs had a senolytic effect when loaded with dasatinib. *In vivo* studies revealed that nanoMIPs tagged with a fluorescent dye could detect senescent cells in the abdominal cavity of naturally aged mice.

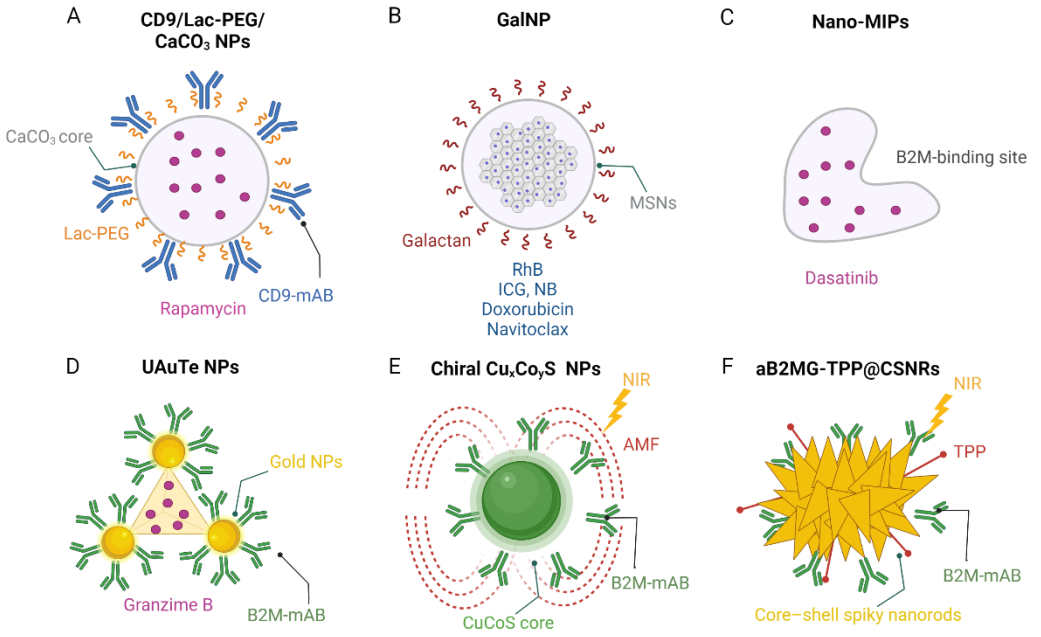

Figure 13 | Scheme of some of the novel nanodevices targeting senescent cells. A) Porous calcium carbonate nanoparticles ($CaCO_3$) loaded with the senomorphic drug rapamycin and functionalized with a lactose-PEG derivative and an anti-CD-9 antibody, a cell surface glycoprotein present in senescent cells. B) Mesoporous silica nanoparticles (MSNs) can be loaded with either dyes such as rhodamine B (RhB), indocyanine green (ICG) or nile blue (NB) or drugs as doxorubicin or navitoclax. GalNP are MSNs functionalized with galactan, a galactose-derived molecule. The SA-β-Gal enzyme cleaves galactose conjugated residues to endocytosed nanoparticles, allowing the release of their cargo within the lysosomal compartment. C) Molecularly imprinted nanoparticles (nanoMIPs) target senescent cells taking advantage of the overexpression in senescent cells of the membrane protein β2 microglobulin (B2MG). NanoMIPs can be loaded with dasatinib or a fluorescent dye. D) Gold tetrahedron nanoparticles (UAuTe) functionalized with the anti-B2M antibody to release granzyme-B in response to near-infrared (NIR) light have also been used to target senescent cells. E) Chiral Cu_xCo_yS nanoparticles functionalized with a B2M antibody have shown to be senolytic using both an alternating magnetic field (AMF) and near-infrared (NIR) light. F) Plasmonic core-shell spiky nanorods (CSNRs) functionalized with anti-B2MG antibody and triphenylphosphonium (TPP) moieties (aB2MG-TPP@CSNRs) were able to target mitochondria in senescent cells.

Anti-B2M antibody has also been used to target senescent cells by using gold tetrahedron nanoparticles (UAuTe) that release granzyme-B in response to near-infrared (NIR) light. Granzyme-B released from UAuTe nanoparticles due to NIR irradiation in a senescence-accelerated (SAMP8) mouse model restores liver function, tissue homeostasis, fur density, and athletic ability.(Qu *et al.*, 2020)

In another approximation, chiral Cu_xCo_yS nanoparticles functionalized with a B2M antibody have shown to be senolytic using both an alternating magnetic field (AMF) and NIR irradiation. In a doxorubicin-treated mouse, Cu_xCo_yS nanoparticles were able to reduce signs of senescence in the liver and kidneys as well as improve fur coverage, mobility, and weight.(Li *et al.*, 2020)

Plasmonic core-shell spiky nanorods (CSNRs) functionalized with anti-B2MG antibody, and triphenylphosphonium (TPP) moieties (aB2MG-TPP@CSNRs) were able to target mitochondria in senescent cells. These photo-induced nanorods (with NIR light) induce apoptosis in senescent cells by increasing mitochondrial ROS. Moreover, they also act as an immune adjuvant having a synergistic effect in restoring the fur density, liver function, and renal function in doxorubicin-induced aging mice.(Lu *et al.*, 2020)

2.8. Clinical translation of silica nanoparticles

Currently, there is no clinical trial evaluating MSNs, albeit their versatility. MSNs are considered safe materials for biomedical applications because of their compatibility and low toxicity (as described above). Therefore, MSNs are expected to serve as versatile drug carriers for clinical purposes. In fact, the FDA has already approved some silica derivatives, such as bulk silica. Bulk silica is cataloged as “Generally Recognized as Safe” by the FDA (US Food and Drug administration, ID Code: 14808-60-7) for its use in cosmetics and food additives. As an example, the food additive E551 is composed of 100 nm silica nanoparticles.

The safety profile of silica nanoparticles in humans is evident from 13 clinical trials (Figure 14) (it has been extensively reviewed in Janjua et al., 2021). In 2007 the first clinical trial using silica-based nanoparticles (NANO-FIM; NCT01270139) started. Core/shell silica-gold NPs in a bioengineered on-artery patch were used for coronary atherosclerosis plasmonic photothermic therapy for angioplasty and artery remodeling. The bioengineered artery patch was grown with allogenous stem cells pre-cultivated in the medium with nanoparticles.(Kharlamov & Gabinsky, 2012) Nanointervention produced significant regression of coronary atherosclerosis by removing the atherosclerosis plaque and remodeling blood vessels.(Kharlamov et al., 2015) Long-term outcomes of the NANO-FIM trial were published in 2017.(Kharlamov et al., 2017) No evidence of cytotoxicity or clinical complications was found in patients who underwent the treatment with the delivery of silica-gold NP in mini surgery implanted bioengineered on-artery patch.

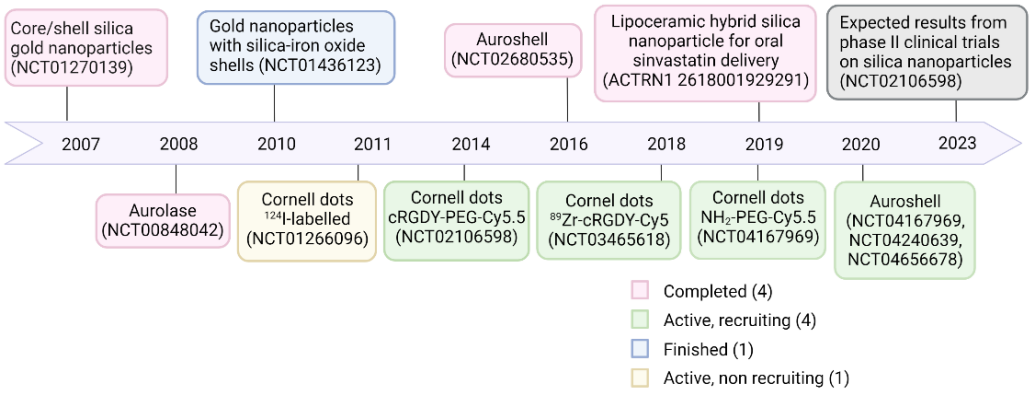

Figure 14 | The timeline shows different types of silica nanoparticles in clinical trials. cRGDY, cyclic arginyl-glycyl-aspartic acid-tyrosine; PEG, polyethylene glycol. Adapted from Jaunja et. al. Nature Reviews Materials. 2021

In addition, these researchers also developed CD68-targeted microbubbles based on gold nanoparticles with silica-iron oxide shells to target macrophages in atherosclerosis plaque and combined with stem cells (NANOM PCI; NCT01436123). In this case, ultrasounds were used to destroy the microbubbles patch and release the nanoparticles,

guided to the target using a magnetic field. However, nanotoxicity was found in the group of patients treated with iron NPs.(Kharlamov et al., 2017)

In 2011, “Cornell dots” (C-dots) entered clinical trials. C-dots are ultrasmall inorganic silica nanoparticles designed as a fluorescent imaging tool for detecting sentinel lymph nodes before cancer surgery.(Phillips *et al.*, 2014) These NPs have an internal silica core labeled with the Cy5 fluorescence dye coated with a PEG polymer and a targeting peptide for tumor and tumor endothelial cells (cyclic arginine–glycine–aspartic acid peptide; cRGDY). C-dots are undergoing clinical trials as an imaging tool for head and neck melanoma (phase I) and also for breast and colorectal malignancies (phase II) (NCT03465618, NCT01266096, NCT02106598, NCT04167969, and NCT02106598). To date, no toxic or adverse events attributable to the particles have been reported, which suggests the safety of these NPs for human cancer diagnostics.(Chen *et al.*, 2017)

Besides, Aurolase (2008) and Auroshell (2016 and 2020) nanoparticles are in clinical trials to identify tumor cells before and during surgery for prostate cancer (NCT04167969) and photothermal ablation of head, neck (NCT00848042) and prostate cancer (NCT04240639, NCT02680535, and NCT04656678). These nanoparticles are based on gold-silica nanoshells. For the prostate cancer pilot clinical trial (NCT04167969), the AuroShells nanoparticles are labeled with the Cy5.5 fluorophore and coated with PEG chains attached to a human prostate-specific membrane antigen (PSMA) inhibitor and labeled, *via* the macrocyclic chelating agent 1,4,7-triazacyclononane-N, N’, N''-triacetic acid (NOTA), with the radioisotope ^{64}Cu (^{64}Cu-NOTA-PSMA-PEG-Cy5.5-C' dot). Preliminary results (n=16) have proved that laser excitation of AuroShell NPs is a safe and technically feasible procedure for the targeted ablation of prostate tumors without causing severe complications or deleterious changes in genitourinary function.(Rastinehad *et al.*, 2019)

In several clinical trials, silica has been used as a formulation to improve drug bioavailability; this is the case of a silica–lipid hybrid formulation to deliver ibuprofen with an increase in bioavailability of 1.95 times compared with the commercially available ibuprofen.(Tan *et al.*, 2014) Also, lipoceramic hybrid silica nanoparticles improved simvastatin pharmacokinetics, showing a 3.5-fold increase in bioavailability compared with the commercial one (ACTRN12618001929291).(Meola *et al.*, 2021)

These clinical trials with silica nanoparticles have shown that silica is not toxic. MSNs can have great potential in the clinic due to their unique characteristics (biocompatibility, designable pore and particle size, high loading capacity, tunable surface through easy chemistry reactions). With these encouraging results, MSNs may open up new horizons for the commercialization of nanomedicine. In order to achieve this goal, future studies should consider key factors when designing MSNs, such as targeting ability, biocompatibility, and clearance pathways.

Objectives

Given the complex role of senescence in tumorigenesis, this doctoral thesis aims to develop effective senescence-inducing and senolytic therapies for cancer treatment. We achieve this general objective through the design, synthesis, *in vitro* characterization and *in vivo* evaluation of several nanodevices and prodrugs in different cancer models as well as through the identification of new senolytic molecules, in order to improve anticancer therapy.

The specific objectives referred to each chapter are:

- To evaluate the negative role of endothelial senescence in promoting metastasis after senescence-inducing chemotherapy in breast cancer.
- To explore the beneficial effects of combined pro-senescence and senolytic therapies to improve the antitumoral activity and to reduce metastatic burden in breast cancer.
- To design and evaluate a targeted-tumor delivery system based on two mesoporous silica nanoparticles that communicate by stigmergy, combining targeted pro-senescence and senolytic therapies.
- To identify and evaluate new senolytic compounds targeting melanoma.

Chapter I | Senolysis reduces senescence in veins and cancer cell migration

Senolysis reduces senescence in veins and cancer cell migration

Alejandra Estepa-Fernández[1,2,3], María Alfonso[1], Ángela Morellá-Aucejo[1,2], Alba García-Fernández[1,2,3*], Araceli Lérida-Viso[1,2,3,4], Beatriz Lozano-Torres[1], Irene Galiana[1,2], Paula Mª Soriano-Teruel[5], Félix Sancenón[1,2,3,4], Mar Orzáez[2,5*], Ramón Martínez-Máñez[1,2,3,4*]

[1] Instituto Interuniversitario de Investigación de Reconocimiento Molecular y Desarrollo Tecnológico (IDM) Universitat Politècnica de València, Universitat de València. *Camino de Vera, s/n. 46022, Valencia, Spain.*

[2] Unidad Mixta UPV-CIPF de Investigación en Mecanismos de Enfermedades y Nanomedicina, Universitat Politècnica de València, Centro de Investigación Príncipe Felipe. *C/ Eduardo Primo Yúfera 3. 46012, Valencia, Spain.*

[3] CIBER de Bioingeniería, Biomateriales y Nanomedicina (CIBER-BBN).

[4] Unidad Mixta de Investigación en Nanomedicina y Sensores. Universitat Politècnica de València, IIS La Fe. *Av. Fernando Abril Martorell, 106 Torre A 7ª planta. 46026, Valencia, Spain*.

[5] Centro de Investigación Príncipe Felipe. *C/ Eduardo Primo Yúfera 3. 46012, Valencia, Spain.*

*Corresponding authors. Email: algarfe4@etsia.upv.es; morzaez@cipf.es; rmaez@qim.upv.es

Published online: August 6, 2021

Graphical abstract

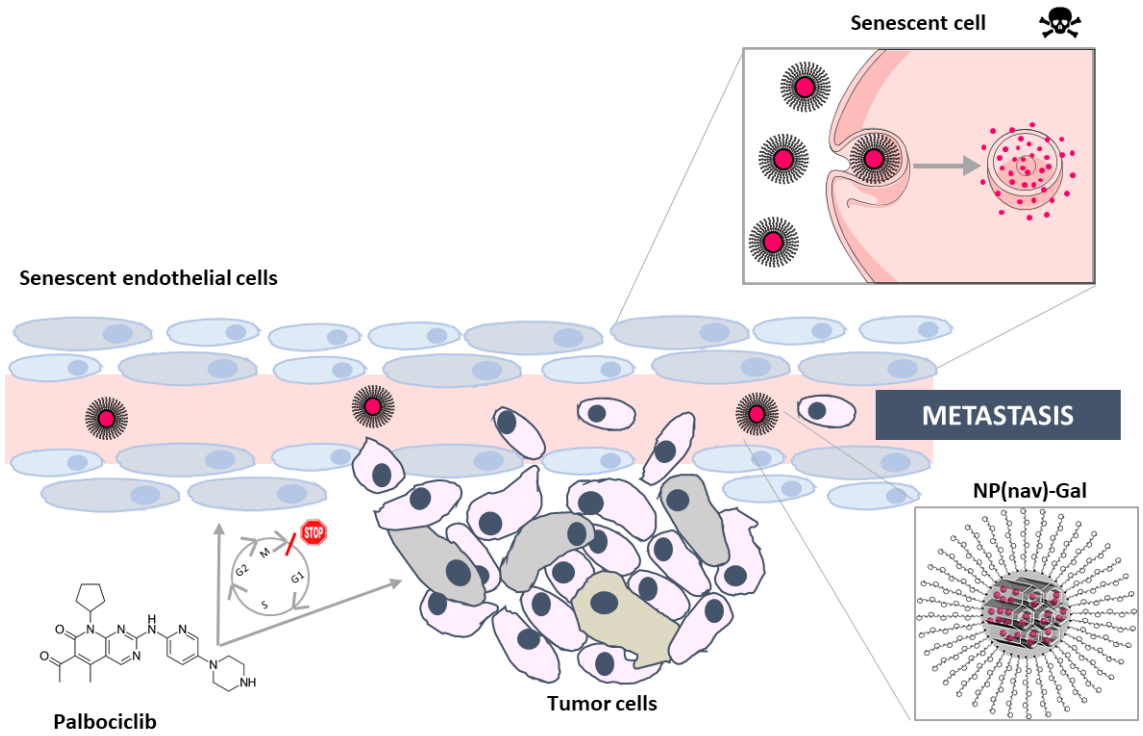

Keywords

Palbociclib, senescence, endothelial cells, triple negative breast cancer, mesoporous nanoparticles, navitoclax

My contribution

I performed in vivo and in vitro experiments except for the nanoparticle synthesis. I also contributed to the experimental design, data analysis, discussion and writing.

1. Abstract

Senescence is a persistent state of cell cycle arrest. Induction of senescence has been explored as a barrier against tumor progression and is used as a therapeutic option. Despite the advantages of the introduction of senescence-inducing compounds in the clinic, recent studies show that their side-effects could be partially masking their antitumor potential. This is due to the deleterious effects that accumulation of senescent cells in tissues and organs causes on tissue microenvironment that confer tumor-promoting properties. In this study, we demonstrate that the presence of senescent endothelium favors cancer cell migration *in vitro* and show that palbociclib systemic treatment induces senescence in veins in an orthotopic triple-negative breast cancer mouse model. Moreover, we found that following palbociclib-induced senogenesis, the elimination of senescent cells using the nanoencapsulated senolytic navitoclax (NP(nav)-Gal) produces the selective elimination of endothelial senescent cells and induces a marked recovery of endothelial tissue functionality. Finally, the treatment with NP(nav)-Gal produces a significant decrease of senescence in veins *in vivo* which is consistent with the decrease in metastasic burden observed. These results evidence the potential of reducing vascular senescence using senolytic therapies as strategy to limit the metastatic dissemination of tumors cells in breast cancer patients subjected to chemotherapeutic treatments.

2. Introduction

Cellular senescence is a stable and long-term cell cycle arrest that can be triggered in proliferating cells as part of development, tissue repair and ageing processes as well as a consequence of a stress response or drug treatment.(Hayflick and Moorhead, 1961; Hernandez-Segura, Nehme and Demaria, 2018) Senescence induction avoids the proliferation of damaged or stressed cells and initiates tissue remodeling processes through the secretion of multiple factors that constitute what is known as the senescence-

associated secretory phenotype (SASP). SASP components are a complex mixture of extracellular factors (such as cytokines, interleukins, metalloproteinases or matrix-degrading proteins) involved in reparation, propagation of senescence, immune clearance, embryogenesis, and tumorigenesis.(Krizhanovsky *et al.*, 2008; Demaria *et al.*, 2014; Yun, Davaapil and Brockes, 2015; Ritschka *et al.*, 2017)

As senescent cells are cell cycle-arrested, the therapeutic induction of senescence has been extensively explored as a mechanism to limit tumor progression.(Acosta and Gil, 2012) Therapeutic induction of senescence in tumor cells is an opportunity to alert and activate the immune system to detect and eliminate them.(Braig *et al.*, 2005; Chen *et al.*, 2005; Collado *et al.*, 2005; Michaloglou *et al.*, 2005) To this end, senescence-inducing compounds have been developed, including cyclin-dependent kinase (CDKs) inhibitors 4 and 6 such as palbociclib. *In vitro*, the inhibition of CDK4/6 results in the restriction of retinoblastoma protein phosphorylation (pRb) causing cell cycle arrest in the G1/S transition phase.(Goel *et al.*, 2018) In this scenario, the induction of senescence in tumor in clinical trials by palbociclib has shown effectiveness in the treatment of advanced breast cancer in combination with letrozole or fulvestrant.(Fry *et al.*, 2004; Finn *et al.*, 2009, 2015, 2016; Pernas *et al.*, 2018) In particular, palbociclib is currently approved by the Food and Drug Administration (FDA) for use in combination with letrozole in HR^+, $HER2^-$ postmenopausal women with metastatic breast cancer or fulvestrant in women with breast cancer that have progressed after endocrine therapy.(Beaver *et al.*, 2015; Walker *et al.*, 2016) Regardless senescence inductors in clinics are effective,(Kwapisz, 2017; Pernas *et al.*, 2018) the role of senescence in tumorigenesis is complex. The accumulation of senescent cells in tissues and organs has proved to cause deleterious effects on the tissue microenvironment producing chronic inflammation and tumor-promoting properties that may drive the formation of secondary tumors or cancer relapse.(Coppé *et al.*, 2010; Kang *et al.*, 2011; Iannello *et al.*, 2013; Eggert *et al.*, 2016; Ruhland, Coussens and Stewart, 2016)

Previous studies have described the crucial role of the endothelium as a barrier against cancer relapse and metastasis.(Kumar *et al.*, 2009; Reymond, D'Água and Ridley, 2013) The endothelium is a thin mono-cellular layer that covers the inner surface of blood vessels.(Lüscher and Barton, 1997) It is involved in nutrient transport to almost all cells in the human body, but it also has a prominent role in inflammatory and immune processes by regulating proliferation and cell migration, as well as adherence and leukocytes activation.(Butler, Kobayashi and Rafii, 2010; El Assar *et al.*, 2012; Al-Soudi, Kaaij and Tas, 2017) A compromised endothelium favors the pass of circulating cancer cells to the tissues favoring metastases in other organs.(Shenoy and Lu, 2016) Senescence is involved in the functional imbalance of the endothelium, through the alteration of the endothelial cytoskeleton and the increase of endothelium permeability, facilitating transendothelial migration, promoting neutrophil infiltration, tumor cell adhesion, and metastasis.(Wieland *et al.*, 2017) Therefore, the reduction of senescent endothelial cells might arise as a feasible strategy to limit cancer cell migration and thus metastasis.

An effective strategy to overcome the negative side effects of senescent cell accumulation is to enhance senolysis; i.e. the selective induction of apoptosis in senescent cells.(Zhu *et al.*, 2015) Thus, the efficacy and safety of two-hit strategies that combine senogenesis and senolysis treatments for the selective elimination of senescent cells are being explored in the context of tumor treatments. Senolytic drugs have proved to alleviate several aging-related diseases that are associated with the accumulation of senescent cells.(Soto-Gamez and Demaria, 2017; Lozano-Torres *et al.*, 2019) However, considering its novelty as well as some toxicity issues derived from its use, only few senolytic drugs have been approved by the FDA yet (Kirkland and Tchkonia, 2020) and the development of new senolytic strategies with higher selectivity and reduced toxicity is an active research field. Among senolytic drugs, navitoclax has shown effectiveness *in vivo* in reducing cancer relapse and delaying the onset of diseases such as atherosclerosis, neurodegenerative diseases or hematopoietic system aging.(Chang *et al.*, 2016; Demaria *et al.*, 2017; Kim *et al.*, 2017; Bussian *et al.*, 2018) However, its clinical use is still limited

by associated hematological toxicity.(Cang *et al.*, 2015) We have recently demonstrated that this effect can be reduced by the design of pro-drugs (González-Gualda *et al.*, 2020) and a nanotechnological-based strategy to specifically deliver navitoclax in senescent cells with high specificity and lack of toxicity.(Agostini *et al.*, 2012; Muñoz-Espín *et al.*, 2018; Galiana *et al.*, 2020; González-Gualda *et al.*, 2020)

Herein, we show that palbociclib induces senescence in endothelial cells and generates an unpaired endothelium that increases breast cancer cell migration. The nanotherapy-targeted senolytic agent (NP(nav)-Gal), based on mesoporous silica nanoparticles loaded with navitoclax, and capped with a hexa-galacto-oligosaccharide, efficiently eliminates endothelial HUVEC senescent cells *in vitro*, improving the endothelial functionality by recovering the ability to form capillary-like structures. We demonstrate that *in vivo* systemic administration of palbociclib induces the accumulation of endothelial senescent cells in a triple-negative breast cancer (TNBC) mice model. Subsequent treatment with the senolytic agent NP(nav)-Gal reduces senescence in veins, and this correlates with a decrease in lung metastasis. Moreover, we demonstrate that palbociclib treatment increases lung metastasis after tail vein injection of TNBC cells in healthy mice. Overall, we provide evidence of the effects derived from chemotherapy-induced senescence in veins and the potential of reducing vascular senescence with senotherapies for limiting cancer cell spreading and thus metastasis.

3. Results

3.1. Endothelial senescence increases the migration of breast cancer MDA-MB-231 cells

The CDK4/6 inhibitor palbociclib induces cell cycle arrest and senescence in different tumors cells.(Wang, Kohli and Demaria, 2020) However, the ability of this drug to induce senescence is not necessarily restricted to tumor cells. This off-target effects could have negative consequences for antitumoral treatments.

We have investigated the effect of palbociclib in endothelial cells and found that treatment with 2 μM palbociclib induces senescence in human umbilical vein endothelial (HUVEC) cells after 7 days of treatment. Induction of cellular senescence was corroborated by the increase in SA β Gal activity assay using the X-Gal test (Figure 1A). Treatment with palbociclib was also accompanied by a change in cell morphology with an increase in cell size and in the number of intracellular vesicles, in agreement to described features for senescent phenotypes.(Hernandez-Segura, Nehme and Demaria, 2018) Senescence induction in the culture was quantified by flow cytometry using the β-galactosidase substrate 5-dodecanoylaminofluorescein di-β-D-galactopyranoside (C_{12}FDG) (Figure 1B). Senescent cells were able to hydrolyze C_{12}FDG yielding a fluorescein derivative which is easily detected in the cells. Results in Figure 1B show that 90.01% of the HUVEC cells in cultures treated with palbociclib were senescent whereas in non-treated cultures only 3.24% presented a senescent phenotype. To confirm cell cycle arrest in palbociclib-treated HUVEC cells, the expression of Ki67 proliferation marker was analyzed by immunofluorescence (Figure 1C). Whereas proliferating HUVEC cells showed a marked Ki67 expression (red emission) this expression was nearly absent in senescent cells. The clonogenic assays also confirmed the proliferation arrest of palbociclib-treated HUVEC cells (Figure 1D). Besides, a marked reduction of phosphorylation of pRb protein together with an up-regulation of the tumor suppressor gene p53 in senescent HUVEC cells was observed when compared with proliferating cells (Figure 1G and S1), thus confirming the palbociclib-induced senescence of endothelial HUVEC cells. Moreover, to determine whether palbociclib-induced senescence in HUVECs can be expanded in a paracrine manner, conditioned media (CM) of senescent endothelial HUVEC cells and triple negative breast cancer MDA-MB-231 and 4T1 cells were added to the recipient proliferating HUVEC cells. Our results suggest that conditioned medium from palbociclib-treated cells change cell morphology and increases X-gal staining in the recipient endothelial cells (Figure S2), thus confirming paracrine-senescence induction.

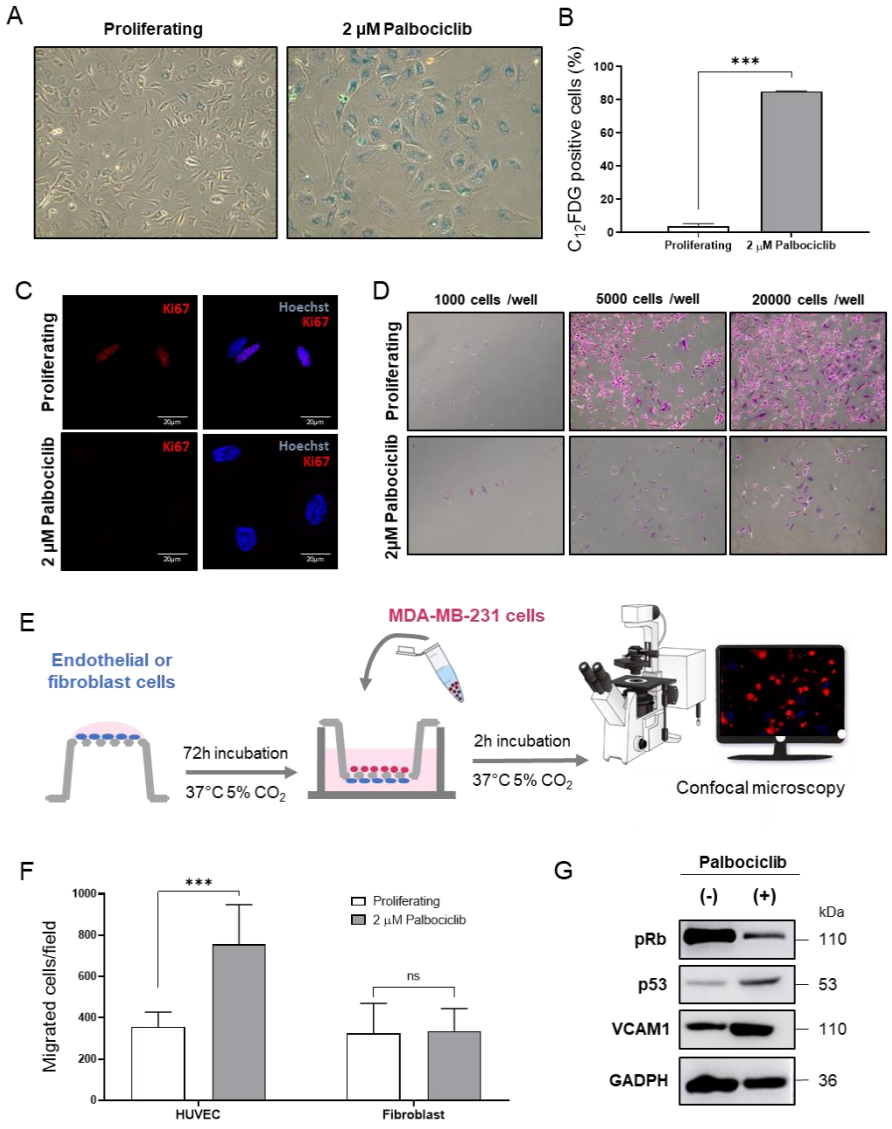

Figure 1 | Endothelial senescence induction upon palbociclib treatment (A) β-Galactosidase staining of proliferating and 2 µM palbociclib-treated HUVEC cells. Senescence induction was confirmed by high β-galactosidase activity (blue color) in palbociclib-treated cells at pH 6. (B) C12FDG staining indicated that β-galactosidase activity increases in palbociclib-treated HUVEC cells when compared with proliferating cells. Values are expressed as mean ± SEM and statistical significance was assessed by the two-tailed Student's T-test: ***p<0.0005. (C) Confocal microscopy images of immunofluorescence of Ki67 (red) in proliferating and senescent HUVEC cells. The proliferation marker Ki67 decreases its expression in senescent HUVEC cells. The nucleus is stained with Hoechst (blue). Scale bar, 20 µm (D) Crystal violet staining of proliferating and senescent

HUVEC cells. Proliferating and one-week palbociclib-treated HUVEC cells were seeded in increasing concentrations in 24-plate wells (1000, 5000 and 20000 cells/wells) and were let to proliferate for one week. (E) Schematic representation of MDA-MB-231 breast cancer cells migration assay. HUVEC or fibroblasts, proliferating or senescent, were seeded in a drop on the bottom of the insert. After 16 h, the drop was aspirated, and new media was added to the insert to let cells grow for 72 h. After 72 h MDA-MB-231 breast cancer cells were stained with 5 µM Cell Tracker Deep Red for 1 h at 37 °C, seeded on the top of the insert and let them migrate for 2 h. HUVEC and fibroblasts were stained with Hoechst. MDA-MB-231 migration was analyzed by confocal microscopy. (F) The presence of senescent endothelial HUVEC cells increases the migration of breast cancer MDA-MB-231 cells (***, p-value <0.0005). The number of migrated tumor cells do not increase when comparing proliferating and senescent fibroblast. Quantification was made with Image J software. (G) Western Blot characterization of proliferating and senescent HUVEC cells. pRb expression decreased after palbociclib treatment (expected band at 110 kDa), both p53 (expected band at 53 kDa) and VCAM1 (expected band at 110 kDa) expression increase after palbociclib treatment. Data represent the means ± SEM of at least three independent experiments.

Once assessed that palbociclib administration induced senescence in endothelial cells we explored the role of endothelial senescence plays in cancer cells migration. In a first step, the expression of the leukocyte receptor of vascular cell adhesion molecule 1 (VCAM1) was analyzed in senescent HUVEC cells. The results showed a remarkable increase of the VCAM1 in HUVEC senescent cells upon palbociclib treatment (Figure 1G and S1). The presentation of the VCAM1 receptor is a signal of endothelial dysfunction(Liao, 2013) and has been described to have a role in increasing tumorigenicity and metastasis.(Schlesinger and Bendas, 2015)

Then, we settled an *in vitro* model to study MDA-MB-231 breast cancer cell migration in the presence of proliferating or senescent HUVEC (Figure 1E). To this end, proliferating or senescent HUVEC cells were seeded in a drop on the bottom of a permeable insert. In the same way, proliferating or senescent fibroblast cells (Figure S3) were used as a control. After cellular adhesion and growth, MDA-MB-231 breast cancer cells were seeded on the top of the insert and let them migrate for 2 h. Migration of MDA-MB-231 breast cancer cells increased when the insert contained endothelial senescent HUVEC cells whereas this effect was not observed when HUVEC cells were not senescent (Figure 1F). Besides, as control, there were no significant differences in migration when proliferating

or senescent fibroblasts were located on the permeable insert. These results demonstrated that endothelial senescence favors cancer cell migration.

3.2. Selection and characterization of drugs to selectively eliminate HUVEC senescent cells

Considering that our objective was the selective elimination of endothelial senescent cells, first we performed a Bcl-2-expression profiling of HUVEC senescent cells. This profiling showed a marked increase of Bcl-2 expression in HUVEC cells upon palbociclib treatment and a marked expression of Bcl-xL in both normal and senescent cells (Figure S3). As senescent cells have been demonstrated to be dependent on Bcl-2 proteins for survival (Childs *et al.*, 2014) we selected navitoclax (ABT-263; nav), the inhibitor of the anti-apoptotic proteins BCL-2, BCL-xL, and BCL-W, as senolytic drug.(Zhu *et al.*, 2016)

To improve navitoclax therapy, by avoiding off-target effects and associated toxicity, we used mesoporous silica nanoparticles (MSNs) coated with a hexa-galactooligosaccharide (galactan) to encapsulate navitoclax (NP(nav)-Gal) (Figure 2A). MSNs are excellent nanocarriers due to their remarkable characteristics such as high loading capacity, homogeneous porosity, easy functionalization and biocompatibility.(Yang, Gai and Lin, 2012; Wu, Mou and Lin, 2013; Aznar *et al.*, 2016; Llopis-Lorente, Lozano-Torres, *et al.*, 2017; Pu *et al.*, 2019; García-Fernández *et al.*, 2020) Gated MSNs have been used satisfactorily in *in vivo* models, improving the solubility of encapsulated drugs and reducing undesired side effects (Zhang *et al.*, 2016; Hu *et al.*, 2017; Muñoz-Espín *et al.*, 2018; Yin *et al.*, 2018; Castillo and Vallet-Regí, 2019; Pu *et al.*, 2019) and also employed in cell sensing and communication protocols.(Llopis-Lorente, DÍez, *et al.*, 2017; de Luis *et al.*, 2019) We have previously reported that galactan-capped MSNs are able to release an entrapped cargo in senescent cells in models of dyskeratosis congenita, chemotherapy-treated xenografts and pulmonary fibrosis.(Agostini *et al.*, 2012; Muñoz-Espín *et al.*, 2018; Galiana *et al.*, 2020) This preferential cargo release is due to the high lysosomal β-galactosidase activity presented in senescent cells which induced

the hydrolysis of the capping ensemble with subsequent pore opening and cargo delivery. A galactan-capped MSN loaded with indocyanine green (ICG,) for tracking purposes and control unloaded nanoparticles capped with galactan (NP(ICG)-Gal and NP-Gal, respectively) were also synthetized and characterized for the study.

Transmission electron microscopy (TEM) images and X-ray diffraction confirmed the preparation of final uniform MSNs of ca. 100 nm, with the typical mesoporous channels visualized as alternate black and white strips (Figure 2B, S4 and S5). Besides, N_2 adsorption-desorption isotherms confirmed the presence of uniform cylindrical mesoporous in the starting MSNs with a pore size of 2.62 nm and a total specific surface area of 1087 $m^2\ g^{-1}$ (Figure S6 and Table S1). Starting calcined MSNs presented a zeta potential value of -21.06 mV which changed to -14.6 and -2.57 mV for NP(ICG)-Gal and NP(nav)-Gal (Figure 2C). Moreover, the hydrodynamic diameter increased from 162.6 nm for the calcined MSNs to 211.6 and 285.6 nm for NP(ICG)-Gal and NP(nav)-Gal (Table S2). Besides, a single population distribution was observed for all solids suggesting that nanoparticles were not aggregated, even after the loading and functionalization process. Thermogravimetric analysis and delivery studies allowed us to determine amounts of navitoclax, ICG and hexa-galacto-oligosaccharide in NP(nav)-Gal and NP(ICG)-Gal (Table S3). Figure 2D and S8 demonstrated that payload delivery from the nanoparticles was negligible in the absence of β-galactosidase, whereas navitoclax and ICG from NP(nav)-Gal and NP(ICG)-Gal were clearly delivered in the presence of the enzyme. Controlled cargo delivery in the presence of β-galactosidase agreed with previous reports.(Muñoz-Espín *et al.*, 2018; Galiana *et al.*, 2020) Cell viability studies in the presence of NP-Gal (without cargo) at different concentrations were performed in HUVEC endothelial cells (Figure S9). After 72 h of treatment cell viability was kept in all cases up to 95% even at the highest NP-Gal concentration (2 mg/mL).

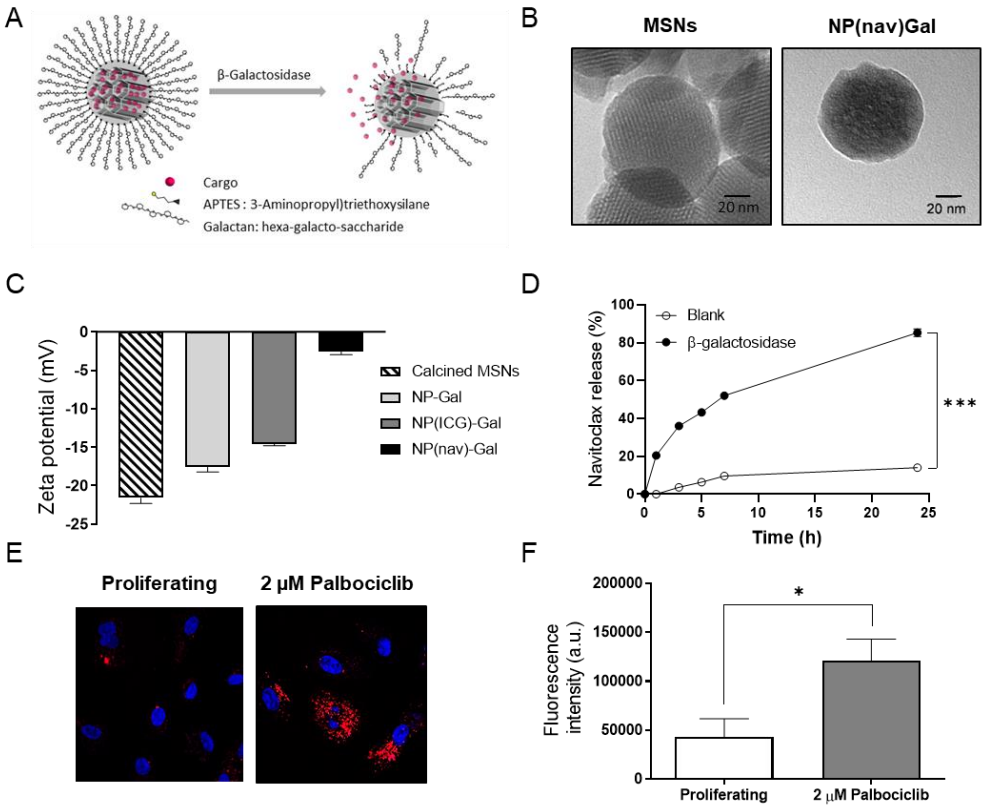

Figure 2 | Physicochemical characterization of NP(nav)-Gal and selective cargo release in HUVEC-senescent cells. (A) Scheme of mesoporous silica nanoparticles (MSNs) loaded with navitoclax or ICG and, functionalized and capped with an oligosaccharide galactan that bounds covalently to APTES. (B) TEM images of NP(nav)-Gal. Scale bar, 20 nm (C) Zeta potential of the steps of the synthesis of the nanodevices: as made MSNs, calcined MSNs, NP-Gal, NP(ICG)-Gal and NP(nav)-Gal. (D) Release profiles of navitoclax from NP(nav)-Gal in the absence or in the presence of β-galactosidase from Aspergillus oryzae in water at pH 4.5. (E) Confocal analysis of NP(ICG)-Gal internalization by HUVEC cells after 6 h of treatment. ICG (red) and nucleus (blue). (F) Mean fluorescence intensity of proliferating and senescent HUVEC cells reflecting the overall particle uptake by the endothelial cells in flow cytometry after NP(ICG)-Gal treatment for 6 h. Statistical significance was assessed by two-tailed Student's T-test (*, p-value <0.05; ***, p-value <0.0005.) Data represent mean ± SEM (n=3).

The preferential ICG delivery from NP(ICG)-Gal in senescent HUVEC cells was studied using confocal microscopy. Figure 2E shows a negligible emission from ICG (far-red fluorescence) in proliferating HUVEC cells, whereas a marked red emission was found in HUVEC senescent cells when treated with NP(ICG)-Gal nanoparticles. This red emission is

consistent with the NP(ICG)-Gal internalization, hydrolysis of the oligosaccharide cap by the overexpressed β-galactosidase enzyme in senescent cells and release of ICG fluorophore. Moreover, flow cytometry studies also indicated preferential cargo delivery from NP(ICG)-Gal in senescent HUVEC endothelial cells (3-fold) versus non-senescent cells (Figure 2F and S10).

Once assessed the preferential internalization and cargo release of NP(ICG)-Gal nanoparticles by HUVEC senescent cells, the senolytic activity of the nanoparticles loaded with navitoclax and free navitoclax was evaluated. Then, proliferating and senescent HUVEC cells were treated with different concentrations of free navitoclax or NP(nav)-Gal and cell viability after 72 h was determined. Free navitoclax and NP(nav)-Gal nanoparticles were non-toxic for proliferating HUVEC cells nearly in all the concentration range tested (Figure 3A). Free navitoclax eliminated senescent HUVEC cells with an estimated IC50 value of 1.4 μM, whereas NP(nav)-Gal nanoparticles preferentially eliminate senescent HUVEC endothelial cells with an IC50 of 0.6 μM. These results confirmed the senolytic properties of navitoclax and NP(nav)-Gal in senescent endothelial cells and show that NP(nav)-Gal improves the senolytic index over navitoclax (7-fold increase when compared to the free drug) indicating that there is an effect of protection of proliferating cells from navitoclax cytotoxicity.

3.3. Navitoclax and NP(nav)-Gal treatment improves the functionality of endothelial tissue in co-cultures of senescent and proliferating HUVEC cells

After assessing the ability of NP(nav)-Gal to eliminate senescent endothelial cells we explored the impact of senescent endothelial cell on angiogenesis. For this purpose, and in a first step, we confirmed the ability of proliferating HUVEC cells to form capillary-like structures (tubes) in an appropriate extracellular matrix support. Proliferating HUVEC cells formed many short tubes with multiple branches, the overall picture resembling that of a honeycomb (Figure 3B). In contrast, senescent HUVEC cells did not form tubular structures and the cells appeared to form clusters reducing the number of branches. In

co-cultures with a 1:3 ratio of proliferating vs senescent HUVEC cells, cells were able to form tubes although the number of branches was reduced when compared with proliferating endothelial cells alone.

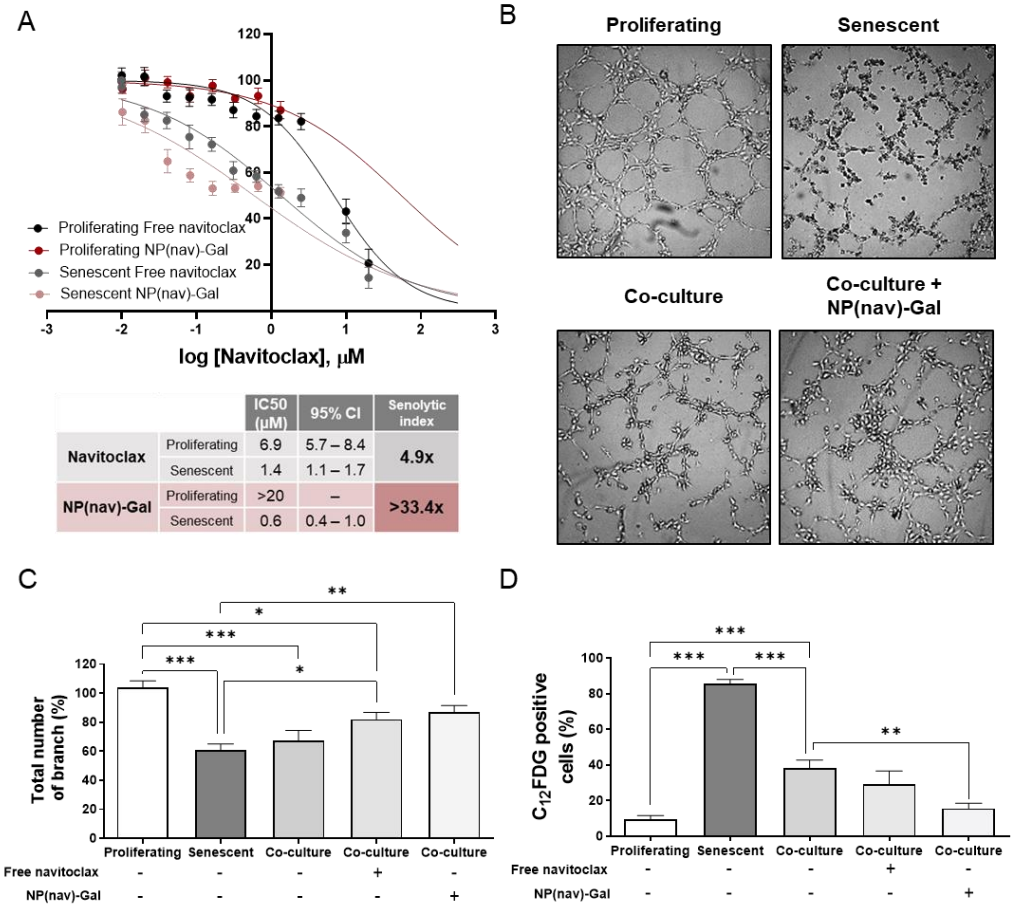

		IC50 (μM)	95% CI	Senolytic index
Navitoclax	Proliferating	6.9	5.7 – 8.4	4.9x
	Senescent	1.4	1.1 – 1.7	
NP(nav)-Gal	Proliferating	>20	–	>33.4x
	Senescent	0.6	0.4 – 1.0	

Figure 3 | Elimination of senescent cells improves endothelial morphology. (A) Cytotoxicity profile of free navitoclax or NP(nav)-Gal in proliferating and senescent HUVEC cells. Cell viability after 72 h of cell treatment with different concentrations of free navitoclax (dark red for proliferating HUVEC and light red for senescent HUVEC) and NP(nav)-Gal (black for proliferating HUVEC and grey for senescent HUVEC. (B) Tube assay formation images of proliferating, senescent and co-culture with the same number of proliferating and senescent HUVEC cells before and after treatment with NP(nav)-Gal for 48 h. (C) Quantification of the total number of branches (Angiotool software). (D) Quantification of C_{12}FDG positive cells by flow cytometry. Pretreatment with NP(nav)-Gal reduced de number of senescent cells. One-way ANOVA followed by Tukey's post-tests were performed to

calculate the statistical significance of the results (*, p-value <0.05; **, p-value <0.05; ***, p-value <0.0005). Data represent the means ± SEM of at least three independent experiments.

To study the efectiveness of senolytic therapies, the effect of senescent cells elimination in co-cultured proliferating and senescent HUVEC cells was assessed. For this purpose, cell co-culture was pretreated with free navitoclax or NP(nav)-Gal nanoparticles (at equivalent navitoclax concentration) for 48 h, and tube formation ability of HUVEC cells and number of branches was evaluated (Figure 3C). As could be seen, proliferating cells presented a higher number of branches than senescent cells. Besides, the number of branches in the co-cultured senescent plus proliferating cells was higher than for senescent cells alone while lower than for proliferating HUVEC cells. Interestingly, the administration of navitoclax to the co-cultures, either in free formulation or encapsulated in NP(nav)-Gal, improved branches formation (reaching values similar to proliferating HUVEC cells) with a final structure resembling that of a honeycomb.

Results above agree with the elimination of senescent cells by navitoclax or NP(nav)-Gal, being the remaining proliferating cells able to form tubular structures with an increased number of branches. This was confirmed by quantifying the number of senescent cells in the co-cultures by C_{12}FDG staining and flow cytometry (Figure 3D). A significant reduction of senescent cells was achieved by free navitoclax and NP(nav)-Gal treatment (ca. 2-fold for NP(nav)-Gal) obtaining levels of senescence similar to those presented in proliferating endothelial cells when co-cultures were treated with NP(nav)-Gal. This reduction of senescent levels with the nanoparticles was ascribed to selective NP(nav)-Gal internalization and subsequent navitoclax delivery in senescent cells. These results support that treatment with navitoclax or NP(nav)-Gal is an effective strategy to recover the functionality of endothelial senescent tissues.

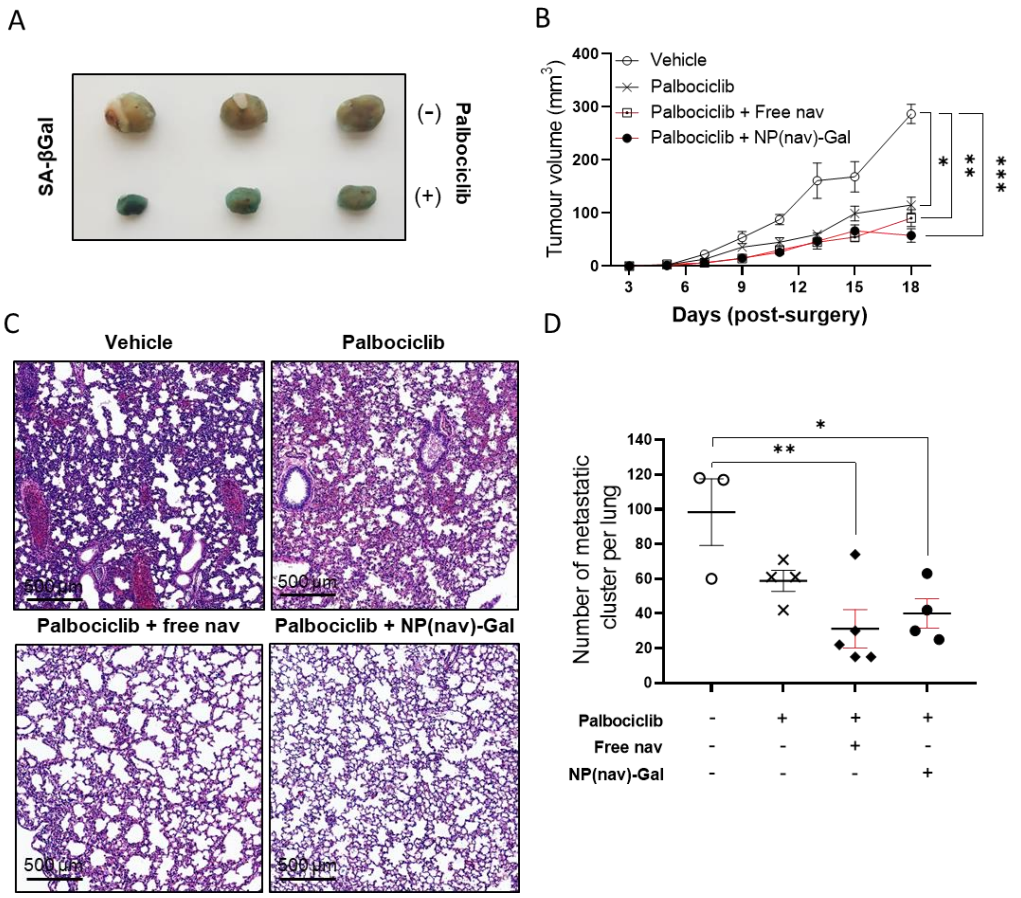

Figure 4 | Balb/cByJ female mice were orthotopically injected with 4T1 breast cancer cells and treated daily with vehicle or palbociclib. Mice were implanted with 0.5×10^6 4T1 cells subcutaneously on mammary pads and palbociclib treatment were given daily (o.g.) for 15 days. One day after palbociclib initiation, daily navitoclax treatment started and was maintained for 17 days (free navitoclax: oral gavage, 25 mg/kg; NP(Nav)-Gal: intraperitoneal injection, 40 mg NP(Nav)-Gal/kg (equivalent to 2.5 mg/kg = free Navitoclax) (n=3-5). (A) Photograph of representative tumor samples stained with X-gal. (B) Tumor volume of the different treatment approaches during all the treatment. (C) H&E staining of representative lung sections taken from xenograft 4T1 tumor-bearing mice for metastatic clusters evaluation. Scale bar, 500 µm (D) Quantification of metastatic lung clusters as representative in the insert were microscopically counted per tissues and plotted in the graph. Statistical analysis was carried out using GraphPad Prism and results were compared by one-way ANOVA followed by Tukey's post-tests (*, p-value <0.05; **, p-value <0.05; ***, p-value <0.0005). Data represent the means ± SEM.

3.4. Evaluation of endothelial senescence in triple-negative breast cancer model by palbociclib-induced senogenesis and NP(nav)-Gal senolysis

Finally, we selected the 4T1 orthotopic triple-negative breast cancer (TNBC) mouse model to study the effect of palbociclib-inducing senescence therapy (senogenesis) followed by navitoclax or NP(nav)-Gal treatment (senolysis) on the vascular endothelium. In this *in vivo* breast cancer models the antitumoral effectiveness of the double senogenesis plus senolysis treatment has been already demonstrated,(Galiana *et al.*, 2020) however the relevance of the endothelium on this process has not been addressed.

The 4T1 mice model is highly tumorigenic and invasive model with close similarities with the human triple negative breast cancer.(Pulaski, Ostrand-Rosenberg and Ostrand-Rosenberg, 2000; DuPré *et al.*, 2007) Balb/cByJ female mice (4-6 weeks) were injected in the mammary pads with 4T1 cells to generate the tumor. After one week of free tumor growth, palbociclib or sodium lactate (vehicle) was administered by daily oral gavage for 17 days (100 mg/kg). One day after palbociclib treatment, free navitoclax (oral gavage, 25 mg/kg) or NP(nav)-Gal (intraperitoneal injection, in a dose equivalent to 2.5 mg/kg of free navitoclax) treatment was given daily for 16 days aiming to eliminate senescence cells. Tumor formation was evaluated every 3 days measuring tumor volume (Figure 4B). After palbociclib treatment, senescence was efficiently induced in tumors as increased X-gal staining revealed (Figure 4A). We also confirmed the effectiveness of combinatorial palbociclib-senogenesis and senolysis treatment for cancer therapy by the reduction of tumor size (Figure 4B and S11)

Lung metastases were evaluated in the 4T1 mice model. Metastatic cell clusters were found in lung sections of 4T1 tumor-bearing mice (Figure 4C) while we detected a decrease tendency, in those animals co-treated with navitoclax either as a free drug or encapsulated (NP(nav)-Gal) (Figure 4D).

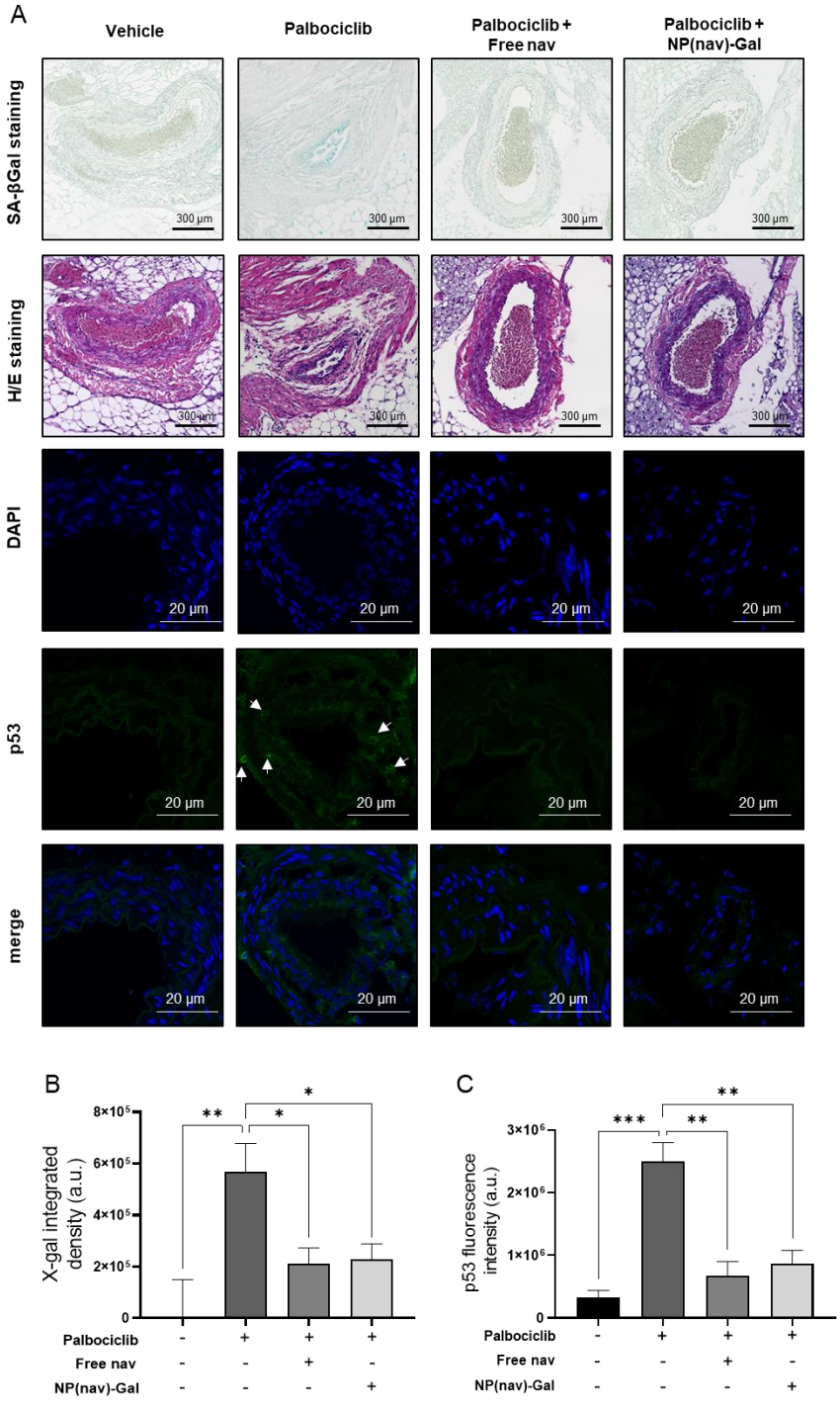
A
Vehicle
Palbociclib
Palbociclib + Free nav
Palbociclib + NP(nav)-Gal
SA-βGal staining
H/E staining
DAPI
p53
merge
300 µm
20 µm
B
X-gal integrated density (a.u.)
8×10⁵
6×10⁵
4×10⁵
2×10⁵
0
**
*
*
Palbociclib - + + +
Free nav - - + -
NP(nav)-Gal - - - +
C
p53 fluorescence intensity (a.u.)
3×10⁶
2×10⁶
1×10⁶
0
***
**
**
Palbociclib - + + +
Free nav - - + -
NP(nav)-Gal - - - +

Figure 5 | Elimination of endothelial senescent cells by treatment with free or encapsulated navitoclax. Inferior cava veins were obtained from Balb/cByJ female mice orthotopically injected with 4T1 breast cancer cells and treated daily with vehicle or palbociclib. (A) Representative images of β-galactosidase staining of mice veins (first line images). Hematoxylin/eosin staining of the mice veins (second line images). Scale bar, 300 µm. Confocal images (third to fifth line) of p53 (green) stained tumor sections. DAPI (blue). Scale bar, 20 µm. (B) Quantification of the β-galactosidase staining was performed using Image J software by measuring integrated density from three random fields per section. (C) Quantification of the p53 fluorescence signal was performed using Image J software by measuring fluorescence integrated density from three random fields per section. Data represent the means ± SEM and statistical significance was assessed by one-way ANOVA followed by Tukey's post-tests (*, p-value <0.05; **, p-value <0.05; ***, p-value <0.0005).

Following our findings above, i.e. (i) palbociclib induces senescence in the endothelium, (ii) senescence favors cancer cell migration and (iii) treatment with free navitoclax or NP(nav)-Gal reduces endothelial senescent cells, we focused our study on the analysis of endothelial cells and found that, at the experimental endpoint, those mice treated systemically with palbociclib developed vascular senescence. In contrast, vascular senescence was not observed in those navitoclax or NP(nav)-Gal treated animals (Figure 5A). Cava veins obtained from mice treated with palbociclib have an increased X-gal staining, p53 and VCAM1 expression (Figure 5 B, 5C and S12). These results demonstrate that oral administration of palbociclib induces senescence in veins in 4T1 orthotopic mice model, while senolytic treatment reduces the senescence burden in the endothelium.

3.5. Palbociclib treatment increases lung metastasis after the tail vein injection of TNBC cells

To corroborate the side effects of palbociclib in development of metastases and to discard the contribution of the primary tumor, healthy Balb/cByJ female mice (4-6 weeks) were treated with palbociclib daily (o.g.) for 15 days. Then, 0.5×10^6 4T1-Luc breast cancer cells were intravenously injected *via* the tail vein. Metastatic spread of cancer cells was monitored every 2-3 days by IVIS measuring luminescence. As we expected, after tail vein injection of the 4T1-Luc (stable luciferase expression) breast cancer cells, lung metastases were developed in all the animals (Figure 6). (Gomez-Cuadrado *et al.*, 2017) However,

animals treated with palbociclib showed an increased lung metastasic burden (Figure 6A and B). As figure 6C shows, palbociclib treatment induced a more rapid progression of metastasis in the lungs, thus suggesting the implication of palbociclib-associated vascular senescence in favoring the spread of cancer cells. Animals were maintained for 10 days until they started to lose weight (Figure S13C). Besides, lungs were obtained for further *ex vivo* analysis by IVIS imaging, thus corroborating the *in vivo* findings (Figure S13A and S13B). Furthermore, histological hematoxylin and eosin analysis of lungs demonstrated that the metastatic area formed by palbociclib treated mice was bigger as well showed more pulmonary metastatic nodules when compared to the vehicle (Figure 6D y 6E).

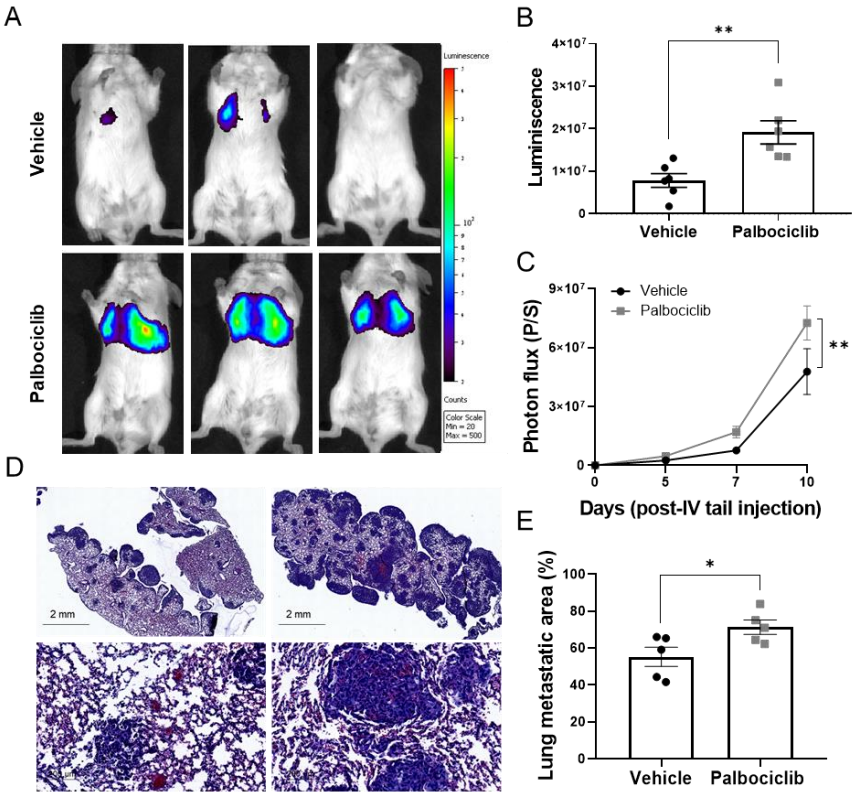

Figure 6 | Lung metastatic burden increases in palbociclib-treated animals. Healthy Balb/cByJ female mice (n=6) were treated with palbociclib daily (o.g.) for 15 days and then, 0.5×106 4T1-Luc breast cancer cells were intravenously injected to evaluate metastasic cell spread. (A) Representative IVIS images. (B) Quantification of tumor burden in lungs from IVIS images (day 10).

Each data point represents one mouse. (C) Quantification of lung photon flux (photons per second) after intravenous tail vein inoculation of cancer cells. (D) Representative H&E–stained lung sections with metastatic lesions: vehicle (left images) and palbociclib-treated mice (right images). Scale bar: 2 mm (top image), 200 μm (bottom image). (E) Quantification of lung metastasic area at day 10. Values are expressed as mean ± SEM and statistical significance was assessed by the two-tailed Student's T-test: *p<0.05.

Overall, these findings are consistent with the role of endothelial senescent cells as metastatic inductors in the tumor microenvironment and support senolysis induction as a method to eliminate them and reduce cancer cell migration limiting metastasis.

4. Discussion and conclusion

In recent years, the cellular senescence field has gained increased interest due to the possibility to use senescence inductors as an antitumor treatments in clinical settings.(Acosta and Gil, 2012) The senescence inductor palbociclib, a CDK 4/6 inhibitor, is currently approved by the FDA for use in combination with letrozole or fulvestrant in some breast cancer therapies(Beaver *et al.*, 2015; Walker *et al.*, 2016) and its efficacy for the treatment of other tumor types is being studied both in preclinical settings and clinical trials.(Grande *et al.*, 2020; Karasic *et al.*, 2020; Qin *et al.*, 2020; Sepúlveda-Sánchez *et al.*, 2020)

However, the incorporation of therapy-induced senescence in clinics is still recent and in a continuous effort to improve patient outcomes. These studies include the fact that persistent senescent cells in tumors can bypass growth arrest and favor tumor relapse.(Wang, Kohli and Demaria, 2020) Besides, senescent cells are also characterized by their associated secretory phenotype (SASP) which involves the secretion of cytokines, chemokines, growth factors, and metalloproteinases.(Rao and Jackson, 2016) SASP can play a detrimental role by creating a chronic sterile inflammation that alters the tissue microenvironment promoting inflammation, tissue damage, and invasion and proliferation of cancer cells which could lead to a potential threat of developing a secondary tumor with increased aggressiveness.(Demaria *et al.*, 2017; Gonzalez-Meljem

et al., 2018) While mechanisms by which CDK4/6 inhibitors block tumor cell proliferation are well-established, knowledge about the impact of these drugs on non-tumor cells is very limited. Senescent nontumor cells in tumor microenvironment also can play a dual role for cancer relapse and tumor cell dissemination.(Zhang, Lam and Sun, 2019)

Considering the functional relevance of endothelium in cancer relapse and metastasis, we evaluated the effect of palbociclib therapy in the endothelial cells. We confirmed that palbociclib induces senescence in human umbilical vein endothelial (HUVEC) cells after 7 days of treatment. Under these conditions, the majority of the HUVEC cells treated with palbociclib were senescent whereas in proliferating cultures only a minority of the population presented a senescence phenotype. HUVEC senescent cells showed a marked decrease in Ki67 expression, an increase in Saβ Gal activity and were cell cycle arrested. Besides, a marked reduction of phosphorylation of pRb protein in senescent HUVEC cells, when compared with proliferating cells, was observed. Interestingly, we found an increase of the expression of the leukocyte receptor VCAM1 in HUVEC senescent cells, which is a signal of endothelial dysfunction.(Liao, 2013) In fact, it has been reported that inflammatory cytokines, such as those secreted by senescence cells, induce the expression of VCAM1 on the endothelial cell surface.(Elices *et al.*, 1990) Endothelial VCAM1 expression enhances not only leukocyte extravasation but also has a role in facilitating tumor cell metastasis by inducing actin stress fiber formation and intercellular gaps.(Schlesinger and Bendas, 2015) The upregulation in VCAM1 expression led to the weakening of cell-to-cell junctions, and thereby to a higher rate of tumor cell transmigration.(Van Wetering *et al.*, 2003; Ferjančič *et al.*, 2013)

Regarding that a critical step in tumor metastasis is transendothelial migration of tumor cells at sites of intravasation and extravasation,(Reymond, D'Água and Ridley, 2013) we expected that the induction of senescence in endothelium might have a role in the metastatic dissemination of tumor cells. We found that migration of MDA-MB-231 breast cancer cells was increased in the presence of endothelial senescent HUVEC cells.

Interestingly, the presence of a monolayer of senescent fibroblasts does not change tumor cells transmigration rate. These results confirmed that endothelial senescence favors cancer cell migration in a specific manner and are align with Hwang et al.(Hwang *et al.*, 2020), who have recently proved that SASP from therapy-induced senescence endothelial cells promotes an aggressive behavior of cancer cells. The presence of senescent endothelial cells in a non-senescent monolayer disrupts tight junction morphology of surrounding young cells and increases the permeability of the monolayer indicating that the barrier function is compromised.(Vincent J D Krouwer, 2012) These results also are in agreement to those reported by Wieland et al.(Wieland *et al.*, 2017) in which the role of endothelial senescence-like phenotype to promote tumor cell migration to the circulation is demonstrated. Also, it has been recently published that, in models of pancreatic cancer, palbociclib-induced senescent cancer cells can alter and remodel the surrounding vasculature through the induction of a pro-angiogenic SASP (Ruscetti *et al.*, 2020), which might also have an impact in cancer cells migration. The disruption of the endothelial barrier in veins might facilitate the entry of tumor cells from the circulation and thereby plays an important role in cancer cell extravasation and metastasis.

Moreover, we also observed that proliferating non-senescent HUVEC cells formed many short tubes with multiple branches while senescent HUVEC cells appeared to form clusters reducing the number of branches. In co-cultures of proliferating and senescent HUVEC cells, tubes are also formed although the number of branches was reduced when compared with proliferating endothelial cells alone. These findings pointed the negative side effects of senescence accumulation for endothelium functionality and therefore tumor progression and metastasis. The blockage of VCAM1 and some inflammatory cytokines has recently been proposed for preventing cancer cell dissemination into other organs.(Swierczak *et al.*, 2015; Wculek and Malanchi, 2015) We postulated the use of the nanoencapsulated senolytic agent navitoclax NP(nav)-Gal as an effective strategy to selectively reduce endothelial senescence, with the aim to overcome the progression of tumor metastasis while avoiding associated toxicities of current navitoclax

therapy.(Galiana *et al.*, 2020) Senescent and non-senescent co-cultured HUVEC cells treated with free navitoclax or with NP(nav)-Gal show a noticeably recovery of the endothelium tube formation ability, recovering the barrier functionality disrupted by palbociclib senescent induction in endothelial cells. Moreover, we show, in a therapy-induced senescence triple negative breast cancer mouse *in vivo* model that treatment with Navitoclax or NP(nav)-Gal produced a reduction of endothelial senescent cells. In accordance with *in vitro* results this reduction correlates with a decrease of lung metastasis. Moreover, to discard the potential contribution of the primary tumor size in this observation, we treat healthy mice with vehicle or palbociclib for 15 days and injected 4T1 breast cancer cells intravenously by the tail vein to evaluate cancer cell spread. The results showed that palbociclib treated mice developed more aggressive lung metastasis than vehicle.

Overall, our findings exhibited that despite the unquestionable benefit that palbociclib has for cancer patients, the accumulation of senescent endothelial cells derived from the palbociclib treatment might be a risk for long term metastasis progression. The derived side effects of systemic palbociclib treatment have not been fully characterized. Considering its use in clinics, a long-term evaluation of possible side effects and the development of more specific delivery strategies might be of importance. Besides, further studies are needed to determine the role of senescence in tumor-promoting properties. In this way, our results strongly suggest that the elimination of endothelial senescent cells can be a suitable strategy to further improve patient outcome reducing cancer cell migration and thus limiting metastasis. These findings open promising complementary doors to improve cancer treatments. Moreover, the elimination of endothelial senescent cells can also serve as a basis for further investigation and involvement in other diseases, opening the possibility of generating new therapies aimed to selectively remove senescent cells.

5. Experimental section

5.1. Cell culture and senescence induction

Human umbilical cord endothelial cells (HUVEC), human breast triple-negative adenocarcinoma MDA-MB-231 cells, 4T1 mouse breast triple-negative adenocarcinoma and human dermal fibroblasts were obtained from ATCC. HUVEC were cultured in F-12K Medium (ATCC 30-2004) supplemented with 10% fetal bovine serum (FBS; Sigma), 0.1 mg/mL heparin (Sigma) and 0.03 mg/mLl endothelial cell growth supplement from bovine neural tissue (ECGS; Sigma). MDA-MB-231, 4T1 and fibroblast cells were maintained in DMEM (Sigma) supplemented with 10% fetal bovine serum (FBS; Sigma). All cell lines were incubated at 37 °C in 5% CO_2. For senescence induction, cells were supplemented with medium containing 2 µM palbociclib for a week (#S1116, Selleckchem) for HUVEC cells and 5 µM palbociclib for MDA-MB-231, 4T1 and fibroblast cells. Cells were routinely tested for mycoplasma contamination.

5.2. β-galactosidase activity assay

β-galactosidase staining was performed using the senescence β-galactosidase staining kit (Cell Signaling, #9860S) following the manufacturer's instructions. Briefly, cells were fixed with the fixative solution at room temperature for 15 min, whereas whole-tissue was fixed with 4% paraformaldehyde overnight. After fixation, cells or tissue were washed two times with PBS and incubated overnight at 37°C without CO_2 with the staining solution containing X-gal in N, N-dimethylformamide. Senescence-associated β-galactosidase enzymatic activity was determined at pH 6. Pictures were taken with a bright-field microscope.

5.3. Flow cytometric determination of β-galactosidase activity

To measure β-galactosidase activity by flow cytometry, we used the fluorogenic substrate C_{12}FDG as described. HUVEC cultures were pretreated with chloroquine (300 mM; Sigma-Aldrich, #C6628) to induce lysosomal alkalization. After 2 h, C_{12}FDG (33 mM; ThermoFisher, #D2893) was added in fresh media and incubated for 4 h at 37 °C under 5% CO_2. At the end of the incubation time, cells were collected using 0.5% Trypsin-EDTA (GIBCO) and resuspended in PBS. Flow cytometry was assessed on a CytoFlex S instrument (Beckman Coulter) followed by data analysis using CytoExpert software.

5.4. Western Blot

Whole-cell extracts were obtained by lysing cells in a buffer containing 25 mM Tris-HCl pH 7.4, 1 mM EDTA, 1% SDS, plus protease and phosphatase inhibitors. The protein concentration was determined by the BCA protein assay. Cell lysates were resolved by SDS-PAGE, transferred to nitrocellulose membranes, blocked with 5% nonfat milk, washed with 0.1% Tween/PBS and incubated overnight with a specific primary antibody. Membranes were washed and probed with the appropriate secondary antibody conjugated to horseradish peroxidase for enhanced chemiluminescence detection (Amersham Pharmacia Biotech).

The antibody against pRb (#9308) was from Cell Signaling, p53 antibody (#ab26) was from Abcam, VCAM1 (#13160) antibody was from Santa Cruz Biotechnology and GADPH antibody (#14C10) was from Cell Signaling. The secondary antibodies used were anti-Rabbit IgG peroxidase antibody (#A6154, Sigma) and peroxidase conjugate-goat anti-Mouse IgG antibody (#A4416, Sigma).

5.5. Ki67 Immunofluorescence

Cells were seeded on coverslips when cells were confluent they were fixed with 4% PFA permeabilized with 0.3% Triton X-100 and blocked with 5% BSA for 1 h. Then cells

were labeled with the primary antibody solution (1% BSA, 0.3% Triton X-100) containing Ki-67 (D3B5) Rabbit (#9129, Cell Signaling), overnight at 4 °C. The following incubation with anti-rabbit IgG Fluor Goat 633 (#A21071, Fisher) was performed for 2 h at room temperature. The coverslips were mounted on glass slides with Mowiol/DAPI (Sigma). Confocal microscopy images were obtained by using a Leica TCS SP8 HyVolution 2 microscope.

5.6. Conditioned media assay

HUVEC ($6 \cdot 10^4$) cells were seeded in 6-well plates and let then attached overnight. Media from proliferating and senescent HUVEC, MDA-MB-231 and 4T1 were obtained, centrifuged to eliminate dead cells (1200 rpm 5 min) and added to HUVEC cells dilute with fresh medium in a relation of 1:1. After 5 days, HUVEC cells were fixed with 4% PFA and X-gal staining was performed.

5.7. Tumor cells migration assay

Proliferating or senescent, HUVEC ($7.5 \cdot 10^4$ cells/insert) or fibroblasts cells ($2.5 \cdot 10^4$ cells/insert) were seeded in a drop on the bottom of a PET permeable (0.8 µM pore size) insert. After 16 h, the drop was aspirated, and new media was added to the insert to let the endothelial cells grow for 72 h. After 72 h MDA-MB-231 breast cancer cells ($3 \cdot 10^5$ cells/insert) were stained with cell tracker deep red (Fisher; #C34565) 5 µM for 1 h at 37 °C, seeded on the top of the insert and let them migrate for 2 h. HUVEC were stained with Hoechst. MDA-MB-231 migration was analyzed by confocal microscopy. IMAGE J was used to quantify the number of migrated MDA-MB-231 cells.

5.8. Synthesis of nanoparticles

Synthesis of the mesoporous silica nanoparticles (MSNs) were performed as described. Briefly, 1 g of N-cetyltrimethylammonium bromide (CTAB, Sigma, #H6269) was dissolved in 480 mL of deionized water and 3.5 mL of NaOH 2 M (Sigma, #1310732) was

added to the solution heated at 80 °C. Then, 5 mL of the polymeric precursor tetraethylorthosilicate (TEOS, Sigma, #131903) were added dropwise to the surfactant solution and the reaction was stirred and heated for further 2 h. The resulting white solid was isolated by centrifugation (10,000 rpm, 20 min) and washed with deionized water until pH 7 was reached. Finally, "as made" MSNs were dried at 70 ^{o}C and then calcined at 550 °C for 5 h using an oxidant atmosphere in order to remove the CTAB template, thus eliminating any residual surfactant that might affect cell viability.

Synthesis of gated MSNs coated with hexa-galactooligosaccharides and loaded with navitoclax (Active BioChem, #A1001) or indocyanine green (Sigma, #I2633) was performed as described in Figure 2 in Supporting Information. For NP(ICG)-Gal, 200 mg of calcined MSNs were suspended in 45 mL of water and 9.5 mg of indocyanine green were added (Sigma, #I2633). The mixture was stirred for 24 h at room temperature, and the nanoparticles were filtered and dried under vacuum (NP(ICG)). Then, the functionalization of the external surface was performed by the addition of 0.28 mL of (3-aminopropyl)triethoxysilane to a suspension of 200 mg of NP(ICG) in 6 mL of anhydrous acetonitrile. After stirring for 5.5 h at room temperature, the solid (NP(ICG)-NH2) was isolated by filtrations and dried under vacuum.

For the synthesis of NP(nav)-Gal, the nanoparticles were loaded with navitoclax by the addition of 155 mg of this drug to a suspension of 200 mg of calcined MSNs in 6 mL of anhydrous dichloromethane. After 24 h of stirring, 0.28 mL of (3-aminopropyl)triethoxysilane were added to the suspension and the stirring was kept for further 5.5 h. Then, the solid was isolated by filtration under vacuum (NP(nav)-NH_2).

On the other hand, NP-NH_2 was synthesized by adding 0.28 mL of (3-aminopropyl)triethoxysilane to a suspension of 200 mg of empty calcined MSNs in 6 mL of anhydrous acetonitrile. After 5.5 h, the functionalized solid was isolated by filtration under vacuum.

For coating with the hexa-galacto-oligosaccharide, the obtained solids functionalized with amino moieties were added to a solution of 500 mg of galactan (Carbosynth, #OG71532, consisting of six repeating galactose monosaccharides linked through β-1,4 glycosidic bonds) in 27 mL of water and stirring was continued at room temperature for 21 h. The final products (NP(ICG)-Gal, NP(nav)-Gal and NP-Gal) were filtered, washed with plenty of water and dried under vacuum. All the final nanoparticles were stored in a desiccator at room temperature.

5.9. Nanodevices characterization

Powder X-ray diffraction (PXRD), thermogravimetric analysis (TGA), transmission electron microscopy (TEM) and N_2 adsorption-desorption isotherms were used for nanoparticles' characterization. PXRD measurements were performed on a Seifert 3000TT diffractometer using Cu-Kα radiation. The thermogravimetric analyses were performed in TGA/SDTA 851e Mettler Toledo equipment in an oxidant atmosphere (air, 80 mL/min) with a heating program that consisted in a heating ramp of 10 ^{o}C/min from 393K to 1273K, and an isothermal heating step at this temperature for 30 min.

TEM images were acquired with a Philips CM10 microscope working at 100 kV. N_2 adsorption-desorption isotherms were recorded on a Micromeritics TriStar II Plus automated analyzer. The samples were degassed at 120 °C under vacuum overnight. The specific surface areas were calculated from the adsorption data in the low pressures range using the Brunauer–Emmett–Teller model. UV-visible spectroscopy was carried out with a Lambda 35 UV-Vis spectrometer (Perkin-Elmer Instruments), and fluorescence spectroscopy with a JASCO spectrofluorometer FP-8300. All the measurements were taken in triplicate.

5.10. Cargo release study of NP(nav)-Gal

For cargo release studies, 4 mg of NP(nav)-Gal nanoparticles were suspended in 10 mL of water at pH 4.5, stirred and the volume was separated in two suspensions of 5 mL. Then, 5 mg of β-galactosidase from Aspergillus oryzae was added to one of the suspensions. After a certain time, aliquots of 200 µL of each suspension were taken and 300 µL of ethyl acetate was added to each one. The mixture was stirred for 1 min, the ethyl acetate was taken, centrifuged and cargo release in the organic phases was measured by UV-vis spectroscopy (absorption band of navitoclax at 275 nm). The same procedure was performed without adding the enzyme to one of the suspensions, as a "blank" control.

5.11. Cargo release study of NP(ICG)-Gal

4 mg of NP(ICG)-Gal nanoparticles were suspended in 10 mL of water at pH 4.5, stirred and this volume was separated into two suspensions of 5 mL. Then, 5 mg of β-galactosidase from Aspergillus oryzae was added to one of the suspensions, and, after a certain time, an aliquot of 300 µL of each suspension was taken. Then, 2 µL of NaOH (0.15 M) was added to the aliquots, vigorously stirred for 3 min, centrifuged for removing the solid and cargo released was measured by fluorescence (λ_{exc} (ICG) = 775 nm, λ_{em} (ICG) = 805 nm). The same procedure was performed without adding the enzyme to one of the suspensions, as a "blank" control.

5.12. Confocal microscopy with NP(ICG)-Gal

Proliferating and senescent HUVEC cells were seeded on 6-multiwell plates at a concentration of 150.000 cells/well. After 24 h, cells were treated for 6 h with a suspension of NP(ICG)-Gal (1 mg/mL) previously filtered. After the incubation time, cells were washed with medium to eliminate non-internalized nanoparticles. For confocal

microscopy, coverslips were mounted and Hoechst 33342 was added for nuclei staining before cell visualization in Leica TCS SP8 HyVolution 2 microscope.

5.13. Flow cytometry with NP(ICG)-Gal

HUVEC cells ($2 \cdot 10^5$ cells/well) were seeded in 6-well plates. After 24 h, cells were treated with NP(ICG)-Gal (1 mg/mL). NP(ICG)-Gal nanoparticles were suspended in cell culture medium, sonicated and agitated for 1 h. After 6 h nanoparticle treatment, cells were collected using 0.5% Trypsin-EDTA (GIBCO) and resuspended in PBS. Flow cytometry was assessed on a CytoFlex S instrument (Beckman Coulter) followed by data analysis using CytoExpert software. As senescent cells are bigger in size than control cells a correction factor was applied by dividing mean intensity by mean FSC-width. We have also considered senescence autofluorescence (by subtracting it).

5.14. Drug toxicity assay

For drug screening assays, cells were trypsinized and replated in flat-bottom-clear 96-well plates (Greiner Bio-One, #655087). Proliferating and senescent HUVEC cells were plated at a density of 10^4 cells per well. After 24 h, free navitoclax or NP(nav)-Gal nanoparticles were added individually to the cells. Free navitoclax was added at a 20 µM final concentration. NP(nav)-Gal were added at a maximum of 2 mg/mL filtered (0.45 µm) which corresponds to 2.66 µM final concentration. After 72 h, viability was measured using CellTiter-Glo® luminescent cell viability assay (Promega, #G7571) kit following the manufacturer's instructions in a PerkinElmer life sciences wallac Victor2TM spectrophotometer. The number of viable cells was normalized to the internal control of untreated cells (DMSO only) of each plate. Non-lineal fit log(inhibitor) vs. response with a variable slope (four parameters) model was used for IC50 estimation in Graphad software. For colony formation assays cells were seeded at different densities in 24-well plates and incubated in a CO_2 incubator at 37 °C for 1 week. Colonies were fixed with 4% PFA and stained with 0.05% crystal violet solution.

5.15. Tube formation assay

Briefly, 65 µL of growth factor reduced matrigel (Corning) was added per well in a 96 well plate, and HUVEC cells (1×10^4 cells) were added and incubated in media with different treatments. 25.000 proliferating cells and 75.000 senescent cells (1:3 ratio) were plated for cocultured. Cells were pretreated with 0.5 mg/mL NP(nav)-Gal filtered (0.66 µM navitoclax) or with 1 µM free navitoclax for 48 h. For quantitative measurements of capillary tube formation, matrigel wells were digitized under a 5x objective (Leica TCS SP8 HyVolution 2) for measurement of the total number of branches at 3 h. AngioTool was used to analyzed tube formation assay.

5.16. 4T1 orthotopic mice model

Female BALB/cByJ wild type mice (28-34 days old) were purchased from Charles River Laboratories, and maintained in ventilated racks under pathogen-free conditions at Principe Felipe Research Centre (Valencia, Spain), with food and water ad libitum and alternate dark and light cycles. All animals were treated humanely and experiments were approved by the Ethical Committee for Research and Animal Welfare. For each group, 4 mice were used for statistical significance. Mice were injected subcutaneously in the second lower right breast with a cellular concentration of $5\cdot10^5$ early passage 4T1 cells as described in Galiana *et al.,* 2020 Palbociclib for senescence induction was administrated for 17 days by daily oral gavage (100 mg/kg) dissolved in sodium lactate 50 mM at 16.5 mg/mL. One day after the start of palbociclib treatment, free navitoclax (oral gavage, 25 mg/kg) or NP(nav)-Gal (intraperitoneal injection, 40 mg NP(nav)-Gal/kg (equivalent to 2.5 mg/kg of free Navitoclax)) treatment was given daily for 16 days. At the end of the treatment, animals were euthanized in a CO_2 atmosphere and tumors, lungs and cava veins were extracted for posterior evaluation.

5.17. 4T1-Luc metastatic model

Female BALB/cByJ wild type mice (28-34 days old) (Charles River Laboratories) were treated for 15 days with palbociclib by daily oral gavage (50 mg/kg) dissolved in sodium lactate 50 mM at 16.5 mg/mL. At the end of the treatment, $5 \cdot 10^5$ early passage 4T1-Luc (4T1 cell line that express constitutively the luciferase gene) cells were injected intravenously in the tail in a volume of 100 µL. Mice were monitored on an IVIS spectrum imaging system. D-luciferin were administered via subcutaneous injection, 10 minutes prior to image acquisition. and bioluminescence signal was analyzed by using the Living Imaging software from Caliper Life Sciences. In vivo lung metastasis was quantified as photons/second.

5.18. Organs X-gal and hematoxylin-eosin staining

Organs were fixed in 4% PFA. After tumor and veins were staining with X-gal. Veins and lungs were embedded in paraffin for tissue sections and hematoxylin-eosin staining. Stained sections were scanned in Leica Aperio Versa at 20x magnification. X-gal positive cells were quantified automatically with Image J software by measuring the mean intensity. Metastatic 4T1 cell clusters were microscopically counted in different lung sections from a minimum of three animals per group.

5.19. Fluorescent Immunohistochemistry

Cava veins were removed, washed 1x PBS and fixed with 4% PFA overnight at 4 °C. The fixative was aspirated, and samples were washed 1x PBS and incubated with 30% sucrose overnight at 4 °C. Fixed tissues were embedded in optimal cutting temperature compound in cryomolds and frozen completely at −20 °C. 10 µm thick tumor sections were then incubated in blocking solution (5% horse serum, 0.3% triton X-100 in 1× PBS) for 1 h and immunostained following incubation with primary antibodies overnight at 4 °C. p53 antibody was used at 1:100 (pAb240) Mouse (ab26, Abcam), VCAM1 antibody was used

at 1:12.5 Mouse (MA5-11447, Invitrogen). Secondary antibodies against rabbit or mouse conjugated to Alexa Fluor 488 (Invitrogen) were used at 1:200 dilution. Sections were mounted on microscope slides using the Mowiol/DAPI (Sigma) and covered with a glass coverslip. Confocal microscopy images were obtained by using a Leica TCS SP8 HyVolution 2 microscope.

5.20. Statistical Analysis

All of the values represent the mean ± SEM of at least three independent experiments. Significance was determined by one-way or two-way ANOVA followed by a Tukey posttest or by Student's T-test using GraphPad Prism software 8. $P < 0.05$ was considered statistically significant.

6. References

Acosta, J. C. and Gil, J. (2012) 'Senescence: A new weapon for cancer therapy', Trends in Cell Biology, pp. 211–219. doi: 10.1016/j.tcb.2011.11.006.

Agostini, A. et al. (2012) 'Targeted cargo delivery in senescent cells using capped mesoporous silica nanoparticles', Angewandte Chemie - International Edition, 51(42), pp. 10556–10560. doi: 10.1002/anie.201204663.

Al-Soudi, A., Kaaij, M. H. and Tas, S. W. (2017) 'Endothelial cells: From innocent bystanders to active participants in immune responses', Autoimmunity Reviews. Elsevier B.V., pp. 951–962. doi: 10.1016/j.autrev.2017.07.008.

El Assar, M. et al. (2012) 'Mechanisms involved in the aging-induced vascular dysfunction', Frontiers in Physiology, 3 MAY. doi: 10.3389/fphys.2012.00132.

Aznar, E. et al. (2016) 'Gated Materials for On-Command Release of Guest Molecules', Chemical Reviews, 116(2), pp. 561–718. doi: 10.1021/acs.chemrev.5b00456.

Beaver, J. A. et al. (2015) 'FDA Approval: Palbociclib for the Treatment of Postmenopausal Patients with Estrogen Receptor-Positive, HER2-Negative Metastatic Breast Cancer.', Clinical cancer research : an official journal of the American Association for Cancer Research, 21(21), pp. 4760–6. doi: 10.1158/1078-0432.CCR-15-1185.

Braig, M. et al. (2005) 'Oncogene-induced senescence as an initial barrier in lymphoma development', Nature, 436(7051), pp. 660–665. doi: 10.1038/nature03841.

Bussian, T. J. et al. (2018) 'Clearance of senescent glial cells prevents tau-dependent pathology and cognitive decline.', Nature, 562(7728), pp. 578–582. doi: 10.1038/s41586-018-0543-y.

Butler, J. M., Kobayashi, H. and Rafii, S. (2010) 'Instructive role of the vascular niche in

promoting tumor growth and tissue repair by angiocrine factors', Nature Reviews Cancer, pp. 138–146. doi: 10.1038/nrc2791.

Cang, S. et al. (2015) 'ABT-199 (venetoclax) and BCL-2 inhibitors in clinical development', Journal of Hematology and Oncology. BioMed Central Ltd. doi: 10.1186/s13045-015-0224-3.

Castillo, R. R. and Vallet-Regí, M. (2019) 'Functional Mesoporous Silica Nanocomposites: Biomedical applications and Biosafety.', International Journal of Molecular Sciences, 20(4), p. 929. doi: 10.3390/ijms20040929.

Chang, J. et al. (2016) 'Clearance of senescent cells by ABT263 rejuvenates aged hematopoietic stem cells in mice', Nature Medicine, 22(1), pp. 78–83. doi: 10.1038/nm.4010.

Chen, Z. et al. (2005) 'Crucial role of p53-dependent cellular senescence in suppression of Pten-deficient tumorigenesis.', Nature, 436(7051), pp. 725–30. doi: 10.1038/nature03918.

Childs, B. G. et al. (2014) 'Senescence and apoptosis: dueling or complementary cell fates?', EMBO reports, 15(11), pp. 1139–1153. doi: 10.15252/embr.201439245.

Collado, M. et al. (2005) 'Senescence in premalignant tumors', 436(7051), pp. 642–642. doi: 10.1038/436642a.

Coppé, J.-P. et al. (2010) 'The Senescence-Associated Secretory Phenotype: The Dark Side of Tumor Suppression', Annual Review of Pathology: Mechanisms of Disease, 5(1), pp. 99–118. doi: 10.1146/annurev-pathol-121808-102144.

Demaria, M. et al. (2014) 'An essential role for senescent cells in optimal wound healing through secretion of PDGF-AA', Developmental Cell, 31(6), pp. 722–733. doi: 10.1016/j.devcel.2014.11.012.

Demaria, M. et al. (2017) 'Cellular senescence promotes adverse effects of chemotherapy and cancer relapse', Cancer Discovery, 7(2), pp. 165–176. doi: 10.1158/2159-8290.CD-16-0241.

DuPré, S. A. et al. (2007) 'The mouse mammary carcinoma 4T1: characterization of the cellular landscape of primary tumors and metastatic tumor foci.', International journal of experimental pathology, 88(5), pp. 351–60. doi: 10.1111/j.1365-2613.2007.00539.x.

Eggert, T. et al. (2016) 'Distinct Functions of Senescence-Associated Immune Responses in Liver Tumor Surveillance and Tumor Progression', Cancer Cell, 30(4), pp. 533–547. doi: 10.1016/j.ccell.2016.09.003.

Elices, M. J. et al. (1990) 'VCAM-1 on activated endothelium interacts with the leukocyte integrin VLA-4 at a site distinct from the VLA-4/Fibronectin binding site', Cell, 60(4), pp. 577–584. doi: 10.1016/0092-8674(90)90661-W.

Ferjančič, Š. et al. (2013) 'VCAM-1 and VAP-1 recruit myeloid cells that promote pulmonary metastasis in mice', Blood, 121(16), pp. 3289–3297. doi: 10.1182/blood-2012-08-449819.

Finn, R. R. S. et al. (2015) 'The cyclin-dependent kinase 4/6 inhibitor palbociclib in combination with letrozole versus letrozole alone as first-line treatment of oestrogen receptor-positive, HER2-negative, advanced breast cancer (PALOMA-

1/TRIO-18): A randomised phase 2 study', The Lancet Oncology, 16(1), pp. 25–35. doi: 10.1016/S1470-2045(14)71159-3.

Finn, R. S. et al. (2009) 'PD 0332991, a selective cyclin D kinase 4/6 inhibitor, preferentially inhibits proliferation of luminal estrogen receptor-positive human breast cancer cell lines in vitro', Breast Cancer Research, 11(5), pp. 1–13. doi: 10.1186/bcr2419.

Finn, R. S. et al. (2016) 'Palbociclib and Letrozole in Advanced Breast Cancer', New England Journal of Medicine, 375(20), pp. 1925–1936. doi: 10.1056/NEJMoa1607303.

Fry, D. W. et al. (2004) 'Specific inhibition of cyclin-dependent kinase 4/6 by PD 0332991 and associated antitumor activity in human tumor xenografts.', Molecular cancer therapeutics, 3(11), pp. 1427–38. Available at: http://www.ncbi.nlm.nih.gov/pubmed/15542782 (Accessed: 4 September 2019).

Galiana, I. et al. (2020) 'Preclinical antitumor efficacy of senescence-inducing chemotherapy combined with a nanoSenolytic', Journal of Controlled Release, 323, pp. 624–634. doi: 10.1016/j.jconrel.2020.04.045.

García-Fernández, A. et al. (2020) 'New Advances in In Vivo Applications of Gated Mesoporous Silica as Drug Delivery Nanocarriers', Small, 16(3), pp. 1–62. doi: 10.1002/smll.201902242.

Goel, S. et al. (2018) 'CDK4/6 Inhibition in Cancer: Beyond Cell Cycle Arrest', Trends in Cell Biology. Elsevier Ltd, pp. 911–925. doi: 10.1016/j.tcb.2018.07.002.

Gomez-Cuadrado, L. et al. (2017) 'Mouse models of metastasis: Progress and prospects', DMM Disease Models and Mechanisms. Company of Biologists Ltd, pp. 1061–1074. doi: 10.1242/dmm.030403.

González-Gualda, E. et al. (2020) 'Galacto-conjugation of Navitoclax as an efficient strategy to increase senolytic specificity and reduce platelet toxicity', Aging Cell, 19(4), pp. 1–19. doi: 10.1111/acel.13142.

Gonzalez-Meljem, J. M. et al. (2018) 'Paracrine roles of cellular senescence in promoting tumorigenesis', 118(10), pp. 1283–1288. Available at: https://pubmed.ncbi.nlm.nih.gov/29670296/ (Accessed: 20 November 2019).

Grande, E. et al. (2020) 'The PALBONET Trial: A Phase II Study of Palbociclib in Metastatic Grade 1 and 2 Pancreatic Neuroendocrine Tumors (GETNE-1407)', The Oncologist, 25(9), p. 745. doi: 10.1634/theoncologist.2020-0033.

Hayflick, L. and Moorhead, P. S. (1961) 'The serial cultivation of human diploid cell strains', Experimental Cell Research, 25(3), pp. 585–621. doi: 10.1016/0014-4827(61)90192-6.

Hernandez-Segura, A., Nehme, J. and Demaria, M. (2018) 'Hallmarks of Cellular Senescence', Trends in Cell Biology, 28(6), pp. 436–453. doi: 10.1016/j.tcb.2018.02.001.

Hu, J.-J. et al. (2017) 'A positive feedback strategy for enhanced chemotherapy based on ROS-triggered self-accelerating drug release nanosystem', Biomaterials, 128, pp. 136–146. doi: 10.1016/J.BIOMATERIALS.2017.03.010.

Hwang, H. J. et al. (2020) 'Endothelial cells under therapy-induced senescence secrete CXCL11, which increases aggressiveness of breast cancer cells', Cancer Letters, 490(June), pp. 100–110. doi: 10.1016/j.canlet.2020.06.019.

Iannello, A. et al. (2013) 'p53-dependent chemokine production by senescent tumor cells supports NKG2D-dependent tumor elimination by natural killer cells', The Journal of Experimental Medicine, 210(10), pp. 2057–2069. doi: 10.1084/jem.20130783.

Kang, T.-W. et al. (2011) 'Senescence surveillance of pre-malignant hepatocytes limits liver cancer development', Nature, 479(7374), pp. 547–551. doi: 10.1038/nature10599.

Karasic, T. B. et al. (2020) ' Phase II Trial of Palbociclib in Patients with Advanced Esophageal or Gastric Cancer ', The Oncologist. doi: 10.1634/theoncologist.2020-0681.

Kim, H.-N. N. et al. (2017) 'DNA damage and senescence in osteoprogenitors expressing Osx1 may cause their decrease with age', Aging Cell, 16(4), pp. 693–703. doi: 10.1111/acel.12597.

Kirkland, J. L. and Tchkonia, T. (2020) 'Senolytic drugs: from discovery to translation', Journal of Internal Medicine, 288(5), pp. 518–536. doi: 10.1111/joim.13141.

Krizhanovsky, V. et al. (2008) 'Senescence of Activated Stellate Cells Limits Liver Fibrosis', Cell, 134(4), pp. 657–667. doi: 10.1016/j.cell.2008.06.049.

Kumar, P. et al. (2009) 'Molecular mechanisms of endothelial hyperpermeability: Implications in inflammation', Expert Reviews in Molecular Medicine. Expert Rev Mol Med. doi: 10.1017/S1462399409001112.

Kwapisz, D. (2017) 'Cyclin-dependent kinase 4/6 inhibitors in breast cancer: palbociclib, ribociclib, and abemaciclib.', Breast cancer research and treatment, 166(1), pp. 41–54. doi: 10.1007/s10549-017-4385-3.

Liao, J. K. (2013) 'Linking endothelial dysfunction with endothelial cell activation', Journal of Clinical Investigation, 123(2), pp. 540–541. doi: 10.1172/JCI66843.

Llopis-Lorente, A., DÍez, P., et al. (2017) 'Interactive models of communication at the nanoscale using nanoparticles that talk to one another', Nature Communications, 8(1), pp. 1–7. doi: 10.1038/ncomms15511.

Llopis-Lorente, A., Lozano-Torres, B., et al. (2017) 'Mesoporous silica materials for controlled delivery based on enzymes', Journal of Materials Chemistry B, 5(17), pp. 3069–3083. doi: 10.1039/c7tb00348j.

Lozano-Torres, B. et al. (2019) 'The chemistry of senescence', Nature Reviews Chemistry, 3(7), pp. 426–441. doi: 10.1038/s41570-019-0108-0.

de Luis, B. et al. (2019) 'An Interactive Model of Communication between Abiotic Nanodevices and Microorganisms', Angewandte Chemie - International Edition, 58(42), pp. 14986–14990. doi: 10.1002/anie.201908867.

Lüscher, T. F. and Barton, M. (1997) 'Biology of the endothelium.', Clinical cardiology, 20(11 Suppl 2), pp. II-3–10. Available at: http://www.ncbi.nlm.nih.gov/pubmed/9422846 (Accessed: 20 November 2019).

Michaloglou, C. et al. (2005) 'BRAFE600-associated senescence-like cell cycle arrest of human naevi', Nature, 436(7051), pp. 720–724. doi: 10.1038/nature03890.

Muñoz-Espín, D. et al. (2018) 'A versatile drug delivery system targeting senescent cells', EMBO Molecular Medicine, 10(9). doi: 10.15252/emmm.201809355.

Pernas, S. et al. (2018) CDK4/6 inhibition in breast cancer: current practice and future directions, Therapeutic Advances in Medical Oncology. SAGE Publications Inc. doi:

10.1177/1758835918786451.

Pu, X. et al. (2019) 'Mesoporous Silica Nanoparticles as a Prospective and Promising Approach for Drug Delivery and Biomedical Applications', Current Cancer Drug Targets, 19(4), pp. 285–295. doi: 10.2174/1568009619666181206114904.

Pulaski, B. A., Ostrand-Rosenberg, S. and Ostrand-Rosenberg, S. (2000) 'Mouse 4T1 Breast Tumor Model', Current Protocols in Immunology, 39(1), pp. 1–16. doi: 10.1002/0471142735.im2002s39.

Qin, Q. et al. (2020) 'CDK4/6 inhibitor palbociclib overcomes acquired resistance to third-generation EGFR inhibitor osimertinib in non-small cell lung cancer (NSCLC)', Thoracic Cancer, 11(9), pp. 2389–2397. doi: 10.1111/1759-7714.13521.

Rao, S. G. and Jackson, J. G. (2016) 'SASP: Tumor Suppressor or Promoter? Yes!', Trends in cancer, 2(11), pp. 676–687. doi: 10.1016/j.trecan.2016.10.001.

Reymond, N., D'Água, B. B. and Ridley, A. J. (2013) 'Crossing the endothelial barrier during metastasis', Nature Reviews Cancer, 13(12), pp. 858–870. doi: 10.1038/nrc3628.

Ritschka, B. et al. (2017) 'The senescence-associated secretory phenotype induces cellular plasticity and tissue regeneration', Genes & Development, 31(2), pp. 172–183. doi: 10.1101/gad.290635.116.

Ruhland, M. K., Coussens, L. M. and Stewart, S. A. (2016) 'Senescence and cancer: An evolving inflammatory paradox', Biochimica et Biophysica Acta - Reviews on Cancer, 1865(1), pp. 14–22. doi: 10.1016/j.bbcan.2015.10.001.

Ruscetti, M. et al. (2020) 'Senescence-Induced Vascular Remodeling Creates Therapeutic Vulnerabilities in Pancreas Cancer', Cell, 181(2), pp. 424-441.e21. doi: 10.1016/j.cell.2020.03.008.

Schlesinger, M. and Bendas, G. (2015) 'Vascular cell adhesion molecule-1 (VCAM-1) - An increasing insight into its role in tumorigenicity and metastasis', International Journal of Cancer. Wiley-Liss Inc., pp. 2504–2514. doi: 10.1002/ijc.28927.

Sepúlveda-Sánchez, J. M. et al. (2020) 'Phase II Trial of Palbociclib in Recurrent Retinoblastoma-Positive Anaplastic Oligodendroglioma: A Study from the Spanish Group for Research in Neuro-Oncology (GEINO)', Targeted Oncology, 15(5), pp. 613–622. doi: 10.1007/s11523-020-00754-6.

Shenoy, A. K. and Lu, J. (2016) 'Cancer cells remodel themselves and vasculature to overcome the endothelial barrier', Cancer Letters. Elsevier Ireland Ltd, pp. 534–544. doi: 10.1016/j.canlet.2014.10.031.

Soto-Gamez, A. and Demaria, M. (2017) 'Therapeutic interventions for aging: the case of cellular senescence', Drug Discovery Today, 22(5), pp. 786–795. doi: 10.1016/j.drudis.2017.01.004.

Swierczak, A. et al. (2015) 'Neutrophils: important contributors to tumor progression and metastasis', Cancer and Metastasis Reviews, 34(4), pp. 735–751. doi: 10.1007/s10555-015-9594-9.

Vincent J D Krouwer (2012) 'Endothelial cell senescence is associated with\rdisrupted cell-cell junctions and increased\rmonolayer permeability', Vascular Cell, 4, pp. 1–10.

Walker, A. J. et al. (2016) 'FDA Approval of Palbociclib in Combination with Fulvestrant for the Treatment of Hormone Receptor-Positive, HER2-Negative Metastatic Breast

Cancer', Clinical Cancer Research, 22(20), pp. 4968–4972. doi: 10.1158/1078-0432.CCR-16-0493.

Wang, B., Kohli, J. and Demaria, M. (2020) 'Senescent Cells in Cancer Therapy: Friends or Foes?', Trends in Cancer, 6(10), pp. 838–857. doi: 10.1016/j.trecan.2020.05.004.

Wculek, S. K. and Malanchi, I. (2015) 'Neutrophils support lung colonization of metastasis-initiating breast cancer cells', Nature, 528(7582), pp. 413–417. doi: 10.1038/nature16140.

Van Wetering, S. et al. (2003) 'VCAM-1-mediated Rac signaling controls endothelial cell-cell contacts and leukocyte transmigration', American Journal of Physiology - Cell Physiology, 285(2 54-2). doi: 10.1152/ajpcell.00048.2003.

Wieland, E. et al. (2017) 'Endothelial Notch1 Activity Facilitates Metastasis', Cancer Cell, 31(3), pp. 355–367. doi: 10.1016/j.ccell.2017.01.007.

Wu, S.-H., Mou, C.-Y. and Lin, H.-P. (2013) 'Synthesis of mesoporous silica nanoparticles', Chemical Society Reviews, 42(9), p. 3862. doi: 10.1039/c3cs35405a.

Yang, P., Gai, S. and Lin, J. (2012) 'Functionalized mesoporous silica materials for controlled drug delivery', Chemical Society Reviews, 41(9), p. 3679. doi: 10.1039/c2cs15308d.

Yin, P. T. et al. (2018) 'Overcoming Chemoresistance in Cancer via Combined MicroRNA Therapeutics with Anticancer Drugs Using Multifunctional Magnetic Core–Shell Nanoparticles', ACS Applied Materials & Interfaces, 10(32), pp. 26954–26963. doi: 10.1021/acsami.8b09086.

Yun, M. H., Davaapil, H. and Brockes, J. P. (2015) 'Recurrent turnover of senescent cells during regeneration of a complex structure.', eLife, 4. doi: 10.7554/eLife.05505.

Zhang, B., Lam, E. W. F. and Sun, Y. (2019) 'Senescent cells: A new Achilles' heel to exploit for cancer medicine?', Aging Cell, 18(1), pp. 1–8. doi: 10.1111/acel.12875.

Zhang, L. et al. (2016) 'Tailored Synthesis of Octopus-type Janus Nanoparticles for Synergistic Actively-Targeted and Chemo-Photothermal Therapy', Angewandte Chemie International Edition, 55(6), pp. 2118–2121. doi: 10.1002/anie.201510409.

Zhu, Y. et al. (2015) 'The Achilles' heel of senescent cells: from transcriptome to senolytic drugs', Aging cell, 14(4), pp. 644–658. doi: 10.1111/acel.12344.

Zhu, Y. et al. (2016) 'Identification of a novel senolytic agent, navitoclax, targeting the Bcl-2 family of anti-apoptotic factors', Aging Cell, 15(3), pp. 428–435. doi: 10.1111/acel.12445.

7. Supporting information

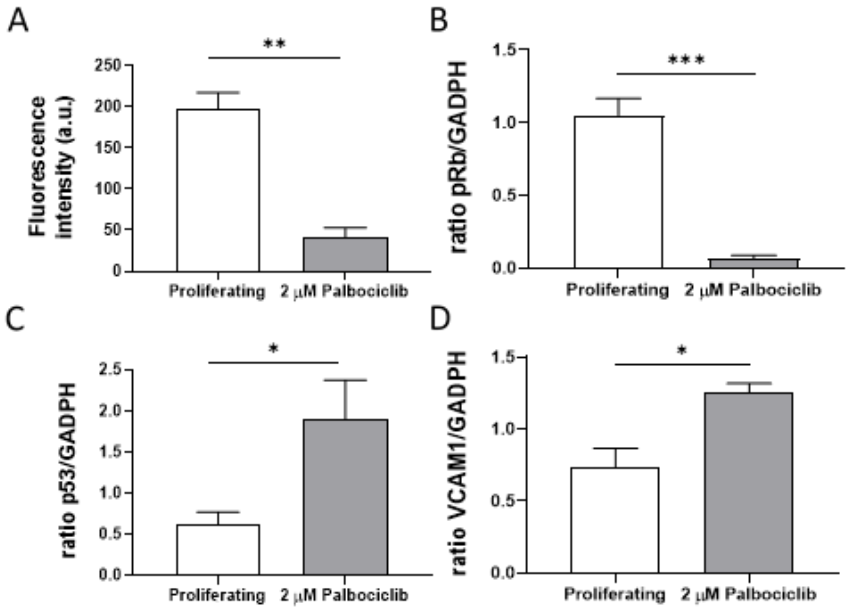

Figure S1 | Characterization of endothelial senescence induced by palbociclib. (A) Quantification of confocal microscopy images of immunofluorescence of Ki67 (red) in proliferating and senescent HUVEC cells. Values are expressed as mean ± SEM and statistical significance was assessed by the two-tailed Student's T-test: ** $p<0.005$. (B) Quantification of the Western Blot pRb bands in proliferating and senescent HUVEC cells using GADPH as a loading control. (C) Quantification of the Western Blot p53 bands in proliferating and senescent HUVEC cells using GADPH as a loading control. (D) Quantification of the Western Blot VCAM1 bands in proliferating and senescent HUVEC cells using GADPH as a loading control. Values are expressed as mean ± SEM and statistical significance was assessed by the two-tailed Student's T-test: *$p<0.05$; **$p<0.005$; ***$p < 0.0005$.

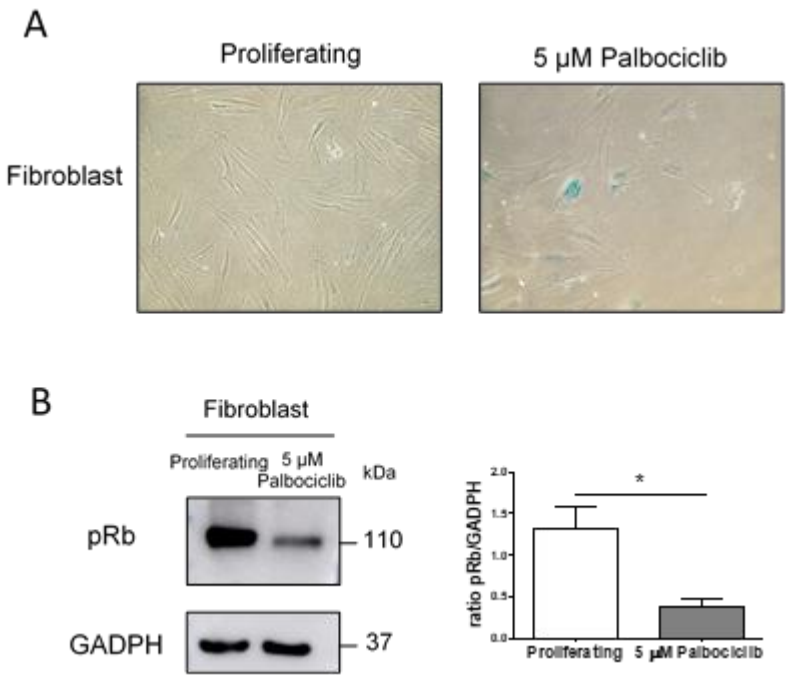

Figure S2 | Characterization of induction of fibroblast senescence. (A) β-Galactosidase staining of proliferating and 5 µM palbociclib-treated fibroblast cells. Senescence induction was confirmed by high β-Galactosidase activity (blue color) in palbociclib-treated cells at pH 6. (B) Western Blot characterization of proliferating and senescent fibroblast. Phosphorylation of retinoblastoma protein (pRb) decreases after palbociclib treatment (expected band at 110 kDa). Quantification of the bands using GADPH as a loading control (n=3) (right panel). Values are expressed as mean ± SD and statistical significance was assessed by the two-tailed Student's T-test: *p<0.05

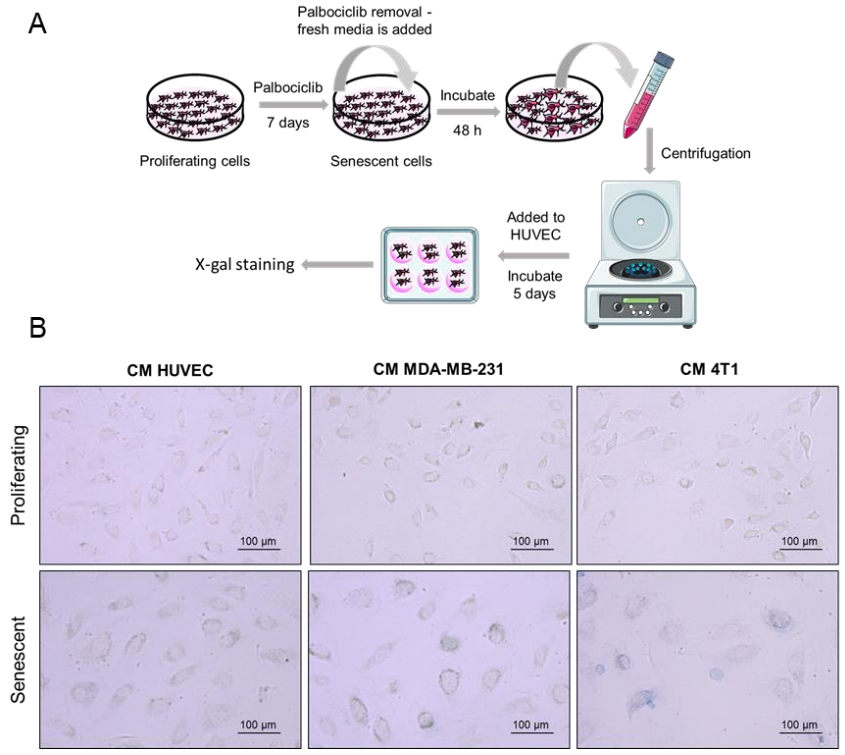

Figure S3 | Conditioned media of senescent HUVEC, MDA-MB-231 or 4T1 breast cancer cells induce senescence. (A) Schematic representation of conditioned media assay. Endothelial HUVEC cells or breast cancer MDA-MB-231 or 4T1 cells were treated with palbociclib for 7 days. After 7 days, palbociclib was removed and fresh media was added to the cell culture. 48 h later, conditioned media (CM) was collected and centrifugated to eliminate death cells. CM were added to proliferating HUVEC cells and incubate for 5 days. X-gal staining was performed afterwards to evaluate induction of senescence. (B) Xgal staining of endothelial HUVEC cells after conditioned media treatment.

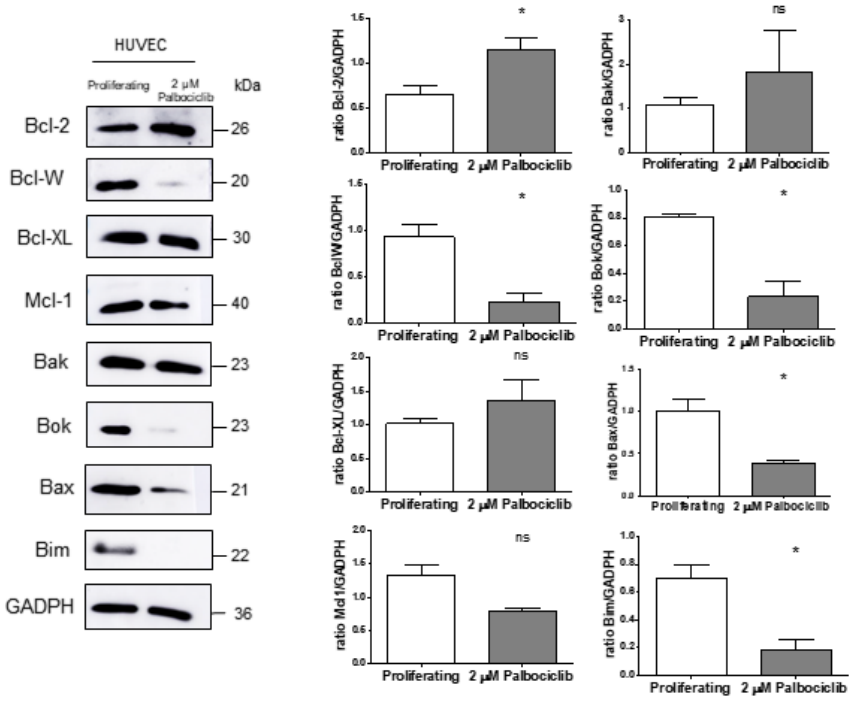

Figure S4 | Western Blot characterization of BCL2 family proteins in proliferating and senescent HUVEC. Quantification of the bands using GADPH as a loading control (n=3) (right panel). Values are expressed as mean ± SD and statistical significance was assessed by the two-tailed Student's T-test: *p<0.05.

7.1. Materials characterization

The PXRD patterns of the "as made" MSNs showed four main peaks at low angles that can be indexed as the (100), (110), (200) and (210) Bragg reflections, that are characteristic of hexagonal ordered mesoporous materials (Figure S6). A slight shift in 2θ values of these reflections in the calcined MSNs was observed, ascribed to the removal of the surfactant and the condensation of silanol groups during the calcination process. In the final nanodevices NP(ICG)-Gal and NP(nav)-Gal the (200) and (210) peaks are lost, most likely due to a reduction of contrast due to pore filling and surface functionalization. However, the preservation of the (100) reflection in their PXRD patterns indicated that the 3D mesoporous structure was preserved during the pore loading process and additional functionalization with the corresponding oligosaccharide. On the other hand, TEM analysis of the prepared nanodevices (Figure S5) showed that nanoparticles exhibited a spherical geometry with a diameter of ca. 100 nm. Besides, TEM images showed the typical channels of the MCM-41 matrix visualized as alternate black and white strips.

N_2 adsorption-desorption isotherms of the calcined MSNs showed a type IV isotherm, typical of the mesoporous silica materials, in which two sharp adsorption steps can be observed (Figure S7A). The first adsorption step at P/P_0 below 0.3 is ascribed to nitrogen condensation inside the empty pores. Moreover, the narrow pore size distribution (inset, Figure S7) and the absence of the hysteresis loop in this range suggested the presence of uniform cylindrical mesopores. In the N_2 adsorption-desorption isotherms of NP-Gal and NP(ICG)-Gal, a significant decrease in the adsorbed N_2 volume and surface area can be observed, as a consequence of the cargo loading inside the mesopores and functionalization of the outer surface with the oligosaccharide (Figures S7B and S7C). Total surface-specific areas were calculated by applying the BET model. Additionally, in order to calculate pore size and volume, the BJH model was applied to the adsorption band of the isotherm for $P/P_0 < 0.6$. All data are summarized in Table S1.

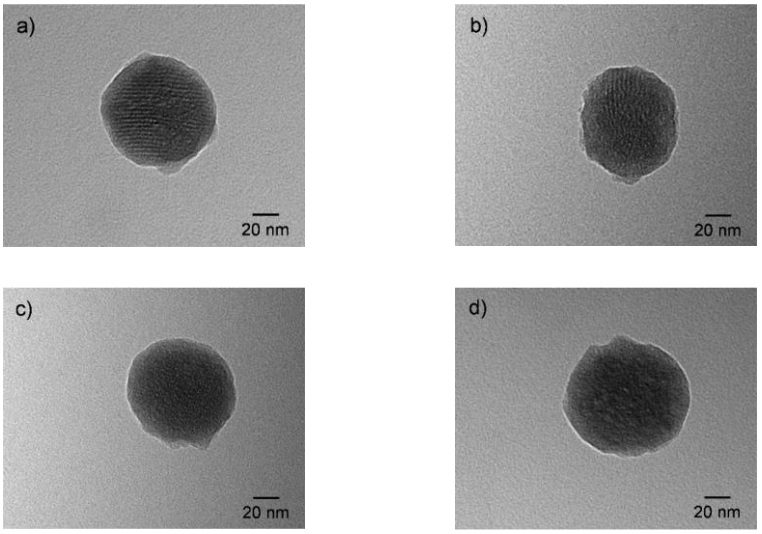

Figure S5 | TEM analysis of (a) calcined MSNs, (b) NP-Gal, (c) NP(nav)-Gal and (d) NP(ICG)-Gal.

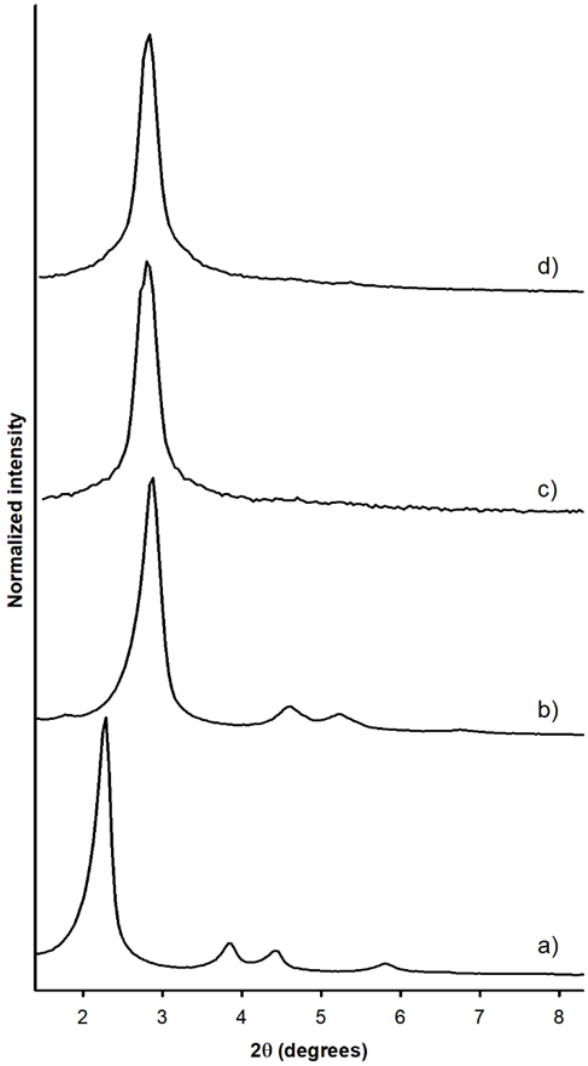

Figure S6 | Powder X-Ray diffraction patterns at low (left) and high (right) angles of (a) starting MSNs, (b) calcined MSNs, (c) NP(ICG)-Gal and (d) NP-Gal.

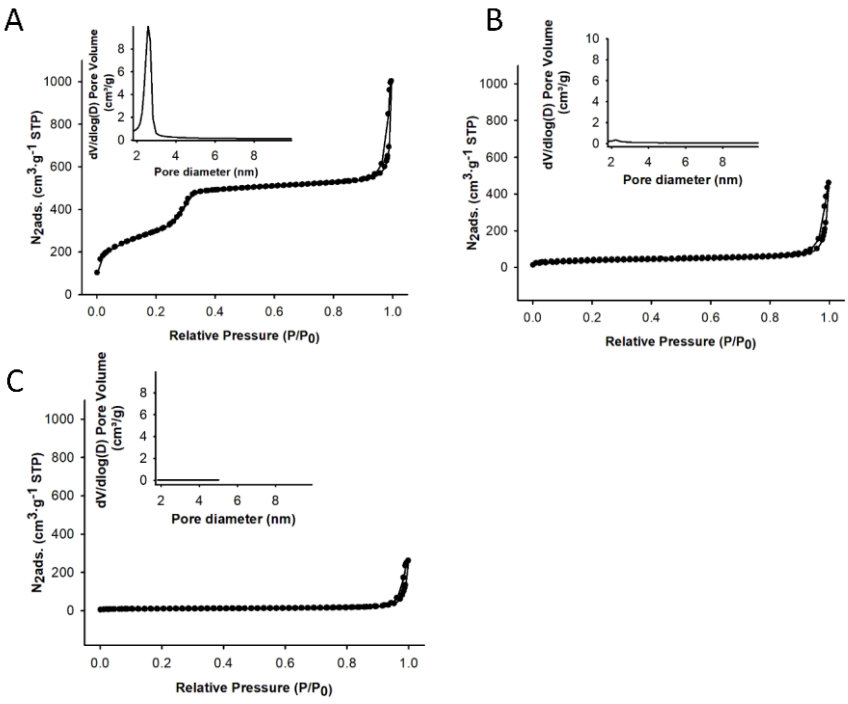

Figure S7| N_2 adsorption-desorption isotherms for (a) calcined MSNs, (b) NP(ICG)-Gal and (c) NP-Gal.

Table S1 | BET specific surface area, pore volumes and pore sizes calculated from N_2 adsorption-desorption isotherms for indicated materials.

Sample	SBET [m^2g^{-1}]	Pore Volume [cm^3g^{-1}]	Pore size [nm]
calcined MSNs	1087.29	0.92	2.62
NP-Gal	28.31	0.01	--
NP(ICG)-Gal	131.12	0.10	--

Table S2 | Hydrodynamic diameter and Zeta potential of selected materials.

Solid	Hydrodynamic particle diameter (nm)	Zeta potential (mV)
calcined MSNs	162.6 ± 1.8	-21.6 ± 0.7
NP-Gal	218.4 ± 1.4	-17.6 ± 0.6
NP(ICG)-Gal	211.6 ± 2.0	-14.6 ± 0.2
NP(nav)-Gal	285.6 ± 3.2	-2.57 ± 0.4

Table S3 | Organic contents of oligosaccharide and cargo for nanodevices NP(ICG)-Gal and NP(nav)-Gal in mg per g of solids.

Solid	$\alpha_{oligosaccharide}$ (mg/g solid)	α_{cargo} (mg/g solid)
NP(ICG)-Gal	181.6	56.4
NP(nav)-Gal	169.0	53.0

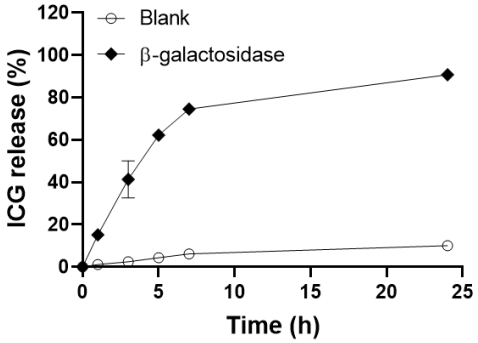

Figure S8 | Release profiles of ICG from NP(ICG)-Gal in the absence or in the presence of β-galactosidase from *Aspergillus oryzae* in water at pH 4.5.

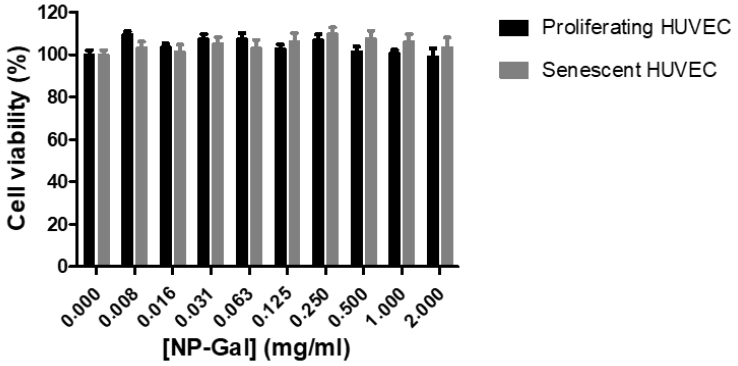

Figure S9 | Cytotoxicity profile of empty NP-Gal in HUVEC cells. Cell viability at different concentrations of nanoparticles at 72h for proliferating HUVEC (black bars) and senescent HUVEC (dark grey bars). Data represent the means ± SEM of at least three independent experiments.

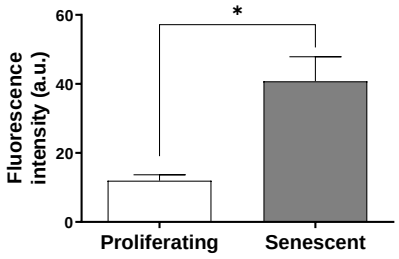

Figure S10 | Mean fluorescence intensity divided by mean FSC-width of proliferating and senescent HUVEC cells reflecting the overall particle uptake by the endothelial cells in flow cytometry after NP(ICG)-Gal treatment for 6 h. Statistical significance was assessed by two-tailed Student's T-test (*, p-value <0.1). Data represent mean ± SEM (n=3).

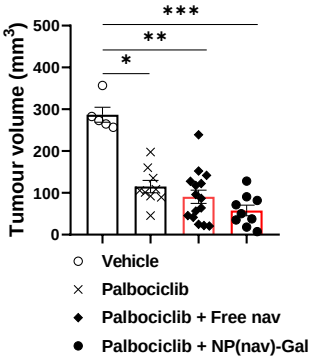

Figure S11 | Tumor volume of the different treatment at the endpoint of the treatment. Values are expressed as mean ± SEM and statistical significance was assessed by one-way ANOVA followed by Tukey's post-tests (*, p-value <0.05; **, p-value <0.05; ***, p-value <0.0005).

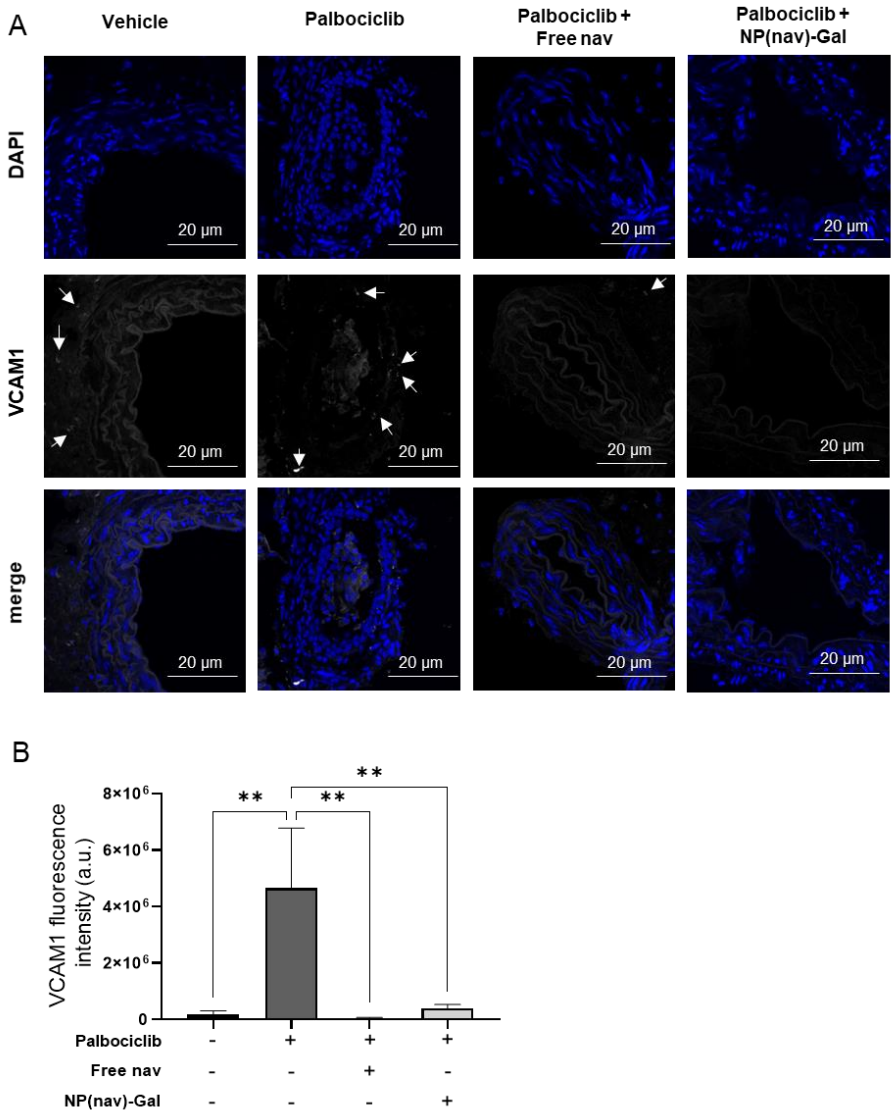

Figure S12 | Inferior cava veins were obtained from Balb/cByJ female mice orthotopically injected with 4T1 breast cancer cells and treated daily with vehicle or palbociclib. (A) Representative images of confocal microscopy of VCAM1 (grey) stained tumor sections. DAPI (blue). Scale bar, 20 µm. (B) Quantification of the VCAM1 fluorescence signal was performed using Image J software by measuring fluorescence integrated density from three random fields per section. Data represent the means ± SEM and statistical significance was assessed by one-way ANOVA followed by Tukey's post-tests (*, p-value <0.05; **, p-value <0.05; ***, p-value <0.0005).

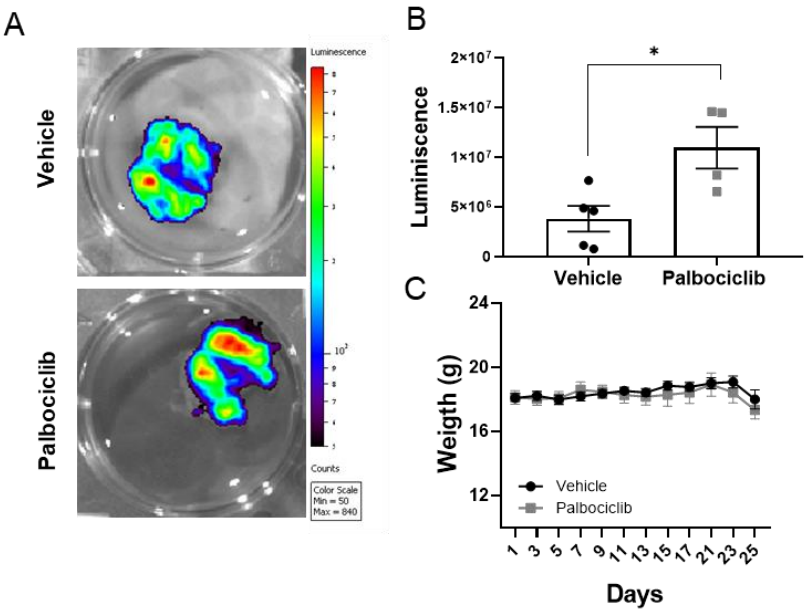

Figure S13 | Healthy Balb/cByJ female mice (n=6) were treated with palbociclib daily (o.g.) for 15 days and then 0.5×10^6 4T1-Luc breast cancer cells were intravenously injected to evaluate cancer cell spread. (A) Representative IVIS images of *ex vivo* lungs. (B) Quantification of tumor burden in lungs from IVIS images (day 10). Each data point represents one lung. (C) Mice weight during the whole experiment. Values are expressed as mean ± SEM and statistical significance was assessed by the two-tailed Student's T-test: *p<0.05.

Chapter II | Combination of palbociclib with navitoclax based-therapies enhances *in vivo* antitumoral activity in triple-negative breast cancer

Combination of palbociclib with navitoclax based-therapies enhances *in vivo* antitumoral activity in triple-negative breast cancer

Alejandra Estepa-Fernández[1,2,3], Alba García-Fernández[1,2,3*], Araceli Lérida-Viso[1,2,3,4], Juan F. Blandez[1,3,4], Irene Galiana[1,2], Félix Sancenon-Galarza[1,2,3,4], Mar Orzáez [2,5*], Ramón Martínez-Máñez[1,2,3,4*]

[1] Instituto Interuniversitario de Investigación de Reconocimiento Molecular y Desarrollo Tecnológico (IDM) Universitat Politècnica de València, Universitat de València. *Camino de Vera, s/n. 46022, Valencia, Spain.*

[2] Unidad Mixta UPV-CIPF de Investigación en Mecanismos de Enfermedades y Nanomedicina, Universitat Politècnica de València, Centro de Investigación Príncipe Felipe. *C/ Eduardo Primo Yúfera 3. 46012, Valencia, Spain.*

[3] CIBER de Bioingeniería, Biomateriales y Nanomedicina (CIBER-BBN).

[4] Unidad Mixta de Investigación en Nanomedicina y Sensores. Universitat Politècnica de València, IIS La Fe. *Av. Fernando Abril Martorell, 106 Torre A 7ª planta. 46026, Valencia, Spain*.

[5] Centro de Investigación Príncipe Felipe. *C/ Eduardo Primo Yúfera 3. 46012, Valencia, Spain.*

**Corresponding authors. Email: algarfe4@etsia.upv.es; morzaez@cipf.es; rmaez@qim.upv.es*

Submitted

Graphical abstract

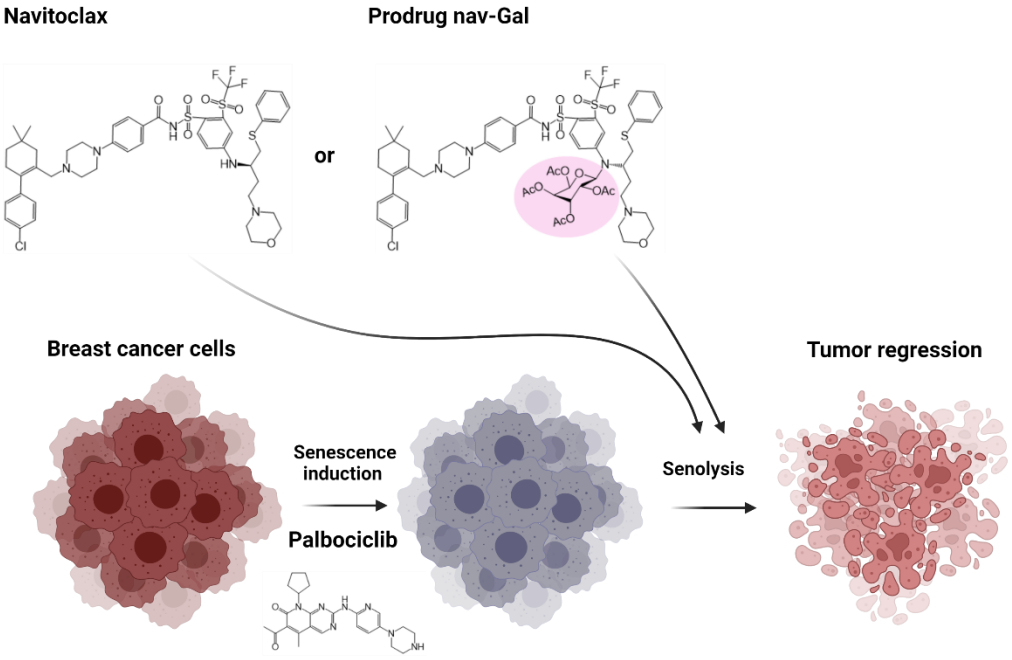

Keywords

TNBC, palbociclib, senolytic, navitoclax, pro-drug, chemotherapy, senescence, targeted-therapies

My contribution

I performed in vivo and in vitro experiments except for the synthesis of Nav-Gal and contributed to the experimental design, data analysis, discussion and writing.

1. Abstract

Triple-negative breast cancer (TNBC) is a very aggressive subtype of breast cancer with a poor prognosis and limited effective therapeutic options. The induction of senescence, arrest of cell proliferation, has been explored as a method to limit tumor progression in metastatic breast cancer. However, relapses occur in some patients, possibly as a result of senescent cancer cells that accumulate in the body after the treatment, thereby promoting tumor recurrence. In this study, we explored the combination of senescence induction and the subsequent elimination of senescent cells (senolysis) as an alternative approach to improve outcomes in TNBC patients. Overall, we demonstrate that a combined treatment using the senescence-inducer palbociclib and the senolytic navitoclax delays tumor growth and reduces metastases in a xenograft mice model of aggressive human TNBC (hTNBC). Besides, considering the off-target effects and toxicity derived from the use of navitoclax, we propose a targeted strategy to minimize associated side effects. We use a galacto-conjugated navitoclax (nav-Gal) as a senolytic pro-drug that can preferentially be activated by β-galactosidase overexpressed in senescent cells. Concomitant treatment with palbociclib and nav-Gal *in vivo* results in the eradication of senescent hTNBC cells with the subsequent reduction of tumor growth while decreasing the cytotoxicity of navitoclax. Collectively, our results support the effectiveness of combined senescence-inducing with senolytic therapy for hTNBC, as well as the development of a targeted approach as an effective and safer therapeutic opportunity.

2. Introduction

Breast cancer is one of the most common cancers in females and the leading cause of cancer-related death in women. Among all breast cancer subtypes, approximately 15–20% of them are triple-negative breast cancer (TNBC).(Morris *et al.*, 2007; Boix-Montesinos *et al.*, 2021) TNBC is characterized by the lack of estrogen (ER) and

progesterone receptor (PR) and human epidermal growth factor receptor 2 (HER2) amplification/overexpression.(Wolff *et al.*, 2013) It has worse prognosis than other breast cancer subtypes. The lack of hormone receptor expression and the aggressive proliferative behavior have limited by now the availability of effective therapies, restricting in most cases the standard of care to chemotherapy.(Garrido-Castro, Lin and Polyak, 2019; Cardoso *et al.*, 2020) Consequently, there is an urgent need for developing non-cytotoxic, targeted therapies to improve the poor prognosis of this aggressive subtype of breast cancer.

From another point of view, senescence is a tumor-suppressing mechanism that has been explored as a therapy for several tumors.(Muñoz-Espín *et al.*, 2018; Galiana *et al.*, 2020; Saleh *et al.*, 2020; Estepa-Fernández *et al.*, 2021) This therapy is already a reality in the clinical practice, for instance, by the use of cell cycle inhibiting drugs such as palbociclib, a highly selective inhibitor of cyclin-dependent kinases 4 and 6 (CDK 4/6). Palbociclib induces cellular senescence in the tumor, thus limiting tumor progression, and has been approved by the US Food and Drug Administration (FDA) to provide a first-line endocrine-based therapy for postmenopausal women with hormone receptor-positive (HR+)/human epidermal growth factor receptor 2 negative (HER2−) advanced or metastatic breast cancer in combination with letrozole or fulvestrant.(Beaver *et al.*, 2015; Walker *et al.*, 2016; Wedam *et al.*, 2019) The good results obtained with this drug has encouraged the study of palbociclib treatment in TNBC patients (NCT03756090, NCT04360941, NCT04494958).(Huang, Wu and Li, 2020) However, despite the benefits of growth suppression after senescence induction in tumors, it has also been demonstrated that the accumulation of senescent cells promotes inflammation, angiogenesis, and can cause cancer recurrence by facilitating senescence escape or invasiveness.(Demaria *et al.*, 2017; Saleh *et al.*, 2018; Galiana *et al.*, 2020; Estepa-Fernández *et al.*, 2021)

In this scenario, the use of senolytics, drugs that specifically kill senescent cells, has been proven to be an effective remedy for alleviating such unwanted senescent cell accumulation.(Estepa-Fernández *et al.*, 2021) Among senolytic drugs, navitoclax has been validated in a variety of preclinical models showing high potency to kill senescent cells, reducing cancer relapses and delaying ageing-related diseases.(Chang *et al.*, 2016; Demaria *et al.*, 2017; Kim *et al.*, 2017; Bussian *et al.*, 2018) Navitoclax inhibits the anti-apoptotic proteins Bcl-2, Bcl-xL and Bcl-w.(Zhu *et al.*, 2016) Senescent cells, in many cases, depend on Bcl-xL for their survival (Yosef *et al.*, 2016), and other cells in the body, such as platelets, do as well.(Schoenwaelder *et al.*, 2011) Therefore, inhibition of Bcl-xL causes thrombocytopenia, the major dose-limiting toxicity effect which has restricted navitoclax use in the clinic.(Kile, 2014; Chang *et al.*, 2016) In this context, it has been recently demonstrated that navitoclax harmful effects can be reduced by the design of pro-drugs (González-Gualda *et al.*, 2020) and nanodevices that selectively deliver navitoclax in senescent cells.(Muñoz-Espín *et al.*, 2018; Galiana *et al.*, 2020; Estepa-Fernández *et al.*, 2021) Galacto-conjugation of navitoclax with acetylated galactose results in the senolytic pro-drug called nav-Gal that can be preferentially activated by β-galactosidase overexpressed in senescent cells. Previous studies from our group based on a similar strategy result in the selective detection of senescent cells.(Lozano-Torres *et al.*, 2017, 2021) The nav-Gal pro-drug has been effective in reducing tumor size in orthotopically transplanted murine lung adenocarcinoma cells and in a tumor xenograft model of human non-small-cell lung cancer by combining senescence-inducing chemotherapies with the senolytic treatment, where it shows reduced hematological toxicity.(González-Gualda *et al.*, 2020)

Based on the above, in this work we explore the combination of senescence induction and the subsequent elimination of senescent cells (senolysis) as an alternative approach to improve outcomes in TNBC patients. Here, we demonstrate that palbociclib therapy-induced senescence (TIS) followed by adjuvant therapy with navitoclax causes a synergistic elimination of senescent cells and reduction of tumor growth and lung

metastasis while decreasing the cytotoxicity of navitoclax in a xenograft mice model of aggressive human TNBC (hTNBC). Our findings support that senescence-inducing therapies combined with senolysis can be a promising strategy for the effective treatment of hTNBC. Moreover, targeted navitoclax-based therapies could facilitate its clinical use as an effective and safer strategy.

3. Results

3.1. Palbociclib induces senescence in MDA-MB-231

Firstly, we studied the capability of palbociclib to induce senescence in hTNBC. For that purpose, MDA-MB-231 cells were treated with palbociclib 5 µM for 7 days, and the senescence-associated β-galactosidase (SA-β-Gal) activity was evaluated. We observed increased positivity for SA-β-Gal staining in cells treated with palbociclib (Figure 1A). Inhibition of CDK4/6 by palbociclib treatment produces the hipophosphorylation of retinoblastoma protein (pRb), causing cell cycle arrest in the G1/S transition phase.(Goel *et al.*, 2018) In palbociclib-treated MDA-MB-231 cells, a decrease in the phosphorylation of the pRb protein is observed when compared to non-treated cells (Figure 1B), indicative of senescence induction. To corroborate cell cycle arrest in palbociclib-treated cells, the expression of the Ki67 proliferation marker was analyzed by immunofluorescence (Figure 1C). Control proliferating MDA-MB-231 cells show a high expression of Ki67 (red emission), whereas palbociclib-treated cells lose the expression of the proliferation marker. Cell cycle analyses by flow cytometry demonstrated accumulation of cells in G1-phase, thus corroborating the cell cycle arrest (Figure 1D). Altogether these results confirm that palbociclib induces senescence in MDA-MB-231 hTNBC cells.

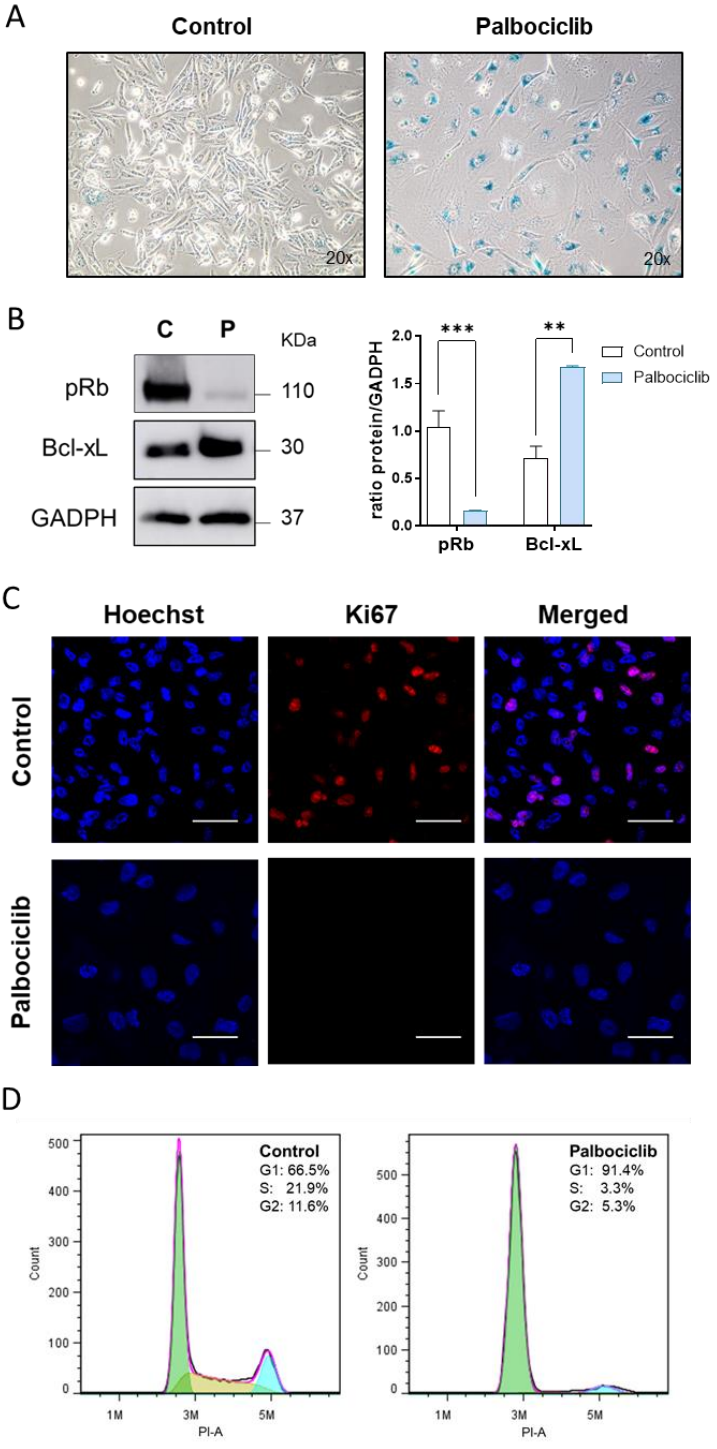
A
Control
Palbociclib
20x
20x
B
C
P
KDa
pRb
Bcl-xL
GADPH
110
30
37
***
**
Control
Palbociclib
ratio protein/GADPH
2.0
1.5
1.0
0.5
0.0
pRb
Bcl-xL
C
Hoechst
Ki67
Merged
Control
Palbociclib
D
Control
G1: 66.5%
S: 21.9%
G2: 11.6%
Palbociclib
G1: 91.4%
S: 3.3%
G2: 5.3%
Count
PI-A
1M
3M
5M

Figure 1 | Palbociclib induces senescence in MDA-MB-231. (A) β-Galactosidase staining (blue color) of control and 5 µm palbociclib-treated MDA-MB-231 cells. (B) Western blot characterization of control (C) and palbociclib-treated (P) MDA-MB-231 cells. pRb expression decreases after palbociclib treatment (expected band at 110 kDa). Bcl-xL expression increases after palbociclib treatment (expected band at 30 kDa). Quantification of western blot using Image J software. Data represent the mean ± SEM of at least three independent experiments and statistical significance was assessed by unpaired T-test (**p<0.01; ***p<0.001). (C) Ki67 immunofluorescence images show staining of Ki67 (red) and nuclei stained with Hoechst (blue) in control and palbociclib treated cells. Scale bars, 20 µm. (D) Propidium iodide (PI) staining of proliferating and palbociclib treated MDA-MB-231 cells. Senescent cells accumulate in cell cycle G1-phase after 7 days of palbociclib treatment.

3.2. Navitoclax and nav-Gal are effective senolytics in TNBC

Once demonstrated the capability of palbociclib to induce senescence in hTNBC cells, we wondered if navitoclax or galacto-conjugated navitoclax, nav-Gal, could be effective for the selective elimination of senescent-hTNBC cells. Navitoclax is preferentially released from the nav-Gal pro-drug due to the hydrolysis of the galactose unit in senescent cells (Figure 2A) as they have increased activity of senescence-associated β-galactosidase.(González-Gualda et al., 2020) Navitoclax will trigger apoptosis by inhibiting Bcl-2, Bcl-w and Bcl-xL proteins causing Bax/Bak oligomerization in the mitochondria membrane.(Zhu et al., 2016) In a first step, we demonstrated that palbociclib-treated hTNBC MDA-MB-231 cells overexpress the anti-apoptotic protein Bcl-xL (Figure 1B), indicating that the inhibition of Bcl-xL by navitoclax could be a potential strategy to eliminate senescent hTNBC cells.(Vivo-Llorca et al., 2020) Nav-gal synthesis was confirmed by HPLC-MS (Figure S1).

To test the senolytic effect of both navitoclax and the pro-drug nav-Gal against senescent cells, we performed cell viability studies in palbociclib-induced MDA-MB-231 senescent cells treated with increasing concentrations of either navitoclax (Figure 2B) or nav-Gal (up to 10 µM) for 72 h (Figure 2C). Navitoclax eliminates senescent MDA-MB-231 cells with an estimated half-maximal inhibitory concentration (IC50) value of 0.5 µM, whereas IC50 for nav-Gal is 0.7 µM (Figure 2D). In addition, IC50 values of 1.3 µM and 2.7

µM were found for navitoclax and nav-Gal, respectively, in control cells. From these data, a senolytic index of 2.6x and 3.9x was found for navitoclax and nav-Gal. The senolytic index was calculated by measuring the ratio of the IC50 values between control and senescent cells. Nav-Gal treatment improved specificity (higher senolytic index) compared to free navitoclax for hTNBC cells, mainly due to nav-Gal reduced toxicity in control cells compared to navitoclax. These results confirmed the senolytic properties of navitoclax and nav-Gal in senescent hTNBC cells and indicate that nav-Gal has lower cytotoxic activity in non-senescent cells.

A

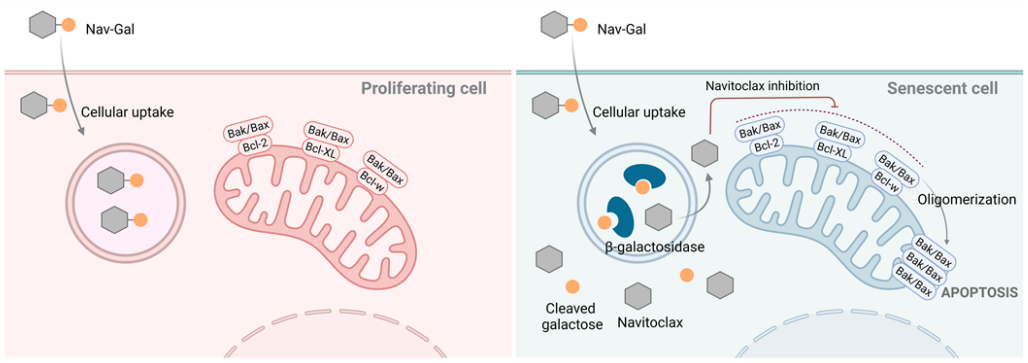

B

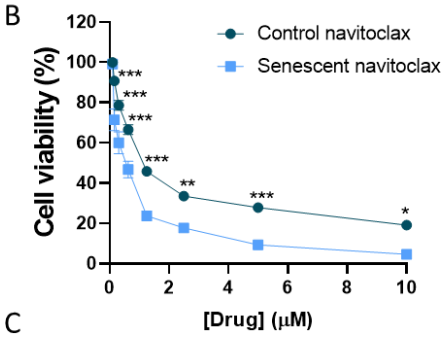

C

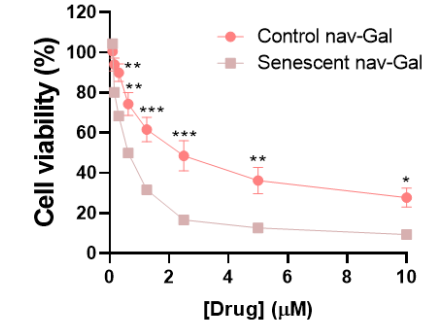

D

		IC50 (µM)	95% CI	Senolytic index
Navitoclax	Control	1.3	1.2 – 1.5	2.6x
	Senescent	0.5	0.4 – 0.6	
Nav-Gal	Control	2.7	2.2 – 3.5	3.9x
	Senescent	0.7	0.6 – 0.8	

E

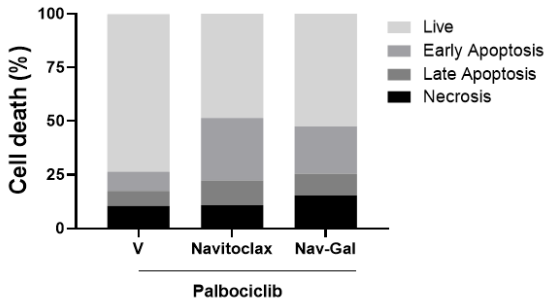

Figure 2 | The use of Nav-Gal, a senolytic pro-drug based on galacto-conjugation of navitoclax, is an efficient strategy for senolysis in TNBC MDA-MB-231 cells. (A) Scheme of the mechanism of action of the nav-Gal pro-drug. Nav-Gal crosses the cell membrane through passive internalization. As senescent cells have increased senescence-associated β-galactosidase activity, navitoclax is released by the hydrolysis of the galactose reaching its target proteins in the mitochondria (Bcl-2, Bcl-w and Bcl-xL). The inhibition of BCL-2 anti-apoptotic proteins by navitoclax causes Bax/Bak oligomerization in the mitochondria membrane triggering apoptosis. (B) Cell viability after 72 h of cell treatment with different concentrations of navitoclax (B) or nav-Gal (C) in control and senescent MDA-MB-231 cells. All values are represented as a percentage of (n≥3) ± SEM, and statistical significance was assessed by two-way ANOVA followed by Sidak's post-tests (*p<0.05, **p<0.01, ***p<0.001). (D) IC50 and senolytic index of navitoclax or nav-Gal treatment in control and senescent MDA-MB-231 cells. (E) Cell death percentage (%) of early apoptotic, late apoptotic, and necrosis cells after navitoclax or nav-Gal (1 μM) treatment for 48 hours. Percentages were measured by Annexin V-FITC and PI expression in flow cytometry. All values are represented as a percentage of (n=3) ± SEM and statistical significance was assessed by two-way ANOVA followed by Sidak's post-tests (**p<0.01, ***p<0.001).

Additionally, we found that treatment with either navitoclax or nav-Gal (1 μM) induced apoptosis (assessed by increased Annexin V staining) preferentially in palbociclib-induced MDA-MB-231 senescent cells, in accordance with previously described results (Figure 2E).(González-Gualda *et al.*, 2020) A strong signal for Annexin V (early and late apoptosis) was observed for both navitoclax (~40% of cells) and nav-Gal (~32% of cells) at equivalent doses after 48h of treatment. The results demonstrate that both navitoclax and nav-Gal senolytics induce apoptosis in senescent cells.

3.3. Combinational treatment of palbociclib and navitoclax or palbociclib and nav-Gal reduces tumor volume in MDA-MB-231 xenografts

The *in vivo* effectivity of the dual treatment, i.e. palbociclib-inducing senescence therapy followed by either navitoclax or nav-Gal treatment (senolysis), was evaluated in an MDA-MB-231 orthotopic hTNBC mouse model. To establish xenografts, MDA-MB-231 breast cancer cells were injected into the second lower right fat-pad of 6–7 weeks old nude BALB/C mice. When tumor volume reached an average of 60 mm^3, daily therapy was initiated with either vehicle (sodium lactate) or 50 mg/kg palbociclib (*via* oral gavage). One day after starting palbociclib treatment, navitoclax administration was initiated

either as a free drug (navitoclax, *via* oral gavage) or as a pro-drug (nav-Gal, *via* i.p. injection) at the same molar dose.

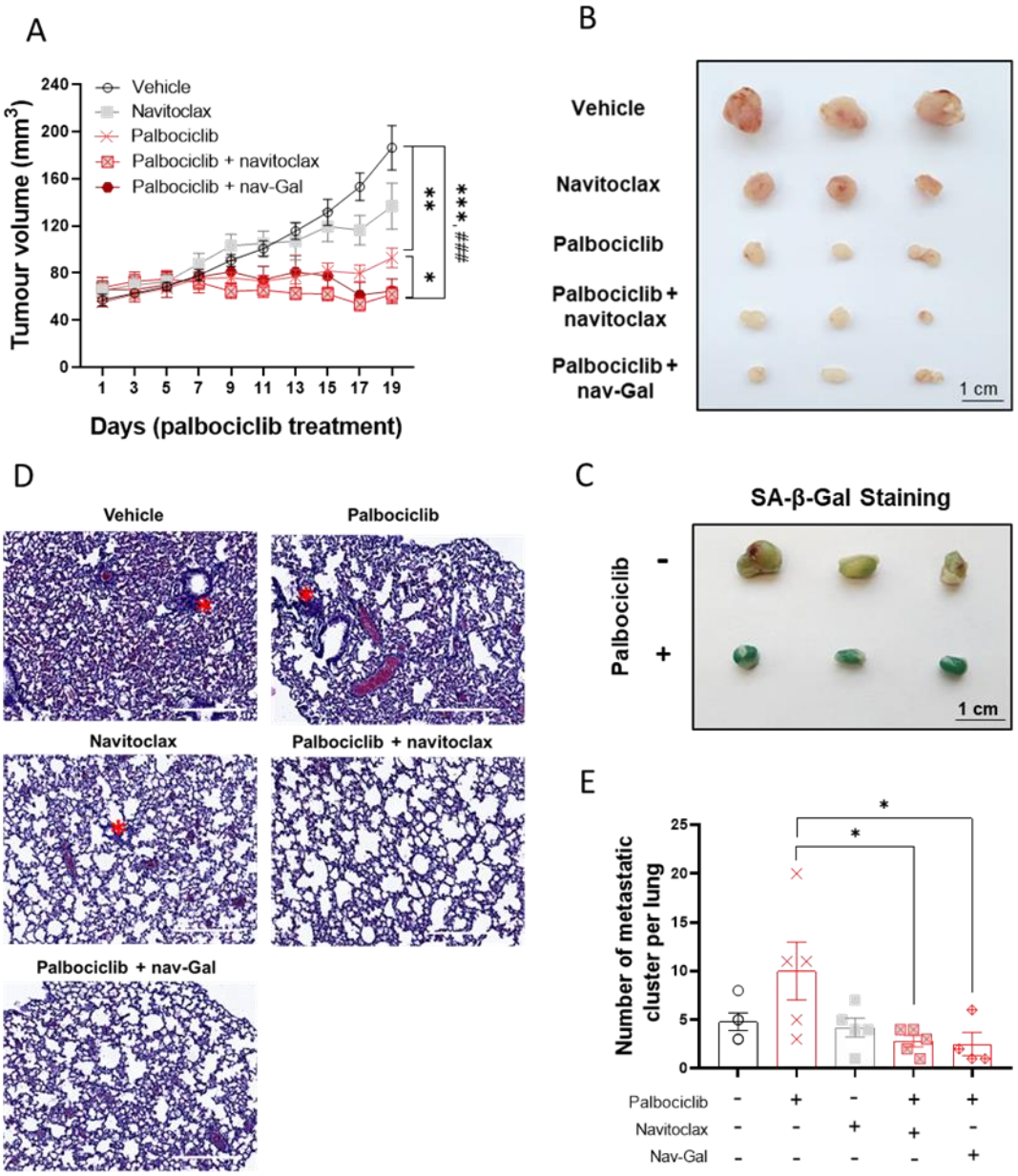

Figure 3 | Concomitant treatment of palbociclib and navitoclax-based therapies reduce tumor size and metastatic burden. BALB/c nude female mice were orthotopically injected with MDA-MB-231

breast cancer cells and treated daily with either vehicle or palbociclib. 2×10^6 MDA-MB-231 cells were subcutaneously implanted on mammary pads. When tumors volume reached 60 mm^3, palbociclib treatment started and was maintained daily (o.g.) for 19 days. Navitoclax and nav-Gal daily treatments started one day after palbociclib treatment (navitoclax: oral gavage, navi-Gal: intraperitoneal injection, molar equivalents). (A) Tumor volume (mm^3) of the different treatment approaches during all the treatment. Statistical analysis was carried out using GraphPad Prism 8 and results were compared by one-way ANOVA followed by Tukey's post-tests (***Vehicle vs palbociclib + navitoclax; ###vehicle vs palbociclib + nav-Gal) (*p<0.05; **p<0.01; ***p<0.001; ###p<0.001). Data represent the mean ± SEM (n = 5). (B) Pictures of representative tumor samples for each treatment. Scale bar, 1 cm. (C) Pictures of representative tumor samples stained with X-gal. Scale bar, 1 cm. (D) H&E staining of representative lung sections taken from xenograft MDA-MB-231 tumor-bearing mice for metastatic clusters evaluation. Scale bar, 500 μm. (E) Quantification of metastatic lung clusters. Representative tissues images were microscopically counted. Statistical analysis was carried out using GraphPad Prism, and results were compared by one-way ANOVA followed by Tukey's post-tests (*p<0.05). Data represent the mean ± SEM (n=5).

As a result of palbociclib treatment, a significant decrease in tumor growth is observed (Figure 3A and 3B) due to the proper induction of senescence in the tumors, confirmed by an increased in X-gal staining (Figure 3C). Treatment with navitoclax alone produces a slight non-significant reduction in tumor volume compared to control mice. In contrast, dual treatment with palbociclib and navitoclax or nav-Gal significantly reduced tumor growth. Concomitant treatment with either palbociclib and navitoclax or palbociclib and nav-Gal reduces animal weight (Figure S2); however, no noteworthy toxicity was found after the treatment (Figure S3).

Interestingly, evaluation of lung metastases in MDA-MB-231 xenograft mice reveals the appearance of initial metastatic cell clusters in lung sections after palbociclib treatment (Figure 3D), while a significant decrease is detected in the number of metastatic nodes in animals co-treated with palbociclib and navitoclax either as a drug or as pro-drug (nav-Gal) (Figure 3E).

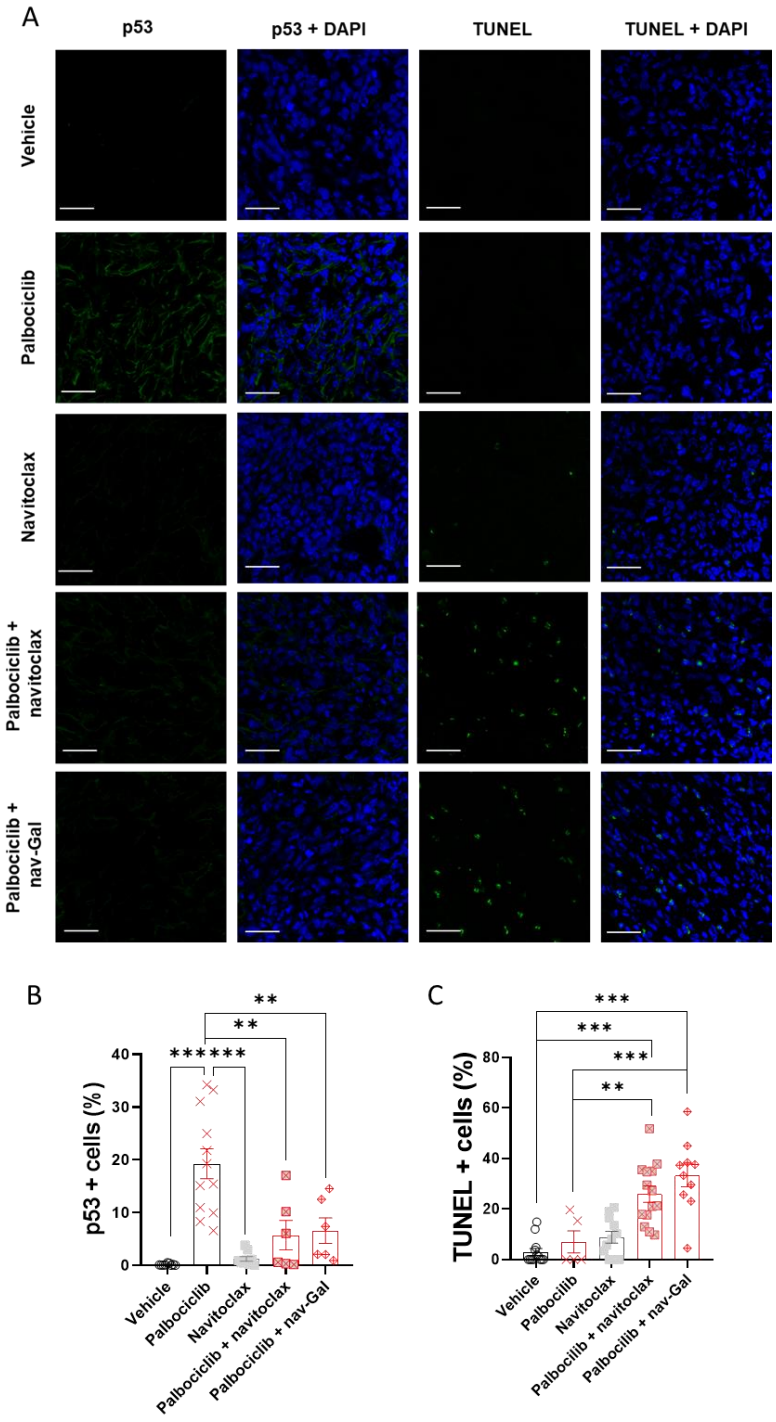
A
p53
p53 + DAPI
TUNEL
TUNEL + DAPI
Vehicle
Palbociclib
Navitoclax
Palbociclib + navitoclax
Palbociclib + nav-Gal
B
p53 + cells (%)
**
**
****
Vehicle
Palbociclib
Navitoclax
Palbociclib + navitoclax
Palbociclib + nav-Gal
C
TUNEL + cells (%)
***
***
***
**
Vehicle
Palbociclib
Navitoclax
Palbociclib + navitoclax
Palbociclib + nav-Gal

Figure 4 | Palbociclib and navitoclax co-treatment produces effective induction of senescence and cell death in tumors. (A) Representative confocal images of p53 immunostaining and TUNEL assay of tumor sections from animals treated with vehicle, palbociclib, navitoclax, or palbociclib and navitoclax or nav-Gal concomitantly (n ≥ 5 tumors per group). TUNEL assay was used to confirm the induction of apoptosis in treated and untreated tumor tissues. Scale bar, 20 µm. (B) Percentage of p53- and (C) TUNEL-positive cells in tumors. Quantification was performed in a total of 3 fields per tumor, covering most of the whole tumor section. Data represent the mean ± SEM (n=5), and statistical significance was assessed by one-way ANOVA followed by Tukey's post-tests (*p<0.05; **p<0.01; ***p<0.001).

Furthermore, histological analyses of the tumors revealed that palbociclib treatment results in increased levels of p53 immunostaining (Figure 4A and 4B), which is a characteristic of cancerous cells in the senescent state. Concomitant treatment with palbociclib and navitoclax or nav-Gal reduced p53 expression, alongside a strong cell death induction, as illustrated by the increase in TUNEL signal (Figure 4A and 4C). These results strongly suggest that apoptosis of senescent cells facilitates the antitumoral effect of co-treatments. Together, the results confirm the benefits of the use of pro-senescent and senolytic therapy in hTNBC xenografts in reducing tumor growth and cancer dissemination to distant organs.

4. Discussion and conclusion

Triple-negative breast cancer (TNBC) is defined as the type of breast cancer that lacks estrogen, progesterone, and HER2 receptors.(Wolff *et al.*, 2013) Due to the loss of such receptors, TNBC is not sensitive to endocrine therapy or molecular targeted therapy. Therefore, treatment options for advanced TNBC patients are limited and ineffective (Yin *et al.*, 2020; O'Reilly, Sendi and Kelly, 2021), with a mortality rate of TNBC patients of 40% within the first 5 years after diagnosis.(Dent *et al.*, 2007) Thus, therapeutic advancements are critical to improve mortality associated with TNBC.

The induction of senescence is a well-established tumor suppressive mechanism due to the characteristic proliferation arrest of senescent cells.(Short *et al.*, 2019; Mongiardi *et al.*, 2021; Park *et al.*, 2021; Prasanna *et al.*, 2021; Wang, Lankhorst and Bernards, 2022) Different classical anticancer therapeutic strategies have been demonstrated to induce senescence in the tumor, such as chemotherapeutic agents, the use of radiotherapy or treatments with CDK4/6 inhibitors.(Wang, Kohli and Demaria, 2020; Wyld *et al.*, 2020) Chemotherapeutic drugs that are widely used clinically and have shown to induce senescence *in vivo* include doxorubicin (Chang *et al.*, 1999), etoposide, (te Poele *et al.*, 2002), cisplatin (Wang *et al.*, 1998) bleomycin, or temozolomide.(Hirose, Berger and Pieper, 2001) The clinically used CDK4/6 inhibitorspalbociclib, abemaciclib, and ribociclib also show senescence induction *in vivo.*(Yoshida, Lee and Diehl, 2016; Torres-Guzmán *et al.*, 2017; Valenzuela *et al.*, 2017; Bortolozzi *et al.*, 2018)

Despite the benefits of stopping cancer proliferation, it has been demonstrated that an excessive accumulation of senescent cells and their secretory phenotype can promote chronic inflammation, angiogenesis, or increase tumor promoting properties that may cause cancer recurrence.(Coppé *et al.*, 2010; Kang *et al.*, 2011; Eggert *et al.*, 2016; Ruhland, Coussens and Stewart, 2016; Estepa-Fernández *et al.*, 2021) Although senescence has always been considered as a permanent and irreversible cell cycle arrest, recent studies have suggested that, under certain conditions, therapy-induced senescent (TIS) tumor cells can escape from this condition and re-enter the cell cycle, thus acquiring an aggressive character.(Roberson *et al.*, 2005; Saleh *et al.*, 2019; Saleh, Tyutyunyk-Massey and Gewirtz, 2019; Triana-Martínez, Loza and Domínguez, 2020; Yu *et al.*, 2020)

On this basis, interventions aimed to limit the deleterious roles of senescent cells are under development *via* the design of senoblockers (drugs that inhibit senescence before it happens), senomorphics (drugs that inhibit senescence-associated secretory phenotype) and senolytics (drugs that eliminate senescent cells).(Lozano-Torres *et al.*, 2019) Senolytics have been intensively investigated and are already being studied in

clinical trials, with very positive preliminary results using dasatinib plus quercetin in patients with idiopathic pulmonary fibrosis and diabetic kidney disease.(Hickson *et al.*, 2019; Justice *et al.*, 2019) Among senolytics, inhibitors of Bcl-2 anti-apoptotic proteins such as navitoclax have proved to be effective in reducing relapse in some cancer models and the onset of several aging associated-diseases.(Chang *et al.*, 2016; Zhu *et al.*, 2016; Demaria *et al.*, 2017; Kim *et al.*, 2017; Bussian *et al.*, 2018) Monotherapy with navitoclax has shown a good antitumoral activity in *in vivo* studies of small cell lung cancer, leukaemia, and lymphoma.(Shoemaker *et al.*, 2008; Tse *et al.*, 2008) In the case of breast cancer, navitoclax is not sufficient to induce tumor death in some breast cancer cell lines (Chen *et al.*, 2011), as we have also observed in MDA-MB-231 xenografts (*vide ante*). However, to enhance the efficacy of navitoclax, combined therapy with TIS agents, such as palbociclib or doxorubicin, has been recently proposed.(Fleury *et al.*, 2019; Galiana *et al.*, 2020; Saleh *et al.*, 2020; Shahbandi *et al.*, 2020) Besides, several phase 1 and phase 1/2 clinical trials combining senescence-inducing chemotherapy and navitoclax are ongoing or completed, including the combination of navitoclax with cisplatin (NCT00878449), etoposide (NCT00878449) or osimertinib (NCT02520778) in lung cancer patients and with dabrafenib or trametinib for patients with metastatic melanoma (NCT01989585). Navitoclax has also been combined with gemcitabine (NCT00887757), paclitaxel (NCT00891605), docetaxel (NCT00888108), irinotecan (NCT01009073), erlotinib (NCT01009073), sorafenib (NCT02143401), or trametinib (NCT02079740) in advanced solid tumors.(Paez-Ribes *et al.*, 2019)

Palbociclib induces senescence by inhibiting CDK4 and CDK6 kinases which decreases the phosphorylation of Rb protein and subsequently induces G1 cell cycle arrest.(Toogood *et al.*, 2005; Rivadeneira *et al.*, 2010) Furthermore, palbociclib has become the standard first-line therapy for advanced metastatic ER+, HER2- negative breast cancer, used in combination with letrozole or fulvestrant.(Beaver *et al.*, 2015; Zeng *et al.*, 2016; Wedam *et al.*, 2019; Llombart-Cussac *et al.*, 2021) Palbociclib in combination with letrozole significantly prolonged median progression-free survival (PFS) compared with placebo

plus letrozole (27.6 vs 14.5 months).(Rugo *et al.*, 2019) Although the effects of palbociclib in TNBC are not well-documented, cell cycle inhibition by palbociclib in MDA-MB-231 suggests its potential use to treat TNBC tumors.(Liu *et al.*, 2017; Huang, Wu and Li, 2020; Bryson *et al.*, 2021; Jost *et al.*, 2021) In addition, beneficial effects have already been found in TNBC by combining palbociclib plus other apoptotic drugs *in vitro* and *in vivo*. For instance, concomitant treatment of palbociclib plus enzalutamide enhanced the palbociclib-induced cytostatic effect in hTNBC MDA-MB-231 cells.(Liu *et al.*, 2017) Besides, the combination of palbociclib plus cisplatin delayed tumor growth in MDA-MB-231 xenografts.(Huang, Wu and Li, 2020)

In this work, we demonstrate that palbociclib treatment induces senescence in xenograft mice bearing hTNBC MDA-MB-231. In addition, treatment with palbociclib followed by navitoclax-based therapies (navitoclax or nav-Gal) results in the reduction of tumor size and the number of metastatic lung clusters. This two-step pro-senescence/senolytic combinatorial treatment regimen selectively induces apoptosis in hTNBC MDA-MB-231 senescent cancer cells causing synergistic reduced tumor growth. In addition, evaluation of lung metastases in the xenograft mice hTNBC model revealed the appearance of initial metastatic cell clusters in lung sections, while a significant decrease in the number of metastatic nodes in animals co-treated with palbociclib and navitoclax or nav-Gal were observed. Previous work from our group already demonstrated that palbociclib-induced senescence increases metastatic clusters in lungs of 4T1 breast cancer mice xenografts by altering the endothelium and that subsequent senolysis with navitoclax decreased the metastatic burden.(Estepa-Fernández *et al.*, 2021) This is relevant as metastasis has a significant role in the clinical management of TNBC. Currently, approximately 25% of TNBC patients relapse with distant metastases. (O'Reilly, Sendi and Kelly, 2021) The reduction of the tumor size and metastatic lung clusters found in this work provides strong support for the potential translation involving palbociclib treatments together with navitoclax in TNBC tumors.

As far as we know, this work is the first time that the combination of palbociclib-induced senescence followed by navitoclax-senolysis in hTNBC has been tested and shown to be effective.(Nor Hisam *et al.*, 2021) In a previous work, we described the effective combination of palbociclib plus navitoclax in a 4T1 mouse model, which is usually considered a TNBC model.(Galiana *et al.*, 2020) Our work here translates the use of the combination of palbociclib plus navitoclax to an hTNBC model. When comparing both models, we have found that monotherapy with palbociclib has more activity arresting the tumor in human MDA-MB-231 xenografts than in 4T1 orthotopic mice models, meaning that senolytic therapy have a better effect in human xenografts. These differences highlight the importance of validating the combination of palbociclib plus navitoclax in both preclinical orthotopic mice and human xenografts models with the objective to make the potential transfer of the treatment to clinical practice more reliable.

Despite its efficacy in preclinical trials, the secondary effects of navitoclax have limited its translation to clinical practice. Among side effects of navitoclax, thrombocytopenia is the most relevant due to platelets dependence on Bcl-xL protein for their survival.(Kaefer *et al.*, 2014) To overcome navitoclax toxicity, recently, a second generation of senolytics have been reported, such as the PZ15227, a Bcl-xL proteolysis-targeting chimera (PROTAC) of navitoclax with limited platelet toxicity.(He *et al.*, 2020) Additionally, several pro-drugs and nanodevices based on β-galactosidase overexpression in senescent cells have been reported (Agostini *et al.*, 2012; Muñoz-Espín *et al.*, 2018; Galiana *et al.*, 2020; Lozano-Torres *et al.*, 2020; Estepa-Fernández *et al.*, 2021), such as the pro-drug nav-Gal,(González-Gualda *et al.*, 2020) ,the galactose-modified duocarmycin (Guerrero *et al.*, 2020), or the gemcitabine-derivative SSK1.(Cai *et al.*, 2020) In the scenario shown here, we proposed the use of the senolytic pro-drug nav-Gal as a targeted strategy to reduce navitoclax toxicity. This galacto-conjugated navitoclax is preferentially activated in senescent cells by the elevated levels of SA-β-gal activity in these cells. Nav-Gal pro-drug has proved to be effective after concomitant treatment with cisplatin in xenografts mice bearing human A549 lung cancer cells and in an orthotopic mice model

using murine lung adenocarcinoma cells.(González-Gualda *et al.*, 2020) Our study demonstrated that a combination of palbociclib and nav-Gal treatment results in more selectivey MDA-MB-231 senescent cells elimination over non-senescence cells. Besides, the concomitant treatment *in vivo* results in the effective removal of senescent hTNBC cells with the subsequent reduction of tumor growth. Our previous results corroborated the proper reduction of platelet toxicity after galacto-conjugation of navitoclax in *ex vivo* experiments with both human and murine blood samples.(González-Gualda *et al.*, 2020) Additionally, platelet count of wild-type C57BL/6J mice treated daily with senotherapy for a total of 10 days exhibited severe thrombocytopenia after navitoclax treatment at day 5.(González-Gualda *et al.*, 2020) This effect was also observed in the human lung cancer xenograft mice model treated with the combined cisplatin-induced senescence and navitoclax senolysis, whereas nav-Gal treatment did not cause this hematological toxicity.(González-Gualda *et al.*, 2020)

Together, our results demonstrate the combination efficacy of palbociclib plus navitoclax-based therapies, providing a strong support for a translational paradigm involving cell cycle arrest treatments together with anti-apoptotic inhibitors in TNBC tumors. Also, we have demonstrated that galacto-conjugation of navitoclax can be used as an effective approach to target senescent cells and limit the toxicity associated with free navitoclax. Overall, we show a safer and more effective therapeutic possibility for the treatment of hTNBC.

5. Experimental section

5.1. Cell culture and senescence induction

Human breast triple-negative adenocarcinoma MDA-MB-231 cells (ATCC) were cultured in DMEM (Sigma) supplemented with 10% fetal bovine serum (FBS; Sigma) and maintained at 37 °C in 5% CO_2. For chemotherapy-induced senescence, we used 5 µM palbociclib (#S1116, Selleckchem) for 7 days.

5.2. Senescence-associated β-galactosidase staining

Senescence-associated β-galactosidase detection was performed using the Senescence β-galactosidase Staining Kit (Cell Signaling, #9860S). Briefly, cells were fixed at room temperature with 1x Fixative Solution, washed, and incubated overnight at 37 °C without CO_2 with fresh 1x Staining Solution containing X-gal in N-N-dimethylformamide. Cells were washed, visualized, and photographed under bright field microscope. For SA-β-Galactosidase staining in tumors, whole-mount tumors were fixed with 4% paraformaldehyde overnight. Then, tumors were washed with PBS and incubated with X-Gal staining solution for 6 h at 37°C.

5.3. Western Blot

Cells were lysed in a buffer containing 25 mM Tris-HCl pH 7.4, 1 mM EDTA, 1% SDS, supplemented with protease and phosphatase inhibitors. Protein concentration was determined by the BCA protein assay. Electrophoresis was performed in SDS-PAGE gels, and proteins were transferred to nitrocellulose membranes. The membranes were blocked for 1 hour with 5% non-fat milk, washed with 0.1% Tween/PBS and incubated with a specific primary antibody at 4°C overnight: pRb (#9308, Cell Signalling), Bcl-xL (#2764, Cell Signalling) and GADPH (#14C10, Cell Signalling). Membranes were washed and incubated with the corresponding secondary antibody conjugated with horseradish peroxidase: anti-Rabbit IgG peroxidase antibody (#A6154, Sigma) or peroxidase conjugated-goat anti-Mouse IgG antibody (#A4416, Sigma). Membranes were visualized using ECL system (GE Healthcare) for chemiluminescent detection of the protein bands.

5.4. Ki67 immunostaining

Cells were seeded on coverslips; when cells were confluent, they were fixed with 4% PFA, permeabilized and blocked for 1h with a solution containing 5% BSA and 0.3% Triton X-100. Then, cells were stained with the primary antibody Ki-67 (D3B5) Rabbit (#9129, Cell

Signaling) overnight at 4 °C. The following incubation with secondary antibody anti-rabbit IgG Fluor Goat 633 (#A21071, Fisher) was performed for 2 h at room temperature. The coverslips were mounted with Mowiol/DAPI (Sigma), and confocal microscopy images were taken using a Leica TCS SP8 HyVolution 2 microscope.

5.5. Cell cycle assay

For apoptosis evaluation assays, proliferating MDA-MB-231 and palbociclib-treated (7 days at 5μM) MDA-MB-231 cells were fixed and permeabilized with ethanol overnight. Then, 0.5 mL of PI/RNAse buffer solution from Immunostep were added to each proliferating or senescent cells (1 x 10^6 cells) and incubated for 15 minutes at room temperature before analysis. Samples were analyzed by flow cytometry using the CytoFLEX S Beckman Coulter.

5.6. Synthesis of nav-Gal pro-drug

Synthesis of nav-Gal was performed as described previously by Gonzalez-Gualda *et al.*(González-Gualda *et al.*, 2020) Briefly, in a round two neck bottom flask, 40 mg of navitoclax from Eurodiagnostico (0.04 mmol), 25 mg of 2,3,4,6-tetra-O-acetyl-α-D-galactopyranosyl-bromide from Sigma (0.06 mmol) and 10.5 mg of K_2CO_3 from Sigma (0.07 mmol) was added. The reaction mixture was purged with an argon atmosphere. Anhydrous acetonitrile (10 mL) was added, and the mixture was stirred at 70 °C for 3 h under an argon atmosphere. The solvent was removed under vacuum pressure. For large stocks used in mouse experiments, the reactions were performed in different batches. Once the desired amount was obtained, all batches were pooled and purified by column chromatography using silica gel (eluent, hexane-ethyl acetate (3:7 v/v; Scharlab) to hexane-ethyl acetate (7:3 v/v)). Purified nav-Gal was obtained as a yellow powder in 35% yield.

5.7. Cytotoxicity assay

Control and senescent MDA-MB-231 cells were plated in white flat-bottom-clear 96-well (Greiner Bio-One) at a density of 10^4 cells per well. After 24 h, navitoclax or nav-Gal were added to the cells at a 10 µM final concentration. After 72 h, viability was measured using CellTiter-Glo® luminescent cell viability assay (Promega, #G7571) kit following the manufacturer's instructions, in a PerkinElmer life sciences wallac Victor2TM spectrophotometer. The number of viable cells was normalized to the internal control of untreated cells (DMSO only) of each plate. The senolytic index of the compounds was calculated by measuring the ratio of the half-maximal inhibitory concentration (IC50) values between control and senescent cells.

5.8. Cell death assay

For the apoptosis evaluation assay, senescent MDA-MB-231 cells were treated with DMSO, navitoclax or nav-Gal 1 µM. After 48 hours of incubation, cells were labelled with Alexa fluorescein isothiocyanate-conjugated Annexin V (BD Bioscience) plus propidium iodide according to the manufacturer's recommendations. Samples were analyzed in the cytometer CytoFLEX S Beckman Coulter.

5.9. Mouse experiments

All mice were treated in strict accordance with the local ethical committee (Ethical Committee for Research and Animal Welfare Generalitat Valenciana, Conselleria d'Agricultura, Medi ambient, Canvi climàtic i Desenvolupament Rural (2020/VSC/PEA/0177)). All mice were maintained in ventilated cages within a specific pathogen-free animal facility. To establish subcutaneous tumor xenografts, 2 x 10^6 MDA-MB-231 breast cancer cells were injected subcutaneously in the second lower right breast of 6–7 weeks old BALB/c nude mice. Tumors were measured with calipers every 2 days, and the tumor volume (mm^3) was calculated with the formula length × $width^2/2$. When

tumor volume reached an average of 60 mm^3, daily therapy was initiated with either vehicle (sodium lactate) or 50 mg/kg palbociclib (via oral gavage). The day after the initiation of palbociclib treatment, navitoclax treatments were initiated at a molar equivalent dose: either 25 mg/kg navitoclax (via oral gavage) or 33.5 mg/kg nav-Gal (via i.p. injection). Navitoclax was prepared in 15% DMSO/ 85% PEG-400 while nav-Gal was prepared in 10% DMSO/ 90% saline. Mice were culled by CO_2 after 3 weeks of treatment, and tumors and lungs were collected for subsequent histological analyses.

5.10. Histology

Tumors were removed, washed with 1× PBS, and fixed with 4% PFA overnight at 4 °C. The fixative was aspirated and the tumor was washed in 1× PBS and incubated with 30% sucrose overnight at 4 °C. Fixed tissues were embedded in cryomolds with OCT and frozen completely at −20 °C. 10 µm thick tumor sections were then incubated in blocking solution (5% horse serum, 0.3% Triton X-100 in 1× PBS) for 1 h and immunostained following incubation with primary antibodies overnight at 4 °C. p53 antibody was used at 1:100 (ab26, Abcam). Secondary antibody against mouse conjugated to Alexa Fluor 488 (Invitrogen) 1:200 dilution. For TUNEL staining, In Situ Cell Death Detection Kit (Merck) was used as per manufacturer's instructions. Sections were mounted on microscope slides using the Mowiol/DAPI (Sigma) and covered with a glass coverslip. Confocal microscopy images were obtained by using a Leica TCS SP8 HyVolution 2 microscope. Positive signal for p53 and TUNEL was quantified with ImageJ or Aperio Versa software.

5.11. Metastasis quantification

Lungs were collected after euthanasia and fixed overnight in 4% PFA. Paraffin-embedded tissue sections (5 µm) on glass slides were processed for hematoxylin-eosin staining, and stained lung sections were scanned in a Leica Aperio Versa 200 equipment at 10x magnification. Metastatic MDA-MB-231 cell clusters were microscopically counted in different lung sections from five animals per group.

5.12. Statistical Analysis

For *in vivo* studies, mice were randomly assigned to treatment groups. All of the values represent the mean ± SEM of at least three independent experiments except the *in vivo* experiment with mice, where a single representative experiment is shown. Significance was determined by one-way ANOVA followed by either Tukey's post-tests or Sidak's post-tests or by Student's T-test using GraphPad Prism 8 software. A p-value below 0.05 was considered statistically significant (*p<0.05; **p<0.01; ***p<0.001).

6. References

Agostini, A. et al. (2012) 'Targeted cargo delivery in senescent cells using capped mesoporous silica nanoparticles', Angewandte Chemie - International Edition, 51(42), pp. 10556–10560. doi: 10.1002/anie.201204663.

Beaver, J. A. et al. (2015) 'FDA Approval: Palbociclib for the Treatment of Postmenopausal Patients with Estrogen Receptor-Positive, HER2-Negative Metastatic Breast Cancer.', Clinical cancer research : an official journal of the American Association for Cancer Research, 21(21), pp. 4760–6. doi: 10.1158/1078-0432.CCR-15-1185.

Boix-Montesinos, P. et al. (2021) 'The past, present, and future of breast cancer models for nanomedicine development', Advanced Drug Delivery Reviews, 173, pp. 306–330. doi: 10.1016/j.addr.2021.03.018.

Bortolozzi, R. et al. (2018) 'Ribociclib, a Cdk4/Cdk6 kinase inhibitor, enhances glucocorticoid sensitivity in B-acute lymphoblastic leukemia (B-All)', Biochemical Pharmacology, 153, pp. 230–241. doi: 10.1016/J.BCP.2018.01.050.

Bryson, B. L. et al. (2021) 'Aberrant induction of a mesenchymal/stem cell program engages senescence in normal mammary epithelial cells', Molecular Cancer Research, 19(4), pp. 651–666. doi: 10.1158/1541-7786.MCR-19-1181.

Bussian, T. J. et al. (2018) 'Clearance of senescent glial cells prevents tau-dependent pathology and cognitive decline.', Nature, 562(7728), pp. 578–582. doi: 10.1038/s41586-018-0543-y.

Cai, Y. et al. (2020) 'Elimination of senescent cells by β-galactosidase-targeted prodrug attenuates inflammation and restores physical function in aged mice', Cell research, 30(7), pp. 574–589. doi: 10.1038/S41422-020-0314-9.

Cardoso, F. et al. (2020) '5th ESO-ESMO international consensus guidelines for advanced breast cancer (ABC 5)', Annals of Oncology, 31(12), p. 1623. doi: 10.1016/J.ANNONC.2020.09.010.

Chang, B. D. et al. (1999) 'A senescence-like phenotype distinguishes tumor cells that undergo terminal proliferation arrest after exposure to anticancer agents.', Cancer

research, 59(15), pp. 3761–7.
Chang, J. et al. (2016) 'Clearance of senescent cells by ABT263 rejuvenates aged hematopoietic stem cells in mice', Nature Medicine, 22(1), pp. 78–83. doi: 10.1038/nm.4010.
Chen, J. et al. (2011) 'The Bcl-2/Bcl-X L/Bcl-w inhibitor, navitoclax, enhances the activity of chemotherapeutic agents in vitro and in vivo', Molecular Cancer Therapeutics, 10(12), pp. 2340–2349. doi: 10.1158/1535-7163.MCT-11-0415.
Coppé, J.-P. et al. (2010) 'The Senescence-Associated Secretory Phenotype: The Dark Side of Tumor Suppression', Annual Review of Pathology: Mechanisms of Disease, 5(1), pp. 99–118. doi: 10.1146/annurev-pathol-121808-102144.
Demaria, M. et al. (2017) 'Cellular senescence promotes adverse effects of chemotherapy and cancer relapse', Cancer Discovery, 7(2), pp. 165–176. doi: 10.1158/2159-8290.CD-16-0241.
Dent, R. et al. (2007) 'Triple-negative breast cancer: clinical features and patterns of recurrence', Clinical cancer research : an official journal of the American Association for Cancer Research, 13(15 Pt 1), pp. 4429–4434. doi: 10.1158/1078-0432.CCR-06-3045.
Eggert, T. et al. (2016) 'Distinct Functions of Senescence-Associated Immune Responses in Liver Tumor Surveillance and Tumor Progression', Cancer Cell, 30(4), pp. 533–547. doi: 10.1016/j.ccell.2016.09.003.
Estepa-Fernández, A. et al. (2021) 'Senolysis Reduces Senescence in Veins and Cancer Cell Migration', Advanced Therapeutics, 2100149, pp. 1–15. doi: 10.1002/adtp.202100149.
Fleury, H. et al. (2019) 'Exploiting interconnected synthetic lethal interactions between PARP inhibition and cancer cell reversible senescence', Nature Communications 2019 10:1, 10(1), pp. 1–15. doi: 10.1038/s41467-019-10460-1.
Galiana, I. et al. (2020) 'Preclinical antitumor efficacy of senescence-inducing chemotherapy combined with a nanoSenolytic', Journal of Controlled Release, 323, pp. 624–634. doi: 10.1016/j.jconrel.2020.04.045.
Garrido-Castro, A. C., Lin, N. U. and Polyak, K. (2019) 'Insights into molecular classifications of triple-negative breast cancer: Improving patient selection for treatment', Cancer Discovery. Cancer Discov, pp. 176–198. doi: 10.1158/2159-8290.CD-18-1177.
Goel, S. et al. (2018) 'CDK4/6 Inhibition in Cancer: Beyond Cell Cycle Arrest', Trends in Cell Biology. Elsevier Ltd, pp. 911–925. doi: 10.1016/j.tcb.2018.07.002.
González-Gualda, E. et al. (2020) 'Galacto-conjugation of Navitoclax as an efficient strategy to increase senolytic specificity and reduce platelet toxicity', Aging Cell, 19(4), pp. 1–19. doi: 10.1111/acel.13142.
Guerrero, A. et al. (2020) 'Galactose-modified duocarmycin prodrugs as senolytics', Aging cell, 19(4). doi: 10.1111/ACEL.13133.
He, Y. et al. (2020) 'Using proteolysis-targeting chimera technology to reduce navitoclax platelet toxicity and improve its senolytic activity', Nature communications, 11(1). doi: 10.1038/S41467-020-15838-0.

Hickson, L. T. J. et al. (2019) 'Senolytics decrease senescent cells in humans: Preliminary report from a clinical trial of Dasatinib plus Quercetin in individuals with diabetic kidney disease', EBioMedicine, 47, pp. 446–456. doi: 10.1016/J.EBIOM.2019.08.069.

Hirose, Y., Berger, M. S. and Pieper, R. O. (2001) 'p53 effects both the duration of G2/M arrest and the fate of temozolomide-treated human glioblastoma cells.', Cancer research, 61(5), pp. 1957–63.

Huang, Y., Wu, H. and Li, X. (2020) 'Novel sequential treatment with palbociclib enhances the effect of cisplatin in RB-proficient triple-negative breast cancer', Cancer Cell International, 20(1), pp. 1–14. doi: 10.1186/s12935-020-01597-x.

Jost, T. et al. (2021) 'Palbociclib Induces Senescence in Melanoma and Breast Cancer Cells and Leads to Additive Growth Arrest in Combination With Irradiation', Frontiers in Oncology, 11, p. 4059. doi: 10.3389/FONC.2021.740002/BIBTEX.

Justice, J. N. et al. (2019) 'Senolytics in idiopathic pulmonary fibrosis: Results from a first-in-human, open-label, pilot study', EBioMedicine, 40, pp. 554–563. doi: 10.1016/J.EBIOM.2018.12.052.

Kaefer, A. et al. (2014) 'Mechanism-based pharmacokinetic/pharmacodynamic meta-analysis of navitoclax (ABT-263) induced thrombocytopenia', Cancer chemotherapy and pharmacology, 74(3), pp. 593–602. doi: 10.1007/S00280-014-2530-9.

Kang, T.-W. et al. (2011) 'Senescence surveillance of pre-malignant hepatocytes limits liver cancer development', Nature, 479(7374), pp. 547–551. doi: 10.1038/nature10599.

Kile, B. T. (2014) 'The role of apoptosis in megakaryocytes and platelets', British Journal of Haematology, 165(2), pp. 217–226. doi: 10.1111/bjh.12757.

Kim, H.-N. N. et al. (2017) 'DNA damage and senescence in osteoprogenitors expressing Osx1 may cause their decrease with age', Aging Cell, 16(4), pp. 693–703. doi: 10.1111/acel.12597.

Liu, C. Y. et al. (2017) 'Combination of palbociclib with enzalutamide shows in vitro activity in RB proficient and androgen receptor positive triple negative breast cancer cells', PLoS ONE, 12(12), pp. 1–14. doi: 10.1371/journal.pone.0189007.

Llombart-Cussac, A. et al. (2021) 'Fulvestrant-Palbociclib vs Letrozole-Palbociclib as Initial Therapy for Endocrine-Sensitive, Hormone Receptor-Positive, ERBB2-Negative Advanced Breast Cancer: A Randomized Clinical Trial', JAMA oncology, 7(12), pp. 1791–1799. doi: 10.1001/JAMAONCOL.2021.4301.

Lozano-Torres, B. et al. (2017) 'An OFF–ON Two-Photon Fluorescent Probe for Tracking Cell Senescence in Vivo', Journal of the American Chemical Society, 139(26), pp. 8808–8811. doi: 10.1021/jacs.7b04985.

Lozano-Torres, B. et al. (2019) 'The chemistry of senescence', Nature Reviews Chemistry, 3(7), pp. 426–441. doi: 10.1038/s41570-019-0108-0.

Lozano-Torres, B. et al. (2020) 'Real-Time In Vivo Detection of Cellular Senescence through the Controlled Release of the NIR Fluorescent Dye Nile Blue', Angewandte Chemie - International Edition, 59(35), pp. 15152–15156. doi: 10.1002/anie.202004142.

Lozano-Torres, B. et al. (2021) 'A Two-Photon Probe Based on Naphthalimide-Styrene

Fluorophore for the in Vivo Tracking of Cellular Senescence', Analytical Chemistry, 93(5), pp. 3052–3060. doi: 10.1021/acs.analchem.0c05447.

Mongiardi, M. P. et al. (2021) 'Cancer Response to Therapy-Induced Senescence: A Matter of Dose and Timing', Cancers 2021, Vol. 13, Page 484, 13(3), p. 484. doi: 10.3390/CANCERS13030484.

Morris, G. J. et al. (2007) 'Differences in breast carcinoma characteristics in newly diagnosed African-American and Caucasian patients: A single-institution compilation compared with the national cancer institute's surveillance, epidemiology, and end results database', Cancer, 110(4), pp. 876–884. doi: 10.1002/cncr.22836.

Muñoz-Espín, D. et al. (2018) 'A versatile drug delivery system targeting senescent cells', EMBO Molecular Medicine, 10(9). doi: 10.15252/emmm.201809355.

Nor Hisam, N. S. et al. (2021) 'Combination therapy of navitoclax with chemotherapeutic agents in solid tumors and blood cancer: A review of current evidence', Pharmaceutics, 13(9). doi: 10.3390/pharmaceutics13091353.

O'Reilly, D., Sendi, M. Al and Kelly, C. M. (2021) 'Overview of recent advances in metastatic triple negative breast cancer', World Journal of Clinical Oncology, 12(3), pp. 164–182. doi: 10.5306/wjco.v12.i3.164.

Paez-Ribes, M. et al. (2019) 'Targeting senescent cells in translational medicine', EMBO Molecular Medicine, 11(12), pp. 1–19. doi: 10.15252/emmm.201810234.

Park, S. S. et al. (2021) 'Senescent tumor cells: an overlooked adversary in the battle against cancer', Experimental & Molecular Medicine 2021 53:12, 53(12), pp. 1834–1841. doi: 10.1038/s12276-021-00717-5.

te Poele, R. H. et al. (2002) 'DNA damage is able to induce senescence in tumor cells in vitro and in vivo.', Cancer research, 62(6), pp. 1876–83.

Prasanna, P. G. et al. (2021) 'Therapy-Induced Senescence: Opportunities to Improve Anticancer Therapy', JNCI J Natl Cancer Inst, 113(10), p. 64. doi: 10.1093/jnci/djab064.

Rivadeneira, D. B. et al. (2010) 'Proliferative Suppression by CDK4/6 Inhibition: Complex Function of the Retinoblastoma Pathway in Liver Tissue and Hepatoma Cells', Gastroenterology, 138(5). doi: 10.1053/j.gastro.2010.01.007.

Roberson, R. S. et al. (2005) 'Escape from therapy-induced accelerated cellular senescence in p53-null lung cancer cells and in human lung cancers', Cancer research, 65(7), pp. 2795–2803. doi: 10.1158/0008-5472.CAN-04-1270.

Rugo, H. S. et al. (2019) 'Palbociclib plus letrozole as first-line therapy in estrogen receptor-positive/human epidermal growth factor receptor 2-negative advanced breast cancer with extended follow-up', Breast Cancer Research and Treatment, 174(3), pp. 719–729. doi: 10.1007/S10549-018-05125-4/FIGURES/4.

Ruhland, M. K., Coussens, L. M. and Stewart, S. A. (2016) 'Senescence and cancer: An evolving inflammatory paradox', Biochimica et Biophysica Acta - Reviews on Cancer, 1865(1), pp. 14–22. doi: 10.1016/j.bbcan.2015.10.001.

Saleh, T. et al. (2018) 'Non-Cell Autonomous Effects of the Senescence-Associated Secretory Phenotype in Cancer Therapy', Frontiers in Oncology, 0(MAY), p. 164.

doi: 10.3389/FONC.2018.00164.
Saleh, T. et al. (2019) 'Tumor cell escape from therapy-induced senescence', Biochemical Pharmacology, 162, pp. 202–212. doi: 10.1016/j.bcp.2018.12.013.
Saleh, T. et al. (2020) 'Clearance of therapy-induced senescent tumor cells by the senolytic ABT-263 via interference with BCL-XL–BAX interaction', Molecular Oncology, 14(10), pp. 2504–2519. doi: 10.1002/1878-0261.12761.
Saleh, T., Tyutyunyk-Massey, L. and Gewirtz, D. A. (2019) 'Tumor cell escape from therapy-induced senescence as a model of disease recurrence after dormancy', Cancer Research, 79(6), pp. 1044–1046. doi: 10.1158/0008-5472.CAN-18-3437.
Schoenwaelder, S. M. et al. (2011) 'Bcl-xL-inhibitory BH3 mimetics can induce a transient thrombocytopathy that undermines the hemostatic function of platelets', Blood, 118(6), pp. 1663–1674. doi: 10.1182/BLOOD-2011-04-347849.
Shahbandi, A. et al. (2020) 'BH3 mimetics selectively eliminate chemotherapy-induced senescent cells and improve response in TP53 wild-type breast cancer', Cell Death and Differentiation, 27(11), pp. 3097–3116. doi: 10.1038/s41418-020-0564-6.
Shoemaker, A. R. et al. (2008) 'Activity of the Bcl-2 family inhibitor ABT-263 in a panel of small cell lung cancer xenograft models', Clinical cancer research : an official journal of the American Association for Cancer Research, 14(11), pp. 3268–3277. doi: 10.1158/1078-0432.CCR-07-4622.
Short, S. et al. (2019) 'Senolytics and senostatics as adjuvant tumor therapy', eBioMedicine, 41, pp. 683–692. doi: 10.1016/J.EBIOM.2019.01.056.
Toogood, P. L. et al. (2005) 'Discovery of a potent and selective inhibitor of cyclin-dependent kinase 4/6', Journal of Medicinal Chemistry, 48(7), pp. 2388–2406. doi: 10.1021/JM049354H/SUPPL_FILE/JM049354HSI20050107_011813.PDF.
Torres-Guzmán, R. et al. (2017) 'Preclinical characterization of abemaciclib in hormone receptor positive breast cancer', Oncotarget, 8(41), p. 69493. doi: 10.18632/ONCOTARGET.17778.
Triana-Martínez, F., Loza, M. I. and Domínguez, E. (2020) 'Beyond Tumor Suppression: Senescence in Cancer Stemness and Tumor Dormancy', Cells, 9(2). doi: 10.3390/cells9020346.
Tse, C. et al. (2008) 'ABT-263: A potent and orally bioavailable Bcl-2 family inhibitor', Cancer Research, 68(9), pp. 3421–3428. doi: 10.1158/0008-5472.CAN-07-5836.
Valenzuela, C. A. et al. (2017) 'Palbociclib-induced autophagy and senescence in gastric cancer cells', Experimental Cell Research, 360(2), pp. 390–396. doi: 10.1016/J.YEXCR.2017.09.031.
Vivo-Llorca, G. et al. (2020) 'MUC1 Aptamer-Capped Mesoporous Silica Nanoparticles for Navitoclax Resistance Overcoming in Triple-Negative Breast Cancer', Chemistry - A European Journal, 26(69), pp. 16318–16327. doi: 10.1002/chem.202001579.
Walker, A. J. et al. (2016) 'FDA Approval of Palbociclib in Combination with Fulvestrant for the Treatment of Hormone Receptor-Positive, HER2-Negative Metastatic Breast Cancer', Clinical Cancer Research, 22(20), pp. 4968–4972. doi: 10.1158/1078-0432.CCR-16-0493.
Wang, B., Kohli, J. and Demaria, M. (2020) 'Senescent Cells in Cancer Therapy: Friends or

Foes?', Trends in Cancer, 6(10), pp. 838–857. doi: 10.1016/j.trecan.2020.05.004.

Wang, L., Lankhorst, L. and Bernards, R. (2022) 'Exploiting senescence for the treatment of cancer', Nature Reviews Cancer 2022, pp. 1–16. doi: 10.1038/s41568-022-00450-9.

Wang, X. et al. (1998) 'Evidence of cisplatin-induced senescent-like growth arrest in nasopharyngeal carcinoma cells.', Cancer research, 58(22), pp. 5019–22.

Wedam, S. et al. (2019) 'FDA Approval Summary: Palbociclib for Male Patients with Metastatic Breast Cancer', Clinical Cancer Research, 26(6). doi: 10.1158/1078-0432.ccr-19-2580.

Wolff, A. C. et al. (2013) 'Recommendations for human epidermal growth factor receptor 2 testing in breast', Journal of Clinical Oncology, 31(31), pp. 3997–4013. doi: 10.1200/JCO.2013.50.9984.

Wyld, L. et al. (2020) 'Senescence and cancer: A review of clinical implications of senescence and senotherapies', Cancers, 12(8), pp. 1–20. doi: 10.3390/cancers12082134.

Yin, L. et al. (2020) 'Triple-negative breast cancer molecular subtyping and treatment progress', Breast Cancer Research, 22(1), pp. 1–13. doi: 10.1186/s13058-020-01296-5.

Yosef, R. et al. (2016) 'Directed elimination of senescent cells by inhibition of BCL-W and BCL-XL', Nature Communications, 7, pp. 1–11. doi: 10.1038/ncomms11190.

Yoshida, A., Lee, E. K. and Diehl, J. A. (2016) 'Induction of therapeutic senescence in vemurafenib-resistant melanoma by extended inhibition of CDK4/6', Cancer Research, 76(10), pp. 2990–3002. doi: 10.1158/0008-5472.CAN-15-2931/652215/AM/INDUCTION-OF-THERAPEUTIC-SENESCENCE-IN-VEMURAFENIB.

Yu, Y. et al. (2020) 'Overexpression of miRNA-3613-3p Enhances the Sensitivity of Triple Negative Breast Cancer to CDK4/6 Inhibitor Palbociclib', Frontiers in Oncology, 10(November), pp. 1–14. doi: 10.3389/fonc.2020.590813.

Zeng, C. et al. (2016) 'Intraoperative identification of liver cancer microfoci using a targeted near-infrared fluorescent probe for imaging-guided surgery', Scientific Reports, 6(November 2015), pp. 1–10. doi: 10.1038/srep21959.

Zhu, Y. et al. (2016) 'Identification of a novel senolytic agent, navitoclax, targeting the Bcl-2 family of anti-apoptotic factors', Aging Cell, 15(3), pp. 428–435. doi: 10.1111/acel.12445.

7. Supporting Information

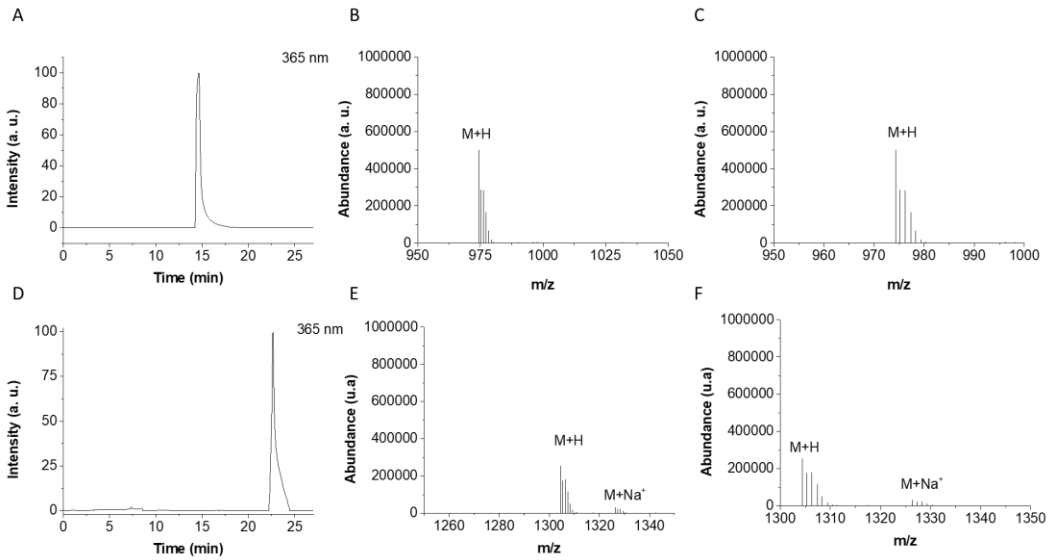

Figure S1 | (A) UV chromatogram of Navitoclax at 365 nm. (B). Mass spectrum for navitoclax obtained from the peak at 14.65 min. (C) Magnification of B showing the 974 m/z value corresponding to M+H. (D) UV chromatogram of nav-Gal at 365 nm. (E). Mass spectrum for Navitoclax obtained from the peak at 22.96 min. (F) Magnification of E showing the 1034 m/z value corresponding to M+H.

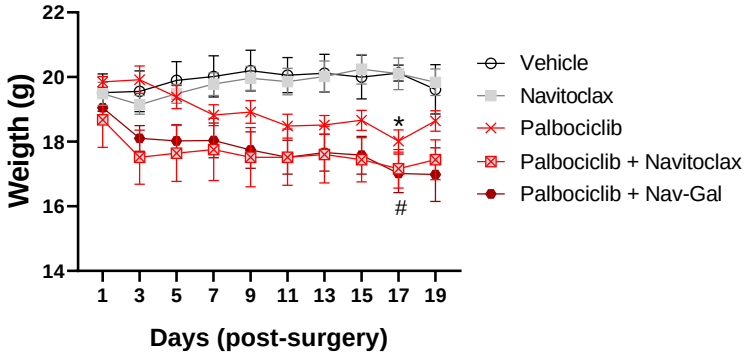

Figure S2 | Mice weight during the whole experiment. Values are expressed as mean ± SEM (n≥5) and statistical significance was assessed by the two-way ANOVA followed by Tukey's post-test: *p<0.05(*Vehicle vs palbociclib + navitoclax); #p<0.05 (#vehicle vs palbociclib + nav-Gal).

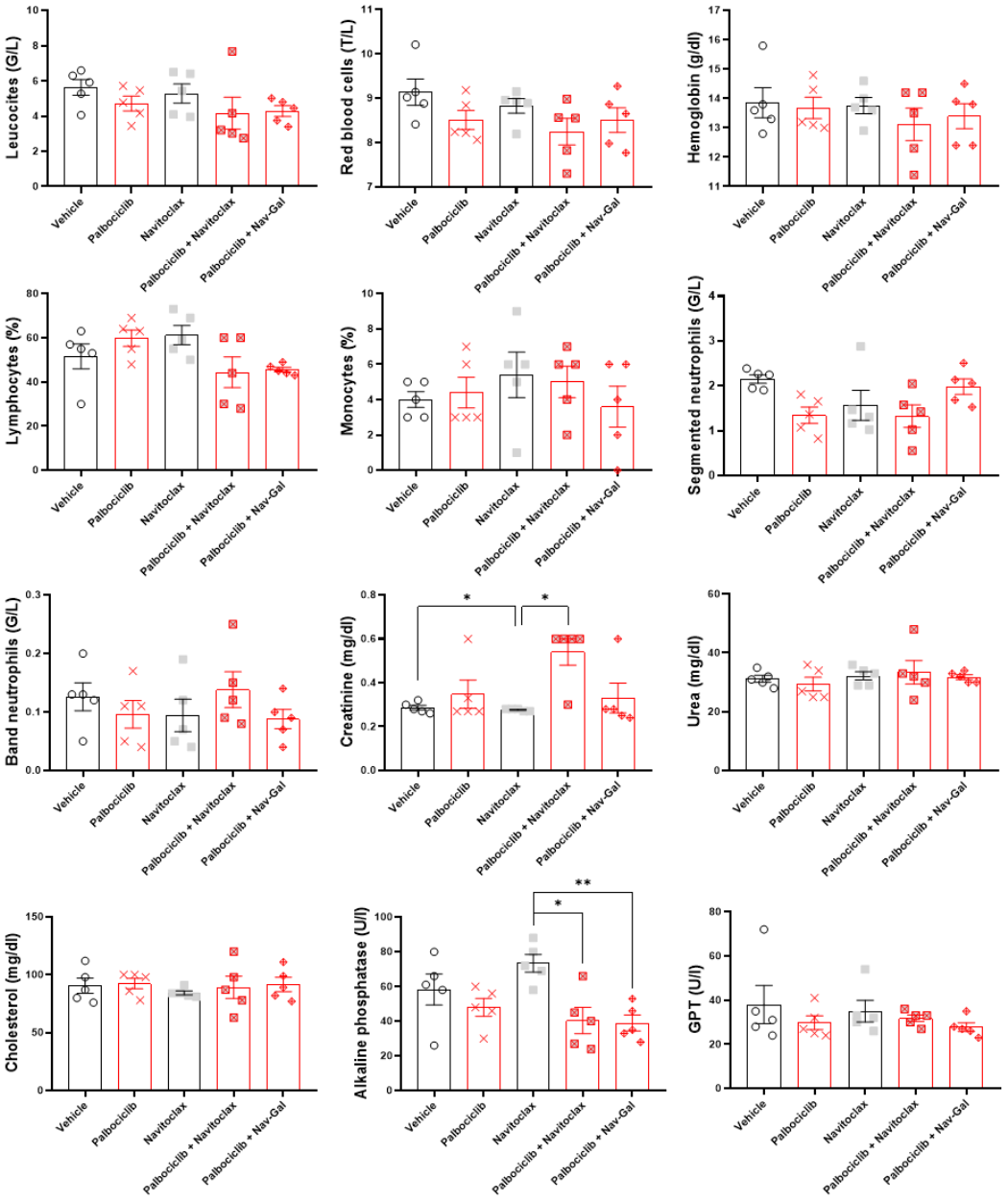

Figure S3 | Hematological and biochemical evaluation of the treatments in nude mice bearing MDA-MB-231 triple-negative breast cancer xenograft. Values are expressed as mean ± SEM (n=5) and statistical significance was assessed by the two-way ANOVA followed by Tukey's post-test (*p<0.05; ** p<0.01; ***p<0.001).

Chapter III | Engineering nanoparticle communication in living systems by stigmergy: an application to enhance antitumor therapy in triple-negative breast cancer

Engineering nanoparticle communication in living systems by stigmergy: an application to enhance antitumor therapy in triple-negative breast cancer

Alejandra Estepa-Fernández,[1,2,3] Alba García-Fernández,[1,2,3*] Araceli Lérida-Viso,[1,2,3,4] Ángela Morellá-Aucejo,[1,2,3] Juan José Esteve-Moreno,[1,2] Juan F. Blandez[1,2,3], María Alfonso,[1] Vicente Candela-Noguera,[1,2] Gema Vivo-Llorca,[1,2] Félix Sancenon-Galarza,[1,2,3,4] Mar Orzáez, [2,5] Ramón Martínez-Máñez[1,2,3,4*]

[1] Instituto Interuniversitario de Investigación de Reconocimiento Molecular y Desarrollo Tecnológico (IDM) Universitat Politècnica de València, Universitat de València. *Camino de Vera, s/n. 46022, Valencia, Spain.*

[2] Unidad Mixta UPV-CIPF de Investigación en Mecanismos de Enfermedades y Nanomedicina, Universitat Politècnica de València, Centro de Investigación Príncipe Felipe. *C/ Eduardo Primo Yúfera 3. 46012, Valencia, Spain.*

[3] CIBER de Bioingeniería, Biomateriales y Nanomedicina (CIBER-BBN).

[4] Unidad Mixta de Investigación en Nanomedicina y Sensores. Universitat Politècnica de València, IIS La Fe. *Av. Fernando Abril Martorell, 106 Torre A 7ª planta. 46026, Valencia, Spain*.

[5] Centro de Investigación Príncipe Felipe. *C/ Eduardo Primo Yúfera 3. 46012, Valencia, Spain.*

* Corresponding authors. Email: algarfe4@etsia.upv.es; rmaez@qim.upv.es

Submitted

Graphical abstract

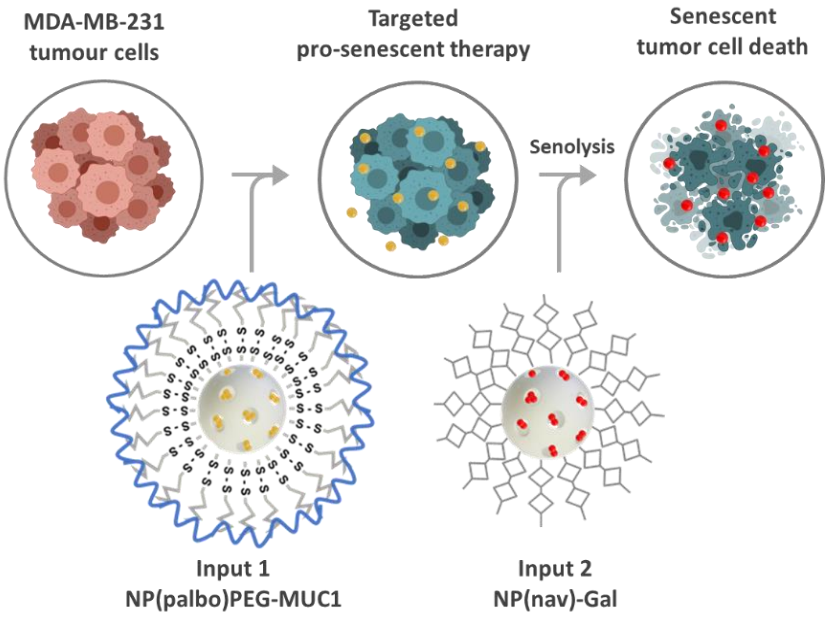

Keywords

Nanoparticle communication, mesoporous silica nanoparticles, senescence, navitoclax, palbociclib, TNBC

My contribution

I performed in vivo and in vitro experiments including the synthesis and characterization of NP(palbo)PEG-MUC1 nanodevice and its derivates. I also contributed to the experimental design, data analysis, discussion and writing.

1. Abstract

The engineering of nanoparticle communication has gained growing attention in the last years, however, efforts to communicate nanoparticles with living systems is still a barely studied emerging topic. Here, we explore a nanoparticle cooperation strategy that involves nanoparticle-cell-nanoparticle communication *in vivo* through stigmergy. Our approach is based on nanodevices that communicate by modifying the environment (stigmergy). First, mesoporous silica nanoparticles loaded with the senescence inductor palbociclib and coated with a heterobifunctional poly(ethylene glycol) that binds covalently to a MUC1-binding aptamer (NP(palbo)PEG-MUC1), were designed to specifically deliver the pro-senescent drug palbociclib in MDA-MB-231 breast cancer cells. Once the first nanoparticle modifies the environment due to the induction of senescence, a second community of nanoparticles, loaded with the senolytic navitoclax and coated with an hexa-oligo-saccharide (NP(nav)-Gal), will release its cargo to selectively eliminate senescent tumor cells. The targeted therapy through stigmergy communication was effective in *in vitro* and *in vivo* delaying tumor growth and reducing metastases in a mouse model of human triple-negative breast cancer while minimizing undesired drugs side effects.

2. Introduction

Since the introduction of nanotechnology concept several years ago, a number of nanoparticles for different applications in areas such as medicine, biotechnology, environmental science, sensing, etc., have been reported. It is possible to design complex nanoparticles for selected purposes.(Zhang *et al.*, 2019) However, nanodevices are usually studied as single non-interactive systems, since communication involving nanoparticles is a scarcely studied topic. Nevertheless, establishing the foundations for communication between nanoparticles and nanoparticles with cells may expand their potential use in

advanced applications allowing them to share information and cooperate.(De Luis *et al.*, 2021)

The concept of communication is essential in living systems and has been crucial for the development of information and communication technologies at the macroscale. In contrast, communication between nanoparticles or nanoparticles with cells is not an easy task and traditional communication technologies are not trivial to apply. A potential approach to establish communication can be achieved by mimicking communications in nature through the use of chemical messengers.(Akyildiz, Brunetti and Blázquez, 2008; de Luis *et al.*, 2021) The use of molecular messengers is the main mechanism of communication in nature and it is ubiquitously used by biological systems. However, very few examples have been reported where micro/nanosystems communicate *via* the interchange of chemical messengers using different enabling technologies. This technologies can be classified by the micro/nanoparticles types (giant liposomes, proteinosomes, coacervates, mesoporous silica, etc.) and by the information processing tools (cell-free transcription-translation machinery (TXTL), DNA displacement reactions, enzymes and responsive molecular ensembles) used.(Giménez *et al.*, 2014; Qiao *et al.*, 2017; Wen *et al.*, 2017; Llopis-Lorente *et al.*, 2018; de Luis *et al.*, 2019, 2021, 2022; Dubuc *et al.*, 2019; Buddingh', Elzinga and van Hest, 2020)

In contrast to the interchange of chemical messengers, many swarm systems in nature communicate through the modification of the environment, a concept that is termed stigmergy.(Bonabeau, Dorigo and Theraulaz, 1999) In this communication protocol, the trace left by an action in a medium stimulates subsequent actions. The concept of stigmergy has been used to analyze self-organizing activities in a wide range of domains including robotics, web communities, human society and social insects.(Theraulaz and Bonabeau, 1999) Stigmergy communication examples in nature involve ants that deposit and sense chemical signals to find food or termites that can build complex structures by modifying their physical environment.(Werfel, Petersen and

Nagpal, 2014) Despite its great potential, the stigmergy paradigm has still been poorly studied in nanotechnology. However, it embraces a completely different mode of communication that can result in several applications and advances in the way we use and design nanoparticles. In this communication protocol one can picture different communities of nanoparticles one of which performs an action and the trace of this action on the medium stimulates the performance of the second community of particles. However, its full power remains underappreciated and examples using nanoparticles and living systems remains almost unexplored.(Ultimo *et al.*, 2020; Maltzahn *et al.*, 2019; Park *et al.*, 2010; Bagley *et al.*, 2013)

Based on the high potential of the stigmergy concept and considering our interest in the design of communication protocols involving nanoparticles, we report herein a stigmergic nanoparticle-cell/tumor-nanoparticle communication applied to enhance tumor therapy in triple-negative breast cancer *in vivo* (Figure 1), taking advantage of the transformation of tumor cells to senescent cells. Briefly, senescence is a cellular state of cell cycle arrest that has traditionally been thought to function as a physiological barrier against tumorigenesis.(Sager, 1991; Campisi, 2001; Collado and Serrano, 2010) However, the accumulation of senescent cells in tumors has been reported to have deleterious effects.(Demaria *et al.*, 2017; Milanovic, Yu and Schmitt, 2018; Saleh *et al.*, 2019, 2020; Estepa-Fernández *et al.*, 2021) Therefore, we envisioned the use of a first population of nanoparticles able to transform tumor cells into senescent cells (transformation of the environment) combined by a second community of nanoparticles able to eliminate senescent cells, with the aim to reduce tumor size by stigmergy. Among senescence-inducing compounds, we used palbociclib, a cyclin-dependent kinase (CDKs) inhibitor already in clinical use.(Finn *et al.*, 2009; Beaver *et al.*, 2015; Walker *et al.*, 2016; Wedam *et al.*, 2019) In relation to senolytic drugs, we used navitoclax, which has shown effectiveness *in vivo* in eliminating senescent cells.(Chang *et al.*, 2016; Zhu *et al.*, 2016; Kim *et al.*, 2017; Bussian *et al.*, 2018) As a consequence of the cooperation by stigmergy

of both nanoparticles, tumor growth reduction, drop of metastases and diminution of drug side effects is observed in a triple-negative breast cancer mice model.

3. Results

3.1. Design, synthesis, and characterization of the final nanodevices

Considering our objective, i.e. to use stigmergy communication concepts to enhance treatment in a mouse model of human triple-negative breast cancer (TNBC) (Figure 1), we prepared two sets of nanodevices using MSNs as an inorganic scaffold (Table S1 and Figure S1). The first nanoparticle is a pro-senescent nanodevice (NP(palbo)PEG-MUC1) and is designed for the targeted induction of senescence in TNBC. To prepare this first nanoparticle, the pores of MSNs were loaded with palbociclib (NP(palbo)) and functionalized with (3-mercaptopropyl)trimethoxysilane. Then, the thiol groups on the surface were reacted first with 2,2'-dipyridyldisulfide and then with a heterobifunctional poly(ethylene glycol) (NHS-PEG-SH) that was finally anchored to the nanoparticles through the formation of disulfide bonds (NP(palbo)PEG). Finally, the 5' amino-modified MUC1-binding aptamer (5' NH_2-GCAGTTGATCCTTTGGATACCCTGG-3') was covalently bonded onto the PEG derivate on the external surface through the formation of amide bonds, yielding the final nanodevice NP(palbo)PEG-MUC1 (Figure 2A). Mucin 1 (MUC1) is a transmembrane glycoprotein considered as an oncomarker due to its overexpression in breast cancer and other carcinomas.(Apostolopoulos, Pietersz and McKenzie, 1999; Vivo-Llorca *et al.*, 2020) Following a similar procedure, nanoparticles NP(saf)PEG, NP(saf)PEG-MUC1 (loaded with safranine O),NP(ICG)PEG, and NP(ICG)PEG-MUC1 (loaded with indocyanine green for *in vivo* tracking purposes) were also prepared. It is hypothesized that these nanoparticles will be internalized selectively by breast cancer cells through MUC1-mediated endocytosis with the subsequent cargo delivery (i.e. palbociclib, safranine O, or ICG) due to the high intracellular concentration of glutathione (GSH), that would reduce the disulfide bonds of the capping PEG in the endocytic

compartment.(Giménez *et al.*, 2015) In order to evaluate the targeting ability of the aptamer functionalized nanoparticles, a similar nanodevice loaded with safranine O but functionalized with a random DNA sequence unable to bind with MUC1 receptor (i.e. 5' NH_2-AAGCACTTTCAGTGGGGAGGAGGGTTGATAGGTTAAGAG-3') was also prepared (NP(saf)PEG-Random). Besides, another set of nanoparticles without any cargo was synthesized to check the biocompatibility of the inorganic support and the gating ensemble (NP-PEG).

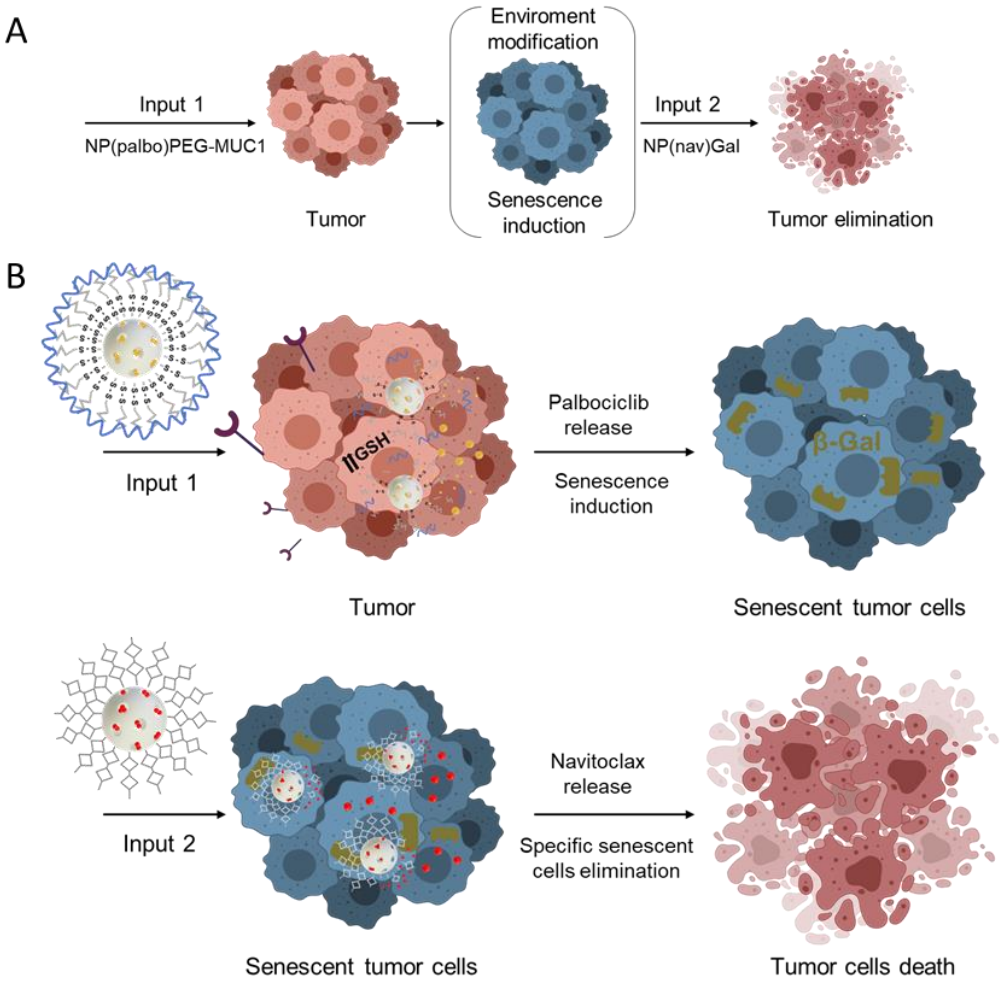

Figure 1 | Nanoparticle communication by stigmergy for enhanced tumor reduction using targeted induction of senescence and senolysis. (A) Schematic representation of stigmergy communication concept. A first community of nanoparticles induces a modification in the environment in such a way that enhances the action of a subsequent community of nanoparticles. (B) NP(palbo)PEG-MUC1 (first community of nanoparticles) releases its cargo in cancer cells due to both (1) the presence of a MUC1-binding aptamer and (2) a high intracellular concentration of glutathione (GSH) that reduces the disulfide bonds of the capping PEG. The release of palbociclib by the first community of nanoparticles modifies the environment by senescence induction in tumor cells. This allows a second community of nanoparticles (NP(nav)-Gal) release their content in senescent cells due to the high lysosomal β-galactosidase activity in these cells. β-Galactosidase induces the hydrolysis of the capping ensemble (galactan) with subsequent delivery of a senolytic cargo (navitoclax) that eliminates senescent cells by apoptosis reducing tumor size.

The second nanoparticle (NP(nav)-Gal) was recently reported by us and we have also described its use in the selective release of entrapped cargos in senescent cells.(Bernardos *et al.*, 2010; Agostini *et al.*, 2012; Muñoz-Espín *et al.*, 2018; Galiana *et al.*, 2020; Lozano-Torres *et al.*, 2020; Estepa-Fernández *et al.*, 2021) To prepare NP(nav)-Gal, MSNs were loaded with navitoclax and externally functionalized with (3-aminopropyl) trimethoxysilane. Finally, the amino moieties reacted with a hexa-galacto-oligosaccharide (galactan), yielding the final system (Figure 2B). Galactan was introduced into the nanoparticle system in order to release the cargo since it can be hydrolyzed due to the elevated lysosomal β-galactosidase activity in senescent cells. Nanoparticles without cargo (NP-Gal) or loaded with the dye nile blue and coated with galactan were also prepared (NP(NB)-Gal) following the same procedure.

Both sets of nanoparticles were characterized using standard procedures (see Supporting Information for more details). The mesoporous structure of the final nanoparticles was clearly observed by powder X-ray diffraction (PXRD) (Figure S2). In all cases the (100) reflection in the PXRD patterns is observed indicating that the 2D mesoporous structure was preserved during the pore loading process and its additional functionalization. N_2 adsorption-desorption isotherms (Figure S3) of the calcined MSNs showed a type IV isotherm typical of the mesoporous silica materials and a BET specific surface area of 1,158.8 m^2/g. In contrast, the N_2 adsorption-desorption isotherm of the

final nanodevices was typical of mesoporous systems with partially filled mesopores with reduced specific surfaces (Table S2). TEM images (Figure S4) show for all nanoparticles a similar reticular spherical geometry with a diameter of ca. 100 nm. Furthermore, TEM-EDX mapping studies for NP(palbo)PEG-MUC1 (Figure 2C) demonstrated the presence of Si (from the silica scaffold), N (from palbociclib and MUC1-targeting aptamer), S (from disulfide bond in the PEG chain), and P (from MUC1 targeting-aptamer). TEM-EDX map for NP(nav)-Gal (Figure 2C) shows the presence of Si (from the silica scaffold), S, F, Cl (from the loaded navitoclax,) and N (from navitoclax and the capping galactan oligosaccharide).

Besides, zeta potential (Figure S5, Table S3) and hydrodynamic diameter (Table S3) measurements were also conducted. Calcined MSNs presented a zeta potential value of -30.9 ± 0.6 mV that changed to 24.0 ± 0.3 mV after pore loading with palbociclib, functionalization of the external surface with mercaptopropyl moieties and subsequent activation with 2,2'-dipyridyldisulfide. After the addition of NHS-PEG-SH, the zeta potential turns to negative values (-32.0 ± 0.3), becoming more negative (-40.3 ± 1.5 mV) when the MUC1-binding aptamer is anchored to give the final NP(palbo)PEG-MUC1 nanoparticle. Moreover, the hydrodynamic diameter increased after the loading and functionalization process from 161.7 ± 2.7 nm for the calcined MSNs to 199.4 ± 6.3 nm for NP(palbo)PEG-MUC1. For NP(nav)-Gal, zeta potential changed from the initial -30.9 ± 0.6 value to 4.03 ± 0.3 mV after loading the pores with navitoclax and grafting of galactan. Besides, the hydrodynamic diameter increased from 161.7 ± 2.7 for MSNs to 253.4 ± 2.2 nm for NP(nav)-Gal. A single population distribution was observed for all the systems suggesting that nanoparticles were not aggregated. Finally, the amount of palbociclib (59 mg/g SiO_2) and PEG (124 mg/g SiO_2) in NP(palbo)PEG were determined by thermogravimetric analysis and by delivery studies in the presence of glutathione. Thermogravimetric analysis and delivery studies were also used to determine the amount of navitoclax (54 mg/g SiO_2) and galactan (167 mg/g SiO_2) in NP(nav)-Gal (Table S4).

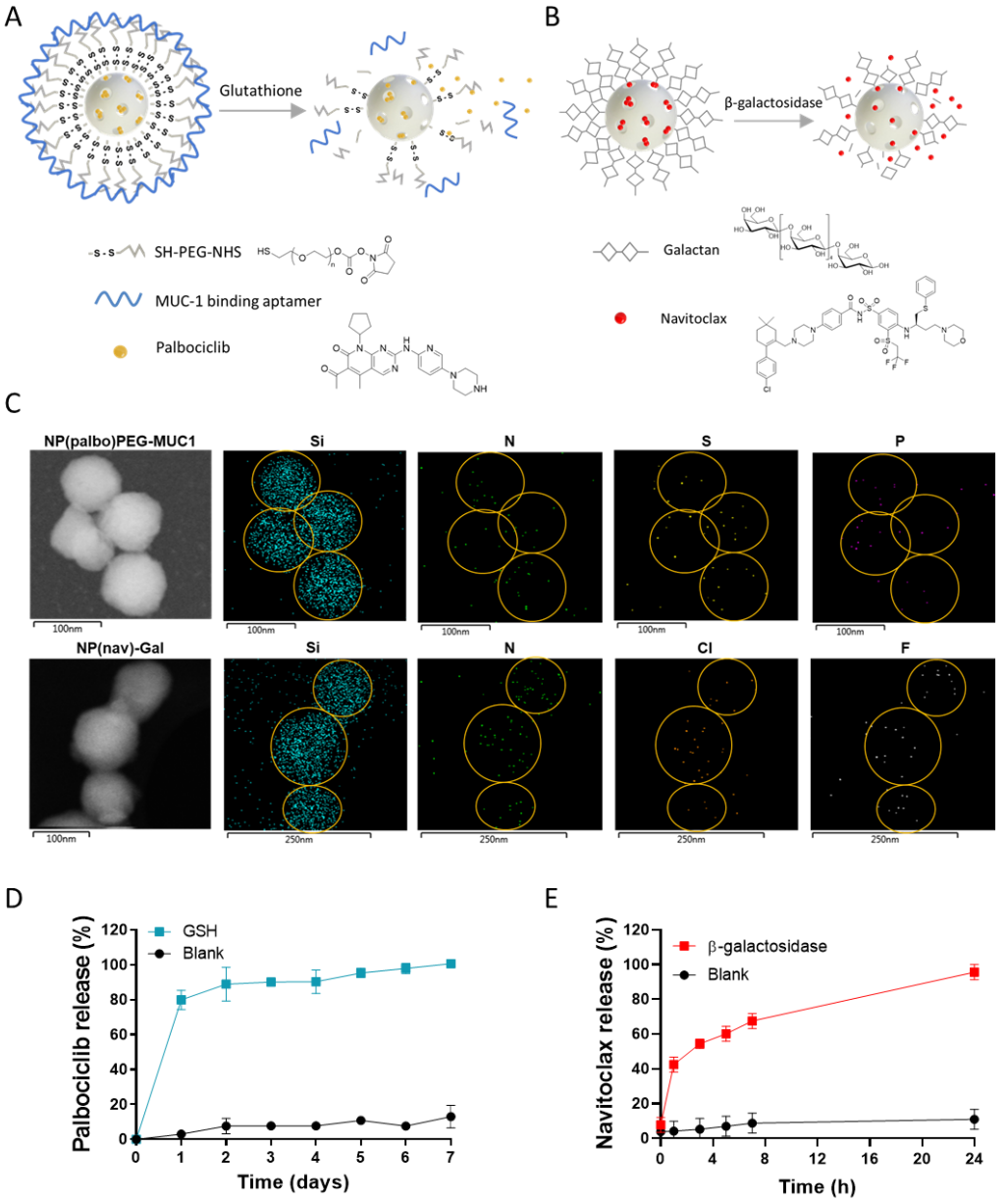

Figure 2 | Nanoparticle design and characterization. (A) Scheme of mesoporous silica nanoparticles (MSNs) loaded with palbociclib and capped with a PEG chain attached to the MUC1-targeting aptamer. (B) Scheme of MSNs loaded with navitoclax and capped with a hexa-galacto-oligosaccharide (galactan). (C) TEM-EDX map for NP(palbo)PEG-MUC1 showing the presence of Si (from the silica scaffold), N (from palbociclib and MUC1-targeting aptamer), S (from the disulfide bond), and P (from MUC1 targeting-aptamer). TEM-EDX map for NP(nav)-Gal shows the presence of Si (from the silica scaffold), S, F,Cl (from the cargo navitoclax), and N (from navitoclax and

galactan). (D) Release profile of palbociclib from NP(palbo)PEG in the absence (black) or presence of GSH (blue) in PBS. Data represent mean ± SEM (n=3). (E) Release profile of navitoclax from NP(nav)-Gal, in the absence (black) or presence of β-galactosidase (red) in water at pH 4.5. Data represent mean ± SD (n=3).

To study the gating ability of the capping PEG, cargo delivery from NP(palbo)PEG was studied in PBS in the presence or the absence of GSH (Figure 2D). GSH is a tripeptide capable of reducing disulfide bonds and its presence has been used for the controlled release of cargos inside cells, as GSH concentration in cells (10 mM) is significantly higher than in blood plasma (2 μM).(Jones *et al.*, 1998) As shown in Figure 2D, a negligible palbociclib release was observed (ca. 10% after 120 h) for NP(palbo)PEG in the absence of GSH. However, a remarkable delivery was found in the presence of GSH. Similar GSH-triggered cargo delivery was observed for NP(saf)PEG and NP(ICG)PEG (Figure S6). Besides, NP(nav)-Gal displayed a negligible drug delivery in solution, while navitoclax was clearly delivered in the presence of the β-galactosidase enzyme (Figure 2E).(Muñoz-Espín *et al.*, 2018; Galiana *et al.*, 2020; Lozano-Torres *et al.*, 2020; Estepa-Fernández *et al.*, 2021) Finally, the biocompatibility of the newly prepared nanodevices was assessed. For this purpose, cell viability studies in the presence of NP-PEG (without cargo) at different concentrations were performed in MDA-MB-231 breast cancer cells (Figure S7A). After 7 days of treatment, cell viability was kept up to 80% even at the highest NP-PEG concentrations (200 μg/mL). We also found that NP-Gal was well-tolerated for MDA-MB-231 cell line (Figure S7B).(Muñoz-Espín *et al.*, 2018; Galiana *et al.*, 2020; Estepa-Fernández *et al.*, 2021)

3.2. Targeted internalization of MUC1-functionalised nanoparticles and induction of senescence *in vitro*

As described above, the pro-senescent nanodevice (first community of nanoparticles) was functionalized with an aptamer designed to target the MUC1 receptor in TNBC MDA-MB-231 cells. MUC1 is a glycoprotein (Gendler, 2001; Pascual *et al.*, 2017) that is overexpressed in MDA-MB-231 cells.(Vivo-Llorca *et al.*, 2020)

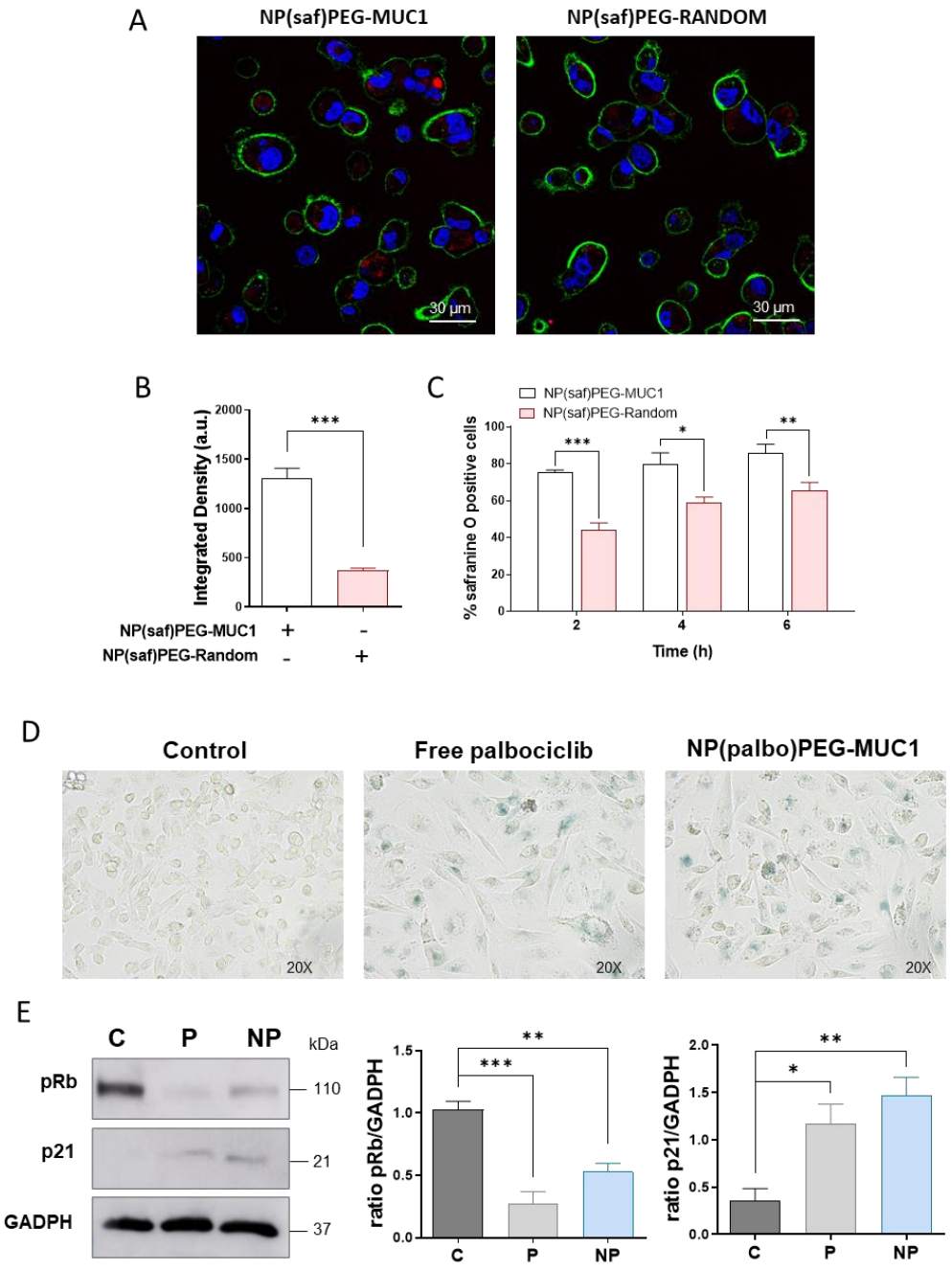

Figure 3 | NP(saf)PEG-MUC1 is preferentially internalized in MDA-MB-231 cells, and NP(palbo)PEG-MUC1 efficiently induces senescence. (A) Representative confocal images of NP(saf)PEG-MUC1 internalization vs NP(saf)PEG-Random internalization by MDA-MB-231 cells after 2 h of treatment (50 µg/mL). Safranine O (red), WGA Alexa 488 (green), and nucleus (blue).

(B) Fluorescence intensity quantification of confocal images of NP(saf)PEG-MUC1 internalization (white bars) vs NP(saf)PEG-Random internalization (red bars) by MDA-MB-231 cells after 2 h of treatment. Data represent mean ± SEM (n=3), and statistical significance was assessed by two-tailed Student's T-test (***p-value<0.001.) (C) Percentage of safranine O positive MDA-MB-231 cells in flow cytometry after 2, 4 and 6 h of NP(saf)PEG-MUC1 (white bars) or NP(saf)PEG-Random (red bars) treatment. Data represent the means ± SEM of at least three independent experiments and statistical significance was assessed by two-way ANOVA followed by Sidak's post-test (*p<0.05; **p<0.01; ***p<0.001) (D) β-Galactosidase staining of control (C), 2.5 μM free palbociclib-treated (P) MDA-MB-231 cells, and 80 μg/mL NP(palbo)PEG-MUC1 (NP) treated MDA-MB-231 cells. Senescence induction was confirmed by high β-galactosidase activity (blue color) in free palbociclib or nanoparticle-treated cells at pH 6. (E) Western Blot characterization of proliferating and senescent MDA-MB-231 cells. After palbociclib treatment pRb (110 kDa) expression decreases whereas p21 (21 kDa) expression increases. Quantification of the bands using GADPH as a loading control (n≥3) (right panels). Values are expressed as mean ± SEM, and statistical significance was assessed by one-way ANOVA followed by a Tukey post-test: *p<0.05; **p<0.01; ***p<0.001.

The preferential internalization of the nanodevice loaded with safranine O (NP(saf)PEG-MUC1) in MDA-MB-231 cells was studied using confocal microscopy and flow cytometry (Figure 3). Confocal images revealed a red emission, ascribed to safranin O, in MDA-MB-231 cells (Figure 3A, left image) after 2 h of treatment with NP(saf)PEG-MUC1. To demonstrate the targeting ability of the capping MUC1-binding aptamer, similar cell internalization studies were performed with nanoparticles functionalized with a random DNA sequence (NP(saf)PEG-Random). When cells were treated with NP(saf)PEG-Random, a much lower safranine O red emission in cells was found (Figure 3A, right image). Quantification of confocal images demonstrated a 3-fold higher safranine O emission in MDA-MB-231 cells treated with NP(saf)PEG-MUC1, when compared to those treated with NP(saf)PEG-Random (Figure 3B). Besides, the safranin O release from NP(saf)PEG-MUC1 and NP(saf)PEG-Random nanoparticles was monitored using flow cytometry (Figure 3C). The results corroborated the preferential uptake of NP(saf)PEG-MUC1 by ca. 80% of the cells after 2 h of treatment, compared to ca. 40% of cells treated with NP(saf)PEG-Random. These results demonstrate the targeting ability of NP(saf)PEG-MUC1 to MDA-MB-231 breast cancer cells.

After demonstrating the ability of NP(saf)PEG-MUC1 to target TNBC cells, we tested if NP(palbo)PEG-MUC1 was able to induce senescence. For that purpose, MDA-MD-231 cells were treated with 80 µg/mL of NP(palbo)PEG-MUC1 for 7 days (corresponds to 2.5 µM of free palbociclib). Free palbociclib at 2.5 µM treatment was used as a control of the senescence induction. Cells treated with free palbociclib or with NP(palbo)PEG-MUC1 have a different morphological appearance when compared with non-treated cells (Figure 3D). Palbociclib-treated cells became larger, flattened, and with higher granularity due to the presence of an expanded lysosomal compartment and the stain in blue when treated with X-Gal due to high activity of β-galactosidase enzyme in senescent cells.(Lozano-Torres *et al.*, 2019) The induction of senescence using encapsulated palbociclib in NP(palbo)PEG-MUC1 was similar to that observed for free palbociclib administration. Besides, western blot assays demonstrated a reduction in the expression of pRb after the treatment with free palbociclib or NP(palbo)PEG-MUC1 (Figure 3E). The hypo-phosphorylation of pRB protein is a recognized mark of senescence induction as a direct consequence of the inhibition of CDK4/6 proteins after palbociclib treatment, which causes cell cycle arrest in the G1/S transition phase.(Goel *et al.*, 2018) Besides, there was an up-regulation of p21 protein when the cells were treated with palbociclib or NP(palbo)PEG-MUC1. These results demonstrated that NP(palbo)PEG-MUC1 induces senescence in MDA-MB-231 cells.

3.3. Cooperative behavior by stigmergy: targeted induction of senescence and senolysis *in vitro*

Once the targeting ability and the pro-senescent capacity of NP(palbo)PEG-MUC1 in MDA-MB-231 cells was assessed, we studied whether the proposed stigmergy communication using nanoparticles could be suitable to enhance cancer therapy. In this respect, MDA-MB-231 cells were treated, in a first step, with free palbociclib or NP(palbo)PEG-MUC1 and, in a second step, with free navitoclax or NP(nav)-Gal. Then, cells were incubated for 72 h and cell viability was measured (Figure 4A). Addition of free

navitoclax to free palbociclib-treated MDA-MB-231 cells resulted in a half-maximal inhibitory concentration (IC50) of 2.71 µM (Figure S8). Remarkably, a higher senolytic activity was obtained when free palbociclib-treated MDA-MB-231 cells were treated with NP(nav)-Gal nanoparticles (Figure 4B) (IC50 value of 1.41 µM). On the other hand, when senescence is first induced by the treatment of MDA-MB-231 cells with NP(palbo)PEG-MUC1, followed with free navitoclax treatment also results in senescent cells death (IC50 of 6.05 µM) (Figure S8). Besides, when MDA-MB-231 cells are treated with the two nanodevices (NP(palbo)-PEG-MUC1 and NP(nav)-Gal), a remarkable IC50 of 1.56 µM is obtained (Figure 4B). These results suggest a beneficial effect due to the combination of NP(palbo)-PEG-MUC1 and NP(nav)-Gal. The stigmergy strategy using the two nanoparticles effectively results in the specific cell death of senescent cells with an increased therapeutic effect compared to the administration of the free drugs.

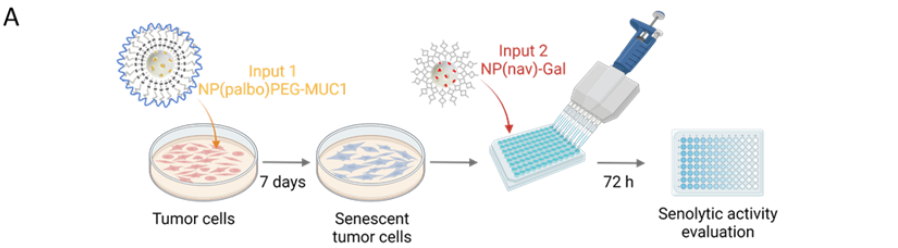

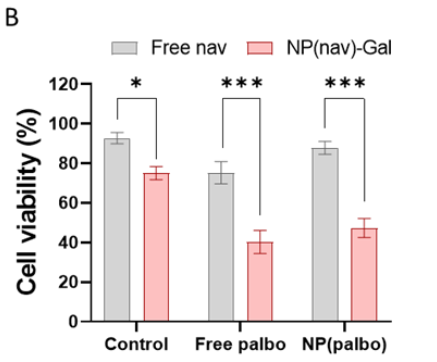

IC50 (µM)	Free palbo	NP(palbo)PEG-MUC1
Free nav	2.71	6.05
NP(nav)-Gal	1.41	1.56

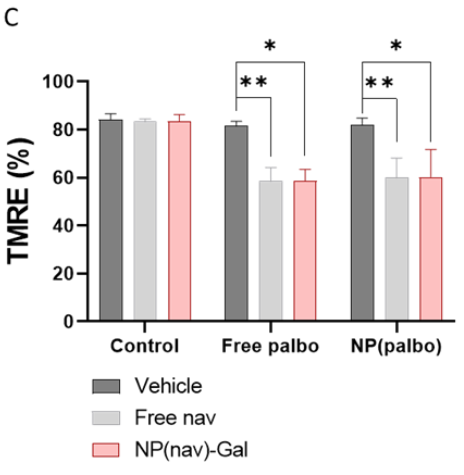

Figure 4 | Cytotoxicity profile of the combination of free palbociclib or NP(palbo)PEG-MUC1 with free navitoclax or NP(nav)-Gal in MDA-MB-231 cells. (A) Scheme of cell viability assays to evaluate the communication system. (B) Cell viability after 72 h of treatment at 0.16 μM and the IC50 values determined for each combined treatment. Control states for non-treated proliferating MDA-MB-231 cells (C) Mitochondrial polarization status in the above-described conditions. Data represent the means ± SEM of at least three independent experiments. Statistical significance was determined by two-way ANOVA followed by Tukey post-test (*p <0.05; **p <0.01 ***p <0.005).

We next investigated the death mechanism of both combinations of the free drugs and the nanodevices in MDA-MB-231 cells. To do so, we studied the mitochondria potential (Figure 4C) using the tetramethylrhodamine ethyl ester (TMRE) dye.(Zamzami *et al.*, 1995; Overbeeke *et al.*, 1999) The results revealed that, following free palbociclib or NP(palbo)PEG-MUC1 treatment, the navitoclax treatment, as a free drug or encapsulated in NP(nav)-Gal, decreased the mitochondrial membrane potential to ca. 60%, indicating apoptosis triggering. These results corroborate the potential of the stigmergy paradigm by using a first community of NP(palbo)PEG-MUC1 nanoparticles to transform tumor cells in senescent cells in combination with a second community of NP(nav)-Gal nanoparticles to eliminate senescent cancer cells.

3.4. Stigmergic communication by targeted induction of senescence and senolysis using nanoparticles *in vivo* in TNBC MDA-MB-231 xenografts

As stated above, stigmergy is a communication method in which individuals (in our case, nanoparticles) communicate with each other by changing the surrounding. The above results demonstrate *in vitro* that a first community of nanoparticles is able to transform tumor cells in senescent cells in combination with a second community of nanoparticles that eliminates senescent cells selectively. However, a most appealing issue of stigmergic communication is its high potential to be applied in highly complex systems such as an *in vivo* environment.

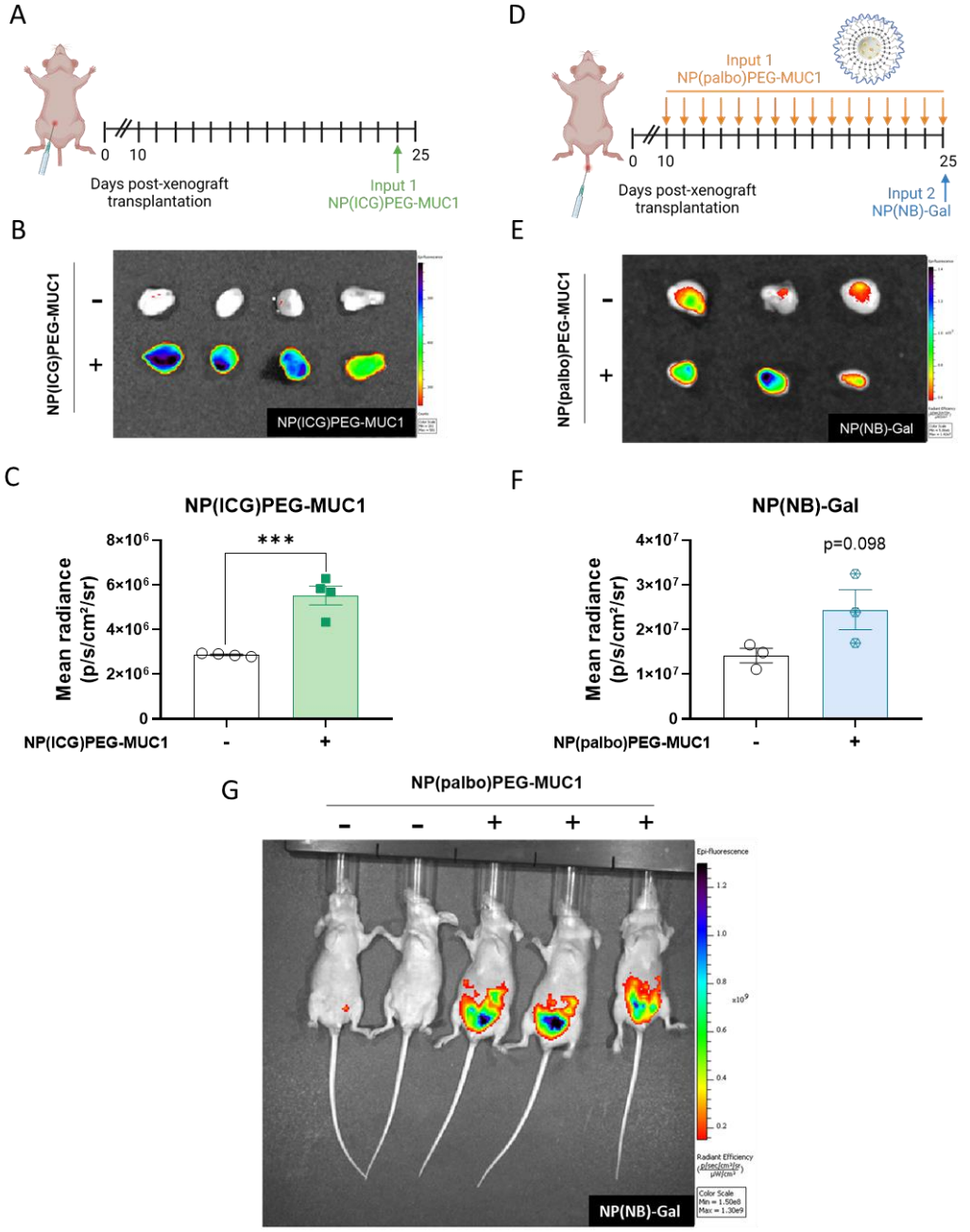

Figure 5 | NP(ICG)PEG-MUC1 nanoparticles selectively release their cargo in the tumors of TNBC model mice, and NP(NB)-Gal nanoparticles selectively release their cargo in the senescent tumors. (A) Balb/c nude female mice were injected on mammary pads with TNBC MDA-MB-231 cells. When tumors volume reached 220 mm^3, NP(ICG)PEG-MUC1 nanoparticles (i.p.) were administered and

IVIS imaging was performed. (B) *Ex vivo* IVIS spectrum imaging of tumors 24 h post-injection of NP(ICG)PEG-MUC1 and (C) fluorescence quantification by Living Image® 4.3.1 software. Data represent mean ± SEM (n=4), and statistical significance was assessed by two-tailed Student's T-test (***p-value<0.001) (D) Balb/c nude female mice were injected on mammary pads with TNBC MDA-MB-231 cells. When tumors volume reached 60 mm^3, palbociclib treatment started (encapsulated in NP(palbo)PEG-MUC1 nanoparticles (i.p)) and was maintained daily for 24 days. On day 24, NP(NB)-Gal nanoparticles (i.p.) were administered and IVIS imaging was performed. (E) *Ex vivo* IVIS spectrum imaging of senescent tumors 24 h post-injection of NP(NB)-Gal and (F) fluorescence quantification by Living Image® 4.3.1 software. Data represent mean ± SEM (n=3), and statistical significance was assessed by two-tailed Student's T-test (*p-value<0.05) (G) *In vivo* imaging studies by IVIS of NP(NB)-Gal distribution after 24 h post-injection in MDA-MB-231 bearing mice previously treated with vehicle (as a control) or NP(palbo)PEG-MUC1 to induce senescence in tumors.

To this aim we first evaluated nanoparticles' ability to target breast cancer tumors *in vivo*. For this purpose, we tracked the activity of the two sets of nanoparticles loaded with fluorescent reporters (i.e. NP(ICG)PEG-MUC1 and NP(NB)-Gal). For that, Balb/c nude female mice were injected on mammary pads with TNBC MDA-MB-231 cells. When tumors volume reached 220 mm^3, NP(ICG)PEG-MUC1 nanoparticles were intraperitoneally administrated (Figure 5A). *Ex vivo* imaging studies of ICG distribution at 24 h post-injection demonstrated the accumulation of the NP(ICG)PEG-MUC1 in MDA-MB-231 tumors with the subsequent release of ICG (Figures 5B and 5C). In an additional experiment, we evaluated if NP(NB)-Gal are able to target senescent tumors induced by the action of the first community of NP(palbo)PEG-MUC1 nanoparticles (Figure 5D). Thus, after two weeks of treatments with NP(palbo)PEG-MUC1, NP(NB)-Gal were intraperitoneally administered. IVIS imaging studies at 24 h post-injection shows the preferential release of the loaded nile blue fluorophore in MDA-MB-231 senescent tumors *ex vivo* (Figure 5E and 5F) and *in vivo* (Figure 5G). These experiments demonstrated that (i) NP(ICG)PEG-MUC1 targets MDA-MB-231 tumors and (ii) previous treatment with the palbociclib-loaded nanoparticles NP(palbo)PEG-MUC1 allows tumor targeting by the second NP(NB)-Gal nanoparticles.

Finally, to validate the proposed therapeutic stigmergic communication, senescence-inducing chemotherapy with NP(palbo)PEG-MUC1 in combination with the senolytic NP(nav)-Gal was tested *in vivo*. MDA-MB-231 cells were injected subcutaneously in the second lower right breast of nude BALB/C mice. When tumor volume reached an average of 60 mm^3, daily therapy was initiated with either vehicle (sodium lactate), 5 mg/kg palbociclib (via oral gavage), or NP(palbo)PEG-MUC1 (via i.p. injection at equivalent palbociclib dose) (Figure 6A). As a result of palbociclib treatment, a significant decrease in tumor growth was observed in mice treated with monotherapy of either free palbociclib or NP(palbo)PEG-MUC1 (Figure 6B). Besides, X-Gal staining showed the overexpression of β-galactosidase in tumor slides of mice treated with either free palbociclib or NP(palbo)PEG-MUC1 (Figure 6C), indicative of the transformation of the environment, from tumors to senescent tumors. Cell senescence induction in tumors was also assessed by immuno-histochemical staining of the proliferation biomarker Ki67 in tumor autopsy samples and by the increase in p53 positive cells (Figure 6C and Figure S9). All these results confirmed the suitability of NP(palbo)PEG-MUC1 nanoparticles for senescence induction in animal models.

In a second step, the effect of the second swarm of nanoparticles NP(nav)-Gal was evaluated. Thus, one day after NP(palbo)PEG-MUC1 administration, senolytic treatment was initiated with NP(nav)-Gal. Remarkably, concomitant treatment with NP(palbo)PEG-MUC1 plus NP(nav)-Gal resulted in a significant reduction of tumor growth (Figure 6B and Figure S10). The results confirmed the proper achievement of therapeutic communication using two sets of nanoparticles that act cooperatively. The modification of cancer cells into senescent cells induced by NP(palbo)PEG-MUC1 (modifying the environment) allows the second community of nanoparticles (NP(nav)-Gal) to deliver the senolytic cargo in senescent cells, resulting in a significant reduction in tumor size. Besides, a similar tumor reduction in mice treated with an equivalent concentration of free palbociclib and free navitoclax was found. However, a remarkable reduction of drug side effects was observed when animals were treated with the encapsulated drugs (*vide infra*).

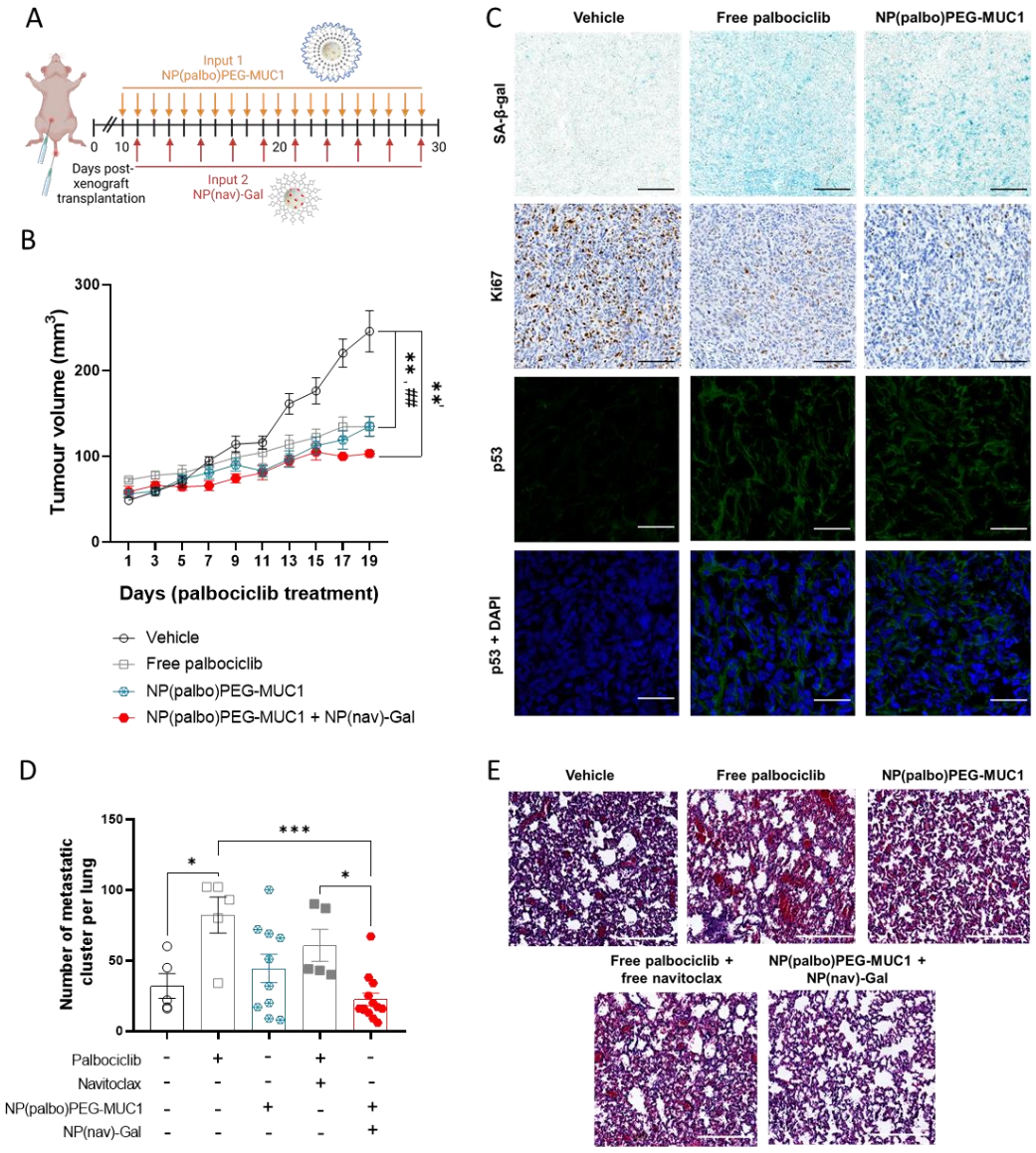

Figure 6 | *In vivo* evaluation of stigmergy communication of NP(palbo)PEG-MUC1 and NP(nav)-Gal in TNBC. (A) Balb/c nude female mice were orthotopically injected with TNBC MDA-MB-231 cells and treated daily with vehicle, free palbociclib, or NP(palbo)PEG-MUC1. 2×10^6 MDA-MB-231 cells were subcutaneously implanted on mammary pads. When tumors volume reached 60 mm^3, palbociclib treatment started (encapsulated in nanoparticles or as a free drug) and was maintained daily for 19 days. NP(nav)-Gal daily treatment started one day after free palbociclib or NP(palbo)PEG-MUC1 treatment. (B) Tumor volume (mm^3) of the different treatment approaches during all the treatments. Statistical analysis was carried out using GraphPad Prism 8, and results

were compared by one-way ANOVA followed by Tukey's post-test (*Vehicle vs free palbociclib; #vehicle vs NP(palbo)PEG-MUC1; **' vehicle vs NP(palbo)PEG-MUC1 + NP(nav)-Gal) (*p<0.05; **p<0.01; ***p<0.001). Data represent the mean ± SEM (n≥5). (C) Photograph of representative tumor sections stained with X-gal, immunostained with Ki67 and p53. Scale bar, 200 µm. (D) Quantification of metastatic lung clusters found in lung sections taken from xenograft MDA-MB-231 tumor-bearing mice. (E) Representative tissue images were microscopically counted. Statistical analysis was carried out using GraphPad Prism 8, and results were compared by one-way ANOVA followed by Tukey's post-test (*p<0.05; **p<0.01; ***p<0.001). Data represent the mean ± SEM (n≥5). E) H&E staining of representative metastatic lung clusters. Scale bar, 500 µm.

Attending to the metastatic profile of TNBC tumors, we also evaluated lung metastasis in the mice bearing MDA-MB-231 tumors model. Metastatic cell clusters were found in lung sections of MDA-MB-231 xenograft mice (Figures 6D and 6E). After free palbociclib treatment, a significant increase in the number of metastatic clusters in lungs is detected. In contrast, a significant decrease was found in those animals co-treated with NP(palbo)PEG-MUC1 and NP(nav)-Gal (Figures 6D and 6E). Histological examination of apoptosis through TUNEL assay in tumor slides evidenced that senescent cells undergo apoptosis after treatment with either free palbociclib plus free navitoclax or NP(palbo)PEG-MUC1 plus NP(nav)-Gal. Moreover, the combinational treatment with the nanoparticles revealed the highest TUNEL signal (Figure 7A and 7B).

To study the safety of the stigmergy strategy using NP(palbo)PEG-MUC1 plus NP(nav)-Gal nanoparticles for two weeks of sustained treatment, blood samples were collected for biochemistry and hematological analyses. In addition, biochemistry analyses were performed to evaluate hepatic and liver function (Figure S11). Besides, to discard a potential pro-inflammatory effect of the nanoparticles, the levels of neutrophils, lymphocytes, and monocytes were analyzed in blood samples (Figure S12). No significant differences between animals untreated or treated with nanoparticles were observed. In conclusion, NP(palbo)PEG-MUC1 plus NP(nav)-Gal treatment does not induce any toxicity or side effects derived from two weeks of sustained nanoparticles administration.

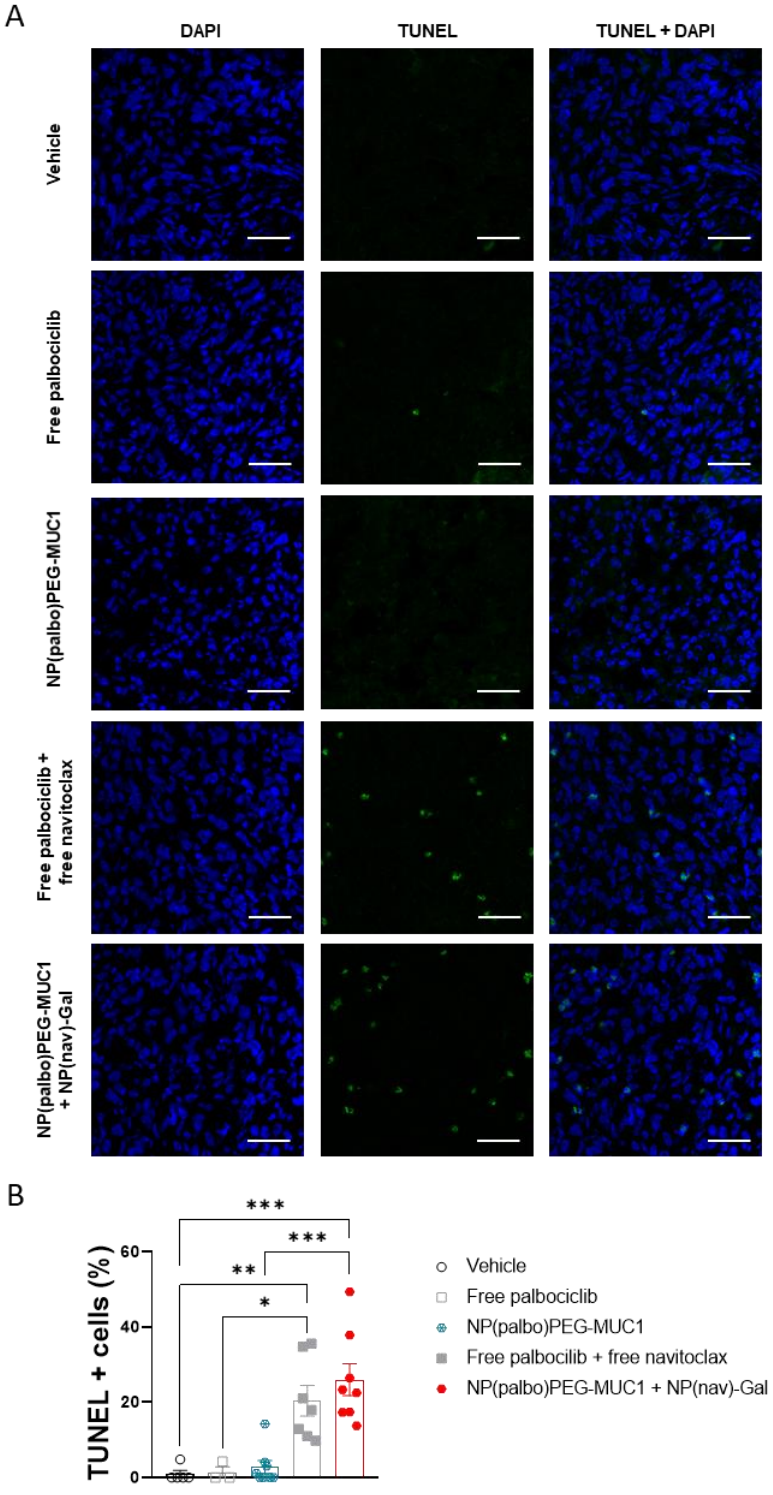
A
DAPI
TUNEL
TUNEL + DAPI
Vehicle
Free palbociclib
NP(palbo)PEG-MUC1
Free palbociclib + free navitoclax
NP(palbo)PEG-MUC1 + NP(nav)-Gal
B
TUNEL + cells (%)
60
40
20
0
***
***
**
*
Vehicle
Free palbociclib
NP(palbo)PEG-MUC1
Free palbocilib + free navitoclax
NP(palbo)PEG-MUC1 + NP(nav)-Gal

Figure 7 | Histological analysis of apoptosis in tumor slides after treatment. (A) Representative confocal images of TUNEL assay of tumor sections from animals treated with vehicle, free palbociclib, NP(palbo)PEG-MUC1, palbociclib + navitoclax, or NP(palbo)PEG-MUC1 + NP(nav)-Gal (n ≥ 5 tumors per group). TUNEL assay was used to confirm the induction of apoptosis in treated and untreated tumor tissues. Scale bar, 20 µm. (B) Percentage of TUNEL-positive cells in tumors. Quantification was performed in a total of 3 fields per tumor, covering most of the whole tumor section. Data represent the mean ± SEM (n≥5) and statistical significance was assessed by one-way ANOVA followed by Tukey's post-test (*p<0.05; **p<0.01; ***p<0.001)

Moreover, biodistribution studies were carried out by determining Si levels in various organs (lung, liver, spleen, kidneys) and tumors by inductively coupled plasma mass spectroscopy (ICP-MS) (Figure S13). The levels of Si detected indicated that the nanoparticles reached the tumors. Besides, Si was also detected in organs associated with nanoparticle elimination. Thus, in the case of NP(palbo)PEG-MUC1, Si was observed in the spleen and kidneys, suggesting renal clearance-(Park *et al.*, 2009) In contrast, when NP(nav)-Gal was added to the treatment, Si content was also observed in the liver, thus suggesting a combined hepatobiliary clearance with renal excretion.(Yu and Zheng, 2015; Zhang *et al.*, 2016)

Regarding the use of palbociclib and navitoclax, we also noticed that encapsulation minimized undesired side effects. Treatment with free palbociclib in monotherapy or concomitant treatment of free palbociclib plus free navitoclax reduces animal weight (Figure S14). Besides, the systemic administration of free palbociclib induces senescence not only in tumors, but it has also been reported that it can induce senescence in veins and thus favor metastasis.(Estepa-Fernández *et al.*, 2021) In contrast, palbociclib encapsulated in the nanoparticle (NP(palbo)PEG-MUC1) significantly reduces mice weight loss, in agreement with a targeted delivery of palbociclib in TNBC tumors compared to the systemic administration. Moreover, encapsulation of palbociclib also resulted in a decrease in metastasis in lungs. In addition, the combined treatment NP(palbo)PEG-MUC1 plus NP(nav)-Gal resulted in a significant decrease in metastasis compared to free drugs. It is also noteworthy that the targeted delivery of navitoclax specifically in

senescent cells has been reported to significantly reduce off-target effects and platelet toxicity.(Galiana *et al.*, 2020; González-Gualda *et al.*, 2020)

Collectively, these results proved the effectiveness of the stigmergy strategy of communication, confirming that this principle could be applied to *in vivo* enhancing therapy in tumors. Targeted pro-senescent and senolytic therapies with both nanosystems have shown their benefits in treating TNBC by effectively reducing tumor growth and metastasis and minimizing undesired side effects.

4. Discussion and conclusion

Senescence is a process of cell-cycle arrest that has a crucial role in aging, development, and antitumor response.(Campisi, 2001; Muñoz-Espín and Serrano, 2014) The induction of senescence is a therapeutic approach used in clinical practice to stop tumor progression. Palbociclib (palbo), a CDK4/6 cell-cycle inhibitor, has shown efficacy in treating advanced breast cancer.(Fry *et al.*, 2004; Finn *et al.*, 2009, 2015, 2016; Pernas *et al.*, 2018) However, an unmet medical need appears with the development of drugs that selectively induce senescence, as the presence of senescent cells in tissues is a double-edged sword (Ohtani *et al.*, 2012) due to their secretory phenotype, that has a negative impact in the tissue microenvironment, triggering tissue dysfunction and/or unfavorable outcomes.(Rao and Jackson, 2016) In this scenario, senolysis (the selective induction of apoptosis in senescent cells) has been demonstrated to eliminate the adverse side effects of senescent cell accumulation.(Zhu *et al.*, 2015; Soto-Gamez and Demaria, 2017)

To enhance the therapeutic effect of nanoparticles targeting tumors and to reduce secondary effects, we envisioned the design of a nanoparticle-cell-nanoparticle system that communicates by stigmergy for cancer treatment. The first set of nanoparticles is loaded with palbociclib and capped with a poly (ethylene glycol) covalently linked to a MUC1-binding aptamer (NP(palbo)PEG-MUC1). The uptake of NP(palbo)PEG-MUC1 by

triple-negative breast cancer MDA-MB-231 cells is enhanced by the overexpression of MUC1, that facilitates the internalization of the nanoparticles. Treatment with NP(palbo)PEG-MUC1 induces senescence in the tumor, demonstrated by the stain of tumor slides with X-Gal and by the increase of the expression levels of Ki67 and p53 makers. NP(palbo)PEG-MUC1 is able to transform the environment in the tumor by inducing senescence, making possible the action of a second community of nanoparticles (NP(nav)-Gal) which are loaded with navitoclax and capped with a hexagalactooligosaccharide (galactan). As a consequence of the cooperation by stigmergy, tumor growth reduction, drop of metastases and diminution of drug side effects is observed in the TNBC mice model.

In this work, we demonstrate the high potential of stigmergy communication strategies involving two communities of nanoparticles. The stigmergy protocol enhances the performance of the nanoparticles, allowing them to be applied in targeted transport and drug delivery, opening up new possibilities for cooperative behaviors. Following this stigmergy communication concept, which involves changes in the environment resulting in cooperation between nanoparticles without any need for planning, simultaneous presence, or mutual awareness between the involved systems, a number of plausible networks aimed at increasing drug efficacy and reducing dosages, side effects, and resistance can be envisioned. Communication at the nanoscale by stigmergy can be useful to develop swarm micro/nanoparticles capable of interacting with their neighbors and local environment, leading to functionalities able to cause a deep impact in the way we treat diseases.

5. Experimental section

5.1. Cell culture and senescence induction

Human breast triple-negative adenocarcinoma MDA-MB-231 cells (ATCC) were maintained in DMEM (Sigma) supplemented with 10 % fetal bovine serum (FBS; Sigma) and incubated at 37°C in 5% CO_2. For senescence induction, cells were treated with 2.5 µM free palbociclib (#S1116, Selleckchem) or with 80 µg/mL NP(palbo)PEG-MUC1 (molar dose of palbociclib equivalent to that of the free drug). Cells were senescent after 7 days of treatment.

5.2. β-galactosidase activity assay

β-galactosidase activity was measured by staining using the Senescence β-galactosidase Staining Kit (Cell Signaling, #9860S). Briefly, cells were fixed with 1x Fixative Solution at room temperature for 15 min. After fixation, cells were washed with PBS, and incubated overnight at 37 °C without CO_2 with 1x Staining Solution containing X-gal in *N*,*N*-dimethylformamide. Senescence-associated β-galactosidase enzymatic activity was determined at pH 6. Pictures were taken with a bright-field microscope.

5.3. Western Blot

Cells were lysed in a buffer containing 25 mM Tris-HCl pH 7.4, 1 mM EDTA, 1% SDS, plus protease and phosphatase inhibitors to obtain whole-cell extracts. Protein concentration was determined by the BCA protein assay. Electrophoresis was performed in SDS-PAGE gels. Proteins were transferred to nitrocellulose membranes, blocked with 5% nonfat milk, washed with 0.1% Tween/PBS and incubated overnight with a specific primary antibody: pRb (#9308, Cell Signalling), p21 (#sc-6246, Santa Cruz), and GADPH (#14C10, Cell Signalling). Membranes were washed and incubated with the appropriate

secondary antibody: anti-Rabbit IgG peroxidase antibody (#A6154, Sigma) or peroxidase conjugate-goat anti-Mouse IgG antibody (#A4416, Sigma).

5.4. Synthesis of MSNs

1 g of *N*-cetyltrimethylammonium bromide (CTAB, Sigma, #H6269) was dissolved in 480 mL of deionized water before adding 3.5 mL of 2 M NaOH (Sigma, #1310732) to the solution. Then, the mixture was heated at 80 °C, 5 mL of the polymeric precursor tetraethylortosilicate (TEOS, Sigma, #131903) were added dropwise, and the reaction was stirred and heated for 2 h. Centrifugation (10,000 rpm, 20 min) was performed to isolate MSNs (white solid) that were washed with deionized water until neutral pH was reached. Finally, the solid was dried at 60 ^{o}C and then calcined at 550 °C (Mufla Furnace) for 5 h using an oxidant atmosphere to remove the surfactant template, that might affect cell viability.

5.5. Synthesis of NP(palbo)PEG-MUC1, NP(saf)PEG-MUC1 and NP(ICG)PEG-MUC1

Gated MSNs loaded with either palbociclib (palbo), safranine O (saf), or indocyanine green (ICG) and coated with polyethylene glycol (PEG, average molecular weight 800 Da) derivative were synthesized. PEG containing thiol and *N*-hydroxysuccinimide (SH-PEG-NHS, Gentaur) was used.

In order to load the pores of calcined MSNs with palbociclib, 100 mg of MSNs were suspended in 3 mL of deionized water containing 40 mg of palbociclib (Selleckchem). To load MSNs with safranine O, 100 mg of calcined MSNs were suspended in 3 mL of acetonitrile containing 28 mg of safranine O (Sigma). To load ICG, 200mg of calcined MSNs were added to a stirred solution of 10 mg indocyanine green (ICG) in 50 mL of water. After the loading, the solids were stirred overnight, filtered off and dried under vacuum.

Afterwards, the loaded solids and 100 mg of empty calcined MSNs were suspended in acetonitrile (3 mL) and (3-mercaptopropyl) trimethoxysilane (MPTMS) (185,6 µL, 10 mmoles/g solid) were added to the mixture and stirred for 5.5 h at room temperature. Then, aldrithiol (220 mg, 10 mmoles/g solid) was added and stirred overnight at room temperature. The solids were isolated by filtration, washed twice with acetonitrile and dried under vacuum. Finally, these prepared solids (100 mg) and the heterobifunctional SH-PEG-NHS (200 mg, 3 mmoles/g solid) were suspended in acetonitrile (10 mL) and stirred overnight. The final products (NP(palbo)PEG, NP(saf)PEG, NP(ICG)PEG, and NP-PEG) were filtered, washed with plenty of water and dried under vacuum.

The 5' amine-modified MUC1-binding aptamer (MUC1) (5' NH_2-GCA GTT GAT CCT TTG GAT ACC CTG G-3'; ThermoFisher) was covalently bonded onto the external surface of NP(palbo)PEG, NP(saf)PEG, and NP(ICG)PEG. In this respect, the solids (20 mg) were resuspended in PBS and mixed with MUC1 (0,6 µmoles). The mixture was stirred for 3 hours and, then, nanoparticles were centrifuged and washed with PBS to get the final solids: NP(palbo)PEG-MUC1, NP(saf)PEG-MUC,1 and NP(ICG)PEG-MUC1. NP(saf)PEG were also coated with a 5' amine-modified non-targeting aptamer (Random) (5' NH_2-AAG CAC TTT CAG TGG GGA GGA GGG TTG ATA GGT TAA GAG-3'; ThermoFisher), that was employed as a negative control in the targeting study, obtaining the nanoparticles referred as NP(saf)PEG-Random. All the final nanoparticles were stored at -20 °C.

5.6. Synthesis of NP(nav)-Gal

Synthesis of gated MSNs loaded with navitoclax (nav) or nile blue (NB) and coated with hexa-galactooligosaccharides (Active BioChem, #A1001) was performed as described previously by our group (NP(nav)-Gal).(Agostini et al., 2012; Muñoz-Espín et al., 2018; Galiana et al., 2020; Estepa-Fernández et al., 2021) The synthesis of NP(NB)-Gal was also previously described.(Lozano-Torres *et al.*, 2020) Briefly, for navitoclax loading, 200 mg of calcined MSNs and 156 mg navitoclax were suspended in 6 mL of anhydrous dichloromethane for 24 h. For nile blue loading, 250 mg of calcined MSNs and 7 mg nile

blue were suspended in 31 mL of anhydrous dichloromethane for 20 h. After the loading, 0.28 mL of (3-aminopropyl) triethoxysilane were added onto the solution and stirring was kept for 5.5 h. The solid was isolated by filtration under vacuum. To obtain the final gated nanoparticles, a solution of 383 mg of galactan (Carbosynth, #OG71532, consisting of six repeating galactose monosaccharides linked through β-1,4 glycosidic bonds) in 25 mL of water was added to the obtained functionalized solids, and stirred at room temperature for 21 h. The final product (NP(nav)-Gal) were centrifuged, washed with plenty of water and ethanol in order to remove the excess of reagents and dried under vacuum. All the final nanoparticles were stored at room temperature in a desiccator.

5.7. Nanoparticles characterization

Powder X-ray diffraction (PXRD), N_2 adsorption-desorption isotherms, thermogravimetric analysis (TGA), transmission electron microscopy (TEM), ζ potential and dynamic light scattering (DLS) were employed for nanoparticle characterization. PXRD measurements were performed on a Seifert 3000TT diffractometer using Cu-Kα radiation. N_2 adsorption-desorption isotherms were recorded on a Micromeritics TriStar II Plus automated analyzer. The samples were degassed at 120 °C under vacuum overnight. The specific surface areas were calculated from the adsorption data in the low pressures range using the Brunauer–Emmett–Teller model. The thermogravimetric analyses were performed in TGA/SDTA 851e Mettler Toledo equipment in an oxidant atmosphere (air, 80 mL/min) with a heating program that consisted of a heating ramp of 10 ^{o}C/min from 393K to 1273K and an isothermal heating step at this temperature for 30 min. ζ potential and dynamic light scattering (DLS) measurements were carried out in a Malvern Zetasizer Nano ZS instrument. TEM images were acquired with a Philips CM10 microscope working at 100 kV. TEM-EDX analysis was performed using a JEOL-JEM-2100 LaB6 electron microscopeat 200 kV accelerating voltage and equipped with an Oxford Instruments INCA x-sight (Si(Li)detector) and a Zeiss SESAM microscope(200kV) equipped with an energy dispersive X-ray(EDX) spectroscopy system from ThermoFisher. UV-visible

spectroscopy was carried out with a Lambda 35 UV/vis spectrometer (Perkin-Elmer Instruments), and cargo delivery assays were performed in fluorescence spectroscopy (JASCO spectrofluorometer FP-8300). All the measurements were taken in triplicate.

5.8. Cargo release studies of NP(palbo)PEG, NP(saf)PEG, and NP(ICG)PEG

1 mg of either NP(palbo)PEG, NP(saf)PEG, or NP(ICG)PEG nanoparticles were suspended in 2 mL of PBS, stirred and the volume was separated in two suspensions of 1 mL. Then, 10 mM glutathione was added to one of the suspensions; the other suspension, without GSH, acts as control. After a certain time, aliquots of 150 μL of each suspension were taken and centrifuged to remove the solid. For NP(palbo)PEG, cargo released was measured by UV-visible spectroscopy (absorption band of palbociclib at 352 nm). For NP(saf)PEG and NP(ICG)PEG cargo, release was measured by fluorescence (λ_{exc} (saf) = 495 nm, λ_{em} (saf) = 587 nm; λ_{exc} (ICG) = 750 nm, λ_{em} (ICG) = 830 nm).

5.9. Cargo release study of NP(nav)-Gal and NP(NB)-Gal

For cargo release studies of NP(nav)-Gal, 4 mg of NP(nav)-Gal nanoparticles were suspended in 10 mL of water at pH 4.5, stirred and the volume was separated in two suspensions of 5 mL. Then, 5 mg of β-galactosidase from *Aspergillus oryzae* were added to one of the suspensions. After a certain time, aliquots of 200 μL of each suspension were taken, and 300 μL of ethyl acetate (to dissolve navitoclax) were added to each one. The mixture was stirred for 1 min, the ethyl acetate was taken, centrifuged, and cargo release in the organic phases was measured by UV-visible spectroscopy (absorption band of navitoclax at 275 nm in ethyl acetate). The same procedure was performed without adding the enzyme to one of the suspensions as a control.

For NP(NB)-Gal cargo release studies, 2 mg of NP(NB)-Gal were suspended in 5 mL of water-DMSO 99:1 v/v mixture at pH 4.5, in the presence or absence of 5 mg of enzyme β-galactosidase from *Aspergillus oryzae*. The suspension was stirred using a magnetic bar.

Sample aliquots of 300 μL mL were taken at scheduled times and were centrifuged to remove the solid. Cargo release was monitored in the absorption band of NB (608 nm).

5.10. Confocal microscopy targeted cellular uptake studies

MDA-MB-231 cells were seeded on coverslips in 6-multiwell plates at a concentration of $4 \cdot 10^5$ cells/well. Two days later, cells were treated with 50 μg/mL suspension of either NP(saf)PEG-MUC1 or NP(saf)PEG-Random. After 30 min, cells were washed with medium in order to eliminate non-internalized nanoparticles and were incubated for a total time of 2 h. For confocal microscopy, coverslips were mounted, and Hoechst and wheat germ agglutinin (WGA) Alexa Fluor 488 were added before cells visualization for nuclei and membrane staining, respectively. Fluorescence intensity was monitored through a Leica TCS SP8 confocal microscope and quantified using Image J software.

5.11. Flow cytometry targeted cellular uptake studies

MDA-MB-231 cells were seeded in 6-multiwell plates at a concentration of $4 \cdot 10^5$ cells/well. After 24 h, cells were treated with a suspension of 50 μg/mL of either NP(saf)PEG-MUC1 or NP(saf)PEG-Random. After 30 min, cells were washed with medium in order to eliminate non-internalized nanoparticles and were incubated for different times, 2, 4 or 6 h. Cells were collected using 0.5% Trypsin-EDTA (GIBCO) and resuspended in PBS. Flow cytometry was assessed on a CytoFlex S instrument (Beckman Coulter) followed by data analysis using CytoExpert software.

5.12. Cytotoxicity assay

Proliferating and senescent MDA-MB-231 cells were plated in flat-bottom-clear 96-well (Greiner Bio-One, #655087) at a density of 10^4 cells per well. After 24 h, free navitoclax or NP(nav)-Gal nanoparticles were added to the cells. Free navitoclax was

added at a 2.5 µM final concentration. NP(nav)-Gal were added, filtered (0.45 µm),at a maximum of 2 mg/mL, which corresponds to 2.66 µM final concentration. After 72 h, viability was measured using the CellTiter-Glo® luminescent cell viability assay (Promega, #G7571) kit, following the manufacturer's instructions in a PerkinElmer life sciences wallac Victor2TM spectrophotometer. The number of viable cells was normalized to the internal control of untreated cells (DMSO only) of each plate.

5.13. TMRE Staining

To address mitochondrial polarization status, proliferating and senescent MDA-MB-231 cells were treated with DMSO, navitoclax (1µM), or NP(nav)-Gal (equivalent dose to 1µM). After 48 hours of incubation, cells were incubated for 30 min at 37 °C/5% CO_2 with 50 nM TMRE dye (Invitrogen, T669). Then, samples were analyzed in a CytoFLEX S flow cytometer.

5.14. Animal experiments

All mice were treated in strict accordance with the local ethical committee (Ethical Committee for Research and Animal Welfare Generalitat Valenciana, Conselleria d'Agricultura, Medi ambient, Canvi climàtic i Desenvolupament Rural (2020/VSC/PEA/0177). In order to evaluate senolytic activity of stigmergy combination on xenografted MDA-MB-231 cells, female 6–7 weeks old BALB/C nude mice were subcutaneously injected with 2 x 10^6 MDA-MB-231 cells. Tumors were measured with calipers every 2 days, and the tumor volume (mm^3) was calculated with the formula length × $width^2/2$. When tumor volume reached an average of 60 mm^3, daily therapy was initiated with either vehicle, 5 mg/kg free palbociclib (via oral gavage; dissolved in 50 mM sodium lactate pH 4.5), 87.5 mg/kg NP(palbo)PEG-MUC1 (via i.p. injection; equivalent dose of palbociclib of 5 mg/kg), or the combination of free palbociclib plus free navitoclax or NP(palbo)PEG-MUC1 plus NP(nav)-Gal. Navitoclax treatments (either as a free drug or encapsulated in the nanoparticles) were initiated the day after the initiation of palbociclib

treatment. Doses: 2.5 mg/kg free navitoclax (via oral gavage; dissolved in 15% DMSO/ 85% PEG-400) or 40 mg/kg NP(nav)-Gal (via i.v. and i.p. injection in alternating days; equivalent navitoclax dose of 2.5 mg/kg). Mice were culled by CO_2 after treatment, and organs were collected for subsequent histological analyses.

5.15. IVIS Imaging

For *in vivo* and *ex vivo* animals or organs fluorescence imaging after nanoparticles treatments, an IVIS Spectrum Imaging System (Caliper LifeSciences) was used. For *in vivo* visualization, animals were anesthetized with 4-4.5% isoflurane in the induction period and maintained at 2-2.5% during the scanning time. For *ex vivo* tumors imaging, animals were euthanized 24 h after nanoparticles injection and tumors were harvested and immediately analyzed. For NP(ICG)PEG-MUC1 IVIS imaging, Balb/c nude female mice were injected with TNBC MDA-MB-231 cells on mammary pads. When tumors volume reached ca. 220 mm^3, NP(ICG)PEG-MUC1 nanoparticles were administered (i.p.), and IVIS imaging was performed. For NP(ICG)-Gal imaging, Balb/c nude female mice were injected with TNBC MDA-MB-231 cells on mammary pads. When tumors volume reached 60 mm^3, palbociclib treatment started (encapsulated in NP(palbo)PEG-MUC1 nanoparticles (i.p.)) and was maintained daily for 24 days. On day 24, NP(NB)-Gal nanoparticles were administered (i.p.), and IVIS imaging was performed. Signal from NP(ICG)PEG-MUC1 nanoparticles loaded with indocyanine green was detected using excitation and emission wavelengths of 745nm and 840nm, respectively. Signal from NP(NB)-Gal nanoparticles loaded with nile blue was detected using excitation and emission wavelengths of 640nm and 680nm, respectively. Fluorescence quantification was performed by Living Image® 4.3.1 software and was measured in photons per second per square centimeter per steradian ($p/s/cm^2/sr$). Fluorophore release was quantified by manually drawing regions of interest (ROIs) over the detected fluorescence signals in organs or tumors.

5.16. Histology

Tumors were removed, washed with 1× PBS and fixed with 4% PFA overnight at 4 °C. The fixative was aspirated, the tumor was washed in 1× PBS and cut in half. Half-tumors were incubated with 30% sucrose overnight at 4 °C. Fixed tissues were embedded in cryomolds with OCT and frozen completely at −20 °C. 10 µm thick tumor sections were then incubated in blocking solution (5% horse serum, 0.3% Triton X-100 in 1× PBS) for 1 h and immunostained by a following incubation with 1:100 p53 primary antibody (ab26, Abcam) overnight at 4 °C. Subsequently, tissue was incubated with secondary antibody (1:200 dilution) against mouse conjugated to Alexa Fluor 488 (Invitrogen) at room temperature for 2 hours. For TUNEL staining, In Situ Cell Death Detection Kit (Merck) was used according to the manufacturer's instructions. Sections were mounted on microscope slides using Mowiol/DAPI (Sigma) and covered with a glass coverslip. Images were obtained using a confocal microscopy Leica TCS SP8 HyVolution 2 microscope. Positive signal for TUNEL was quantified with ImageJ software.

The other half-tumors were included in paraffin for immunohistological Ki67 staining. 5 mm paraffin sections were deparaffinized and re-hydrated. Antigen retrieval was carried out using 10mM Sodium Citrate and 0.05% Tween 20 buffer at pH 6.0 for 30 minutes. Tumor sections were incubated in blocking solution (5% horse serum, 0.3% Triton X-100 in 1× PBS) for 1 h and incubated with Ki67 (Abcam) antibody at 4 °C overnight. Ki67 immunostaining was developed using 3,3-diaminobenzidine tetrahydrochloride (DAB) and nuclei counterstained with hematoxylin. Sections were scanned in Leica Aperio Versa 200 equipment at 10x magnification.

5.17. Metastasis quantification

Lungs were collected and fixed overnight in 4% PFA. Paraffin-embedded tissue sections (5 µm) were stained with hematoxylin-eosin and scanned in a Leica Aperio Versa

200 equipment at 10x magnification. Metastatic 4T1 cell clusters were microscopically counted from at least five animals per group in different lung sections.

5.18. Silica biodistribution

Selected organs (lungs, liver, spleen, kidneys, and tumor) were extracted and conserved for silicon (Si) detection. Organs were first weighted and then individually introduced in polytetrafluoroethylene (PTFE) bottles. 1mL of tetramethylammonium hydroxide solution (TMAH, #331635, Sigma) was added to each recipient, bottles were firmly closed, and digestion was carried out for 2h at 80 °C using a digestion unit Bloc digest 20 (Selecta). After cooling, digested samples were diluted with distilled water to 10 mL in polypropylene tubes, filtered in 0.45µm filters (#17463443, Scharlab) and kept in polystyrene tubes until determination. For the analysis, 0.5 mL of the sample was diluted to 10 mL with a solution of 2% nitric acid and 1% hydrochloric acid. Silicon determination was performed in an Inductively Coupled Plasma Mass Spectrometer System (ICP-MS) Agilent 7900 in H2 mode, using germanium as internal standard. A calibration curve was also prepared from silicon standard for ICP (#08729, Sigma), and standard solutions were digested and treated the same way as the mice samples. Data are expressed as µg Si/g sample.

5.19. Statistical Analysis

All the values represent the mean ± SEM of at least three independent experiments except the *in vivo* experiment with mice, where a single representative experiment is shown. Significance was determined by one-way ANOVA or two-way ANOVA followed by Tukey's post-test, Sidak's post-test, or Student's T-test using GraphPad Prism 8 software. A p-value below 0.05 was considered statistically significant (*$p<0.05$; **$p<0.01$; ***$p<0.001$) or (#$p<0.05$; ##$p<0.01$; ###$p<0.001$). For *in vivo* studies, mice were randomly assigned to treatment groups; the sample size was not pre-determined

6. References

Agostini, A. et al. (2012) 'Targeted cargo delivery in senescent cells using capped mesoporous silica nanoparticles', Angewandte Chemie - International Edition, 51(42), pp. 10556–10560. doi: 10.1002/anie.201204663.

Akyildiz, I. F., Brunetti, F. and Blázquez, C. (2008) 'Nanonetworks: A new communication paradigm'. doi: 10.1016/j.comnet.2008.04.001.

Apostolopoulos, V., Pietersz, G. A. and McKenzie, I. F. C. (1999) 'MUC1 and breast cancer', Current Opinion in Molecular Therapeutics, pp. 98–103.

Bagley, A. F. et al. (2013) 'Plasmonic photothermal heating of intraperitoneal tumors through the use of an implanted near-infrared source', ACS nano, 7(9), pp. 8089–8097. doi: 10.1021/NN4033757.

Beaver, J. A. et al. (2015) 'FDA Approval: Palbociclib for the Treatment of Postmenopausal Patients with Estrogen Receptor-Positive, HER2-Negative Metastatic Breast Cancer.', Clinical cancer research : an official journal of the American Association for Cancer Research, 21(21), pp. 4760–6. doi: 10.1158/1078-0432.CCR-15-1185.

Bernardos, A. et al. (2010) 'Enzyme-responsive intracellular controlled release using nanometric silica mesoporous supports capped with "saccharides"', ACS Nano, 4(11), pp. 6353–6368. doi: 10.1021/nn101499d.

Bonabeau, E., Dorigo, M. and Theraulaz, G. (1999) Swarm Intelligence: From Natural to Artificial Systems ., Oxford University Press. doi: 10.1086/393972.

Buddingh', B. C., Elzinga, J. and van Hest, J. C. M. (2020) 'Intercellular communication between artificial cells by allosteric amplification of a molecular signal', Nature Communications 2020 11:1, 11(1), pp. 1–10. doi: 10.1038/s41467-020-15482-8.

Bussian, T. J. et al. (2018) 'Clearance of senescent glial cells prevents tau-dependent pathology and cognitive decline.', Nature, 562(7728), pp. 578–582. doi: 10.1038/s41586-018-0543-y.

Campisi, J. (2001) 'Cellular senescence as a tumor-suppressor mechanism', Trends in Cell Biology, 11(11), pp. 27–31. doi: 10.1016/S0962-8924(01)02151-1.

Chang, J. et al. (2016) 'Clearance of senescent cells by ABT263 rejuvenates aged hematopoietic stem cells in mice', Nature Medicine, 22(1), pp. 78–83. doi: 10.1038/nm.4010.

Collado, M. and Serrano, M. (2010) 'Senescence in tumors: evidence from mice and humans', Nature reviews. Cancer, 10(1), pp. 51–57. doi: 10.1038/NRC2772.

Demaria, M. et al. (2017) 'Cellular senescence promotes adverse effects of chemotherapy and cancer relapse', Cancer Discovery, 7(2), pp. 165–176. doi: 10.1158/2159-8290.CD-16-0241.

Dubuc, E. et al. (2019) 'Cell-free microcompartmentalised transcription-translation for the prototyping of synthetic communication networks', Current opinion in biotechnology, 58, pp. 72–80. doi: 10.1016/J.COPBIO.2018.10.006.

Estepa-Fernández, A. et al. (2021) 'Senolysis Reduces Senescence in Veins and Cancer Cell Migration', Advanced Therapeutics, 2100149, pp. 1–15. doi:

10.1002/adtp.202100149.

Finn, R. R. S. et al. (2015) 'The cyclin-dependent kinase 4/6 inhibitor palbociclib in combination with letrozole versus letrozole alone as first-line treatment of oestrogen receptor-positive, HER2-negative, advanced breast cancer (PALOMA-1/TRIO-18): A randomised phase 2 study', The Lancet Oncology, 16(1), pp. 25–35. doi: 10.1016/S1470-2045(14)71159-3.

Finn, R. S. et al. (2009) 'PD 0332991, a selective cyclin D kinase 4/6 inhibitor, preferentially inhibits proliferation of luminal estrogen receptor-positive human breast cancer cell lines in vitro', Breast Cancer Research, 11(5), pp. 1–13. doi: 10.1186/bcr2419.

Finn, R. S. et al. (2016) 'Palbociclib and Letrozole in Advanced Breast Cancer', New England Journal of Medicine, 375(20), pp. 1925–1936. doi: 10.1056/NEJMoa1607303.

Fry, D. W. et al. (2004) 'Specific inhibition of cyclin-dependent kinase 4/6 by PD 0332991 and associated antitumor activity in human tumor xenografts.', Molecular cancer therapeutics, 3(11), pp. 1427–38. Available at: http://www.ncbi.nlm.nih.gov/pubmed/15542782 (Accessed: 4 September 2019).

Galiana, I. et al. (2020) 'Preclinical antitumor efficacy of senescence-inducing chemotherapy combined with a nanoSenolytic', Journal of Controlled Release, 323, pp. 624–634. doi: 10.1016/j.jconrel.2020.04.045.

Gendler, S. J. (2001) 'MUC1, The Renaissance Molecule', Journal of Mammary Gland Biology and Neoplasia 2001 6:3, 6(3), pp. 339–353. doi: 10.1023/A:1011379725811.

Giménez, C. et al. (2014) 'Towards chemical communication between gated nanoparticles', Angewandte Chemie - International Edition, 53(46), pp. 12629–12633. doi: 10.1002/anie.201405580.

Giménez, C. et al. (2015) 'Gated mesoporous silica nanoparticles for the controlled delivery of drugs in cancer cells', Langmuir, 31(12), pp. 3753–3762. doi: 10.1021/acs.langmuir.5b00139.

Goel, S. et al. (2018) 'CDK4/6 Inhibition in Cancer: Beyond Cell Cycle Arrest', Trends in Cell Biology. Elsevier Ltd, pp. 911–925. doi: 10.1016/j.tcb.2018.07.002.

González-Gualda, E. et al. (2020) 'Galacto-conjugation of Navitoclax as an efficient strategy to increase senolytic specificity and reduce platelet toxicity', Aging Cell, 19(4), pp. 1–19. doi: 10.1111/acel.13142.

Jones, D. P. et al. (1998) 'Glutathione measurement in human plasma. Evaluation of sample collection, storage and derivatization conditions for analysis of dansyl derivatives by HPLC', Clinica chimica acta; international journal of clinical chemistry, 275(2), pp. 175–184. doi: 10.1016/S0009-8981(98)00089-8.

Kim, H.-N. N. et al. (2017) 'DNA damage and senescence in osteoprogenitors expressing Osx1 may cause their decrease with age', Aging Cell, 16(4), pp. 693–703. doi: 10.1111/acel.12597.

Llopis-Lorente, A. et al. (2018) 'Hybrid Mesoporous Nanocarriers Act by Processing Logic Tasks: Toward the Design of Nanobots Capable of Reading Information from the Environment', ACS Applied Materials and Interfaces, 10(31), pp. 26494–26500.

doi: 10.1021/acsami.8b05920.

Lozano-Torres, B. et al. (2019) 'The chemistry of senescence', Nature Reviews Chemistry, 3(7), pp. 426–441. doi: 10.1038/s41570-019-0108-0.

Lozano-Torres, B. et al. (2020) 'Real-Time In Vivo Detection of Cellular Senescence through the Controlled Release of the NIR Fluorescent Dye Nile Blue', Angewandte Chemie - International Edition, 59(35), pp. 15152–15156. doi: 10.1002/anie.202004142.

de Luis, B. et al. (2019) 'An Interactive Model of Communication between Abiotic Nanodevices and Microorganisms', Angewandte Chemie - International Edition, 58(42), pp. 14986–14990. doi: 10.1002/anie.201908867.

de Luis, B. et al. (2021) 'A chemical circular communication network at the nanoscale', Chemical Science, 12(4), pp. 1551–1559. doi: 10.1039/d0sc04743k.

de Luis, B. et al. (2022) 'Nanoprogrammed Cross-Kingdom Communication Between Living Microorganisms', Nano Letters, 22(5), pp. 1836–1844. doi: 10.1021/ACS.NANOLETT.1C02435/SUPPL_FILE/NL1C02435_SI_001.PDF.

De Luis, B. et al. (2021) 'Engineering chemical communication between micro/nanosystems', Chemical Society Reviews. The Royal Society of Chemistry, pp. 8829–8856. doi: 10.1039/d0cs01048k.

Von Maltzahn, G. et al. (2011) 'Nanoparticles that communicate in vivo to amplify tumor targeting', Nature Materials, 10(7), pp. 545–552. doi: 10.1038/nmat3049.

Milanovic, M., Yu, Y. and Schmitt, C. A. (2018) 'The Senescence–Stemness Alliance – A Cancer-Hijacked Regeneration Principle', Trends in Cell Biology, 28(12), pp. 1049–1061. doi: 10.1016/j.tcb.2018.09.001.

Muñoz-Espín, D. and Serrano, M. (2014) 'Cellular senescence: From physiology to pathology', Nature Reviews Molecular Cell Biology, 15(7), pp. 482–496. doi: 10.1038/nrm3823.

Muñoz-Espín, D. et al. (2018) 'A versatile drug delivery system targeting senescent cells', EMBO Molecular Medicine, 10(9). doi: 10.15252/emmm.201809355.

Ohtani, N. et al. (2012) 'Cellular senescence: A double-edged sword in the fight against cancer', Experimental Dermatology, 21(SUPPL.1), pp. 1–4. doi: 10.1111/j.1600-0625.2012.01493.x.

Overbeeke, R. et al. (1999) 'Sequential occurrence of mitochondrial and plasma membrane alterations, fluctuations in cellular Ca2+ and pH during initial and later phases of cell death', Apoptosis : an international journal on programmed cell death, 4(6), pp. 455–460. doi: 10.1023/A:1009604510329.

Park, J. H. et al. (2009) 'Biodegradable luminescent porous silicon nanoparticles for in vivo applications', Nature Materials 2009 8:4, 8(4), pp. 331–336. doi: 10.1038/nmat2398.

Park, J. H. et al. (2010) 'Cooperative nanomaterial system to sensitize, target, and treat tumors', Proceedings of the National Academy of Sciences of the United States of America, 107(3), pp. 981–986. doi: 10.1073/pnas.0909565107.

Pascual, L. et al. (2017) 'MUC1 aptamer-capped mesoporous silica nanoparticles for controlled drug delivery and radio-imaging applications', Nanomedicine: Nanotechnology, Biology, and Medicine, 13(8), pp. 2495–2505. doi:

10.1016/j.nano.2017.08.006.

Pernas, S. et al. (2018) CDK4/6 inhibition in breast cancer: current practice and future directions, Therapeutic Advances in Medical Oncology. SAGE Publications Inc. doi: 10.1177/1758835918786451.

Qiao, Y. et al. (2017) 'Predatory behaviour in synthetic protocell communities', Nature chemistry, 9(2), pp. 110–119. doi: 10.1038/NCHEM.2617.

Rao, S. G. and Jackson, J. G. (2016) 'SASP: Tumor Suppressor or Promoter? Yes!', Trends in cancer, 2(11), pp. 676–687. doi: 10.1016/j.trecan.2016.10.001.

Sager, R. (1991) 'Senescence as a mode of tumor suppression.', Environmental Health Perspectives, 93, p. 59. doi: 10.1289/EHP.919359.

Saleh, T. et al. (2019) 'Tumor cell escape from therapy-induced senescence', Biochemical Pharmacology, 162, pp. 202–212. doi: 10.1016/j.bcp.2018.12.013.

Saleh, T. et al. (2020) 'Clearance of therapy-induced senescent tumor cells by the senolytic ABT-263 via interference with BCL-XL–BAX interaction', Molecular Oncology, 14(10), pp. 2504–2519. doi: 10.1002/1878-0261.12761.

Soto-Gamez, A. and Demaria, M. (2017) 'Therapeutic interventions for aging: the case of cellular senescence', Drug Discovery Today, 22(5), pp. 786–795. doi: 10.1016/j.drudis.2017.01.004.

Taylor-Papadimitriou, J. et al. (1999) 'MUC1 and cancer.', Biochimica et biophysica acta, 1455(2–3), pp. 301–13. doi: 10.1016/s0925-4439(99)00055-1.

Theraulaz, G. and Bonabeau, E. (1999) 'A brief history of stigmergy', Artificial Life. Artif Life, pp. 97–116. doi: 10.1162/106454699568700.

Ultimo, A. et al. (2020) 'Nanoparticle-cell-nanoparticle communication by stigmergy to enhance poly(I:C) induced apoptosis in cancer cells', Chemical Communications, 56(53), pp. 7273–7276. doi: 10.1039/d0cc02795b.

Vivo-Llorca, G. et al. (2020) 'MUC1 Aptamer-Capped Mesoporous Silica Nanoparticles for Navitoclax Resistance Overcoming in Triple-Negative Breast Cancer', Chemistry - A European Journal, 26(69), pp. 16318–16327. doi: 10.1002/chem.202001579.

Walker, A. J. et al. (2016) 'FDA Approval of Palbociclib in Combination with Fulvestrant for the Treatment of Hormone Receptor-Positive, HER2-Negative Metastatic Breast Cancer', Clinical Cancer Research, 22(20), pp. 4968–4972. doi: 10.1158/1078-0432.CCR-16-0493.

Wedam, S. et al. (2019) 'FDA Approval Summary: Palbociclib for Male Patients with Metastatic Breast Cancer', Clinical Cancer Research, 26(6). doi: 10.1158/1078-0432.ccr-19-2580.

Wen, P. et al. (2017) 'Coordinated Membrane Fusion of Proteinosomes by Contact-Induced Hydrogel Self-Healing', Small (Weinheim an der Bergstrasse, Germany), 13(22). doi: 10.1002/SMLL.201700467.

Yu, M. and Zheng, J. (2015) 'Clearance Pathways and Tumor Targeting of Imaging Nanoparticles', ACS Nano, 9(7), pp. 6655–6674. doi: 10.1021/ACSNANO.5B01320/SUPPL_FILE/NN5B01320_SI_001.PDF.

Zamzami, N. et al. (1995) 'Reduction in mitochondrial potential constitutes an early

irreversible step of programmed lymphocyte death in vivo', The Journal of Experimental Medicine, 181(5), p. 1661. doi: 10.1084/JEM.181.5.1661.

Zhang, X. et al. (2019) 'The Pathway to Intelligence: Using Stimuli-Responsive Materials as Building Blocks for Constructing Smart and Functional Systems', Advanced materials (Deerfield Beach, Fla.), 31(11). doi: 10.1002/ADMA.201804540.

Zhang, Y. N. et al. (2016) 'Nanoparticle-liver interactions: Cellular uptake and hepatobiliary elimination', Journal of controlled release : official journal of the Controlled Release Society, 240, pp. 332–348. doi: 10.1016/J.JCONREL.2016.01.020.

Zhu, Y. et al. (2015) 'The Achilles' heel of senescent cells: from transcriptome to senolytic drugs', Aging cell, 14(4), pp. 644–658. doi: 10.1111/acel.12344.

Zhu, Y. et al. (2016) 'Identification of a novel senolytic agent, navitoclax, targeting the Bcl-2 family of anti-apoptotic factors', Aging Cell, 15(3), pp. 428–435. doi: 10.1111/acel.12445.

7. Supporting information

Table S1 | Nanoparticles nomenclature and composition.

Nanoparticle nomenclature	Gate	Cargo	Support	Used for
as made **MSNs**			MSNs	Nanoparticle synthesis and characterization
calcined **MSNs**			MSNs	Nanoparticle synthesis and characterization
NP(palbo)		Palbociclib	MSNs	Nanoparticle synthesis and characterization
NP(palbo)PEG	PEG	Palbociclib	MSNs	Nanoparticle synthesis and characterization
NP(palbo)PEG-MUC1	PEG-MUC1	Palbociclib	MSNs	Nanoparticle characterization, induction of senescence, cell viability assays, cell death mechanism, stigmergy communication
NP(saf)PEG	PEG	Safranine O	MSNs	Nanoparticle synthesis and characterization
NP(saf)PEG-MUC1	PEG-MUC1	Safranine O	MSNs	Nanoparticle characterization, *in vitro* targeting assays
NP(saf)PEG-Radom	PEG-Random	ICG	MSNs	Nanoparticle characterization, *in vitro* targeting assays
NP-PEG	PEG		MSNs	Nanoparticle synthesis, nanoparticle characterization and biocompatibility
NP(ICG)PEG	PEG-MUC1	ICG	MSNs	Nanoparticle synthesis and characterization
NP(ICG)PEG-MUC1	PEG-MUC1	ICG	MSNs	Nanoparticle synthesis, nanoparticle characterization and IVIS targeting assays
NP-Gal	Galactan		MSNs	Nanoparticle synthesis, nanoparticle characterization and biocompatibility
NP(nav)-Gal	Galactan	Navitoclax	MSNs	Nanoparticle characterization, cell viability assays, cell death mechanism, stigmergy communication
NP(NB)-Gal	Galactan	Nile-Blue	MSNs	Nanoparticle characterization, IVIS targeting assays

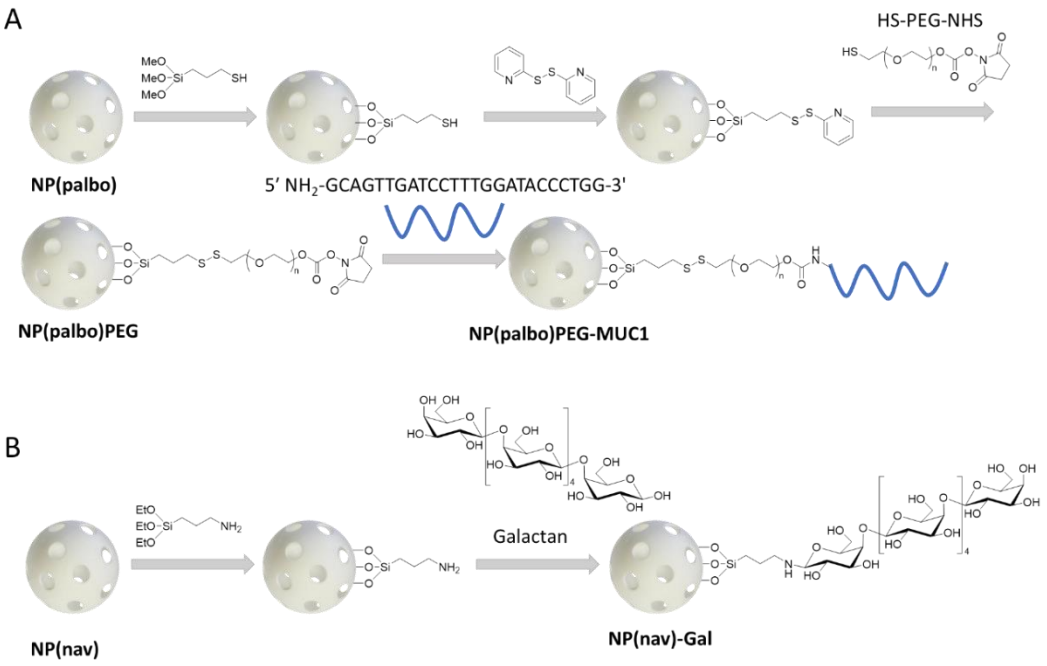

Figure S1 | Schematic representation of the synthetic procedure for NP(palbo)PEG-MUC1 (A) and NP(nav)-Gal (B).

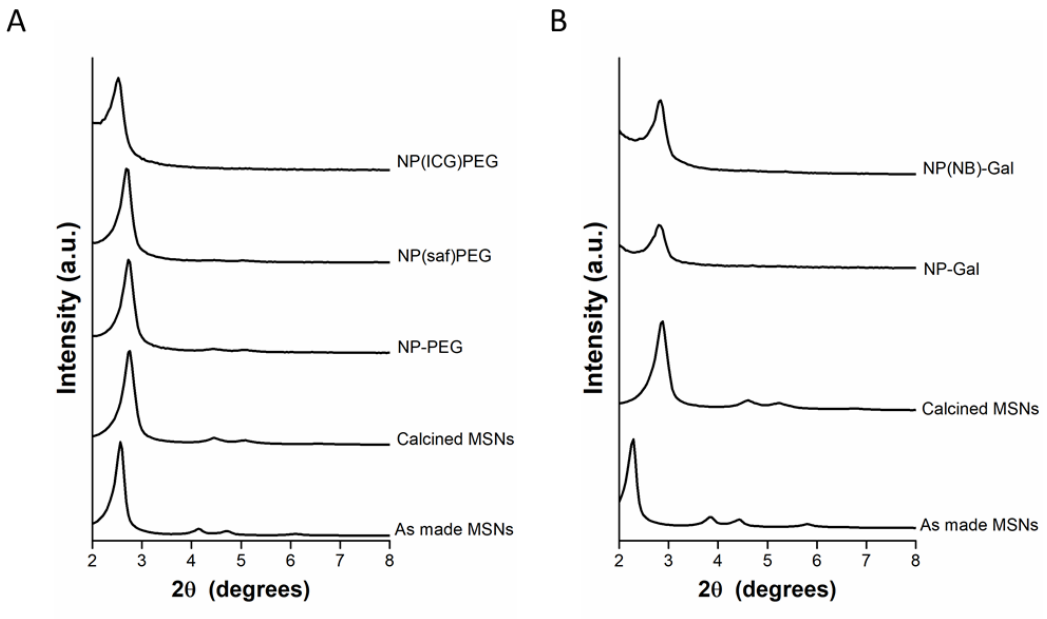

Figure S2 | Powder X-ray diffraction pattern at low (left) and high (right) angles of (A) as made MSNs, calcined MSNs, NP-PEG, NP(saf)PEG and NP(ICG)PEG; (B) as made MSNs, calcined MSNs, NP-Gal and NP(NB)-Gal.

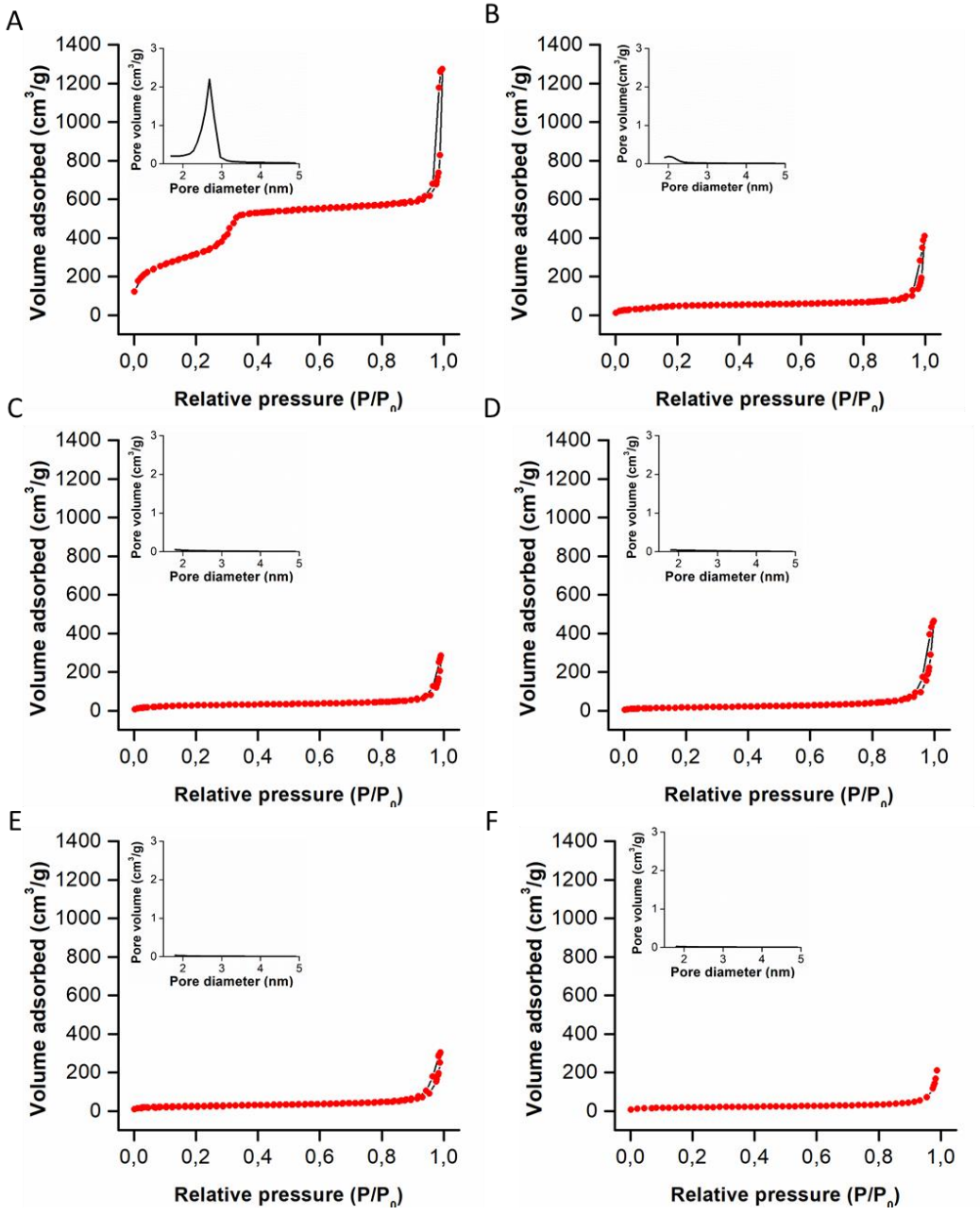

Figure S3 | N_2 adsorption-desorption isotherms for (A) calcined MSNs, (B) NP(saf)PEG, (C) NP-PEG, (D) NP(ICG)-PEG, (E) NP-Gal, and (F) NP(NB)-Gal

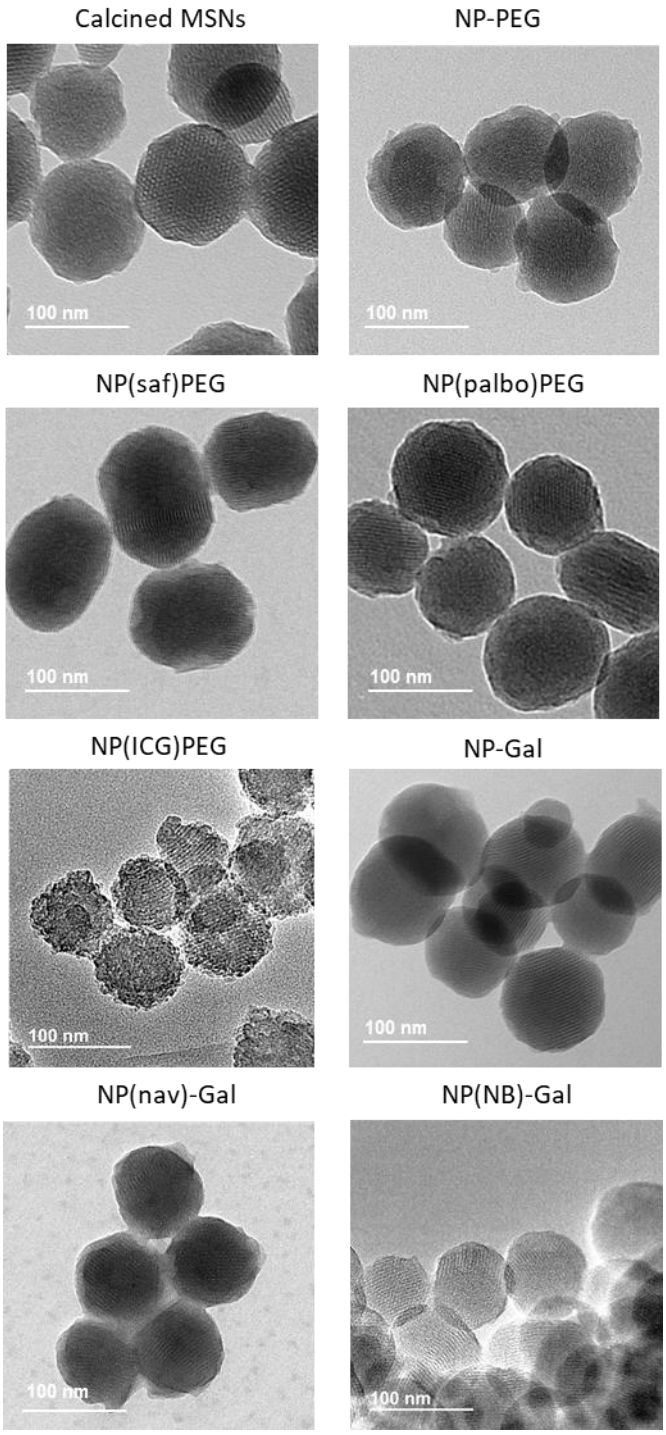

Figure S4 | TEM analysis of the synthetized nanoparticles.

Table S2 | BET specific surface area, pore volumes, and pore sizes calculated from N2 adsorption-desorption isotherms for the indicated materials.

Sample	SBET (m^2g^{-1})	Pore volume (cm^3g^{-1})	Pore size (nm)
calcined MSNs	1158.80	0.95	2.57
NP-PEG	95.13	0.05	-
NP(saf)PEG	183.13	0.11	-
NP(ICG)PEG	57.69	0.05	-
NP-Gal	86.36	0.04	-
NP(NB)-Gal	62.12	0.04	-

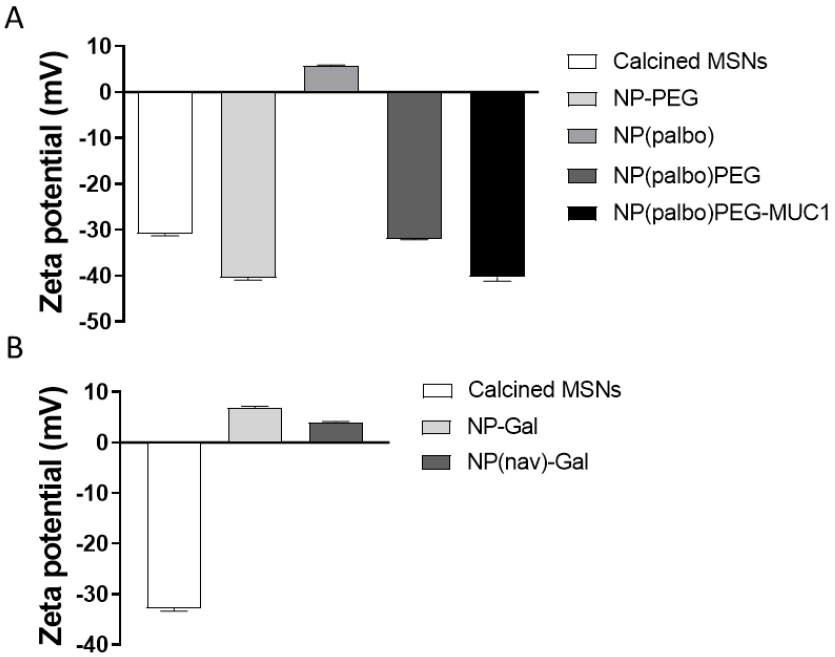

Figure S5 | Zeta potential of (A) all the steps of the synthesis of NP(palbo)PEG-MUC1: calcined MSNs, NP-PEG, NP(palbo), NP(palbo)PEG, and NP(palbo)PEG-MUC1; (B) calcined MSNs, NP-Gal and NP(nav)-Gal. Data represent mean ± SEM (n=3).

Table S3 | Hydrodynamic diameter and Zeta potential of selected materials.

Solid	Hydrodynamic particle diameter (nm)	Zeta potential (mV)
as made MSNs	180.9 ± 5.4	48.5 ± 1.2
calcined MSNs	161.7 ± 2.7	-30.9 ± 0.6
NP-PEG	171.9 ± 3.2	-40.5 ± 0.8
NP(saf)PEG-MUC1	191.6 ± 3.0	-37.8 ± 5.3
NP(ICG)PEG-MUC1	205.4 ± 3.0	-25.9 ± 0.2
NP(palbo)	288.4 ± 2.0	5.7 ± 0.2
NP(palbo)PEG	187.2 ± 5.9	-32.0 ± 0.3
NP(palbo)PEG-MUC1	199.4 ± 6.3	-40.3 ± 1.5
NP-Gal	186.6 ± 4.0	6.94 ± 0.4
NP(nav)-Gal	253.4 ± 2.2	4.03 ± 0.3
NP(NB)-Gal	262.1 ± 5.6	-34.7± 1.7

Table S4 | Organic contents of the molecular gate (poly(ethylene glycol) (PEG) or galactan and cargo for the synthetized nanodevices in mg per g of solids.

Solid	α_{gate} (mg/g solid)	α_{cargo} (mg/g solid)
NP(saf)PEG	106	46
NP(ICG)PEG	171	68
NP(palbo)PEG	124	59
NP(NB)-Gal	218	143
NP(nav)-Gal	281	31

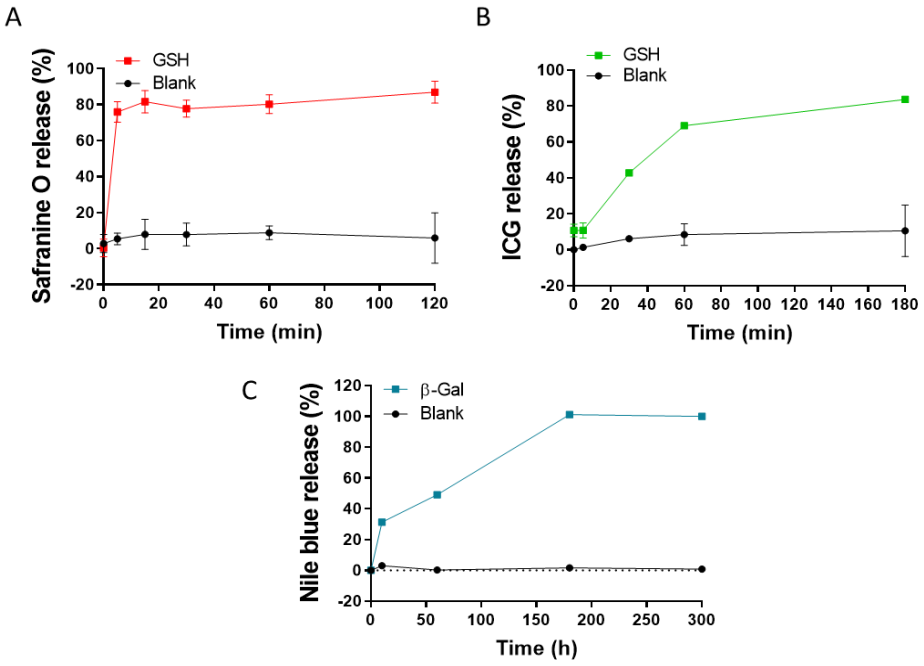

Figure S6 | Release profile of Safranine O (A) from NP(saf)PEG-MUC1 and ICG (B) from NP(ICG)PEG-MUC1 in the absence (black) or presence of glutathione (GSH) (red or green) in PBS. (C) Release profile of nile blue from NP(NB)-Gal in the absence (black) or presence of β-galactosidase (β-Gal) (blue) in water with 1%DMSO. Data represent mean ± SEM.

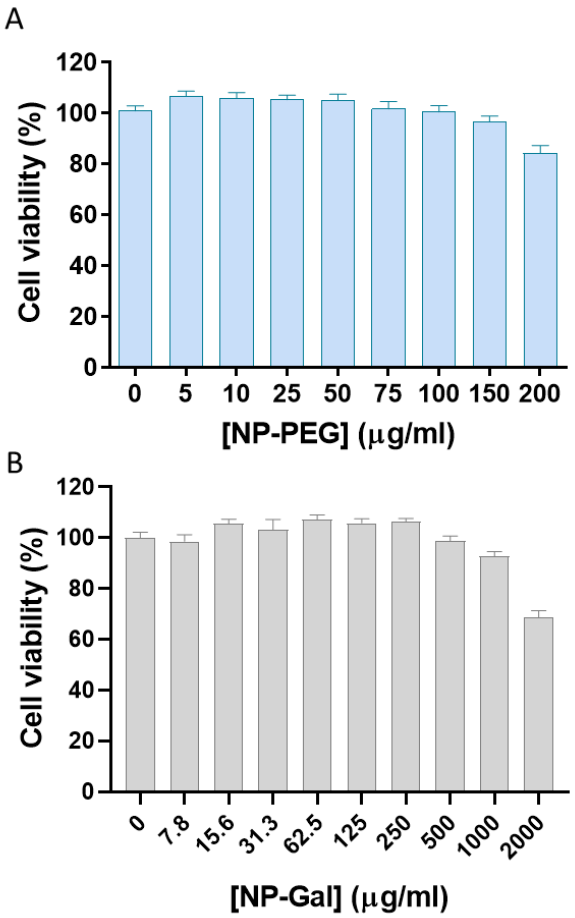

Figure S7 | Cytotoxicity profile of empty NP-PEG (A) and NP-Gal (B) in MDA-MB-231 cells. Cell viability at different concentrations of NP-PEG at 7 days and NP-Gal at 72h. Data represent the means ± SEM of at least three independent experiments.

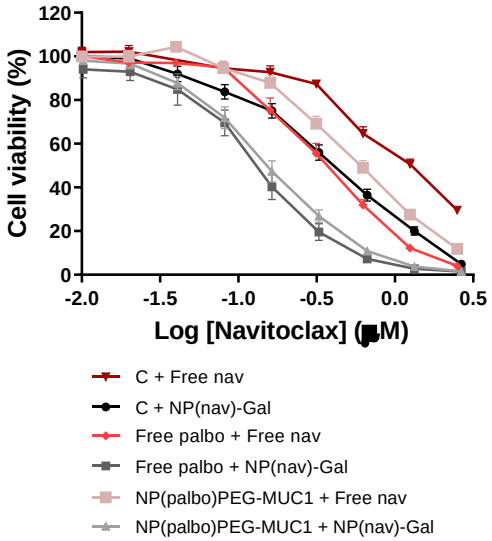

Figure S8 | Cell viability after 72 h of treatment with different concentrations of free navitoclax (dark red for control (C) proliferating MDA-MB-231 cells, bright red for free palbociclib treated cells, and light red for NP(palbo)PEG-MUC1 treated cells) or NP(nav)-Gal (black for control (C) proliferating cells, dark grey for free palbociclib treated cells and light grey for NP(palbo)PEG-MUC1 treated cells).

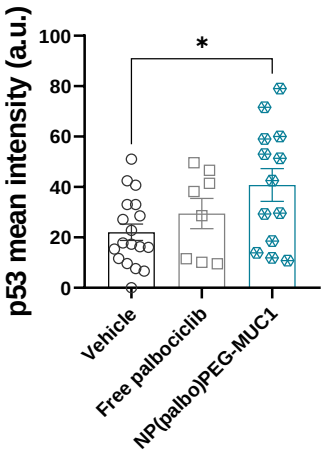

Figure S9 | Percentage of p53 mean intensity in tumors slides. Quantification was performed in a total of 3 fields per tumor, covering most of the total tumor section. Data represent the mean ± SEM (n≥5) and statistical significance was assessed by one-way ANOVA followed by Sidak's post-test (*p<0.05).

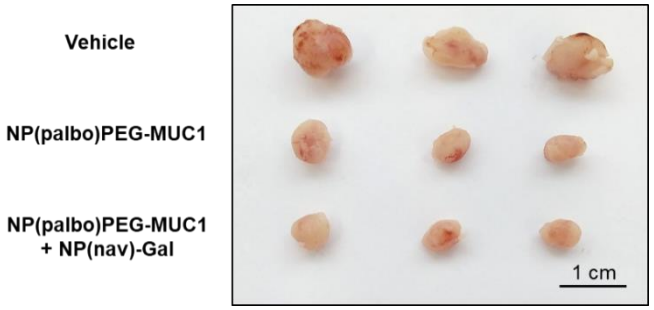

Figure S10 | Photograph of representative tumor samples for each treatment. Scale bar, 1 cm.

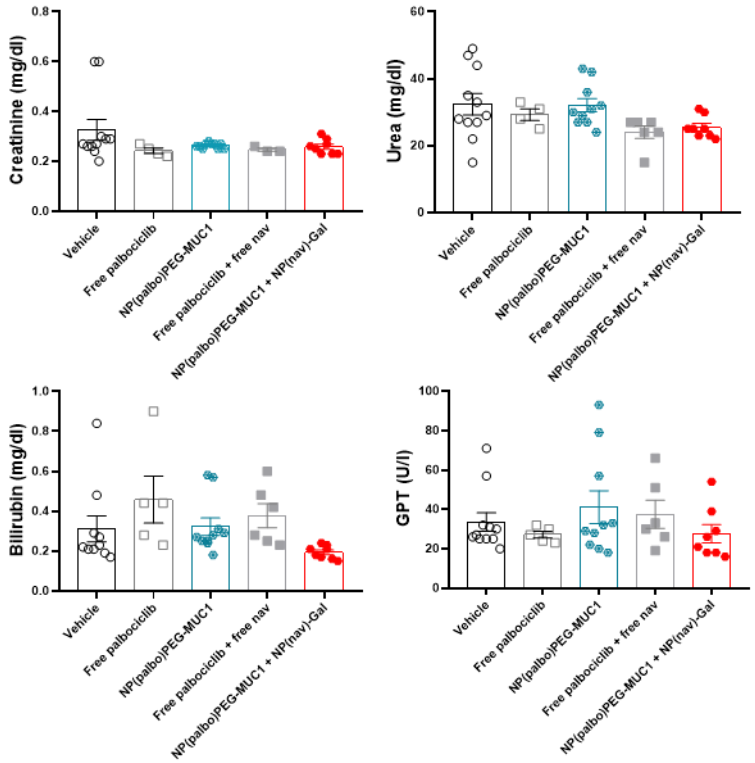

Figure S11 | Biochemistry blood analyses of MDA-MB-231 xenografts after the different treatments. Data represent means ± SEM and statistical significance was assessed by the two-way ANOVA followed by Tukey's post-test (*p<0.05; **p<0.01; ***p<0.001)

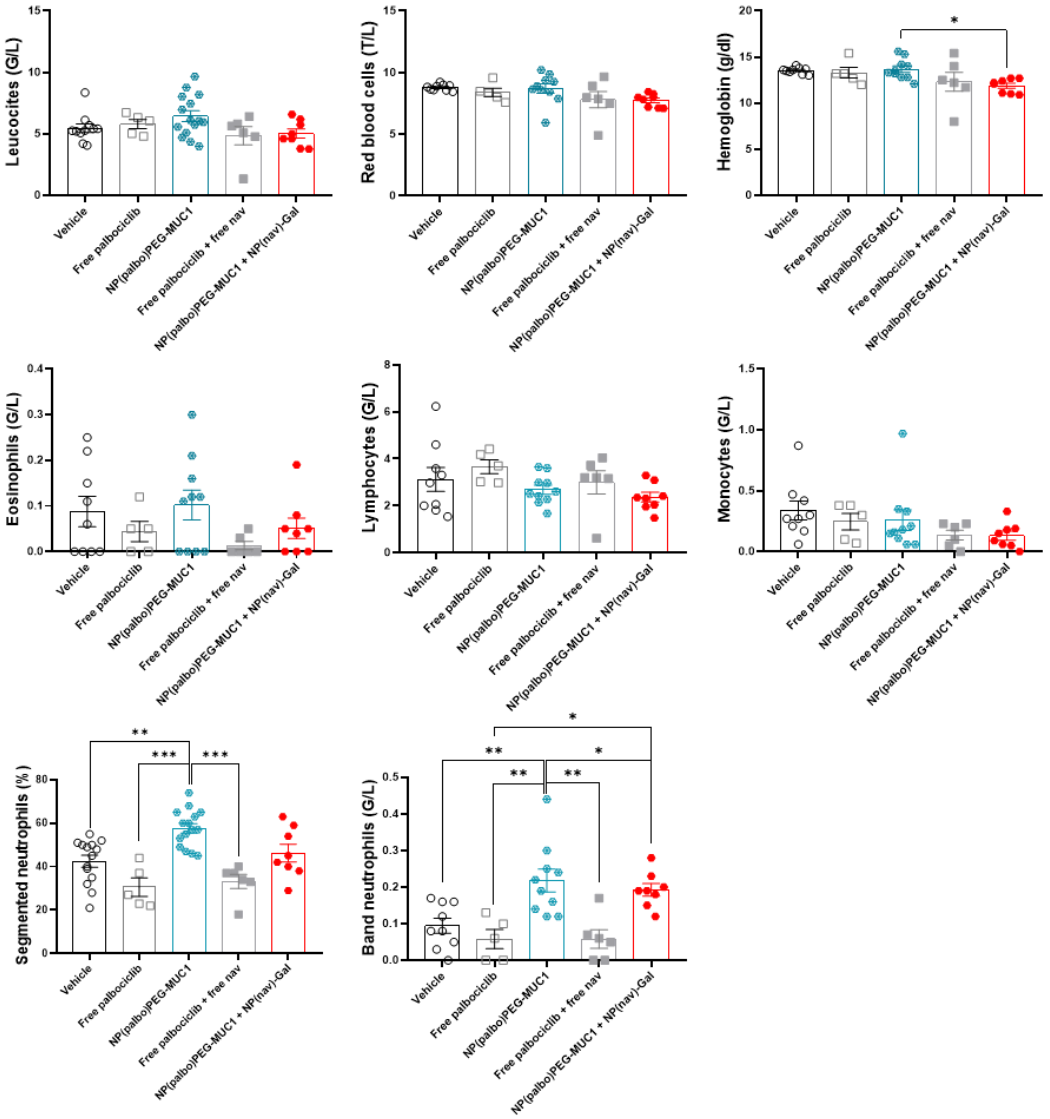

Figure S12 | Hemogram blood analyses of MDA-MB-231 xenografts after the different treatments. Data represent means ± SEM (n≥5) and statistical significance was assessed by the two-way ANOVA followed by Tukey's post-test (*p<0.05; **p<0.01; ***p<0.001)

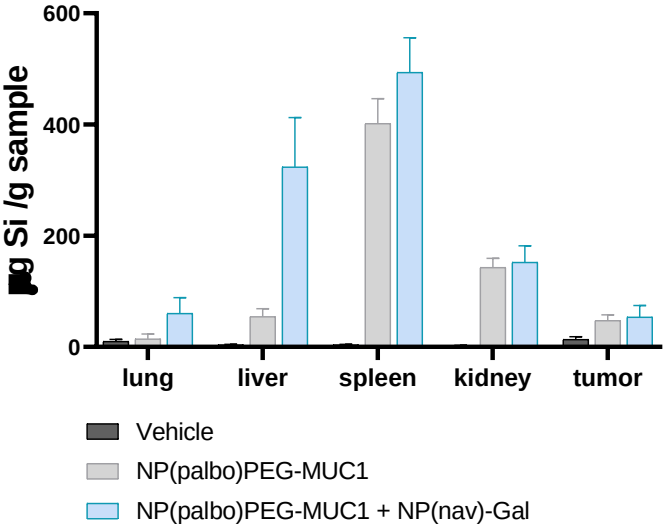

Figure S13 | Biodistribution of the nanoparticles in mice organs. Si levels were analyzed by Inductively Coupled Plasma Mass Spectroscopy (ICP-MS). Data are expressed as mean ± SEM (n=5) and represented as µg Si per g of sample.

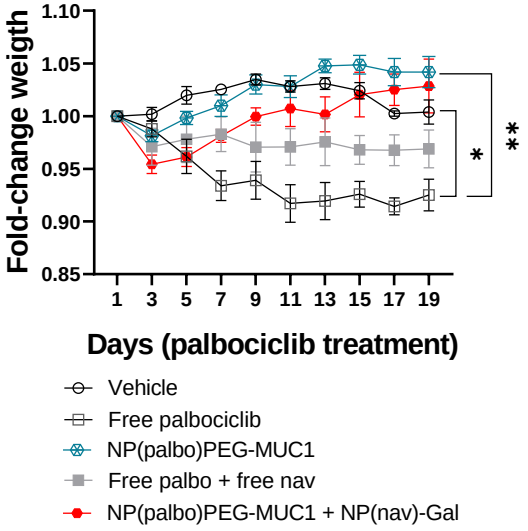

Figure S14 | Fold-change of weight changes of MDA-MB-231 xenografts during the whole experiment. Values are expressed as mean ± SEM (n≥5) and statistical significance was assessed by the two-way ANOVA followed by Tukey's post-test (*p<0.05; **p<0.01).

Chapter IV | Identification of novel senolytic hexapeptide for malignant melanoma

Identification of novel senolytic hexapeptide for malignant melanoma

Alejandra Estepa-Fernández[1,2,3‡], Irene Galiana[1,2‡], Araceli Lérida-Viso[1,2,3,4], Alicia Belén García-Jareño[2,5], Alba García-Fernández[1,2,3], Félix Sancenon-Galarza[1,2,3,4], Mar Orzáez [2,5*], Ramón Martínez-Máñez[1,2,3,4*]

[1] Instituto Interuniversitario de Investigación de Reconocimiento Molecular y Desarrollo Tecnológico (IDM) Universitat Politècnica de València, Universitat de València. *Camino de Vera, s/n. 46022, Valencia, Spain.*

[2] Unidad Mixta UPV-CIPF de Investigación en Mecanismos de Enfermedades y Nanomedicina, Universitat Politècnica de València, Centro de Investigación Príncipe Felipe. *C/ Eduardo Primo Yúfera 3. 46012, Valencia, Spain.*

[3] CIBER de Bioingeniería, Biomateriales y Nanomedicina (CIBER-BBN).

[4] Unidad Mixta de Investigación en Nanomedicina y Sensores. Universitat Politècnica de València, IIS La Fe. *Av. Fernando Abril Martorell, 106 Torre A 7ª planta. 46026, Valencia, Spain*.

[5] Centro de Investigación Príncipe Felipe. *C/ Eduardo Primo Yúfera 3. 46012, Valencia, Spain.*

[‡] Both authors have contributed equally.

*Corresponding authors: rmaez@qim.upv.es, morzaez@cipf.es.

Submitted

Graphical abstract

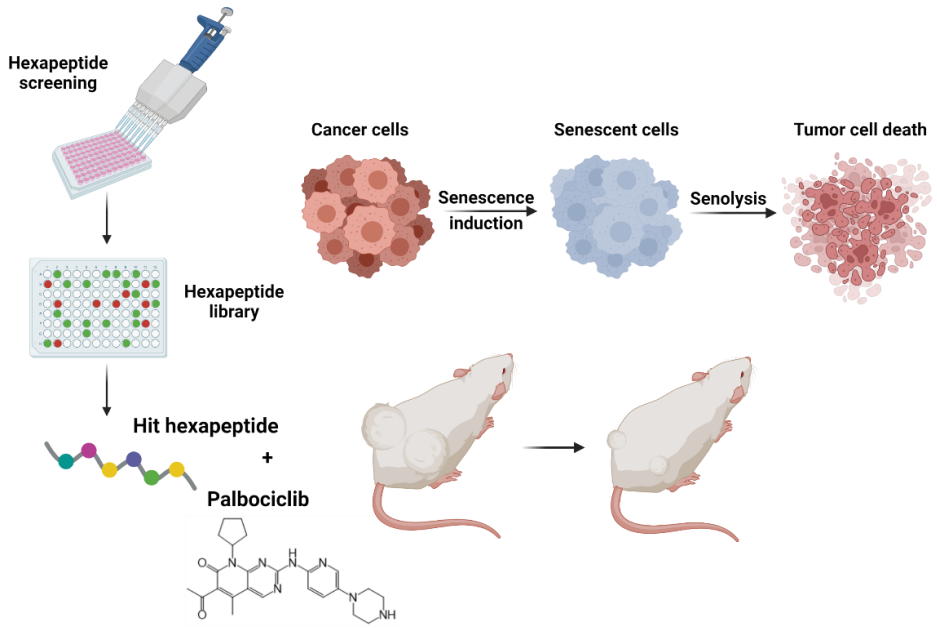

Keywords

Hexapeptide, senolytic drug, melanoma, senescence, screening

My contribution

I performed in vitro and in vivo evaluation of hexapeptide H8 and H14. I also contributed to the experimental design, data analysis, discussion and writing.

1. Abstract

Senescence is a cellular state of proliferative growth arrest whose main role in cancer is to prevent damaged cells from proliferating. Therapy-induced senescence is effective in clinical practice as a tumor-suppressive mechanism. However, the accumulation of senescent cells can also exacerbate tumorigenesis due to their pro-inflammatory and tumor-promoting secretory phenotype. Senolytics, drugs that selectively eliminate senescent cells, can ameliorate senescence-associated pathologies in many preclinical mouse models, including cancer and age-related diseases. Here, we report the identification of a novel senolytic peptide, H14, for the treatment of malignant melanoma, which selectively induces apoptosis in senescent cells. We show that combination treatment of the pro-senescent inductor palbociclib and the senolytic peptide H14 eradicates tumors in SK-MEL-103 mice xenografts. Our findings evidence the potential of the hexapeptide H14 for malignant melanoma treatment.

2. Introduction

Senescence is a cellular state of proliferative growth arrest that plays a role in aging, development, wound healing, and preventing carcinogenesis. (Muñoz-Espín and Serrano, 2014) Senescent cells are mainly characterized by morphological and epigenetic changes, increased activity of lysosomal β-galactosidase, and an associated secretory phenotype (SASP).(Lozano-Torres *et al.*, 2019) SASP factors provide signals for immune clearance of senescence cells and promote repair in adult damaged tissue.(Acosta *et al.*, 2013; Hernandez-Segura, Nehme and Demaria, 2018) However, in the aging process, senescent cells tend to accumulate in human tissues as a result of a defective elimination by an aged immune system.(Aiello *et al.*, 2019) Senescent cells in aged tissues contribute to the development of several age-related diseases including diabetes, tumorigenesis, atherosclerosis, osteoporosis, pulmonary and liver fibrosis, cardiac and brain disorders, and kidney disease.(Jimenez *et al.*, 2005; Yang and Fogo, 2010; Muñoz-Espín and Serrano,

2014; Chandrasekaran, Idelchik and Melendez, 2017; Farr *et al.*, 2017; Schafer *et al.*, 2017; Sun *et al.*, 2017; Baker and Petersen, 2018; Wandrer *et al.*, 2018; Hernandez-Segura, Nehme and Demaria, 2018; Khosla, Farr and Kirkland, 2018; McHugh and Gil, 2018) Consequently, the early detection of senescent cells represents a key issue in the development and monitoring of senolytic therapies.(Lozano-Torres *et al.*, 2017; Lozano-Torres, Blandez, Galiana, *et al.*, 2021; Lozano-Torres, Blandez, Sancenón, *et al.*, 2021; Lozano-Torres *et al.*, 2022)

Due to its tumor-suppressive function, drug-induced senescence is currently approved to treat locally advanced metastatic breast cancer patients and under clinical trials for its use in many other cancer types.(Levitin *et al.*, 2005; Webster *et al.*, 2006; Jugdaohsingh, 2007; Guenther *et al.*, 2019; Wang, Lankhorst and Bernards, 2022) To this end, senescence-inducing compounds, such as the CDK4/6 inhibitor, palbociclib, have been developed.(Finn *et al.*, 2015; Kwapisz, 2017; Whittaker *et al.*, 2017) Despite the effectiveness of senescence inducers for antitumor treatment in clinics, patients still suffer from cancer relapses. In fact, the accumulation of senescent cells in tissues and organs has harmful effects on the tissue, generating a pro-inflammatory microenvironment prone to becoming a metastatic niche .(Demaria *et al.*, 2017; Saleh *et al.*, 2018; Liao, Xiao and Liu, 2020; Estepa-Fernández *et al.*, 2021)

In recent years, there has been an intensive effort to identify pharmacological compounds with the ability to specifically target and eliminate senescent cells (senolytics).(Dou *et al.*, 2015; Fuhrmann-Stroissnigg *et al.*, 2017; Jeon *et al.*, 2017; Kirkland *et al.*, 2017; Zhu *et al.*, 2017; Fuhrmann-Stroissnigg, Niedernhofer and Robbins, 2018; Zhang *et al.*, 2018; Triana-Martínez *et al.*, 2019; Galiana *et al.*, 2020) Senolytic drugs, such as navitoclax, have demonstrated effectivity in reducing cancer relapse and delaying the onset of several aging associated-diseased such as atherosclerosis, neurodegenerative diseases, or hematopoietic system aging.(Chang *et al.*, 2016; Demaria *et al.*, 2017; Kim *et al.*, 2017; Bussian *et al.*, 2018). Besides, senolytic treatments, extend both health and life

span in naturally aged and progeroid syndrome mice.(Xu *et al.*, 2018; Yousefzadeh *et al.*, 2018a). Several pharmacological senolytics like navitoclax, fisetin, and the combination of dasatinib plus quercetin, are already being evaluated in clinical trials.(Hickson *et al.*, 2019; Justice *et al.*, 2019; Kirkland and Tchkonia, 2020; Verdoorn *et al.*, 2021; Morsli, Doherty and Muñoz-Espín, 2022) A major drawback of these senolytics is that they frequently have prevalent inherent toxicity which limits their therapeutic window and availability. For instance, navitoclax treatment causes thrombocytopenia, impaired osteoprogenitor function, and trabecular bone loss. (Kaefer *et al.*, 2014; Sharma *et al.*, 2020). Up to day, there is no universal senolytic drug capable of effectively removing all types of senescent cells, nor a specific senolytic drug capable of selectively eliminating one senescent cell type over another. Therefore, finding senolytic selective therapies for removing specific senescent cells could be a therapy of great potential for precision treatments.

In this context, combinatorial chemistry offers a powerful tool to provide new senolytic candidates. Combinatorial libraries are formed by compound mixtures organized to permit the screening of a large number of compounds in a simple process.(Aina *et al.*, 2007) In particular, synthetic peptide libraries have the potential to incorporate D-amino acids and other unnatural amino acids, as well as specific secondary structures to enhance biological activity by avoiding degradation.(Liu *et al.*, 2017; Bozovičar and Bratkovič, 2020)

From another point of view, one of the cancer subtypes where senescence induction has shown therapeutic potential is melanoma,(Ohanna *et al.*, 2011; Mao *et al.*, 2021; Tubita *et al.*, 2022) an aggressive skin cancer that metastasizes rapidly and is resistant to many commonly used anticancer drugs.(Gray-Schopfer, Wellbrock and Marais, 2007) Clinical management of melanoma involves treatment with drugs that are highly toxic resulting in damage to healthy cells and a decrease in immunity, consequently inducing patient suffering.(Mattia *et al.*, 2018; Kozar *et al.*, 2019) These tumor types, as previously demonstrated for breast cancer. (Fry *et al.*, 2004; Finn *et al.*, 2009, 2015, 2016; Beaver *et*

al., 2015; Walker *et al.*, 2016; Pernas *et al.*, 2018), could benefit from specific "one-two punch" therapies capable of first inducing senescence and then specifically eliminate senescent tumoral cells.

Based on the above, in this work, we have identified two promising senolytic hexapeptides for the treatment of malignant melanoma from the screening of a combinatorial library of D-amino acid hexapeptides. The screening has been performed in a melanoma cell model upon a "first shot- treatment" with the senescence-inducer palbociclib. The two new hexapeptides (i.e. H8 and H14) display specific senolytic activity for SK-Mel-103 melanoma cells. Concomitant treatment with palbociclib and H14 in a xenograft melanoma mice model results in the apoptosis of senescent tumor cells and the subsequent reduction of tumor growth.

3. Results

3.1. Identification of melanoma senolytic hexapeptides from the screening of a positional hexapeptide combinatorial library

To identify new senolytic compounds, we selected a combinatorial library of D-amino acid hexapeptides with a positional scanning format.(Blondelle *et al.*, 1995) We focused on this type of library for several reasons. First, peptides have important advantages as drugs such as low toxicity and great efficacy in mimicking protein-protein interactions relevant to biological activity. Since the use of insulin as a drug, several other peptides have reached the clinics successfully.(Muttenthaler *et al.*, 2021) Secondly, the use of D-amino acids avoids problems of peptide degradation. And finally, the positional scanning format of the library provides the opportunity to easily screen millions of hexapeptides organized in only 120 mixtures where the position of one amino acid is known, and the rest of the positions are occupied by equimolar mixtures of all the 20 amino acids (Figure S1).(Canela *et al.*, 2006) Following this approach, we performed the screening in the human melanoma cell line SK-Mel-103. These cells efficiently underwent

senescence upon treatment with 5 µM palbociclib, as revealed by their increased cellular size and augmented SA-βgal activity (Figure 1A). Besides, this was accompanied by hipophosphorylation of pRB and increased expression of p53 and p21 (Figure 1B and 1C) as expected for a senescent phenotype.

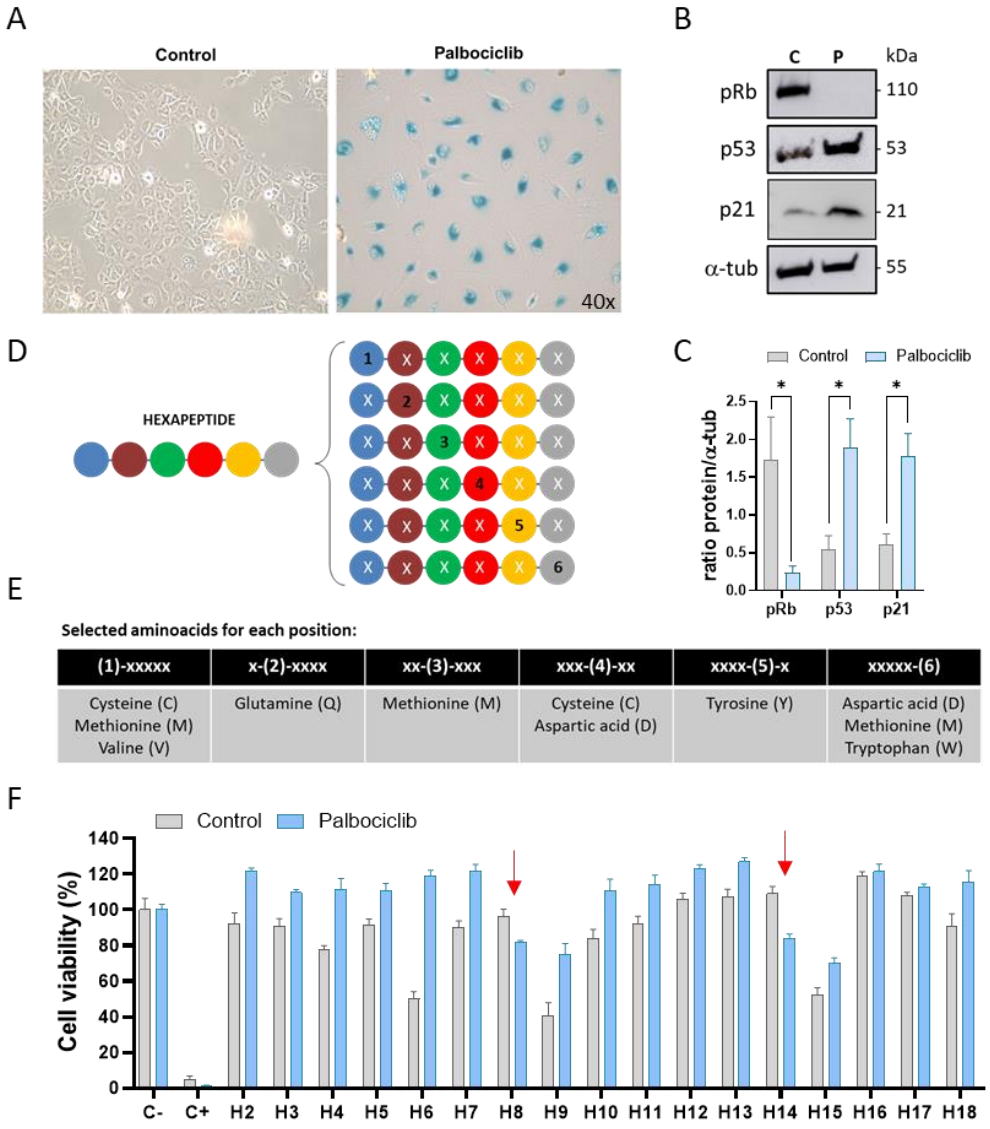

Figure 1 | Identification of senolytic hexapeptides on melanoma cultures from the screening of a positional hexapeptide combinatorial library. (A) Control and senescent SK-Mel-103 cells (treated

with 5 µM palbociclib, 7 days) after staining of β-galactosidase activity. (B) Western Blot analysis of pRB, p53, and p21 expression of control (C) and palbociclib-treated (P) SK-Mel-103 cells. α-tubulin (α-tub) was used as a loading control. (C) Quantification of western blot using Image J software. Data represent the mean ± SEM of at least three independent experiments, and statistical significance was assessed by unpaired T-test (*p<0.05). (D) Schematic representation of the 6 sub-chemical libraries of hexapeptides with a defined amino acid position. (E) Amino acids selected for each position in the hexapeptide. (F) Cytotoxicity evaluation of hexapeptide candidates (50 µM) in proliferating (grey bars) and senescent SK-Mel-103 (blue bars) based on the senolytic activity of the synthesized defined sequence hexapeptides (H2-H18). The negative (C-) and positive (C+) internal controls are included. C- is 1% DMSO, and C+ is 0.5 µM doxorubicin for control cells and 10 µM navitoclax for senescent cells. Data represent means ± SEM (n=3).

To identify hit candidates, we first evaluated the senolytic activity of the hexapeptide library with a total number of 20^6 peptides, distributed in 120 mixtures. (Figure 1D and S2) Based on the senolytic activity of each mixture in the SK-Mel-103 melanoma cell line, amino acids were selected for each of the six possible hexapeptide positions (Table S1). The combination of best amino acids chosen for each position led us to synthesize 18 hexapeptides with defined composition (3·1·1·2·1·3 = 18) (Figure 1E). Once the 18 candidate hexapeptides were synthesized, we evaluated the newly defined peptides for identifying the best senolytic activity (detailed explanation can be found in Supporting Information). Evaluation of defined peptides rendered two hexapeptides, H8 (MQMCYM) and H14 (VQMCYM), with senolytic activity, as could be inferred for the different cell viability observed between control cells and senescent SK-Mel-103 cells, upon peptide treatment (Figure 1F).

The senolytic activity of H8 and H14, was confirmed in viability assays where control cells and senescent melanoma SK-Mel-103 cells were treated for 48h with concentrations from 0 to 25 µM of each peptide, and then fixed and stained with crystal violet (Figure 2A). Treated control melanoma cells presented a monolayer of cells in all the concentrations evaluated for both hexapeptides, whose density could be practically compared to the density of non-treated cells. However, senescent cells began to visibly

decrease their viability at concentrations of 5 µM and 10 µM for H14 and H8 treatment, respectively. Practically no cells remained alive at 25 µM concentration for both peptides.

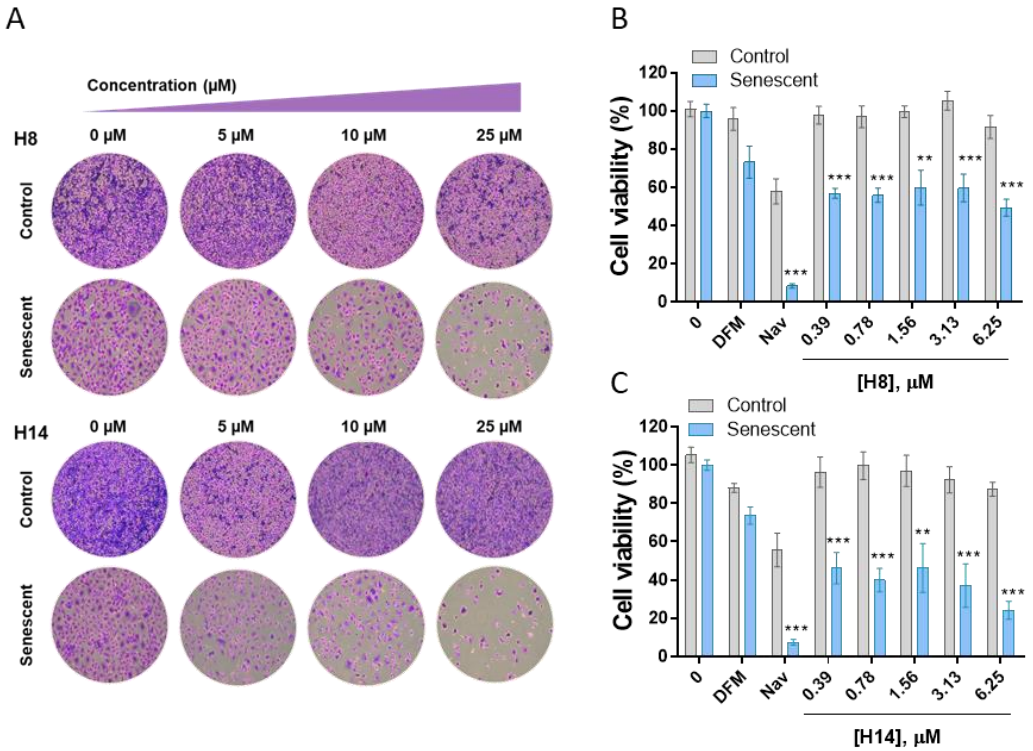

Figure 2 | Analysis of the senolytic activity of hexapeptide H8 and H14. (A) Crystal violet staining of control cells versus senescent cells at different H8 (upper panel) and H14 (lower panel) hexapeptide concentrations. (B) H8 cytotoxicity evaluation in proliferating (grey bars) and senescent SK-Mel-103 (black bars). Navitoclax (Nav, 10 µM) was used as positive senolytic control. Data represent means ± SEM (n=4). (C) H14 cytotoxicity evaluation in proliferating (grey bars) and senescent SK-Mel-103 (black bars). Navitoclax (10 µM) was used as positive senolytic control. Data represent means ± SEM (n=4). Statistical analysis was carried out using GraphPad Prism 8, and results were compared by multiple T-tests followed by Holm-Sidak post-tests (**p<0.01; ***p<0.001).

To further confirm the senolytic activity of both hexapeptides, cell viability assays were also evaluated after 72h of treatment by ATP measurement. Both hexapeptides were non-toxic for non-senescent SK-Mel-103 cells nearly in all the concentration range tested as cell viability was maintained up to 80% (Figure 2B and 2C). Hexapeptide H8 eliminated senescent melanoma cells with an estimated IC50 value of 4.6 µM, whereas

hexapeptide H14 eliminated them with an IC50 of 1 µM. The senolytic index was calculated by measuring the ratio of the IC50 values between control and senescent cells. An estimated senolytic index of 36.2x and 1.5x was found from these data for H14 and H8. These results confirmed the senolytic properties of both hexapeptides *in vitro* in senescent malignant melanoma cells. Due to the higher senolytic activity of H14, we decide to focus on this hexapeptide for further assays.

3.2. H14 induces cell death by apoptosis in melanoma senescent cells.

To address the cell death mechanism triggered by H14 in senescent cells, we investigated the possible induction of apoptosis. First, we analyzed the exposure of phosphatidylserine to the outer plasma membrane leaflet, a typical characteristic of cells undergoing cell death by apoptosis. For this purpose, we analyzed by flow cytometry cells double-stained with Annexin V/FITC, a phosphatidylserine affinity dye, and propidium iodide to identify dead cells. Treatment with the hexapeptide H14 (3.5 µM) mainly triggered apoptosis of palbociclib-induced SK-Mel-103 senescent cells (~18.22% early apoptosis (Annexin +/PI-), ~21.64% late apoptosis (Annexin +/PI+) ~6.66% necrosis (Annexin - /PI +)) (Figure 3A). Similarly, after the treatment with H14, we also observed the induction of active Caspase-3, the main executor of cell death by apoptosis (~3-fold increase when compared with non-treated senescent cells) (Figure 3B). Moreover, pre-treatment with the irreversible pan-caspase inhibitor Z-VAD-FMK (Zvad) protected senescent cells from cell death induced by H14 (Figure 3B), thus confirming that apoptosis is the preferential mechanism of cell death triggered by this compound.

There are two main pathways of apoptosis induction, intrinsic or mitochondrial and extrinsic (receptor-mediated) pathways (D'Arcy, 2019). To discern which of these two pathways was activated by H14, we studied the mitochondria functionality to identify a potential decrease in mitochondrial potential (Zamzami *et al.*, 1995; Overbeeke *et al.*, 1999). Analysis by flow cytometry of cells stained with tetramethylrhodamine ethyl ester

(TMRE) dye that accumulates in active polarized mitochondria revealed that hexapeptide H14 causes the loss of mitochondrial polarization in ~53% of cells (Figure 3C), confirming the activation of the intrinsic pathway. In summary, these results confirmed that the senolytic activity of H14 mainly relays on its capacity to induce cell death by activating the mitochondrial apoptosis pathway.

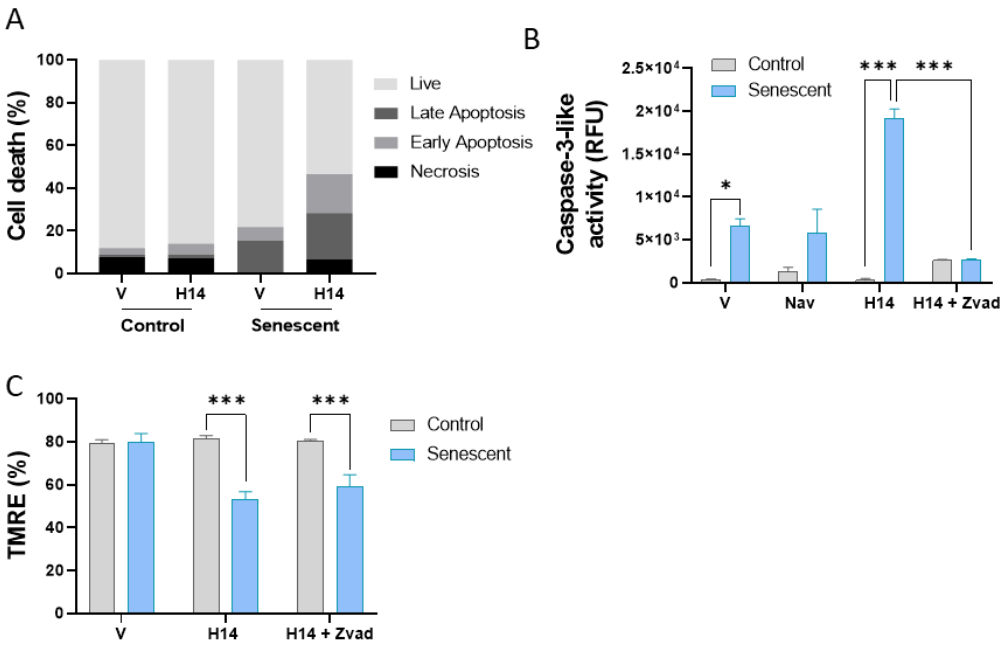

Figure 3 | Analysis of senescent cell death after H14 treatment. (A) Cell death percentage (%) of live, early apoptotic, late apoptotic, and necrosis cells after DMSO (vehicle, V) or H14 (3.5 µM) treatment for 48 hours. Percentages were measured by Annexin V-FITC and PI expression in flow cytometry. All values are represented as means (n ≥ 3) ± SEM. (B) Caspase 3 activity was measured in cytosolic extracts of proliferating and senescent SK-Mel-103 cells after treatment with H14 (3.5 µM). Navitoclax (Nav, 5 µM) was used as a positive control. Zvad is a pan-caspase inhibitor that blocks apoptosis. (C) Mitochondrial polarization status was measured with TMRE. Data represent means ± SEM (n=3). Statistical significance was determined by two-way ANOVA and Sidak's post-test (*p <0.05; **p <0.01 ***p <0.005).

3.3. H14 induces cell death in *in vivo* models of senescent melanoma tumors

Given the proper capacity of H14 to selectively eliminate senescent cells *in vitro*, we move one step forward to evaluate both the security and the antitumor activity of H14 in malignant melanoma *in vivo*. To address this issue, we first evaluated the acute toxicity of hexapeptide H14 in healthy mice. For this purpose, mice were treated with a single dose of H14 at 13 mg/kg, the maximum dose possible given peptide solubility, and were observed periodically during the first 24 hours and daily for 14 days. All animals survived the H14 treatment without any apparent affectation on their wellness or behavior (Figure S3A). Next, we evaluated the sustained toxicity in mice daily treated with H14 for a week (accumulated dose of 91 mg/kg; 13 mg/kg daily). After 8 days, all the animals did not show any toxic effects (Figure S3B). In hemograms and biochemistry blood analytics, all the measured parameters were maintained in normal ranges, corroborating normal renal and liver function and the absence of alterations in the red and white blood cell lineages. (Figure S4). Histological analysis of the major organs (lungs, heart, liver, spleen, and kidney) did not reveal any evident pathological alteration, in terms of morphology and structure, in H14 treated animals (Figure S3C).

Once we evaluated the security, we analyzed the *in vivo* senolytic activity of H14 on xenografted SK-Mel-103 athymic nude mice. Navitoclax treatment was included as a control of senolytic activity for further comparison with the hexapeptide treatment. (Chang *et al.*, 2016; Zhu *et al.*, 2016; Galiana *et al.*, 2020). Mice were subcutaneously injected with $5 \cdot 10^5$ SK-Mel-103 cells in the two flanks, and tumor formation was evaluated every 2 days, measuring tumor volume until it reached an average of 50 mm^3. Then, a daily therapy was initiated with either vehicle, 50 mg/kg palbociclib (via oral gavage) to induce senescence, 13 mg/kg H14 (via i.p. injection), 25 mg/kg navitoclax (via oral gavage), or a combination of palbociclib with either H14 or navitoclax (Figure 4A). Senolytic treatment (H14 or navitoclax) started one day after palbociclib treatment and was given daily for 15 days.

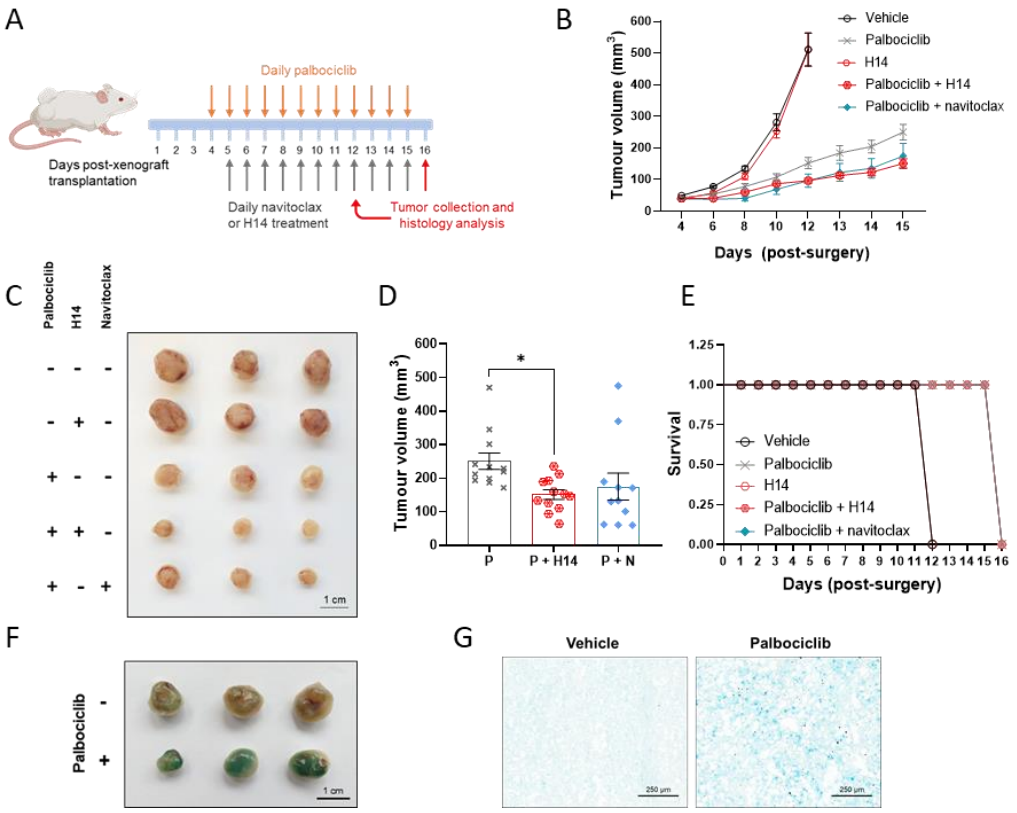

Figure 4 | H14 induces senolysis in melanoma tumors. (A) Athymic nude female mice were subcutaneously injected with SK-Mel-103 melanoma cancer cells and treated daily with either vehicle or palbociclib. When tumors volume reached 50 mm^3, palbociclib treatment started and was maintained daily (o.g.) for 15 days. H14 and navitoclax daily therapy started one day after palbociclib treatment (H14, 13 mg kg^{-1} intraperitoneal injection, navitoclax: oral gavage, 25 mg kg^{-1}) (n = 12). (B) Tumor volume (mm^3) of SK-Mel-103 xenografts after the different treatments. Data represents means ± SEM. (C) Photograph of representative tumor samples for each treatment. Scale bar, 1 cm. (D) Tumor volume (mm^3) of SK-Mel-103 xenografts at endpoint after either palbociclib (P), palbociclib plus H14 (P + H14) or palbociclib plus navitoclax (P + N) treatment. Data represents means ± SEM (n≥10). Statistical significance was determined by one-way ANOVA and Sidak's post-test (*p <0.05). (E) Kaplan-Meier curve during the experimental period in response to the treatments. All the treatments enhance the survival of melanoma model mice. (F) Photograph of representative tumor stained with X-gal. Scale bar, 1 cm. (G) SA-β-gal staining of representative tumor sections. Scale bar, 250 µm.

After palbociclib treatment, a significant reduction in tumor size was observed compared with non-palbociclib treated groups (Figure 4B). Besides, the treatment of animals with H14 hexapeptide did not exhibit any sign of tumor reduction. Of note, vehicle-treated mice and H14-treated mice had to be sacrificed on day 12 due to the exponential growth of the tumor that affected their well-being (Figure 4E). In contrast, a significant tumor size decrease was achieved when animals were treated with the combination of palbociclib with H14 hexapeptide. The induction of senescence is required to obtain a robust therapeutic effect with the hexapeptide H14, thus confirming its senolytic activity. Combinatorial palbociclib plus H14, achieved a similar reduction of tumor size (Figure 4C and 4D) to that observed for palbociclib plus navitoclax treatment, thus reinforcing H14 senolytic effectiveness for malignant melanoma therapy. Indeed, concomitant palbociclib plus H14 treatment slightly improved tumor size compared to treatment with palbociclib plus navitoclax (Figure 4C and 4D). Mice did not have any significant body weight loss (Figure S5) or biochemistry and hematological alterations (Figure S6 and S7), indicating the lower systemic toxicity of the hexapeptide.

Besides, the induction of senescence was confirmed in tumors. Increased X-gal staining was observed in whole tumors (Figure 4F) and in tumor sections (Figure 4G). Besides, Ki67 expression decreased after palbociclib treatment (Figure 5A). Moreover, histological evaluation of tumors showed an increase in p53 and p21 expression after palbociclib treatment (Figure 5A and 5B). A reduction of p53 and p21 expression was observed after concomitant treatment with palbociclib plus H14 or palbociclib plus navitoclax. TUNEL signal was also evaluated in tumor sections (Figure 5A and 5B), with an increased signal after palbociclib plus either H14 or navitoclax treatment, strongly suggesting apoptosis of senescent cells facilitates the antitumor effect. These results demonstrate that oral administration of palbociclib induces senescence in tumors in SK-Mel-103 xenografts mice model, while H14 senolytic treatment reduces the senescence burden in the tumors.

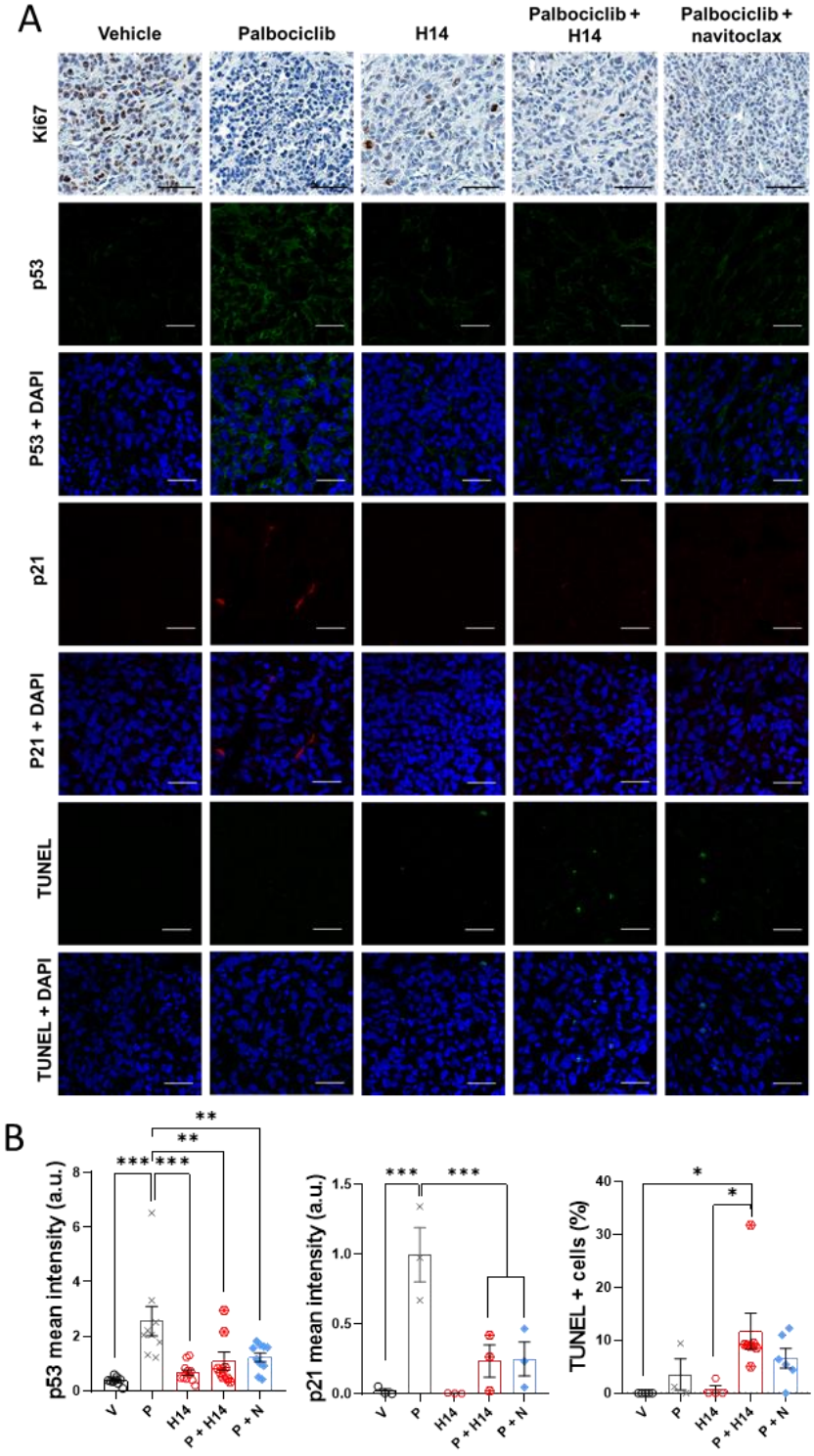
A
Vehicle
Palbociclib
H14
Palbociclib + H14
Palbociclib + navitoclax
Ki67
p53
P53 + DAPI
p21
P21 + DAPI
TUNEL
TUNEL + DAPI
B
p53 mean intensity (a.u.)
p21 mean intensity (a.u.)
TUNEL + cells (%)
V
P
H14
P + H14
P + N

Figure 5 | Simultaneous treatment with palbociclib and H14 significantly inhibits tumor growth in a human melanoma xenograft mouse model. (A) Representative histological images of SK-Mel-103 xenografts tumors at the end of the treatments stained for Ki67, p53, and p21 expression and labelled using TUNEL staining. Scale bar = 100 µm. (B) Percentage of p53- (top), p21- (middle), and TUNEL-positive (bottom) cells in tumors from animals treated with vehicle (V), palbociclib (P), hexapeptide H14, or palbociclib (P), and H14 or navitoclax (N) concomitantly (n ≥ 12 tumors per group). For quantification, at least 3 tumors were analyzed. Data represent the mean ± SEM, and statistical significance was assessed by one-way ANOVA followed by Tukey post-test (*p <0.05; **p <0.01 ***p <0.005).

4. Discussion and conclusion

Cellular senescence is a state of permanent growth arrest that can be triggered by several stresses.(Hernandez-Segura, Nehme and Demaria, 2018) In this work, we focus on the therapy-induced senescence (TIS) in cancer cells in response to treatment with the chemotherapeutic agent palbociclib. Traditionally, TIS presents a desirable strategy for cancer treatment since it can stop cancer cell proliferation.(Sager, 1991; Campisi, 2001; Collado and Serrano, 2010) However, once cancer cells become senescent, they can be either cleared by the immune system or escape from it and accumulated in the tissues.(Liao, Xiao and Liu, 2020) Senescence-associated secretory phenotype (SASP) of senescent cells also has an important role in immunosuppression and creating a pro-tumoral microenvironment.(Rao and Jackson, 2016; Gonzalez-Meljem *et al.*, 2018; Faget, Ren and Stewart, 2019; Ruscetti *et al.*, 2020) Furthermore, senescence cells can escape from the senescence state, entering a stem-like state with high aggressiveness that eventually facilitates cancer recurrence.(Demaria *et al.*, 2017; Milanovic *et al.*, 2018; Saleh *et al.*, 2018) To avoid these negative effects, one-two punch strategies have been developed using a combined therapy of senescence-inducing chemotherapy followed by senotherapy.(Sieben *et al.*, 2018; Short *et al.*, 2019; Galiana *et al.*, 2020; Estepa-Fernández *et al.*, 2021; Park *et al.*, 2021; Wang, Lankhorst and Bernards, 2022) Senotherapies are drugs aimed to limit the deleterious effects of senescent cells either by eliminating senescent cells (senolytics), inhibiting the SASP (senomorphics), or inhibiting senescence before it happens (senoblockers). Over the last few years, several senolytics have been

reported, including dasatinib and quercetin, Bcl-2 family inhibitors, piperlongumine, fisetin, HSP90 inhibitors, and cardiac glycosides, among many others.(Zhu *et al.*, 2015, 2017; Chang *et al.*, 2016; Yosef *et al.*, 2016; Baar *et al.*, 2017; Fuhrmann-Stroissnigg *et al.*, 2017; Kang *et al.*, 2017; Yousefzadeh *et al.*, 2018b; Zhang *et al.*, 2018). Up to date, there is no universal senolytic drug capable of effectively eliminating all types of senescent cells nor a specific senolytic able to eliminate selectively one senescent cell type over another. Therefore, finding a selective method for removing a specific senescent cell type could be a therapy of importance for precision cancer treatment.

Melanoma prognosis has advanced significantly in recent years with the use of BRAF/MEK inhibitors and anti-PD1 antibodies that have improved the clinical management of this disease (Davis, Shalin and Tackett, 2019). However, not all patients benefit from these therapies or maintain their benefits over the long term; thus, new and effective drugs are urgently needed. In particular, palbociclib and other CDK4/6 inhibitors have already had a huge impact on the clinical management of different cancer types, such as breast cancer. Melanoma patients may promptly benefit from their clinical utility as palbociclib therapy is already in clinical trials for melanoma treatment (NCT03454919, NCT04720768, NCT01037790, NCT02202200, NCT02065063A, NCT02465060).(Garutti *et al.*, 2021; Mao *et al.*, 2021). In this scenario, and due to the induction of senescence by palbociclib, senolytic compounds can provide an excellent therapeutic opportunity to explore a combination strategy to improve patient outcomes.

Taking everything into account, in this study, we aim to identify novel senolytics agents that can target malignant melanoma senescent cells with optimal *in vivo* efficacy and safety. To identify new senolytic compounds, we selected a combinatorial library of D-amino acid hexapeptides with a positional scanning format and identified two six-amino acid peptides, H8 and H14, with senolytic activity *in vitro* in the human melanoma cell line SK-Mel-103 but with limited cytotoxicity to proliferating cells. The hexapeptide H14 causes cell death in senescent cells by apoptosis induction. In addition, we moved

one step forward and evaluated both the safety and the antitumor activity of H14 in malignant melanoma *in vivo*. No acute toxicity or sustained toxicity in mice was found upon treatment with H14 and hemograms and biochemistry blood analysis maintained normal levels. Besides, histological analysis of major organs did not reveal pathological alterations. Moreover, efficacy analysis of the use of H14 was tested on xenografted SK-Mel-103 athymic nude mice. A significant decrease in tumor size was achieved when animals were treated with the combination of palbociclib plus H14 hexapeptide. Besides, the induction of senescence was confirmed in tumors. TUNEL signal evaluated in tumor sections upon treatment with palbociclib plus H14 evidenced apoptosis of senescent cells which facilitates the antitumor effect. Our results demonstrate that palbociclib induces senescence in tumors in SK-Mel-103 xenografts mice model, while H14 senolytic treatment reduces the senescence burden in the tumors.

Combination of palbociclib and H14, achieved a similar reduction of tumor size to that observed for palbociclib plus navitoclax treatment, thus reinforcing the H14 senolytic activity in malignant melanoma. Moreover, navitoclax, an inhibitor of BCL-2 anti-apoptotic proteins, is effective *in vivo* in reducing relapse in some cancer models and the onset of several aging associated-diseased.(Chang *et al.*, 2016; Zhu *et al.*, 2016; Demaria *et al.*, 2017; Kim *et al.*, 2017; Bussian *et al.*, 2018). Also, early-phase clinical data indicate the potential role of navitoclax in cancer treatments, even though it is not yet routinely used in clinical practice (NCT00445198; NCT02591095; NCT02520778; NCT02079740) and we have probed the efficacy of the combinational treatment of palbociclib plus navitoclax in SK-Mel-103 xenografts mice.(Muñoz-Espín *et al.*, 2018) However, navitoclax frequently causes thrombocytopenia, (Wilson *et al.*, 2010; Cang *et al.*, 2015; Muñoz-Espín *et al.*, 2018) however that was not observed upon H14 treatment (Fig S7). Besides, mice treated with H14 alone or in combination with palbociclib did not show any significant body weight loss or biochemistry and hematological alterations indicating no systemic toxicity of the hexapeptide and providing evidence for *in vivo* safety of this senolytic.

In summary, we have identified two new hexapeptides with promising senolytic activities that could eventually eliminate senescent cells in melanoma patients undergoing chemotherapy treatments that induce senescence, overcoming the long-term negative effects caused by the accumulation of senescent cancer cells.

5. Experimental section

5.1. Cell lines

Human melanoma SK-Mel-103 cell line was obtained from ATCC and maintained in DMEM medium supplemented with 10% fetal bovine serum (FBS) (Sigma). The cells were kept in incubation at 37°C under conditions of O_2 20% and CO_2 5%. For senescence induction, the culture medium was supplemented with palbociclib at 5 µM and held for 7 days.

5.2. Peptide libraries

The library was a combinatorial library of hexapeptides of D-amino acids (they do not degrade in cells) that consisted of a total of 20^6 compounds (stock 3.9 mM in water 5% DMSO) (#DD05273, DiverDrugs). All individual peptides were prepared using simultaneous multiple peptide synthesis.(Canela *et al.*, 2006) H14 for *in vivo* experiment was synthesized by Nzytech and purified by HPLC by 96,45% (Figure S8).

5.3. HPLC and MS characterization

Conditions of HPLC chromatograms: 4.6 x 250 mm, GS-120-5-C18 column, 1 mL/min, (solvent A: 0.1% trifluoroacetic acid in 100% acetonitrile, solvent B: 0,1% trifluoroacetic acid in 100% water): gradient elution: 26:74 0 min, 51:49 25 min, 100:0 25.1 min. ESI-MS chromatograms were acquired with the mass spectrometer Single Quadrupole LC/MS Agilent. Conditions: 0.2 mL/min, (50% H_2O: 50% acetonitrile).

5.4. Positional tracking of the entire library

To carry out the first screening tests of the whole library, the activity of the hexapeptides was tested at three different and considerably high concentrations: 500, 600, and 700 µM. Proliferating and senescent cells were seeded in parallel in 96 well plates, at densities of 3500 and 5000 cells per well (respectively). After 24 hours, hexapeptide treatment (final concentration in well: 500-600-700 µM) was added, or the respective treatments with 0.5 µM doxorubicin (Carbosynth) or 5 µM navitoclax (Active Biochem) in the case of the wells corresponding to the positive controls. Both positive and negative controls were included on each plate to validate the viability readings. The treatments were allowed to incubate with the cells for 48 hours, after which time the viability readings were done directly on each plate with the CellTiter-Glo® Luminescent Cell Viability Assay kit (Promega).

5.5. Staining of senescence-associated β-galactosidase

Senescence-associated β-galactosidase was performed using the Senescence β-galactosidase Staining Kit (Cell Signaling). The assay was carried out following the manufacturer's instructions; the cells were incubated overnight at 37°C with the staining solution (X-gal dissolved in N-N-dimethylformamide, pH 6)

5.6. Viability test with deconvolved hexapeptides

The 18 hexapeptides with a defined sequence (synthesized from the deconvolution of the results obtained from the initial screening of the library) were again tested in feasibility tests to continue studying their senolytic activity. Control and senescent cells were plated in parallel in 96-well plates: 3500 and 5000 proliferating and senescent cells (respectively) per well. The following day, the different synthesized hexapeptides were added and tested at two different final concentrations: 50 µM and 100 µM. Positive controls (doxorubicin for control cells, navitoclax for senescent cells) and negative

controls were included in each plate. In addition, an extra plate was included to which hexapeptide treatment was added in the absence of cells to rule out a possible baseline luminescence signal. After 48 hours of incubation of the cells with the corresponding treatments, the viability reading of each plate was carried out using the CellTiter-Glo® Luminescent Cell Viability Assay kit (Promega). The senolytic index of the compounds was calculated by measuring the ratio of the half-maximal inhibitory concentration (IC50) values between control and senescent cells.

5.7. Viability validation test

The final validation of the senolytic activity of the two selected defined sequence hexapeptides (H8 and H14) was performed using a viability test based on crystal violet. For this, control cells and senescent cells were seeded in 24-well dishes, at densities of 4 x 10^5 cells/mL and 2.15 x 10^5 cells/mL, respectively. The two hexapeptides were tested the following day at 5, 10, and 25 µM for 48 h. After the incubation time, cells were washed several times with PBS and fixed with 4% paraformaldehyde (15 minutes, room temperature). Then cells were washed, and crystal violet solution (0.05%) was added (45 min) for staining the cells that had remained attached to the plate. Finally, dishes were washed with water to remove the excess of dye not retained in the cells and dried at room temperature before visualization.

5.8. Cell death assay

For the apoptosis evaluation assay, proliferating and senescent SK-Mel-103 cells were treated with H14 (3.5 µM). According to the manufacturer's recommendations, after 48 hours of incubation, cells were labeled with Alexa fluorescein isothiocyanate-conjugated Annexin V (BD Bioscience) plus propidium iodide. Samples were analyzed in the cytometer CytoFLEX S.

5.9. Caspase 3 Activity

Proliferating and senescent SK-Mel-103 cells were treated with H14 (3.5 μM). After 48 hours of incubation, cells were harvested, and the pellets were resuspended in lysis buffer (10.2 mM HEPES pH 7.4, 10 mM KCl, 1.5 mM $MgCl_2$, 1 mM EDTA, 1 mM EGTA, and 1 mM DTT, supplemented with a protease inhibitor cocktail). The pellets were frozen and thawed three times using liquid nitrogen and cell lysates, then centrifuged at 13,200 rpm for 10 min. The supernatants were collected, and total protein concentration was quantified using the BCA method. For caspase 3 kinetics, 50 μg protein was mixed with 200 μL caspase assay buffer (PBS, 10% glycerol, and 2 mM DTT) containing 20 μM Ac-DEVD-AFC. Caspase activity was monitored using a Wallac 1420 Victor2 Workstation (λ_{exc} 400 and λ_{em} 508 nm). To block apoptosis induction, pan-caspase inhibitor Z-VAD-FMK (Enzo Life Sciences) 5 μM for 24 h was used.

5.10. TMRE Staining

For addressing mitochondrial polarization status, proliferating and senescent SK-Mel-103 cells were treated with H14 (3.5 μM). After 48 hours of incubation, cells were incubated with 50 nM TMRE dye (Invitrogen, T669) at 37ºC/5% CO_2 for 30 min. Then, samples were analyzed in a CytoFLEX S flow cytometer. As a positive control of mitochondrial depolarization, cells pre-treated with 20 μM FCCP for 10 min were used (data not shown). To block apoptosis induction, the pan-caspase inhibitor Z-VAD-FMK (Enzo Life Sciences) 5 μM for 24 h was used.

5.11. Mice experiments

Animal procedures were approved by Ethical Committee for Research and Animal Welfare Generalitat Valenciana, Conselleria dÀgricultura, Medi ambient, Canvi climàtic i Desenvolupament Rural (license number 2020/VSC/PEA/0176). Female 8-10 weeks old athymic nude mice (Hsd: Athymic Nude-Foxn1nu, Envigo) were used.

To evaluate the toxicity of the hexapeptide H14, single health mice were treated with H14 (13 mg/kg) at 48 h intervals. Mice were observed individually at least once during the first 30 minutes after dosing, periodically during the first 24 hours, and then daily for 14 days. After 14 days, 3 consecutive animals survived the H14 treatment without any visual affectation of their wellness or behavior. Also, 5 mice were daily treated (13 mg/kg) with H14 for a week to evaluate sustained toxicity. After 14 days, animals did not show any toxic effects.

In order to evaluate senolytic activity of the H14 hexapeptide on xenografted SK-Mel-103 cells, female 8-10 weeks old athymic nude mice (Hsd: Athymic Nude-Foxn1nu, Envigo) were subcutaneously injected in two flanks with 5 x 10^5 SK-Mel-103 cells. Tumors were measured with calipers every 2 days, and the tumor volume (mm^3) was calculated with the formula length × $width^2/2$. When tumor volume reached an average of 50 mm^3, daily therapy was initiated with either vehicle, 50 mg/kg palbociclib (via oral gavage), 13 mg/kg H14 (via i.p. injection), 25 mg/kg navitoclax (via oral gavage), or a combination of the mentioned drugs.

5.12. Histology

Tumors were fixed (4% PFA, overnight, 4 °C), washed in 1×PBS, incubated with 30% sucrose (overnight, 4 °C) and embedded in cryomolds with OCT. 10 µm thick tumor sections were then incubated in blocking solution (5% horse serum, 0.3% Triton X-100 in 1× PBS) for 1 h and immunostained following incubation with primary antibodies overnight at 4 °C. p53 antibody was used at 1:100 (ab26, Abcam), and p21 antibody was used at 1:100 (ab107099, Abcam). Secondary antibodies against rat or mouse conjugated to Alexa Fluor 488 (Invitrogen) or Alexa Fluor 587 (Invitrogen) were used at 1:200 dilutions. For TUNEL staining, In Situ Cell Death Detection Kit (Merck) was used following the manufacturer's instructions. Sections were mounted using the Mowiol/DAPI (Sigma) and covered with a glass coverslip. Confocal microscopy images were obtained using a

Leica TCS SP8 HyVolution 2 microscope. Positive signal for p21, p53, and TUNEL was quantified with ImageJ.

Tumors were also included in paraffin for Ki67 staining. 5 µm paraffin sections were deparaffinized and re-hydrated. Antigen retrieval was carried out using 10mM Sodium Citrate and 0.05% Tween 20 buffer at pH 6.0 for 30 minutes. Tumor sections were incubated in blocking solution (5% horse serum, 0.3% Triton X-100 in 1× PBS) for 1 h and incubated with Ki67 (Abcam) antibody at 4°C overnight. Ki67 immunostaining was developed using 3,3-diaminobenzidine tetrahydrochloride (DAB) and nuclei counterstained with hematoxylin. Sections were scanned in Leica Aperio Versa 200 equipment at 10x magnification.

5.13. Statistical Analysis

For *in vivo* studies, mice were randomly assigned to treatment groups; sample size was not pre-determined. All of the values represent the mean ± SEM of at least three independent experiments except the *in vivo* experiment with mice, and a single representative experiment is shown. Significance was determined by one-way ANOVA followed by Tukey post-tests or two-way ANOVA followed by Sidak's post-tests as indicated in the figures using GraphPad 8 software. A p-value below 0.05 was considered statistically significant and indicated with asterisk: *$p < 0.05$, **$p < 0.01$ and ***$p < 0.005$.

6. References

Acosta, J. C. et al. (2013) ‘A complex secretory program orchestrated by the inflammasome controls paracrine senescence’, Nature Cell Biology, 15(8), pp. 978–990. doi: 10.1038/ncb2784.

Aiello, A. et al. (2019) ‘Immunosenescence and its hallmarks: How to oppose aging strategically? A review of potential options for therapeutic intervention’, Frontiers in Immunology, 10(SEP), p. 2247. doi: 10.3389/FIMMU.2019.02247/BIBTEX.

Aina, O. H. et al. (2007) ‘From combinatorial chemistry to cancer-targeting peptides’, Molecular Pharmaceutics. Mol Pharm, pp. 631–651. doi: 10.1021/mp700073y.

Baar, M. P. et al. (2017) 'Targeted Apoptosis of Senescent Cells Restores Tissue Homeostasis in Response to Chemotoxicity and Aging', Cell, 169(1), pp. 132-147.e16. doi: 10.1016/j.cell.2017.02.031.

Baker, D. J. and Petersen, R. C. (2018) 'Cellular senescence in brain aging and neurodegenerative diseases: evidence and perspectives', Journal of Clinical Investigation, 128(4), pp. 1208–1216. doi: 10.1172/JCI95145.

Beaver, J. A. et al. (2015) 'FDA Approval: Palbociclib for the Treatment of Postmenopausal Patients with Estrogen Receptor-Positive, HER2-Negative Metastatic Breast Cancer.', Clinical cancer research : an official journal of the American Association for Cancer Research, 21(21), pp. 4760–6. doi: 10.1158/1078-0432.CCR-15-1185.

Blondelle, S. E. et al. (1995) 'The antimicrobial activity of hexapeptides derived from synthetic combinatorial libraries', Journal of Applied Bacteriology, 78(1), pp. 39–46. doi: 10.1111/J.1365-2672.1995.TB01671.X.

Bozovičar, K. and Bratkovič, T. (2020) 'Evolving a peptide: Library platforms and diversification strategies', International Journal of Molecular Sciences. MDPI AG. doi: 10.3390/ijms21010215.

Bussian, T. J. et al. (2018) 'Clearance of senescent glial cells prevents tau-dependent pathology and cognitive decline.', Nature, 562(7728), pp. 578–582. doi: 10.1038/s41586-018-0543-y.

Campisi, J. (2001) 'Cellular senescence as a tumor-suppressor mechanism', Trends in Cell Biology, 11(11), pp. 27–31. doi: 10.1016/S0962-8924(01)02151-1.

Canela, N. et al. (2006) 'Identification of an Hexapeptide That Binds to a Surface Pocket in Cyclin A and Inhibits the Catalytic Activity of the Complex Cyclin-dependent Kinase 2-Cyclin A', Journal of Biological Chemistry, 281(47), pp. 35942–35953. doi: 10.1074/JBC.M603511200.

Cang, S. et al. (2015) 'ABT-199 (venetoclax) and BCL-2 inhibitors in clinical development', Journal of Hematology and Oncology. BioMed Central Ltd. doi: 10.1186/s13045-015-0224-3.

Chandrasekaran, A., Idelchik, M. del P. S. and Melendez, J. A. (2017) 'Redox control of senescence and age-related disease', Redox Biology, 11, pp. 91–102. doi: 10.1016/J.REDOX.2016.11.005.

Chang, J. et al. (2016) 'Clearance of senescent cells by ABT263 rejuvenates aged hematopoietic stem cells in mice', Nature Medicine, 22(1), pp. 78–83. doi: 10.1038/nm.4010.

Collado, M. and Serrano, M. (2010) 'Senescence in tumors: evidence from mice and humans', Nature reviews. Cancer, 10(1), pp. 51–57. doi: 10.1038/NRC2772.

D'Arcy, M. S. (2019) 'Cell death: a review of the major forms of apoptosis, necrosis and autophagy', Cell Biology International. John Wiley & Sons, Ltd, pp. 582–592. doi: 10.1002/cbin.11137.

Davis, L. E., Shalin, S. C. and Tackett, A. J. (2019) 'Current state of melanoma diagnosis and treatment', Cancer Biology and Therapy, 20(11), pp. 1366–1379. doi: 10.1080/15384047.2019.1640032.

Demaria, M. et al. (2017) 'Cellular senescence promotes adverse effects of chemotherapy

and cancer relapse', Cancer Discovery, 7(2), pp. 165–176. doi: 10.1158/2159-8290.CD-16-0241.

Dou, Z. et al. (2015) 'Autophagy mediates degradation of nuclear lamina', Nature, 527(7576), pp. 105–109. doi: 10.1038/nature15548.

Estepa-Fernández, A. et al. (2021) 'Senolysis Reduces Senescence in Veins and Cancer Cell Migration', Advanced Therapeutics, 2100149, pp. 1–15. doi: 10.1002/adtp.202100149.

Faget, D. V., Ren, Q. and Stewart, S. A. (2019) 'Unmasking senescence: context-dependent effects of SASP in cancer', Nature reviews. Cancer, 19(8), pp. 439–453. doi: 10.1038/S41568-019-0156-2.

Farr, J. N. et al. (2017) 'Targeting cellular senescence prevents age-related bone loss in mice', Nature Medicine, 23(9), pp. 1072–1079. doi: 10.1038/nm.4385.

Finn, R. R. S. et al. (2015) 'The cyclin-dependent kinase 4/6 inhibitor palbociclib in combination with letrozole versus letrozole alone as first-line treatment of oestrogen receptor-positive, HER2-negative, advanced breast cancer (PALOMA-1/TRIO-18): A randomised phase 2 study', The Lancet Oncology, 16(1), pp. 25–35. doi: 10.1016/S1470-2045(14)71159-3.

Finn, R. S. et al. (2009) 'PD 0332991, a selective cyclin D kinase 4/6 inhibitor, preferentially inhibits proliferation of luminal estrogen receptor-positive human breast cancer cell lines in vitro', Breast Cancer Research, 11(5), pp. 1–13. doi: 10.1186/bcr2419.

Finn, R. S. et al. (2016) 'Palbociclib and Letrozole in Advanced Breast Cancer', New England Journal of Medicine, 375(20), pp. 1925–1936. doi: 10.1056/NEJMoa1607303.

Fry, D. W. et al. (2004) 'Specific inhibition of cyclin-dependent kinase 4/6 by PD 0332991 and associated antitumor activity in human tumor xenografts.', Molecular cancer therapeutics, 3(11), pp. 1427–38. Available at: http://www.ncbi.nlm.nih.gov/pubmed/15542782 (Accessed: 4 September 2019).

Fuhrmann-Stroissnigg, H. et al. (2017) 'Identification of HSP90 inhibitors as a novel class of senolytics', Nature Communications, 8(1). doi: 10.1038/s41467-017-00314-z.

Fuhrmann-Stroissnigg, H., Niedernhofer, L. J. and Robbins, P. D. (2018) 'Hsp90 inhibitors as senolytic drugs to extend healthy aging', Cell Cycle, pp. 1–8. doi: 10.1080/15384101.2018.1475828.

Galiana, I. et al. (2020) 'Preclinical antitumor efficacy of senescence-inducing chemotherapy combined with a nanoSenolytic', Journal of Controlled Release, 323, pp. 624–634. doi: 10.1016/j.jconrel.2020.04.045.

Garutti, M. et al. (2021) 'CDK4/6 Inhibitors in Melanoma: A Comprehensive Review', Cells, 10(6). doi: 10.3390/CELLS10061334.

Gonzalez-Meljem, J. M. et al. (2018) 'Paracrine roles of cellular senescence in promoting tumorigenesis', 118(10), pp. 1283–1288. Available at: https://pubmed.ncbi.nlm.nih.gov/29670296/ (Accessed: 20 November 2019).

Gray-Schopfer, V., Wellbrock, C. and Marais, R. (2007) 'Melanoma biology and new targeted therapy', Nature 2007 445:7130, 445(7130), pp. 851–857. doi: 10.1038/nature05661.

Guenther, L. M. et al. (2019) 'A combination CDK4/6 and IGF1R inhibitor strategy for Ewing sarcoma', Clinical Cancer Research, 25(4), pp. 1343–1357. doi: 10.1158/1078-0432.CCR-18-0372/72965/AM/A-COMBINATION-CDK4-6-AND-IGF1R-INHIBITOR-STRATEGY.

Hernandez-Segura, A., Nehme, J. and Demaria, M. (2018) 'Hallmarks of Cellular Senescence', Trends in Cell Biology, 28(6), pp. 436–453. doi: 10.1016/j.tcb.2018.02.001.

Hickson, L. T. J. et al. (2019) 'Senolytics decrease senescent cells in humans: Preliminary report from a clinical trial of Dasatinib plus Quercetin in individuals with diabetic kidney disease', EBioMedicine, 47, pp. 446–456. doi: 10.1016/J.EBIOM.2019.08.069.

Jeon, O. H. et al. (2017) 'Local clearance of senescent cells attenuates the development of post-traumatic osteoarthritis and creates a pro-regenerative environment', Nature Medicine, 23(6), pp. 775–781. doi: 10.1038/nm.4324.

Jimenez, R. et al. (2005) 'Replicative senescence in patients with chronic kidney failure', Kidney International, 68, pp. S11–S15. doi: 10.1111/j.1523-1755.2005.09903.x.

Jugdaohsingh, R. (2007) 'Silicon and bone health', in Journal of Nutrition, Health and Aging. Europe PMC Funders, pp. 99–110.

Justice, J. N. et al. (2019) 'Senolytics in idiopathic pulmonary fibrosis: Results from a first-in-human, open-label, pilot study', EBioMedicine, 40, pp. 554–563. doi: 10.1016/J.EBIOM.2018.12.052.

Kaefer, A. et al. (2014) 'Mechanism-based pharmacokinetic/pharmacodynamic meta-analysis of navitoclax (ABT-263) induced thrombocytopenia', Cancer chemotherapy and pharmacology, 74(3), pp. 593–602. doi: 10.1007/S00280-014-2530-9.

Kang, H. T. et al. (2017) 'Chemical screening identifies ATM as a target for alleviating senescence', Nature Chemical Biology, 13(6), pp. 616–623. doi: 10.1038/nchembio.2342.

Khosla, S., Farr, J. N. and Kirkland, J. L. (2018) 'Inhibiting Cellular Senescence: A New Therapeutic Paradigm for Age-Related Osteoporosis', The Journal of Clinical Endocrinology & Metabolism, 103(4), pp. 1282–1290. doi: 10.1210/jc.2017-02694.

Kim, H.-N. N. et al. (2017) 'DNA damage and senescence in osteoprogenitors expressing Osx1 may cause their decrease with age', Aging Cell, 16(4), pp. 693–703. doi: 10.1111/acel.12597.

Kirkland, J. L. et al. (2017) 'The Clinical Potential of Senolytic Drugs', Journal of the American Geriatrics Society, 65(10), pp. 2297–2301. doi: 10.1111/jgs.14969.

Kirkland, J. L. and Tchkonia, T. (2020) 'Senolytic drugs: from discovery to translation', Journal of Internal Medicine, 288(5), pp. 518–536. doi: 10.1111/joim.13141.

Kozar, I. et al. (2019) 'Many ways to resistance: How melanoma cells evade targeted therapies', Biochimica et Biophysica Acta (BBA) - Reviews on Cancer, 1871(2), pp. 313–322. doi: 10.1016/J.BBCAN.2019.02.002.

Kwapisz, D. (2017) 'Cyclin-dependent kinase 4/6 inhibitors in breast cancer: palbociclib, ribociclib, and abemaciclib.', Breast cancer research and treatment, 166(1), pp.

41–54. doi: 10.1007/s10549-017-4385-3.
Levitin, F. et al. (2005) 'The MUC1 SEA module is a self-cleaving domain', Journal of Biological Chemistry, 280(39), pp. 33374–33386. doi: 10.1074/jbc.M506047200.
Liao, C., Xiao, Y. and Liu, L. (2020) 'The dynamic process and its dual effects on tumors of therapy-induced senescence', Cancer Management and Research, 12, pp. 13553–13566. doi: 10.2147/CMAR.S285083.
Liu, R. et al. (2017) 'Tumor-targeting peptides from combinatorial libraries', Advanced Drug Delivery Reviews. Elsevier B.V., pp. 13–37. doi: 10.1016/j.addr.2016.05.009.
Lozano-Torres, B. et al. (2017) 'An OFF–ON Two-Photon Fluorescent Probe for Tracking Cell Senescence in Vivo', Journal of the American Chemical Society, 139(26), pp. 8808–8811. doi: 10.1021/jacs.7b04985.
Lozano-Torres, B. et al. (2019) 'The chemistry of senescence', Nature Reviews Chemistry, 3(7), pp. 426–441. doi: 10.1038/s41570-019-0108-0.
Lozano-Torres, B., Blandez, J. F., Galiana, I., et al. (2021) 'A Two-Photon Probe Based on Naphthalimide-Styrene Fluorophore for the In Vivo Tracking of Cellular Senescence', Analytical chemistry, 93(5), pp. 3052–3060. doi: 10.1021/ACS.ANALCHEM.0C05447.
Lozano-Torres, B., Blandez, J. F., Sancenón, F., et al. (2021) 'Chromo-fluorogenic probes for β-galactosidase detection', Analytical and bioanalytical chemistry, 413(9), pp. 2361–2388. doi: 10.1007/S00216-020-03111-8.
Lozano-Torres, B. et al. (2022) 'Lipofuscin labelling through biorthogonal strain-promoted azide-alkyne cycloaddition for the detection of senescent cells', The FEBS journal. doi: 10.1111/FEBS.16477.
Mao, L. et al. (2021) 'Palbociclib in advanced acral melanoma with genetic aberrations in the cyclin-dependent kinase 4 pathway', European journal of cancer (Oxford, England : 1990), 148, pp. 297–306. doi: 10.1016/J.EJCA.2021.02.021.
Mattia, G. et al. (2018) 'Cell death-based treatments of melanoma:conventional treatments and new therapeutic strategies', Cell Death & Disease 2018 9:2, 9(2), pp. 1–14. doi: 10.1038/s41419-017-0059-7.
McHugh, D. and Gil, J. (2018) 'Senescence and aging: Causes, consequences, and therapeutic avenues', Journal of Cell Biology, 217(1), pp. 65–77. doi: 10.1083/JCB.201708092.
Milanovic, M. et al. (2018) 'Senescence-associated reprogramming promotes cancer stemness', Nature, 553(7686), pp. 96–100. doi: 10.1038/nature25167.
Morsli, S., Doherty, G. J. and Muñoz-Espín, D. (2022) 'Activatable senoprobes and senolytics: Novel strategies to detect and target senescent cells', Mechanisms of Ageing and Development, 202(October 2021), p. 111618. doi: 10.1016/j.mad.2021.111618.
Muñoz-Espín, D. and Serrano, M. (2014) 'Cellular senescence: From physiology to pathology', Nature Reviews Molecular Cell Biology, 15(7), pp. 482–496. doi: 10.1038/nrm3823.
Muñoz-Espín, D. et al. (2018) 'A versatile drug delivery system targeting senescent cells',

EMBO Molecular Medicine, 10(9). doi: 10.15252/emmm.201809355.
Muttenthaler, M. et al. (2021) 'Trends in peptide drug discovery', Nature Reviews Drug Discovery 2021 20:4, 20(4), pp. 309–325. doi: 10.1038/s41573-020-00135-8.
Ohanna, M. et al. (2011) 'Senescent cells develop a PARP-1 and nuclear factor-{kappa}B-associated secretome (PNAS)', Genes & development, 25(12), pp. 1245–1261. doi: 10.1101/GAD.625811.
Overbeeke, R. et al. (1999) 'Sequential occurrence of mitochondrial and plasma membrane alterations, fluctuations in cellular Ca2+ and pH during initial and later phases of cell death', Apoptosis : an international journal on programmed cell death, 4(6), pp. 455–460. doi: 10.1023/A:1009604510329.
Park, S. S. et al. (2021) 'Senescent tumor cells: an overlooked adversary in the battle against cancer', Experimental & Molecular Medicine 2021 53:12, 53(12), pp. 1834–1841. doi: 10.1038/s12276-021-00717-5.
Pernas, S. et al. (2018) 'CDK4/6 inhibition in breast cancer: current practice and future directions', Therapeutic Advances in Medical Oncology. SAGE Publications Inc. doi: 10.1177/1758835918786451.
Rao, S. G. and Jackson, J. G. (2016) 'SASP: Tumor Suppressor or Promoter? Yes!', Trends in cancer, 2(11), pp. 676–687. doi: 10.1016/j.trecan.2016.10.001.
Ruscetti, M. et al. (2020) 'Senescence-Induced Vascular Remodeling Creates Therapeutic Vulnerabilities in Pancreas Cancer', Cell, 181(2), pp. 424-441.e21. doi: 10.1016/j.cell.2020.03.008.
Sager, R. (1991) 'Senescence as a mode of tumor suppression.', Environmental Health Perspectives, 93, p. 59. doi: 10.1289/EHP.919359.
Saleh, T. et al. (2018) 'Non-Cell Autonomous Effects of the Senescence-Associated Secretory Phenotype in Cancer Therapy', Frontiers in Oncology, 0(MAY), p. 164. doi: 10.3389/FONC.2018.00164.
Schafer, M. J. et al. (2017) 'Cellular senescence mediates fibrotic pulmonary disease', Nature Communications, 8. doi: 10.1038/ncomms14532.
Sharma, A. K. et al. (2020) 'The Senolytic Drug Navitoclax (ABT-263) Causes Trabecular Bone Loss and Impaired Osteoprogenitor Function in Aged Mice', Frontiers in Cell and Developmental Biology, 8, p. 354. doi: 10.3389/FCELL.2020.00354.
Short, S. et al. (2019) 'Senolytics and senostatics as adjuvant tumor therapy', eBioMedicine, 41, pp. 683–692. doi: 10.1016/J.EBIOM.2019.01.056.
Sieben, C. J. et al. (2018) 'Two-Step Senescence-Focused Cancer Therapies', Trends in Cell Biology, xx(9), pp. 1–15. doi: 10.1016/j.tcb.2018.04.006.
Sun, R. et al. (2017) 'Senescence as a novel mechanism involved in β-adrenergic receptor mediated cardiac hypertrophy', PLOS ONE. Edited by S. Gupta, 12(8), p. e0182668. doi: 10.1371/journal.pone.0182668.
Triana-Martínez, F. et al. (2019) 'Identification and characterization of Cardiac Glycosides as senolytic compounds', Nature Communications, 10(1), pp. 1–12. doi: 10.1038/s41467-019-12888-x.
Tubita, A. et al. (2022) 'Inhibition of ERK5 Elicits Cellular Senescence in Melanoma via the Cyclin-Dependent Kinase Inhibitor p21', Cancer Research, 82(3), pp. 447–457. doi:

10.1158/0008-5472.CAN-21-0993/674088/AM/INHIBITION-OF-ERK5-ELICITS-CELLULAR-SENESCENCE-IN.

Verdoorn, B. P. et al. (2021) 'Fisetin for COVID-19 in skilled nursing facilities: Senolytic trials in the COVID era', Journal of the American Geriatrics Society, 69(11), pp. 3023–3033. doi: 10.1111/JGS.17416.

Walker, A. J. et al. (2016) 'FDA Approval of Palbociclib in Combination with Fulvestrant for the Treatment of Hormone Receptor-Positive, HER2-Negative Metastatic Breast Cancer', Clinical Cancer Research, 22(20), pp. 4968–4972. doi: 10.1158/1078-0432.CCR-16-0493.

Wandrer, F. et al. (2018) 'Senescence mirrors the extent of liver fibrosis in chronic hepatitis C virus infection', Alimentary Pharmacology & Therapeutics, 48(3), pp. 270–280. doi: 10.1111/apt.14802.

Wang, L., Lankhorst, L. and Bernards, R. (2022) 'Exploiting senescence for the treatment of cancer', Nature Reviews Cancer 2022, pp. 1–16. doi: 10.1038/s41568-022-00450-9.

Webster, A. C. et al. (2006) 'Target of Rapamycin Inhibitors (Sirolimus and Everolimus) for Primary Immunosuppression of Kidney Transplant Recipients: A Systematic Review and Meta-Analysis of Randomized Trials', Transplantation, 81(9), pp. 1234–1248. doi: 10.1097/01.tp.0000219703.39149.85.

Whittaker, S. R. et al. (2017) 'Inhibitors of cyclin-dependent kinases as cancer therapeutics', Pharmacology & Therapeutics, 173, pp. 83–105. doi: 10.1016/j.pharmthera.2017.02.008.

Wilson, W. H. et al. (2010) 'Navitoclax, a targeted high-affinity inhibitor of BCL-2, in lymphoid malignancies: a phase 1 dose-escalation study of safety, pharmacokinetics, pharmacodynamics, and antitumor activity', The Lancet. Oncology, 11(12), pp. 1149–1159. doi: 10.1016/S1470-2045(10)70261-8.

Xu, M. et al. (2018) 'Senolytics Improve Physical Function and Increase Lifespan in Old Age', Nature medicine, 24(8), p. 1246. doi: 10.1038/S41591-018-0092-9.

Yang, H. and Fogo, A. B. (2010) 'Cell Senescence in the Aging Kidney', Journal of the American Society of Nephrology, 21(9), pp. 1436–1439. doi: 10.1681/ASN.2010020205.

Yosef, R. et al. (2016) 'Directed elimination of senescent cells by inhibition of BCL-W and BCL-XL', Nature Communications, 7, pp. 1–11. doi: 10.1038/ncomms11190.

Yousefzadeh, M. J. et al. (2018a) 'Fisetin is a senotherapeutic that extends health and lifespan', EBioMedicine, 36, pp. 18–28. doi: 10.1016/J.EBIOM.2018.09.015.

Yousefzadeh, M. J. et al. (2018b) 'Fisetin is a senotherapeutic that extends health and lifespan', EBioMedicine, 36, pp. 18–28. doi: 10.1016/j.ebiom.2018.09.015.

Zamzami, N. et al. (1995) 'Reduction in mitochondrial potential constitutes an early irreversible step of programmed lymphocyte death in vivo', The Journal of Experimental Medicine, 181(5), p. 1661. doi: 10.1084/JEM.181.5.1661.

Zhang, X. X. et al. (2018) 'Oxidation resistance 1 is a novel senolytic target', Aging Cell, p. e12780. doi: 10.1111/acel.12780.

Zhu, Y. et al. (2015) 'The Achilles' heel of senescent cells: from transcriptome to senolytic drugs', Aging cell, 14(4), pp. 644–658. doi: 10.1111/acel.12344.
Zhu, Y. et al. (2016) 'Identification of a novel senolytic agent, navitoclax, targeting the Bcl-2 family of anti-apoptotic factors', Aging Cell, 15(3), pp. 428–435. doi: 10.1111/acel.12445.
Zhu, Y. et al. (2017) 'New agents that target senescent cells: The flavone, fisetin, and the BCL-XL inhibitors, A1331852 and A1155463', Aging, 9(3), pp. 1–9. doi: 10.18632/aging.101202.

7. Supporting Information

7.1. Hexapeptide screening

For deconvolute the library, positional tracking format was used (Pinilla C, Appel JR, Blanc P 1992). After evaluation of the biological activity for each sub- library, the active mixtures were selected from the deconvolution process, and the synthesis of the defined compounds was carried out. These defined hexapeptides were studied to confirm the results of the library deconvolution and thus the most active peptides were identified.

As explained graphically in Figure S1, this library consists of a series of mixtures composed of hexapeptides with a defined position (P_n) for a selected aminoacid and in the rest of positions equimolar mixtures of all amino acids (X). The library is therefore composed of 6 sub-libraries, each of them composed of 20 mixtures with only one defined position (P_n). The total number of peptides in the library is 20^6 compounds, distributed in 120 mixtures. Thus, for example, the sub-library corresponding to "position 1" (represented in blue in Figure S1) is made up of twenty mixtures of different hexapeptides, in each of which the amino acid that occupies the first place is known - 20 possible amino acids.

To perform the screening, control and senescent melanoma SK-Mel-103 cells were treated with the different peptide mixtures at three different concentrations (500, 600, and 700 μM) to maximize the detection of differences in viability between control cells and senescent cells (Figure S2, Supporting Information). Each graph represents the set of

the 20 hexapeptide mixtures in each of the 6 positions defined in the library. Thus, combining the three viability results for each hexapeptide mix, we can select the best senolytic activity depending on the position of the amino acid. Before proceeding with the selection, all the viability data obtained for each mixture were normalized, by calculating, the difference between the viability percentages obtained for control and senescent cells. The amino acid selection criteria for each position were based on: (1) defined position of the amino acids that caused higher senescent death compared to control cells, (2) the reproducibility of inter-assay results, and (3) that the sum of the viability differences between control cells and senescent cells at the different concentrations was greater than or equal to 0.5. An example of this analysis performed for the P_n position defined by a cysteine (Cys) is shown in Table S1.

7.2. References

Pinilla C, Appel JR, Blanc P, H. R. (1992). Rapid identification of high affinity peptide ligands using positional scanning synthetic peptide combinatorial libraries. *BioTechniques*, *13*(6), 901-905.

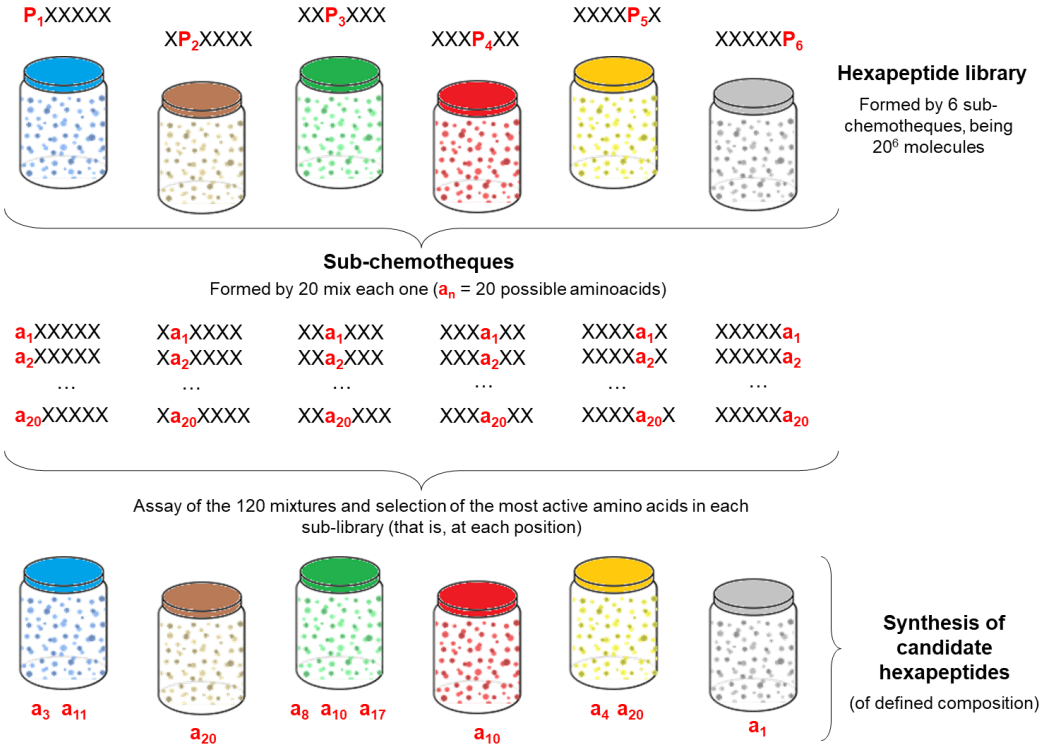

Figure S1 | Scheme of the deconvolution process of a D-amino acid hexapeptide library using positional screening methodology. The hexapeptide library was formed by 6 sub-libraries with hexapeptides with a defined amino acid position (Pn) being an any of the 20 possible amino acids.

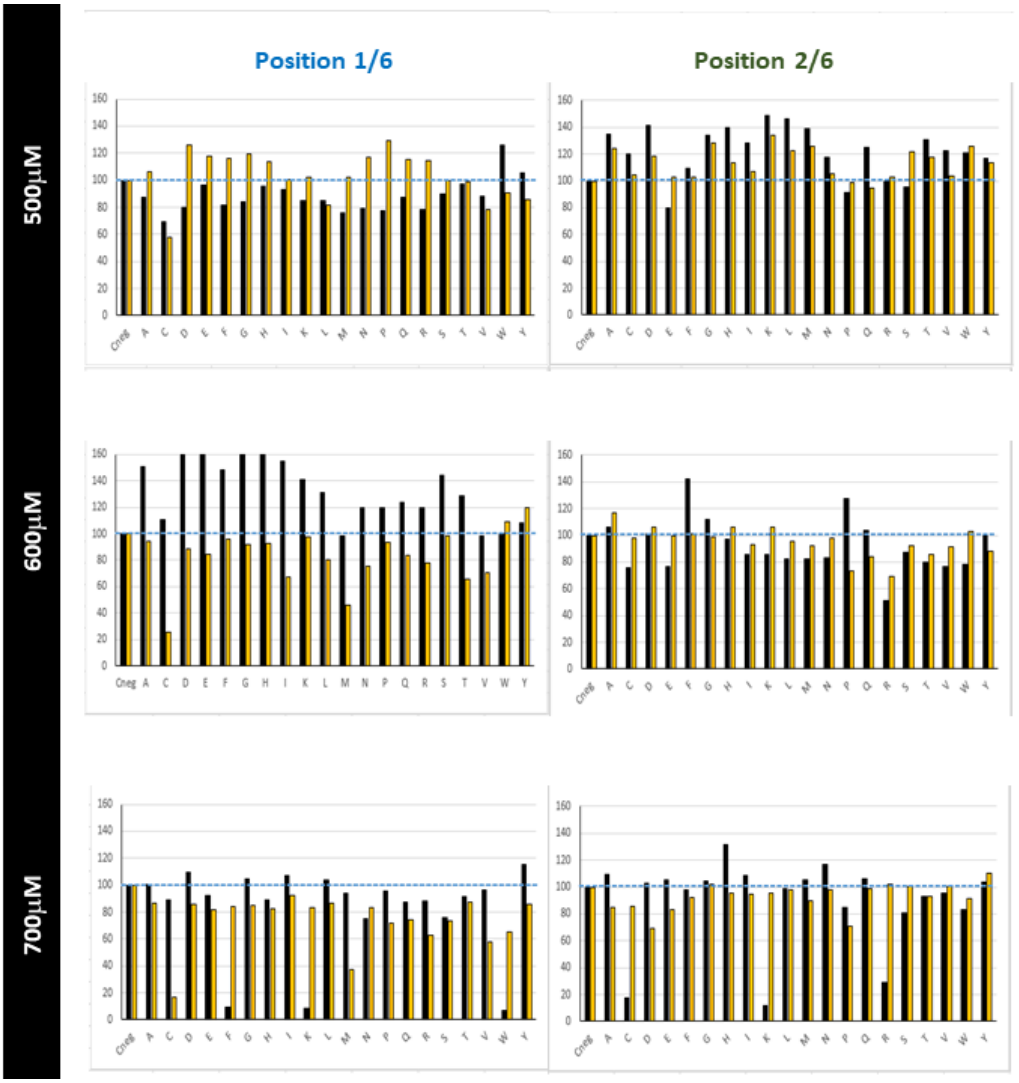
500µM
600µM
700µM
Position 1/6
Position 2/6

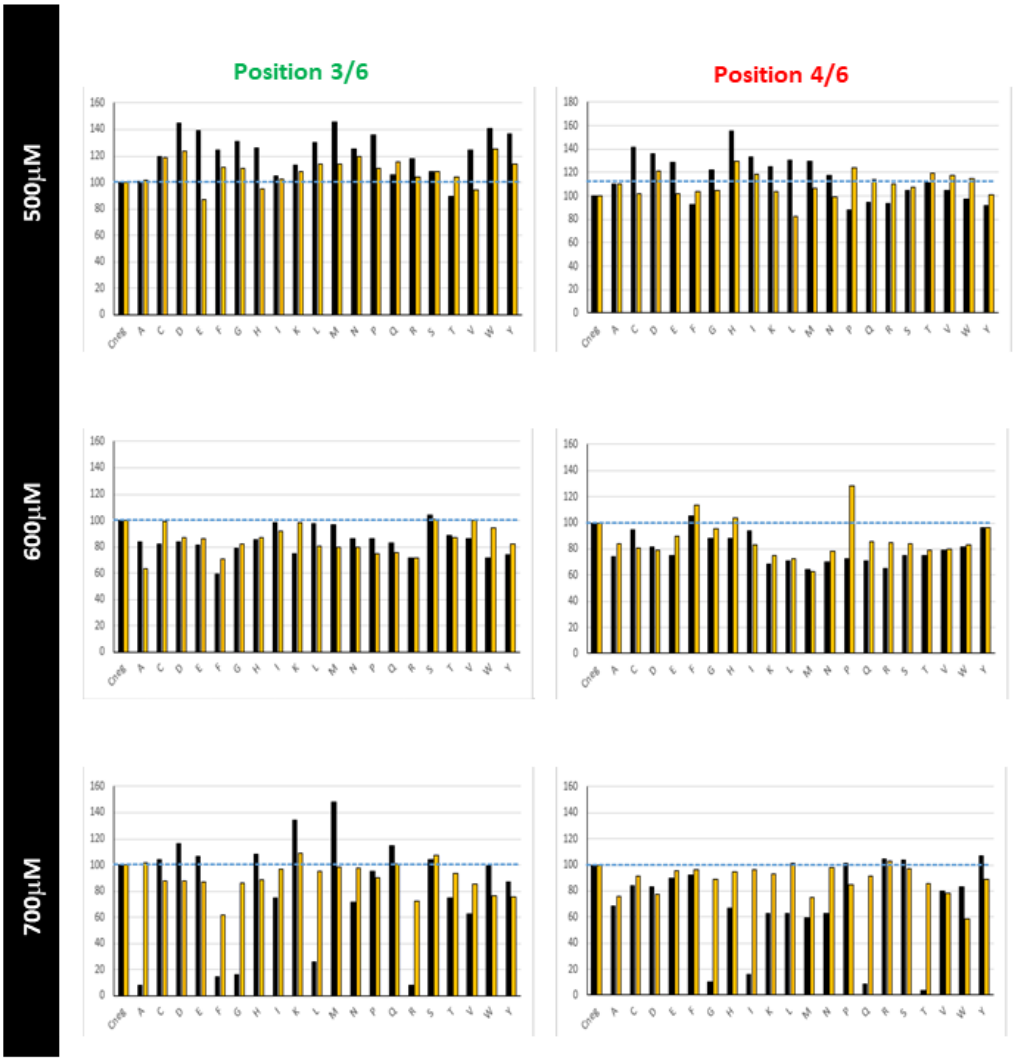
Position 3/6
Position 4/6
500µM
600µM
700µM

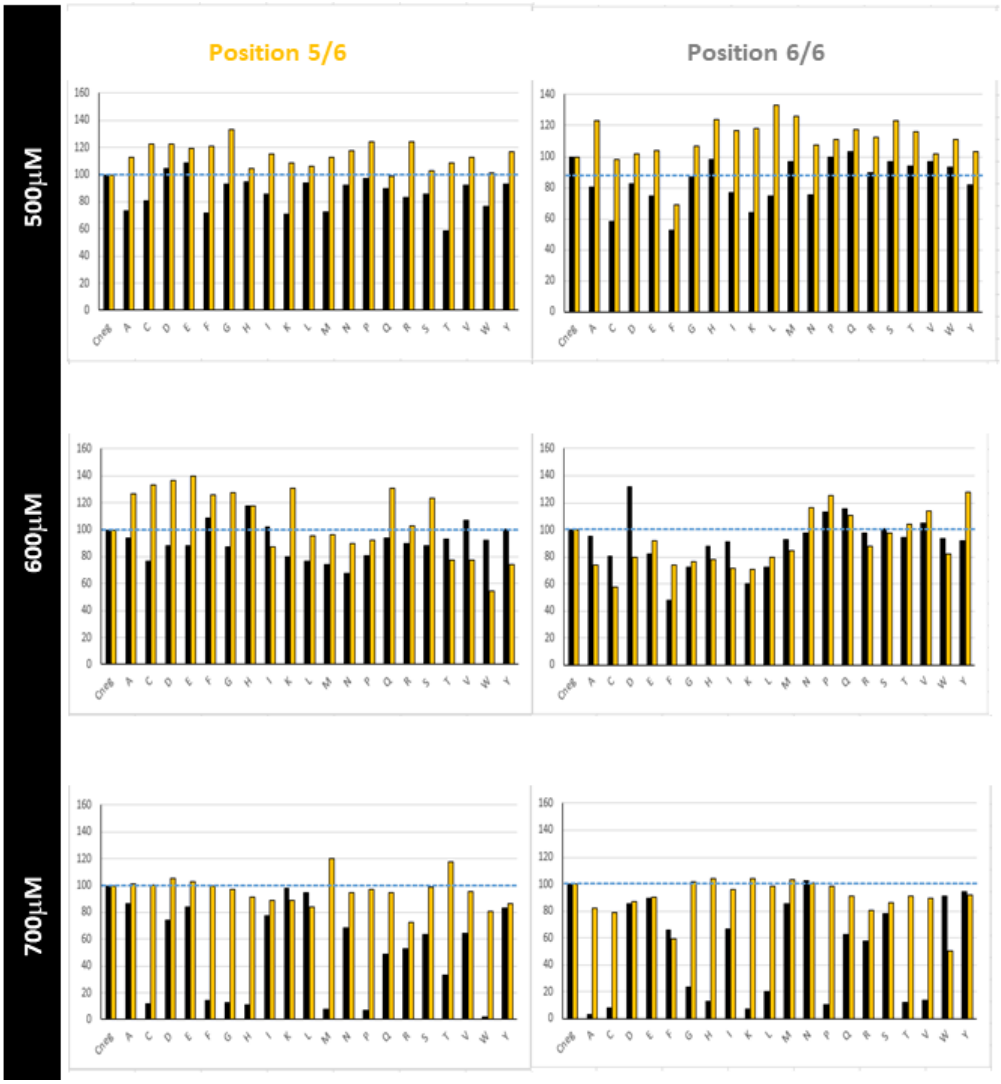

Figure S2 | Cell viability graphs obtained for control cells (black bar) and senescent cells (yellow bar) treated with three different concentrations of the hexapeptide library (500, 600, 700 µM). Each graph corresponds to the 20 peptide mixtures available for each position, the X axis representing the amino acid defined in each of these mixtures.

Table S1 | Example of the selection criteria applied in the choice of candidate amino acids for each position of the hexapeptide.

	Viability data			Viability data			Viability data			
Pn	**Control 500µM**	**Palbo 500µM**	**(C-S)**	**Control 600µM**	**Palbo 600µM**	**(C-S)**	**Control 700µM**	**Palbo 700µM**	**(C-S)**	**Σ**
Cys	1.22	0.99	**0.3**	1.19	0.92	**0.3**	1.25	1.03	**0.2**	0.8

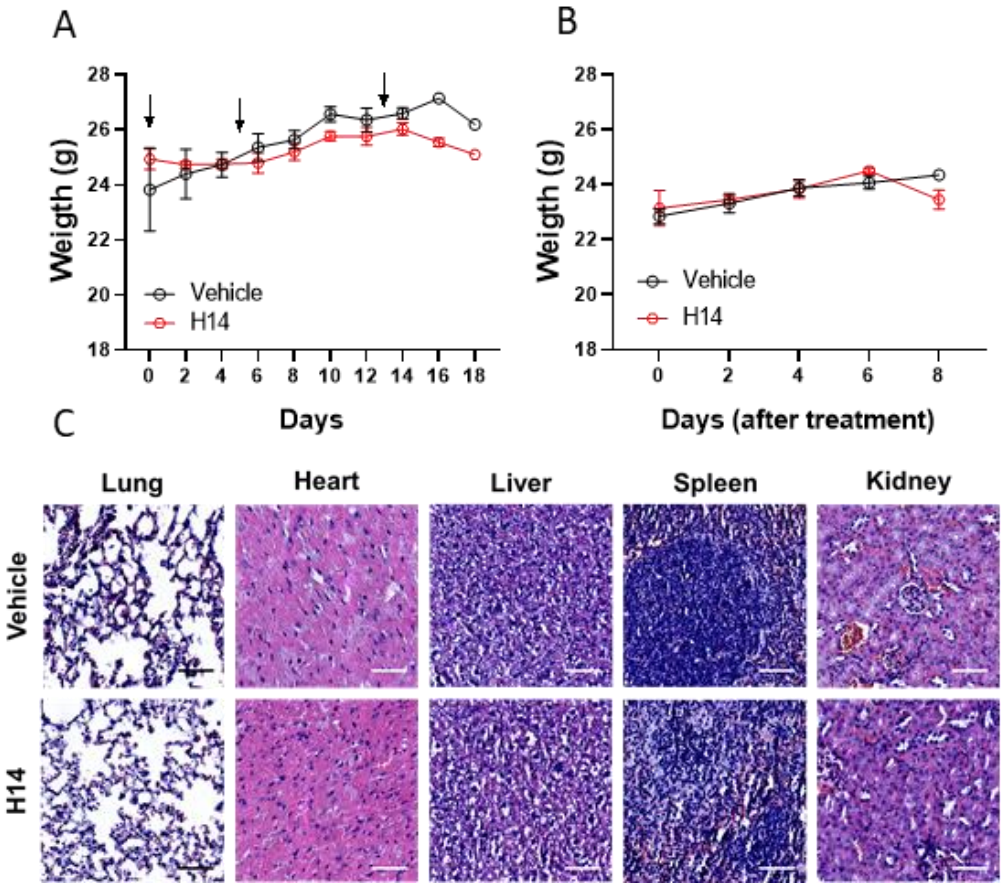

Figure S3 | Weight changes (g) in H14 toxicity assays of point treatments (A) and daily treatments for a week (B). Data represents means ± SEM. (C) H/E staining of main organs after being treated daily with H14 for a week. Scale Bar, 100 µm.

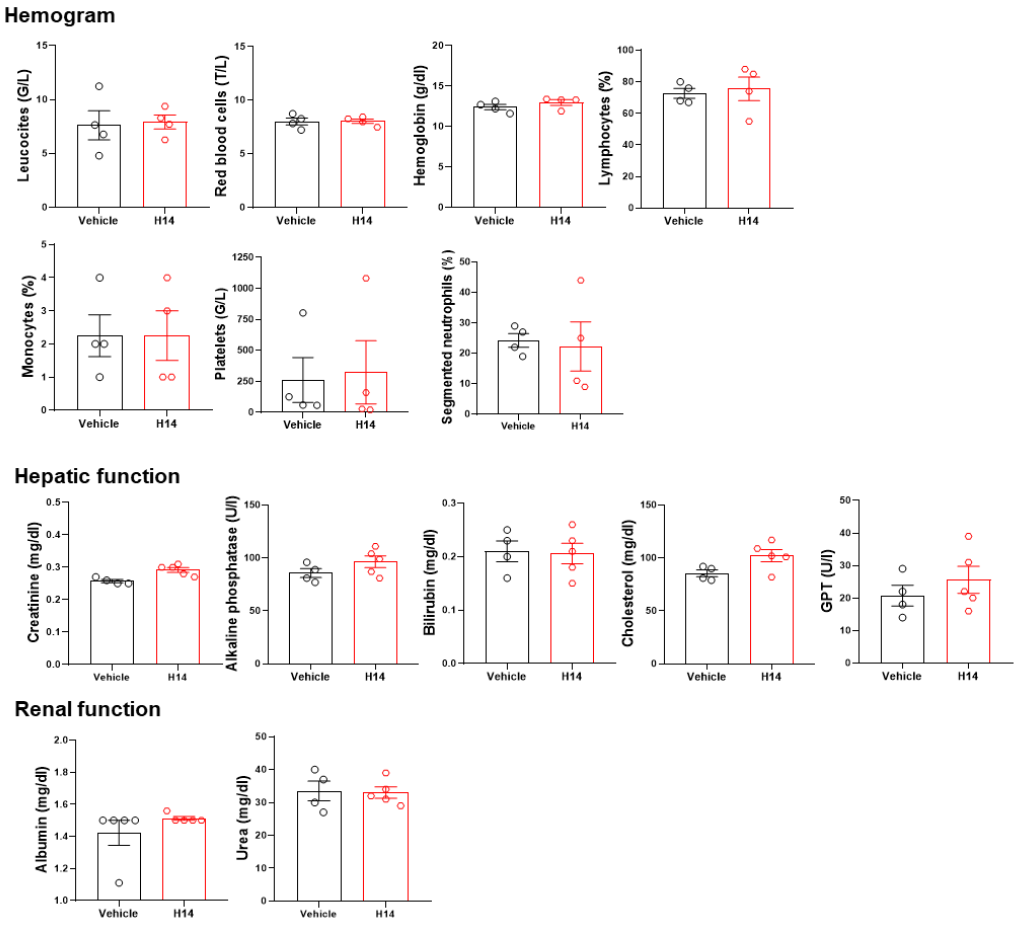

Figure S4 | Hemogram and biochemistry blood analyses of healthy mice treated daily with H14 for a week. Data represents means ± SEM.

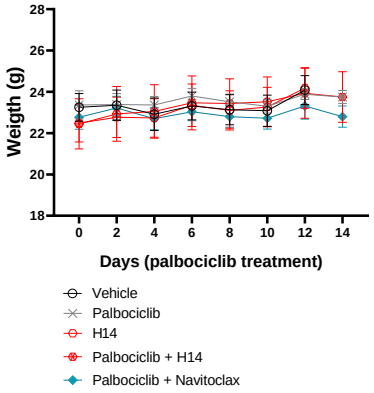

Figure S5 | Weight changes (g) of SK-Mel-103 xenografts after the different treatments. Data represents means ± SEM.

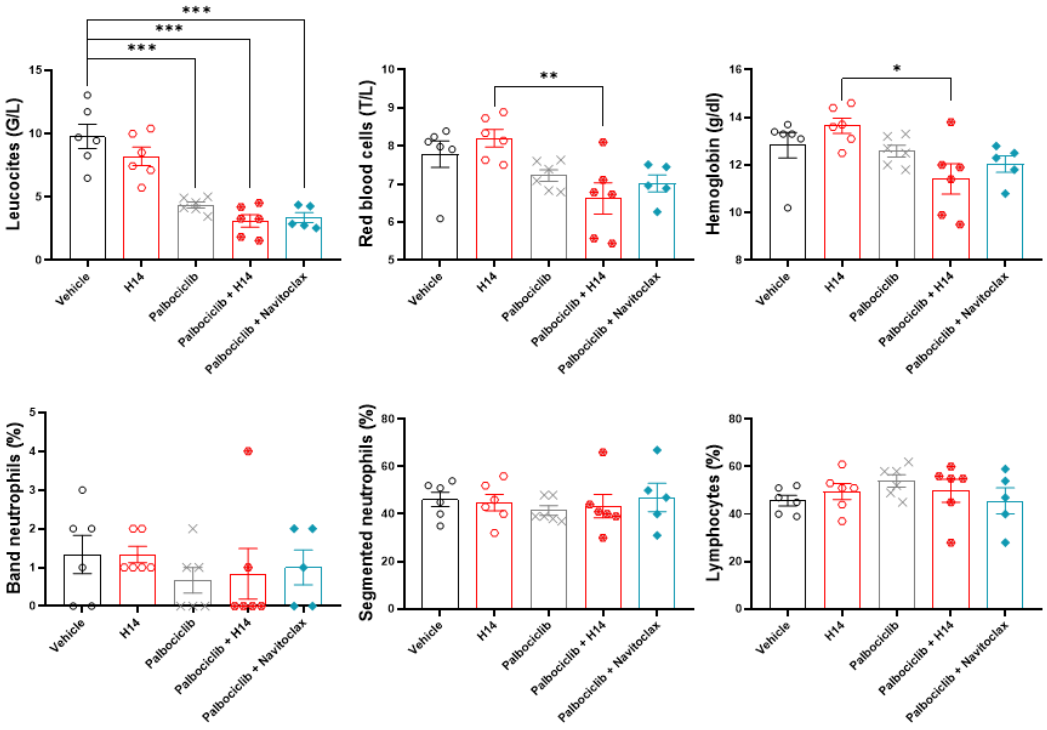

Figure S6 | Hemogram of SK-Mel-103 xenografts after the different treatments. Data represents means ± SEM.

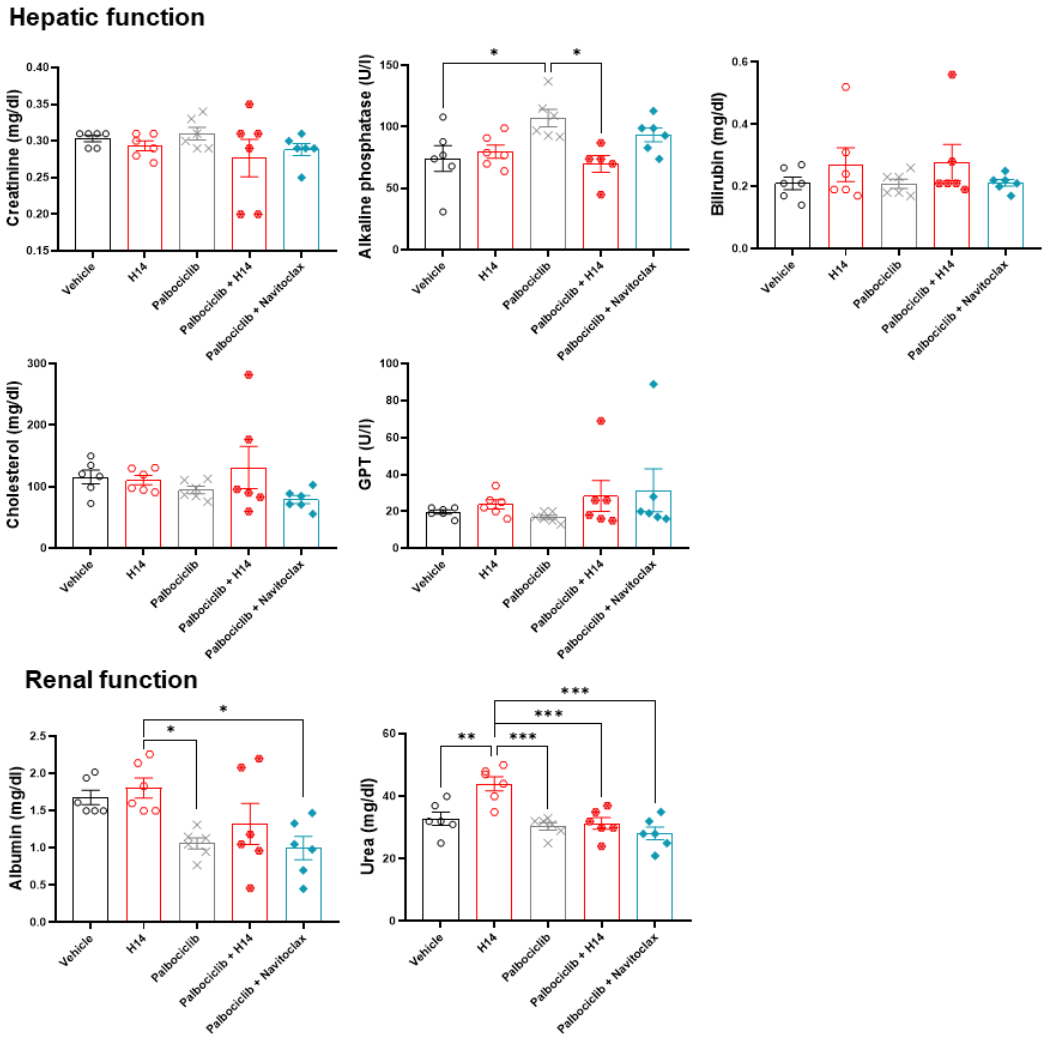

Figure S7 | Biochemistry blood analysis of SK-Mel-103 xenografts after the different treatments. Data represents means ± SEM.

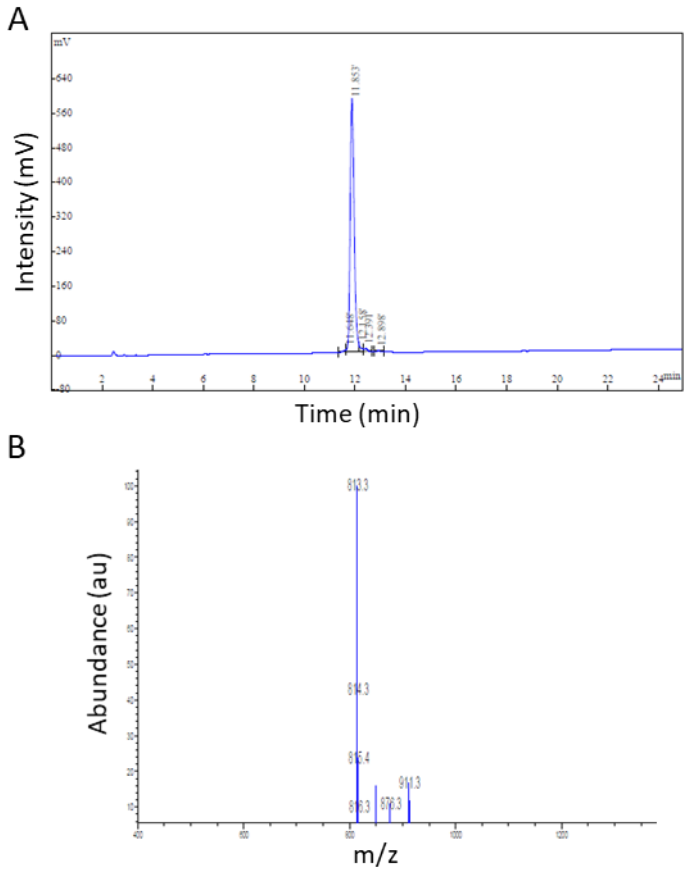

Figure S8 | (A) HPLC chromatogram of H14. (B) Mass spectrum for H14 showing the 813.3 m/z value.

Future perspectives and conclusions

This PhD thesis has explored senescence-induction as a therapeutic option in cancer treatment through the design, synthesis, and preclinical evaluation of several nanodevices and prodrugs and the identification of a novel senolytic.

Regarding the first objective of this thesis, in the third chapter, we have demonstrated that systemic treatment with palbociclib in an orthotopic triple-negative breast cancer (TNBC) mouse model induces senescence in vascular endothelial cells, generating an unpaired endothelium that favors breast cancer cell migration. A one-two punch strategy that combines palbociclib pro-senescence therapy followed by nanotherapy-targeted navitoclax senolysis selectively eliminates vascular endothelial senescent cells and induces a marked recovery of endothelial tissue functionality, recovering the ability to form capillary-like structures. Nanotherapy-targeted senolysis was performed using a nanodevice based on MSNs loaded with navitoclax and functionalized with a hexa-galacto-oligosaccharide (galactan). Cargo release from NP(nav)-Gal was achieved through the high lysosomal β-galactosidase activity enzyme presented in senescent cells, which induced the hydrolysis of the capping linker with subsequent pore opening and navitoclax delivery. Importantly, subsequent treatment with palbociclib and the targeted senolytic agent NP(nav)-Gal reduces senescence in veins *in vivo,* which is consistent with the decrease in metastatic lung burden observed. Moreover, we have demonstrated that palbociclib treatment increases lung metastasis after tail vein injection of triple-negative breast cancer cells in healthy mice. Overall, in this chapter, we provided evidence of the effects that chemotherapy-induced senescence has on vascular endothelial cells and the potential to reduce vascular senescence using senolytic therapies as a strategy to limit metastatic dissemination of tumor cells in breast cancer patients subjected to chemotherapeutic treatments.

In the fourth chapter, a one-two punch strategy combining senescence induction and the subsequent elimination of senescent cells (senolysis) was developed as an alternative approach to improve outcomes in triple-negative breast cancer patients. We

demonstrate that palbociclib therapy-induced senescence (TIS) followed by adjuvant therapy with navitoclax causes a synergistic elimination of senescent cells and reduction of tumor growth and lung metastasis in a xenograft mice model of aggressive human TNBC (hTNBC). Considering the off-target effects and toxicity derived from navitoclax, we proposed a targeted strategy to minimize thrombocytopenia-associated navitoclax side effects. We used a galactose-conjugated navitoclax (nav-Gal) as a senolytic prodrug that can be preferentially activated by lysosomal β-galactosidase overexpressed in senescent cells. Concomitant treatment with palbociclib and nav-Gal *in vivo* results in the eradication of senescent hTNBC cells with the subsequent reduction of tumor growth while decreasing the cytotoxicity of navitoclax. Collectively, our findings support the effectiveness of this two-step approach. Combined senescence-inducing with senolytic therapy can be a promising strategy for the effective treatment of hTNBC. In light of the encouraging results, we conclude that targeted navitoclax therapies could facilitate its clinical use as an effective and safer therapeutic opportunity.

Attending to the third objective of this work, engineering a novel nanoparticle communication system by stigmergy to enhance tumor therapy using targeted pro-senescent and senolytic therapies, two nanocarriers consisting of gated MSNs were prepared in the fifth chapter. The first nanodevice (NP(palbo)PEG-MUC1) was loaded with palbociclib and functionalized, though disulfide bonds, with a poly (ethylene glycol) that binds an aptamer cap that targets the MUC1 surface protein, overexpressed in breast tumor cells. The second nanodevice was the senolytic NP(nav)-Gal already described in chapter 1. For the pro-senescence NP(palbo)PEG-MUC1 nanodevice, the cargo was only released in the presence of glutathione, which can reduce the disulfide bond that linked the poly(ethylene glycol) to the nanoparticle surface. Our studies demonstrate the preferential accumulation of the nanodevices in the targeted cells *in vitro* and *in vivo*. NP(palbo)PEG-MUC1 showed a great therapeutic effect in the induction of senescence in the triple-negative breast cancer xenografts. A synergistic effect was achieved when both sets of nanoparticles were sequentially administered, delaying tumor growth and

reducing metastases in the TNBC mice model. As far as we know, this is the first work that presents a sustained administration of two nanoparticles *in vivo,* combining the novel pro-senescent and senolytic strategy for cancer treatment. Collectively, these results supported the effectiveness of the proposed communication strategy, confirming the principle that communication could amplify drug delivery in tumors and thus enhance therapy. The conceptual idea of nanoparticle communication opens the opportunity to develop multifunctional systems loaded with different drug combinations, aimed to provide more therapeutic options to solve the needs of the patients.

The last objective of this thesis was accomplished in the sixth chapter. We aimed to identify novel senolytic agents with optimal *in vivo* efficacy and safety to target malignant melanoma senescent cells. We report the identification of two hexapeptides (H8 and H14) with specific senolytic activity for senescent SK-Mel-103 melanoma cells but with limited cytotoxicity to proliferating cells. A one-two punch strategy of palbociclib-senescence induction plus H14-senolysis achieves a better reduction of tumor growth than monotherapy. We compare the senolytic activity of H14 with the well-known senolytic navitoclax. Our study has identified new hexapeptides with promising senolytic activities that could eventually allow the elimination of senescent cells in melanoma patients who have undergone senescence inducing chemotherapy treatments, thus overcoming the long-term adverse effects caused by the accumulation of senescent cancer cells. Next steps in this project will include the identification of the molecular target of H14 in senescent cells.

Developing nanomaterials and prodrugs to eliminate senescent cells *in vivo* could be a promising approach in cancer treatment and helpful in the treatment of cancer and other age-related diseases. Since these systems are still in the early stages of their biomedicine application, some challenges need to be addressed.

One main challenge that senescence research still needs to overcome is understanding the role of systemic induction of senescence when treating tumors. The

heterogeneity of tumors may limit the effectiveness of senescence induction, which may even cause tumor relapses due to the variable tumor responses to drug treatment. It will be crucial to better understand the synergy between pro-senescence therapy and senotherapies. It may be possible that not all pro-senescence therapies and not all cancer types will benefit from a one-two punch combination with senotherapies. Also, it will be important to understand how the SASP produced by senescent cancer cells impacts the interaction between senescent cancer cells and the immune system.

Another challenge is the search for gold standard biomarkers for the senescent state. No single marker can clearly discriminate between senescence and other growth-arrested states. Clinical translation will be facilitated by a deeper understanding of human senescence, including identifying novel biomarkers on the surfaceome, secretome, metabolome, and intracellular signaling pathways. Recent advances have already allowed the development of dyes and fluorescent nanodevices as well as multi-gene signatures or cytokine panels to detect senescent cells *in vivo*. Non-invasive imaging methods would be optimal to measure tumor senescence induction in patients during treatment.

A further issue that needs to be solved is the lack of either a specific or universal senolytic drug. The most commonly used senolytic has highly variable activity as senolytic. Thus, on the one hand, the field needs a broad spectrum senolytic. But there is also a need for specific senolytics to exploit the vulnerabilities of senescent cancer cells without affecting the tissue microenvironment. Besides, the field demands a better understanding of the clinical contexts in which senotherapeutic tools may be useful.

It is also worth highlighting that the commonly used senolytics have well-known side-effects (e.g., thrombocytopenia in the case of navitoclax). In this scenario, nanotechnology presents a powerful strategy to overcome many of the limitations of such therapies, due to their capability to specifically release the drugs in the targeted site, increasing the therapeutic effect while diminishing side effects.

Nanoparticles and prodrugs have shown efficacy as senotherapy in preclinical models. However, it is important to fully evaluate their potential effects on the organisms and their benefit-to-risk ratio. We still have a long way before nanoparticles are fully incorporated into clinical routines. Future efforts should be directed towards a better understanding of their biodistribution, pharmacokinetics, persistence, and clearance in living organisms for a successful clinic translation.

Future breakthroughs in the field of cellular senescence treatment are expected. We hope that the results achieved in this PhD thesis will open new research opportunities and inspire the development of advanced strategies with smart nanodevices and prodrugs for their application in the field of cellular senescence or in other biomedical areas such as sensing, and communication technologies to solve patient needs.

References

Abuodeh, Y., Venkat, P. and Kim, S. (2016) 'Systematic review of case reports on the abscopal effect', Current problems in cancer, 40(1), pp. 25–37. doi: 10.1016/J.CURRPROBLCANCER.2015.10.001.

Acosta, J. C. et al. (2013) 'A complex secretory program orchestrated by the inflammasome controls paracrine senescence', Nature Cell Biology, 15(8), pp. 978–990. doi: 10.1038/ncb2784.

Adjei, I. M., Sharma, B. and Labhasetwar, V. (2014) 'Nanoparticles: cellular uptake and cytotoxicity', Advances in experimental medicine and biology, 811, pp. 74–91. doi: 10.1007/978-94-017-8739-0_5.

Agostini, A. et al. (2012) 'Targeted cargo delivery in senescent cells using capped mesoporous silica nanoparticles', Angewandte Chemie - International Edition, 51(42), pp. 10556–10560. doi: 10.1002/anie.201204663.

Al-Soudi, A., Kaaij, M. H. and Tas, S. W. (2017) 'Endothelial cells: From innocent bystanders to active participants in immune responses', Autoimmunity Reviews. Elsevier B.V., pp. 951–962. doi: 10.1016/j.autrev.2017.07.008.

Alessio, N. et al. (2021) 'Different Stages of Quiescence, Senescence, and Cell Stress Identified by Molecular Algorithm Based on the Expression of Ki67, RPS6, and Beta-Galactosidase Activity', International journal of molecular sciences, 22(6), pp. 1–13. doi: 10.3390/IJMS22063102.

Alimonti, A. et al. (2010) 'A novel type of cellular senescence that can be enhanced in mouse models and human tumor xenografts to suppress prostate tumorigenesis', The Journal of clinical investigation, 120(3), pp. 681–693. doi: 10.1172/JCI40535.

Althubiti, M. et al. (2014) 'Characterization of novel markers of senescence and their prognostic potential in cancer', Cell Death and Disease, 5(11), pp. e1528-10. doi: 10.1038/cddis.2014.489.

Anselmo, A. C. et al. (2021) 'Nanoparticles in the clinic: An update post COVID-19 vaccines', Bioengineering & Translational Medicine, 6(3), p. e10246. doi: 10.1002/BTM2.10246.

Asghar, U. et al. (2015) 'The history and future of targeting cyclin-dependent kinases in cancer therapy', Nature reviews. Drug discovery, 14(2), pp. 130–146. doi: 10.1038/NRD4504.

El Assar, M. et al. (2012) 'Mechanisms involved in the aging-induced vascular dysfunction', Frontiers in Physiology, 3 MAY. doi: 10.3389/fphys.2012.00132.

Aznar, E. et al. (2009) 'pH- and Photo-Switched Release of Guest Molecules from Mesoporous Silica Supports', Journal of the American Chemical Society, 131(19), pp. 6833–6843. doi: 10.1021/JA810011P.

Aznar, E. et al. (2016) 'Gated Materials for On-Command Release of Guest Molecules', Chemical Reviews, 116(2), pp. 561–718. doi: 10.1021/acs.chemrev.5b00456.

Baker, D. J. et al. (2011) 'Clearance of p16Ink4a-positive senescent cells delays ageing-associated disorders', Nature, 479(7372), pp. 232–236. doi: 10.1038/nature10600.

Baker, D. J. et al. (2016) 'Naturally occurring p16Ink4a-positive cells shorten healthy lifespan', Nature, 530(7589), pp. 184–189. doi: 10.1038/nature16932.

Baker, D. J. and Petersen, R. C. (2018) 'Cellular senescence in brain aging and

neurodegenerative diseases: evidence and perspectives', Journal of Clinical Investigation, 128(4), pp. 1208–1216. doi: 10.1172/JCI95145.

Barnes, P. J. (2015) 'Mechanisms of development of multimorbidity in the elderly', European Respiratory Journal, 45(3), pp. 790–806. doi: 10.1183/09031936.00229714.

Basisty, N. et al. (2020) 'A proteomic atlas of senescence-associated secretomes for aging biomarker development', PLoS biology, 18(1), p. e3000599. doi: 10.1371/JOURNAL.PBIO.3000599.

Baskar, R. et al. (2012) 'Cancer and radiation therapy: Current advances and future directions', International Journal of Medical Sciences, 9(3), pp. 193–199. doi: 10.7150/IJMS.3635.

Beaver, J. A. et al. (2015) 'FDA Approval: Palbociclib for the Treatment of Postmenopausal Patients with Estrogen Receptor-Positive, HER2-Negative Metastatic Breast Cancer.', Clinical cancer research : an official journal of the American Association for Cancer Research, 21(21), pp. 4760–6. doi: 10.1158/1078-0432.CCR-15-1185.

Bernardos, A. et al. (2008) 'Controlled release of vitamin B2 using mesoporous materials functionalized with amine-bearing gate-like scaffoldings', Journal of controlled release : official journal of the Controlled Release Society, 131(3), pp. 181–189. doi: 10.1016/J.JCONREL.2008.07.037.

Bernardos, A. et al. (2009) 'Enzyme-Responsive Controlled Release Using Mesoporous Silica Supports Capped with Lactose', Angewandte Chemie International Edition, 48(32), pp. 5884–5887. doi: 10.1002/anie.200900880.

Besancenot, R. et al. (2010) 'A Senescence-Like Cell-Cycle Arrest Occurs During Megakaryocytic Maturation: Implications for Physiological and Pathological Megakaryocytic Proliferation', PLOS Biology, 8(9), p. e1000476. doi: 10.1371/JOURNAL.PBIO.1000476.

De Biasi, S. et al. (2020) 'Marked T cell activation, senescence, exhaustion and skewing towards TH17 in patients with COVID-19 pneumonia', Nature Communications 2020 11:1, 11(1), pp. 1–17. doi: 10.1038/s41467-020-17292-4.

Bielak-Zmijewska, A., Mosieniak, G. and Sikora, E. (2018) 'Is DNA damage indispensable for stress-induced senescence?', Mechanisms of Ageing and Development, 170, pp. 13–21. doi: 10.1016/j.mad.2017.08.004.

Biran, A. et al. (2017) 'Quantitative identification of senescent cells in aging and disease', Aging Cell, 16(4), pp. 661–671. doi: 10.1111/acel.12592.

Birch, J. and Gil, J. (2020) 'Senescence and the SASP: Many therapeutic avenues', Genes and Development, 34(23–24), pp. 1565–1576. doi: 10.1101/gad.343129.120.

Bloom, J. and Cross, F. R. (2007) 'Multiple levels of cyclin specificity in cell-cycle control', Nature Reviews Molecular Cell Biology, 8(2), pp. 149–160. doi: 10.1038/nrm2105.

Bodnar, A. G. et al. (1998) 'Extension of life-span by introduction of telomerase into normal human cells.', Science (New York, N.Y.), 279(5349), pp. 349–52.

Braig, M. et al. (2005) 'Oncogene-induced senescence as an initial barrier in lymphoma development', Nature, 436(7051), pp. 660–665. doi: 10.1038/nature03841.

Braumüller, H. et al. (2013) 'T-helper-1-cell cytokines drive cancer into senescence',

Nature 2013 494:7437, 494(7437), pp. 361–365. doi: 10.1038/nature11824.

Bringas, E. et al. (2012) 'Triggered release in lipid bilayer-capped mesoporous silica nanoparticles containing SPION using an alternating magnetic field', Chemical Communications, 48(45), pp. 5647–5649. doi: 10.1039/C2CC31563G.

Burd, C. E. E. et al. (2013) 'Monitoring Tumorigenesis and Senescence In Vivo with a p16INK4a-Luciferase Model', Cell, 152(1–2), pp. 340–351. doi: 10.1016/J.CELL.2012.12.010.

Burton, D. G. A. and Krizhanovsky, V. (2014) 'Physiological and pathological consequences of cellular senescence', Cellular and molecular life sciences : CMLS, 71(22), pp. 4373–4386. doi: 10.1007/S00018-014-1691-3.

Burton, D. G. A. and Stolzing, A. (2018) 'Cellular senescence: Immunosurveillance and future immunotherapy', Ageing research reviews, 43, pp. 17–25. doi: 10.1016/J.ARR.2018.02.001.

Bussian, T. J. et al. (2018) 'Clearance of senescent glial cells prevents tau-dependent pathology and cognitive decline.', Nature, 562(7728), pp. 578–582. doi: 10.1038/s41586-018-0543-y.

Butler, J. M., Kobayashi, H. and Rafii, S. (2010) 'Instructive role of the vascular niche in promoting tumor growth and tissue repair by angiocrine factors', Nature Reviews Cancer, pp. 138–146. doi: 10.1038/nrc2791.

Cai, Y. et al. (2020) 'Elimination of senescent cells by β-galactosidase-targeted prodrug attenuates inflammation and restores physical function in aged mice', Cell research, 30(7), pp. 574–589. doi: 10.1038/S41422-020-0314-9.

Campisi, J. (2001) 'Cellular senescence as a tumor-suppressor mechanism', Trends in Cell Biology, 11(11), pp. 27–31. doi: 10.1016/S0962-8924(01)02151-1.

Campisi, J. et al. (2011) 'Cellular senescence: A link between cancer and age-related degenerative disease?', Seminars in Cancer Biology, 21(6), pp. 354–9. doi: 10.1016/j.semcancer.2011.09.001.

Campisi, J. and d'Adda di Fagagna, F. (2007) 'Cellular senescence: when bad things happen to good cells', Nature Reviews Molecular Cell Biology, 8(9), pp. 729–740. doi: 10.1038/nrm2233.

Cang, S. et al. (2015) 'ABT-199 (venetoclax) and BCL-2 inhibitors in clinical development', Journal of Hematology and Oncology. BioMed Central Ltd. doi: 10.1186/s13045-015-0224-3.

Cardoso, F. et al. (2020) '5th ESO-ESMO international consensus guidelines for advanced breast cancer (ABC 5)', Annals of Oncology, 31(12), p. 1623. doi: 10.1016/J.ANNONC.2020.09.010.

Castillo, R. R. and Vallet-Regí, M. (2019) 'Functional Mesoporous Silica Nanocomposites: Biomedical applications and Biosafety.', International Journal of Molecular Sciences, 20(4), p. 929. doi: 10.3390/ijms20040929.

Cauda, V., Argyo, C. and Bein, T. (2010) 'Impact of different PEGylation patterns on the long-term bio-stability of colloidal mesoporous silica nanoparticles', Journal of Materials Chemistry, 20(39), pp. 8693–8699. doi: 10.1039/C0JM01390K.

Chandra, T. et al. (2015) 'Global reorganization of the nuclear landscape in senescent

cells', Cell reports, 10(4), pp. 471–483. doi: 10.1016/J.CELREP.2014.12.055.
Chandrasekaran, A., Idelchik, M. del P. S. and Melendez, J. A. (2017) 'Redox control of senescence and age-related disease', Redox Biology, 11, pp. 91–102. doi: 10.1016/J.REDOX.2016.11.005.
Chang, B D et al. (1999) 'A senescence-like phenotype distinguishes tumor cells that undergo terminal proliferation arrest after exposure to anticancer agents.', Cancer research, 59(15), pp. 3761–7.
Chang, Bey Dih et al. (1999) 'A senescence-like phenotype distinguishes tumor cells that undergo terminal proliferation arrest after exposure to anticancer agents', Cancer Research, 59(15), pp. 3761–3767.
Chang, J. et al. (2016) 'Clearance of senescent cells by ABT263 rejuvenates aged hematopoietic stem cells in mice', Nature Medicine, 22(1), pp. 78–83. doi: 10.1038/nm.4010.
Chaudhury, K. et al. (2014) 'Regenerative nanomedicine: current perspectives and future directions', International Journal of Nanomedicine, 9(1), p. 4153. doi: 10.2147/IJN.S45332.
Chen, C. et al. (2011) 'Polyvalent nucleic acid/mesoporous silica nanoparticle conjugates: dual stimuli-responsive vehicles for intracellular drug delivery', Angewandte Chemie (International ed. in English), 50(4), pp. 882–886. doi: 10.1002/ANIE.201005471.
Chen, F. et al. (2017) 'Cancer-Targeting Ultrasmall Silica Nanoparticles for Clinical Translation: Physicochemical Structure and Biological Property Correlations', Chemistry of Materials, 29(20), pp. 8766–8779. doi: 10.1021/acs.chemmater.7b03033.
Chen, Y. et al. (2013) 'In vivo distribution and antitumor activity of doxorubicin-loaded N-isopropylacrylamide-co-methacrylic acid coated mesoporous silica nanoparticles and safety evaluation', European Journal of Pharmaceutics and Biopharmaceutics, 85(3 PART A), pp. 406–412. doi: 10.1016/j.ejpb.2013.06.015.
Chen, Z. et al. (2005) 'Crucial role of p53-dependent cellular senescence in suppression of Pten-deficient tumorigenesis.', Nature, 436(7051), pp. 725–30. doi: 10.1038/nature03918.
Chicas, A. et al. (2010) 'Dissecting the unique role of the retinoblastoma tumor suppressor during cellular senescence', Cancer cell, 17(4), pp. 376–387. doi: 10.1016/J.CCR.2010.01.023.
Childs, B. G. et al. (2014) 'Senescence and apoptosis: dueling or complementary cell fates?', EMBO reports, 15(11), pp. 1139–1153. doi: 10.15252/embr.201439245.
Childs, B. G. et al. (2016) 'Senescent intimal foam cells are deleterious at all stages of atherosclerosis.', Science (New York, N.Y.), 354(6311), pp. 472–477. doi: 10.1126/science.aaf6659.
Childs, B. G. et al. (2017) 'Senescent cells: An emerging target for diseases of ageing', Nature Reviews Drug Discovery, 16(10), pp. 718–735. doi: 10.1038/nrd.2017.116.
Choi, Y. H. and Han, H. K. (2018) 'Nanomedicines: current status and future perspectives in aspect of drug delivery and pharmacokinetics', Journal of Pharmaceutical

Investigation, 48(1), pp. 43–60. doi: 10.1007/S40005-017-0370-4/FIGURES/1.

Choi, Y. L. et al. (2011) 'Controlled release using mesoporous silica nanoparticles functionalized with 18-crown-6 derivative', Journal of Materials Chemistry, 21(22), pp. 7882–7885. doi: 10.1039/C1JM11334H.

Chung, Y. H. et al. (2020) 'COVID-19 Vaccine Frontrunners and Their Nanotechnology Design', ACS nano, 14(10), pp. 12522–12537. doi: 10.1021/ACSNANO.0C07197.

Chuprin, A. et al. (2013) 'Cell fusion induced by ERVWE1 or measles virus causes cellular senescence', Genes & development, 27(21), pp. 2356–2366. doi: 10.1101/GAD.227512.113.

Cindrova-Davies, T. et al. (2018) 'Evidence of oxidative stress-induced senescence in mature, post-mature and pathological human placentas', Placenta, 68, pp. 15–22. doi: 10.1016/J.PLACENTA.2018.06.307.

Coll, C. et al. (2011) 'Enzyme-mediated controlled release systems by anchoring peptide sequences on mesoporous silica supports', Angewandte Chemie (International ed. in English), 50(9), pp. 2138–2140. doi: 10.1002/ANIE.201004133.

Collado, M. et al. (2005) 'Senescence in premalignant tumors', 436(7051), pp. 642–642. doi: 10.1038/436642a.

Collado, M., Blasco, M. A. and Serrano, M. (2007) 'Cellular Senescence in Cancer and Aging', Cell, 130(2), pp. 223–233. doi: 10.1016/J.CELL.2007.07.003.

Collado, M. and Serrano, M. (2010) 'Senescence in tumors: evidence from mice and humans', Nature reviews. Cancer, 10(1), pp. 51–57. doi: 10.1038/NRC2772.

Cong, Y. et al. (2017) 'Abscopal regression following SABR for non-small-cell-lung cancer: A case report', Cancer biology & therapy, 18(1), pp. 1–3. doi: 10.1080/15384047.2016.1264541.

Coppé, J.-P. et al. (2010) 'The Senescence-Associated Secretory Phenotype: The Dark Side of Tumor Suppression', Annual Review of Pathology: Mechanisms of Disease, 5(1), pp. 99–118. doi: 10.1146/annurev-pathol-121808-102144.

Coppé, J. P. et al. (2008) 'Senescence-associated secretory phenotypes reveal cell-nonautonomous functions of oncogenic RAS and the p53 tumor suppressor.', PLoS biology, 6(12). doi: 10.1371/journal.pbio.0060301.

Coppé, J. P. et al. (2011) 'Tumor Suppressor and Aging Biomarker p16INK4a Induces Cellular Senescence without the Associated Inflammatory Secretory Phenotype', Journal of Biological Chemistry, 286(42), pp. 36396–36403. doi: 10.1074/JBC.M111.257071.

Cox, L. S. and Redman, C. (2017) 'The role of cellular senescence in ageing of the placenta', Placenta, 52, pp. 139–145. doi: 10.1016/j.placenta.2017.01.116.

Cristofanilli, M. et al. (2016) 'Fulvestrant plus palbociclib versus fulvestrant plus placebo for treatment of hormone-receptor-positive, HER2-negative metastatic breast cancer that progressed on previous endocrine therapy (PALOMA-3): final analysis of the multicentre, double-blind, phas', 17(4), pp. 425–439. doi: 10.1016/S1470-2045(15)00613-0.

Croissant, J. G. et al. (2016) 'Protein-gold clusters-capped mesoporous silica nanoparticles for high drug loading, autonomous gemcitabine/doxorubicin co-delivery, and in-

vivo tumor imaging', Journal of Controlled Release, 229, pp. 183–191. doi: 10.1016/j.jconrel.2016.03.030.

Croissant, J. G. et al. (2018) 'Mesoporous Silica and Organosilica Nanoparticles: Physical Chemistry, Biosafety, Delivery Strategies, and Biomedical Applications', Advanced Healthcare Materials. Wiley-VCH Verlag. doi: 10.1002/adhm.201700831.

Croissant, J. G., Fatieiev, Y. and Khashab, N. M. (2017) 'Degradability and Clearance of Silicon, Organosilica, Silsesquioxane, Silica Mixed Oxide, and Mesoporous Silica Nanoparticles', Advanced Materials, 29(9). doi: 10.1002/adma.201604634.

Däbritz, J. H. M. et al. (2016) 'CD20-targeting immunotherapy promotes cellular senescence in B-cell lymphoma', Molecular Cancer Therapeutics, 15(5), pp. 1074–1081. doi: 10.1158/1535-7163.MCT-15-0627.

Danhier, F., Feron, O. and Préat, V. (2010) 'To exploit the tumor microenvironment: Passive and active tumor targeting of nanocarriers for anti-cancer drug delivery', Journal of controlled release : official journal of the Controlled Release Society, 148(2), pp. 135–146. doi: 10.1016/J.JCONREL.2010.08.027.

Demaria, M. et al. (2014) 'An essential role for senescent cells in optimal wound healing through secretion of PDGF-AA', Developmental Cell, 31(6), pp. 722–733. doi: 10.1016/j.devcel.2014.11.012.

Demaria, M. et al. (2017) 'Cellular senescence promotes adverse effects of chemotherapy and cancer relapse', Cancer Discovery, 7(2), pp. 165–176. doi: 10.1158/2159-8290.CD-16-0241.

Van Deursen, J. M. (2014) 'The role of senescent cells in ageing', Nature, 509(7501), pp. 439–446. doi: 10.1038/NATURE13193.

Di, X. et al. (2008) 'A chemotherapy-associated senescence bystander effect in breast cancer cells', http://dx.doi.org/10.4161/cbt.7.6.5861, 7(6), pp. 864–872. doi: 10.4161/CBT.7.6.5861.

Dimri, G. P. et al. (1995) 'A biomarker that identifies senescent human cells in culture and in aging skin in vivo.', Proceedings of the National Academy of Sciences of the United States of America, 92(20), pp. 9363–7.

Dobrovolskaia, M. A. et al. (2008) 'Preclinical studies to understand nanoparticle interaction with the immune system and its potential effects on nanoparticle biodistribution', Molecular Pharmaceutics, 5(4), pp. 487–495. doi: 10.1021/mp800032f.

Dogra, P. et al. (2018) 'Establishing the effects of mesoporous silica nanoparticle properties on in vivo disposition using imaging-based pharmacokinetics', Nature Communications, 9(1), pp. 1–14. doi: 10.1038/s41467-018-06730-z.

Dörr, J. R. et al. (2013) 'Synthetic lethal metabolic targeting of cellular senescence in cancer therapy', Nature, 501(7467), pp. 421–425. doi: 10.1038/NATURE12437.

Efeyan, A. et al. (2007) 'Induction of p53-Dependent Senescence by the MDM2 Antagonist Nutlin-3a in Mouse Cells of Fibroblast Origin', Cancer Research, 67(15), pp. 7350–7357. doi: 10.1158/0008-5472.CAN-07-0200.

Ehlerding, E. B., Chen, F. and Cai, W. (2015) 'Biodegradable and renal clearable inorganic nanoparticles', Advanced Science, 3(2), pp. 1–8. doi: 10.1002/advs.201500223.

Ekpenyong-Akiba, A. E. et al. (2019) 'Detecting and targeting senescent cells using molecularly imprinted nanoparticles', Nanoscale Horizons, 4(3), pp. 757–768. doi: 10.1039/c8nh00473k.

Elmore, L. W. et al. (2005) 'Evasion of a single-step, chemotherapy-induced senescence in breast cancer cells: implications for treatment response', Clinical cancer research : an official journal of the American Association for Cancer Research, 11(7), pp. 2637–2643. doi: 10.1158/1078-0432.CCR-04-1462.

Estepa-Fernández, A. et al. (2021) 'Senolysis Reduces Senescence in Veins and Cancer Cell Migration', Advanced Therapeutics, 2100149, pp. 1–15. doi: 10.1002/adtp.202100149.

Evangelou, K. et al. (2017) 'Robust, universal biomarker assay to detect senescent cells in biological specimens.', Aging cell, 16(1), pp. 192–197. doi: 10.1111/acel.12545.

Faget, D. V., Ren, Q. and Stewart, S. A. (2019) 'Unmasking senescence: context-dependent effects of SASP in cancer', Nature reviews. Cancer, 19(8), pp. 439–453. doi: 10.1038/S41568-019-0156-2.

Fang, J., Islam, W. and Maeda, H. (2020) 'Exploiting the dynamics of the EPR effect and strategies to improve the therapeutic effects of nanomedicines by using EPR effect enhancers', Advanced Drug Delivery Reviews. doi: 10.1016/j.addr.2020.06.005.

Farokhzad, O. C. and Langer, R. (2009) 'Impact of nanotechnology on drug delivery', ACS nano, 3(1), pp. 16–20. doi: 10.1021/NN900002M.

Farr, J. N. et al. (2017) 'Targeting cellular senescence prevents age-related bone loss in mice', Nature Medicine, 23(9), pp. 1072–1079. doi: 10.1038/nm.4385.

Finn, R. R. S. et al. (2015) 'The cyclin-dependent kinase 4/6 inhibitor palbociclib in combination with letrozole versus letrozole alone as first-line treatment of oestrogen receptor-positive, HER2-negative, advanced breast cancer (PALOMA-1/TRIO-18): A randomised phase 2 study', The Lancet Oncology, 16(1), pp. 25–35. doi: 10.1016/S1470-2045(14)71159-3.

Finn, R. S. et al. (2009) 'PD 0332991, a selective cyclin D kinase 4/6 inhibitor, preferentially inhibits proliferation of luminal estrogen receptor-positive human breast cancer cell lines in vitro', Breast Cancer Research, 11(5), pp. 1–13. doi: 10.1186/bcr2419.

Finn, R. S. et al. (2016) 'Palbociclib and Letrozole in Advanced Breast Cancer', New England Journal of Medicine, 375(20), pp. 1925–1936. doi: 10.1056/NEJMoa1607303.

Fleury, H. et al. (2019) 'Exploiting interconnected synthetic lethal interactions between PARP inhibition and cancer cell reversible senescence', Nature Communications 2019 10:1, 10(1), pp. 1–15. doi: 10.1038/s41467-019-10460-1.

Frescas, D. et al. (2017) 'Senescent cells expose and secrete an oxidized form of membrane-bound vimentin as revealed by a natural polyreactive antibody', Proceedings of the National Academy of Sciences of the United States of America, 114(9), pp. E1668–E1677. doi: 10.1073/PNAS.1614661114.

Freund, A. et al. (2010) 'Inflammatory networks during cellular senescence: causes and consequences', Trends in Molecular Medicine, 16(5), pp. 238–246. doi: 10.1016/J.MOLMED.2010.03.003.

Freund, A. et al. (2012) 'Lamin B1 loss is a senescence-associated biomarker', Molecular

biology of the cell, 23(11), pp. 2066–2075. doi: 10.1091/MBC.E11-10-0884.

Frickenstein, A. N. et al. (2021) 'Mesoporous silica nanoparticles: Properties and strategies for enhancing clinical effect', Pharmaceutics. Pharmaceutics. doi: 10.3390/pharmaceutics13040570.

Fry, D. W. et al. (2004) 'Specific inhibition of cyclin-dependent kinase 4/6 by PD 0332991 and associated antitumor activity in human tumor xenografts.', Molecular cancer therapeutics, 3(11), pp. 1427–38. Available at: http://www.ncbi.nlm.nih.gov/pubmed/15542782 (Accessed: 4 September 2019).

Fuhrmann-Stroissnigg, H. et al. (2017) 'Identification of HSP90 inhibitors as a novel class of senolytics', Nature Communications, 8(1). doi: 10.1038/s41467-017-00314-z.

Fuhrmann-Stroissnigg, H., Niedernhofer, L. J. and Robbins, P. D. (2018) 'Hsp90 inhibitors as senolytic drugs to extend healthy aging', Cell Cycle, pp. 1–8. doi: 10.1080/15384101.2018.1475828.

Galiana, I. et al. (2020) 'Preclinical antitumor efficacy of senescence-inducing chemotherapy combined with a nanoSenolytic', Journal of Controlled Release, 323, pp. 624–634. doi: 10.1016/j.jconrel.2020.04.045.

Gao, J. J. et al. (2020) 'CDK4/6 inhibitor treatment for patients with hormone receptor-positive, HER2-negative, advanced or metastatic breast cancer: a US Food and Drug Administration pooled analysis', The Lancet Oncology, 21(2), pp. 250–260. doi: 10.1016/S1470-2045(19)30804-6.

García-Fernández, A. et al. (2020) 'New Advances in In Vivo Applications of Gated Mesoporous Silica as Drug Delivery Nanocarriers', Small, 16(3), pp. 1–62. doi: 10.1002/smll.201902242.

Georgakopoulou, E. et al. (2012) 'Specific lipofuscin staining as a novel biomarker to detect replicative and stress-induced senescence. A method applicable in cryo-preserved and archival tissues', Aging, 5(1), pp. 37–50. doi: 10.18632/aging.100527.

Gerdes, J. et al. (1984) 'Cell cycle analysis of a cell proliferation-associated human nuclear antigen defined by the monoclonal antibody Ki-67.', The Journal of Immunology, 133(4), pp. 1710 LP – 1715. Available at: http://www.jimmunol.org/content/133/4/1710.abstract.

Gil-Gil, M. et al. (2021) 'The role of CDK4/6 inhibitors in early breast cancer', Breast, 58, pp. 160–169. doi: 10.1016/j.breast.2021.05.008.

Giménez, C. et al. (2015) 'Gated mesoporous silica nanoparticles for the controlled delivery of drugs in cancer cells', Langmuir, 31(12), pp. 3753–3762. doi: 10.1021/acs.langmuir.5b00139.

Gisbert-Garzarán, M., Lozano, D. and Vallet-Regí, M. (2020) 'Mesoporous Silica Nanoparticles for Targeting Subcellular Organelles', International journal of molecular sciences, 21(24), pp. 1–18. doi: 10.3390/IJMS21249696.

Goel, S. et al. (2016) 'Overcoming Therapeutic Resistance in HER2-Positive Breast Cancers with CDK4/6 Inhibitors', Cancer Cell, 29(3), pp. 255–269. doi: 10.1016/J.CCELL.2016.02.006.

Goel, S. et al. (2017) 'CDK4/6 inhibition triggers anti-tumor immunity', Nature 2017

548:7668, 548(7668), pp. 471–475. doi: 10.1038/nature23465.
Goel, S. et al. (2018) 'CDK4/6 Inhibition in Cancer: Beyond Cell Cycle Arrest', Trends in Cell Biology. Elsevier Ltd, pp. 911–925. doi: 10.1016/j.tcb.2018.07.002.
Gong, X. et al. (2017) 'Genomic Aberrations that Activate D-type Cyclins Are Associated with Enhanced Sensitivity to the CDK4 and CDK6 Inhibitor Abemaciclib', Cancer Cell, 32(6), pp. 761-776.e6. doi: 10.1016/J.CCELL.2017.11.006.
González-Gualda, E. et al. (2020) 'Galacto-conjugation of Navitoclax as an efficient strategy to increase senolytic specificity and reduce platelet toxicity', Aging Cell, 19(4), pp. 1–19. doi: 10.1111/acel.13142.
González-Gualda, E. et al. (2021) 'A guide to assessing cellular senescence in vitro and in vivo', FEBS Journal, 288(1), pp. 56–80. doi: 10.1111/febs.15570.
Gorgoulis, V. et al. (2019) 'Cellular Senescence: Defining a Path Forward', Cell, 179(4), pp. 813–827. doi: 10.1016/J.CELL.2019.10.005.
Grandhi, T. S. P. and Rege, K. (2014) 'Design, synthesis, and functionalization of nanomaterials for therapeutic drug delivery', Advances in Experimental Medicine and Biology, 811, pp. 157–182. doi: 10.1007/978-94-017-8739-0_9.
Guan, X. et al. (2017) 'Stromal Senescence By Prolonged CDK4/6 Inhibition Potentiates Tumor Growth', Molecular cancer research : MCR, 15(3), pp. 237–249. doi: 10.1158/1541-7786.MCR-16-0319.
Guerrero, A., Herranz, N., et al. (2020) 'Cardiac glycosides are broad-spectrum senolytics', 1(11), pp. 1074–1088. doi: 10.1038/s42255-019-0122-z.Cardiac.
Guerrero, A., Guiho, R., et al. (2020) 'Galactose-modified duocarmycin prodrugs as senolytics', Aging cell, 19(4). doi: 10.1111/ACEL.13133.
Hampel, B. et al. (2004) 'Differential regulation of apoptotic cell death in senescent human cells', Experimental gerontology, 39(11–12), pp. 1713–1721. doi: 10.1016/J.EXGER.2004.05.010.
Han, D., Williams, E. and Cadenas, E. (2001) 'Mitochondrial respiratory chain-dependent generation of superoxide anion and its release into the intermembrane space', Biochemical Journal, 353(2), pp. 411–416. doi: 10.1042/BJ3530411.
Han, Z. et al. (2002) 'Role of p21 in apoptosis and senescence of human colon cancer cells treated with camptothecin.', The Journal of biological chemistry, 277(19), pp. 17154–60. doi: 10.1074/jbc.M112401200.
Hanahan, D. (2022) 'Hallmarks of Cancer: New Dimensions.', Cancer discovery, 12(1), pp. 31–46. doi: 10.1158/2159-8290.CD-21-1059.
Hanahan, D. and Weinberg, R. A. (2011) 'Hallmarks of cancer: the next generation', Cell, 144(5), pp. 646–674. doi: 10.1016/J.CELL.2011.02.013.
Harley, C. B., Futcher, A. B. and Greider, C. W. (1990) 'Telomeres shorten during ageing of human fibroblasts', Nature, 345(6274), pp. 458–460. doi: 10.1038/345458a0.
Hashimoto, M. et al. (2016) 'Elimination of p19 ARF-expressing cells enhances pulmonary function in mice', JCI insight, 1(12). doi: 10.1172/JCI.INSIGHT.87732.
Hayflick, L. (1965) 'The limited in vitro lifetime of human diploid cell strains', Experimental Cell Research, 37(3), pp. 614–636. doi: 10.1016/0014-4827(65)90211-9.
Hayflick, L. and Moorhead, P. S. (1961) 'The serial cultivation of human diploid cell strains',

Experimental Cell Research, 25(3), pp. 585–621. doi: 10.1016/0014-4827(61)90192-6.

He, Q. et al. (2011) 'In vivo biodistribution and urinary excretion of mesoporous silica nanoparticles: Effects of particle size and PEGylation', Small, 7(2), pp. 271–280. doi: 10.1002/smll.201001459.

He, Y. et al. (2020) 'Using proteolysis-targeting chimera technology to reduce navitoclax platelet toxicity and improve its senolytic activity', Nature communications, 11(1). doi: 10.1038/S41467-020-15838-0.

Hernandez-Segura, A. et al. (2017) 'Unmasking Transcriptional Heterogeneity in Senescent Cells', Current Biology, 27(17), pp. 2652-2660.e4.

Hernandez-Segura, A., Nehme, J. and Demaria, M. (2018) 'Hallmarks of Cellular Senescence', Trends in Cell Biology, 28(6), pp. 436–453. doi: 10.1016/j.tcb.2018.02.001.

Hickson, L. T. J. et al. (2019) 'Senolytics decrease senescent cells in humans: Preliminary report from a clinical trial of Dasatinib plus Quercetin in individuals with diabetic kidney disease', EBioMedicine, 47, pp. 446–456. doi: 10.1016/J.EBIOM.2019.08.069.

Hildebrand, D. G. et al. (2013) 'α-Fucosidase as a novel convenient biomarker for cellular senescence', Cell Cycle, 12(12), pp. 1922–1927. doi: 10.4161/cc.24944.

Hirose, Y., Berger, M. S. and Pieper, R. O. (2001) 'p53 effects both the duration of G2/M arrest and the fate of temozolomide-treated human glioblastoma cells.', Cancer research, 61(5), pp. 1957–63.

Hoffmann, F. et al. (2006) 'Silica-based mesoporous organic-inorganic hybrid materials', Angewandte Chemie - International Edition. Angew Chem Int Ed Engl, pp. 3216–3251. doi: 10.1002/anie.200503075.

Hortobagyi, G. N. G. et al. (2016) 'Ribociclib as First-Line Therapy for HR-Positive, Advanced Breast Cancer', 375(18), pp. 1738–1748. doi: 10.1056/NEJMOA1609709/SUPPL_FILE/NEJMOA1609709_DISCLOSURES.PDF.

Hu, J.-J. et al. (2017) 'A positive feedback strategy for enhanced chemotherapy based on ROS-triggered self-accelerating drug release nanosystem', Biomaterials, 128, pp. 136–146. doi: 10.1016/J.BIOMATERIALS.2017.03.010.

Huang, F.-C. et al. (2012) 'Induction of senescence in cancer cells by the G-quadruplex stabilizer, BMVC4, is independent of its telomerase inhibitory activity', British Journal of Pharmacology, 167(2), pp. 393–406. doi: 10.1111/j.1476-5381.2012.01997.x.

Huang, X. et al. (2011) 'The shape effect of mesoporous silica nanoparticles on biodistribution, clearance, and biocompatibility in vivo', ACS Nano, 5(7), pp. 5390–5399. doi: 10.1021/nn200365a.

Hudgins, A. D. et al. (2018) 'Age- and Tissue-Specific Expression of Senescence Biomarkers in Mice', Frontiers in genetics, 9(FEB). doi: 10.3389/FGENE.2018.00059.

Hwang, H. J. et al. (2020) 'Endothelial cells under therapy-induced senescence secrete CXCL11, which increases aggressiveness of breast cancer cells', Cancer Letters, 490(June), pp. 100–110. doi: 10.1016/j.canlet.2020.06.019.

Janjua, T. I. et al. (2021) 'Clinical translation of silica nanoparticles', Nature Reviews Materials. Nature Publishing Group, pp. 1072–1074. doi: 10.1038/s41578-021-00385-x.

Jeon, O. H. et al. (2017) 'Local clearance of senescent cells attenuates the development of post-traumatic osteoarthritis and creates a pro-regenerative environment', Nature Medicine, 23(6), pp. 775–781. doi: 10.1038/nm.4324.

Jimenez, R. et al. (2005) 'Replicative senescence in patients with chronic kidney failure', Kidney International, 68, pp. S11–S15. doi: 10.1111/j.1523-1755.2005.09903.x.

Jones, K. R. et al. (2005) 'p53-Dependent accelerated senescence induced by ionizing radiation in breast tumor cells', International journal of radiation biology, 81(6), pp. 445–458. doi: 10.1080/09553000500168549.

Jun, J. Il and Lau, L. F. (2010) 'Cellular senescence controls fibrosis in wound healing', Aging, 2(9), pp. 627–631. doi: 10.18632/AGING.100201.

Justice, J. N. et al. (2019) 'Senolytics in idiopathic pulmonary fibrosis: Results from a first-in-human, open-label, pilot study', EBioMedicine, 40, pp. 554–563. doi: 10.1016/J.EBIOM.2018.12.052.

Kaefer, A. et al. (2014) 'Mechanism-based pharmacokinetic/pharmacodynamic meta-analysis of navitoclax (ABT-263) induced thrombocytopenia', Cancer chemotherapy and pharmacology, 74(3), pp. 593–602. doi: 10.1007/S00280-014-2530-9.

Kang, C. et al. (2015) 'The DNA damage response induces inflammation and senescence by inhibiting autophagy of GATA4', Science (New York, N.Y.), 349(6255). doi: 10.1126/SCIENCE.AAA5612.

Kang, T.-W. et al. (2011) 'Senescence surveillance of pre-malignant hepatocytes limits liver cancer development', Nature, 479(7374), pp. 547–551. doi: 10.1038/nature10599.

Katz, M. L. et al. (1984) 'Lipofuscin accumulation resulting from senescence and vitamin E deficiency: Spectral properties and tissue distribution', Mechanisms of Ageing and Development, 25(1–2), pp. 149–159. doi: 10.1016/0047-6374(84)90137-4.

Khan, Z. H. et al. (2016) 'Introduction to nanomaterials', in Advanced Structured Materials, pp. 1–23. doi: 10.1007/978-81-322-2668-0_1.

Khosla, S., Farr, J. N. and Kirkland, J. L. (2018) 'Inhibiting Cellular Senescence: A New Therapeutic Paradigm for Age-Related Osteoporosis', The Journal of Clinical Endocrinology & Metabolism, 103(4), pp. 1282–1290. doi: 10.1210/jc.2017-02694.

Kile, B. T. (2014) 'The role of apoptosis in megakaryocytes and platelets', British Journal of Haematology, 165(2), pp. 217–226. doi: 10.1111/bjh.12757.

Killilea, D. W. et al. (2003) 'Iron accumulation during cellular senescence in human fibroblasts in vitro', Antioxidants & redox signaling, 5(5), pp. 507–516. doi: 10.1089/152308603770310158.

Kim, H.-N. N. et al. (2017) 'DNA damage and senescence in osteoprogenitors expressing Osx1 may cause their decrease with age', Aging Cell, 16(4), pp. 693–703. doi: 10.1111/acel.12597.

Kim, Y. H. et al. (2017) 'Senescent tumor cells lead the collective invasion in thyroid cancer', 8. Available at: https://pubmed.ncbi.nlm.nih.gov/28489070/ (Accessed:

26 November 2019).
Kirkland, J. L. and Tchkonia, T. (2020) 'Senolytic drugs: from discovery to translation', Journal of Internal Medicine, 288(5), pp. 518–536. doi: 10.1111/joim.13141.
Knaś, M. et al. (2012) 'The profile of lysosomal exoglycosidases in replicative and stress-induced senescence in early passage human fibroblasts', Folia Histochemica et Cytobiologica, 50(2), pp. 220–227. doi: 10.5603/FHC.2012.0031.
Krizhanovsky, V. et al. (2008) 'Senescence of Activated Stellate Cells Limits Liver Fibrosis', Cell, 134(4), pp. 657–667. doi: 10.1016/j.cell.2008.06.049.
Krpetić, Ž. et al. (2014) 'Nanomaterials: impact on cells and cell organelles', Advances in experimental medicine and biology, 811, pp. 135–156. doi: 10.1007/978-94-017-8739-0_8.
Krtolica, A. et al. (2001) 'Senescent fibroblasts promote epithelial cell growth and tumorigenesis: a link between cancer and aging', Proceedings of the National Academy of Sciences of the United States of America, 98(21), pp. 12072–12077. doi: 10.1073/PNAS.211053698.
Kuilman, T. et al. (2010) 'The essence of senescence', Genes & development, 24(22), pp. 2463–2479. doi: 10.1101/GAD.1971610.
Kulkarni, J. A. et al. (2020) 'Spontaneous, solvent-free entrapment of siRNA within lipid nanoparticles', Nanoscale, 12(47), pp. 23959–23966. doi: 10.1039/D0NR06816K.
Kumar, P. et al. (2009) 'Molecular mechanisms of endothelial hyperpermeability: Implications in inflammation', Expert Reviews in Molecular Medicine. Expert Rev Mol Med. doi: 10.1017/S1462399409001112.
Kwon, Y. et al. (2017) 'Autophagy Is Pro-Senescence When Seen in Close-Up, but Anti-Senescence in Long-Shot', Molecules and cells, 40(9), pp. 607–612. doi: 10.14348/MOLCELLS.2017.0151.
Laprise-Pelletier, M. et al. (2015) 'Metal chelate grafting at the surface of mesoporous silica nanoparticles (MSNs): Physico-chemical and biomedical imaging assessment', Journal of Materials Chemistry B, 3(5), pp. 748–758. doi: 10.1039/c4tb01423e.
Lazarovits, J. et al. (2015) 'Nanoparticle-blood interactions: The implications on solid tumor targeting', Chemical Communications, 51(14), pp. 2756–2767. doi: 10.1039/c4cc07644c.
Lee, A. C. et al. (1999) 'Ras proteins induce senescence by altering the intracellular levels of reactive oxygen species', The Journal of biological chemistry, 274(12), pp. 7936–7940. doi: 10.1074/JBC.274.12.7936.
Lee, S. et al. (2021) 'Virus-induced senescence is a driver and therapeutic target in COVID-19', Nature 2021 599:7884, 599(7884), pp. 283–289. doi: 10.1038/s41586-021-03995-1.
Leontieva, O. V. and Blagosklonny, M. V. (2013) 'CDK4/6-inhibiting drug substitutes for p21 and p16 in senescence: Duration of cell cycle arrest and MTOR activity determine geroconversion', Cell Cycle, 12(18), pp. 3063–3069. doi: 10.4161/cc.26130.
Li, H. et al. (2018) 'In vivo near infrared fluorescence imaging and dynamic quantification

of pancreatic metastatic tumors using folic acid conjugated biodegradable mesoporous silica nanoparticles', Nanomedicine: Nanotechnology, Biology, and Medicine, 14(6), pp. 1867–1877. doi: 10.1016/j.nano.2018.04.018.

Li, S. et al. (2020) ' Chiral Cu x Co y S Nanoparticles under Magnetic Field and NIR Light to Eliminate Senescent Cells ', Angewandte Chemie, 132(33), pp. 14019–14026. doi: 10.1002/ANGE.202004575.

Li, Z., Zhang, Y. and Feng, N. (2019) 'Mesoporous silica nanoparticles: synthesis, classification, drug loading, pharmacokinetics, biocompatibility, and application in drug delivery', Expert opinion on drug delivery, 16(3), pp. 219–237. doi: 10.1080/17425247.2019.1575806.

Lin, Q. et al. (2010) 'Anticancer drug release from a mesoporous silica based nanophotocage regulated by either a one- or two-photon process', Journal of the American Chemical Society, 132(31), pp. 10645–10647. doi: 10.1021/JA103415T.

Ling, X. et al. (2014) 'FL118 Induces p53-Dependent Senescence in Colorectal Cancer Cells by Promoting Degradation of MdmX', Cancer Research, 74(24), pp. 7487–7497. doi: 10.1158/0008-5472.CAN-14-0683.

Liu, Z. et al. (2008) 'Circulation and long-term fate of functionalized, biocompatible single-walled carbon nanotubes in mice probed by Raman spectroscopy', Proceedings of the National Academy of Sciences, 105(5), pp. 1410 LP – 1415. doi: 10.1073/pnas.0707654105.

Llopis-Lorente, A. et al. (2017) 'Mesoporous silica materials for controlled delivery based on enzymes', Journal of Materials Chemistry B, 5(17), pp. 3069–3083. doi: 10.1039/c7tb00348j.

Longmire, M., Choyke, P. L. and Kobayashi, H. (2008) 'Clearance properties of nano-sized particles and molecules as imaging agents: considerations and caveats', Nanomedicine (London, England), 3(5), pp. 703–717. doi: 10.2217/17435889.3.5.703.

López-Otín, C. et al. (2013) 'The Hallmarks of Aging', Cell, 153(6), pp. 1194–1217. doi: 10.1016/j.cell.2013.05.039.

Lu, C. H. and Willner, I. (2015) 'Stimuli-responsive DNA-functionalized nano-/microcontainers for switchable and controlled release', Angewandte Chemie (International ed. in English), 54(42), pp. 12212–12235. doi: 10.1002/ANIE.201503054.

Lu, M. et al. (2020) 'Mitochondria-Targeting Plasmonic Spiky Nanorods Increase the Elimination of Aging Cells in Vivo', Angewandte Chemie International Edition, 59(22), pp. 8698–8705. doi: 10.1002/ANIE.202002576.

Lüscher, T. F. and Barton, M. (1997) 'Biology of the endothelium.', Clinical cardiology, 20(11 Suppl 2), pp. II-3–10. Available at: http://www.ncbi.nlm.nih.gov/pubmed/9422846 (Accessed: 20 November 2019).

Maciejowski, J. and De Lange, T. (2017) 'Telomeres in cancer: tumor suppression and genome instability', Nature reviews. Molecular cell biology, 18(3), pp. 175–186. doi: 10.1038/NRM.2016.171.

Malumbres, M. and Barbacid, M. (2009) 'Cell cycle, CDKs and cancer: a changing

paradigm', 9(3), pp. 153–166. doi: 10.1038/nrc2602.

Mansilla, S., Piña, B. and Portugal, J. (2003) 'Daunorubicin-induced variations in gene transcription: commitment to proliferation arrest, senescence and apoptosis.', The Biochemical journal, 372(Pt 3), pp. 703–11. doi: 10.1042/BJ20021950.

Manzano, M. and Vallet-Regí, M. (2019) 'Ultrasound responsive mesoporous silica nanoparticles for biomedical applications', Chemical Communications, 55(19), pp. 2731–2740. doi: 10.1039/C8CC09389J.

Manzano, M. and Vallet-Regí, M. (2020) 'Mesoporous Silica Nanoparticles for Drug Delivery', Advanced Functional Materials, 30(2), p. 1902634. doi: 10.1002/ADFM.201902634.

Marconett, C. N. et al. (2011) 'Indole-3-carbinol downregulation of telomerase gene expression requires the inhibition of estrogen receptor-alpha and Sp1 transcription factor interactions within the hTERT promoter and mediates the G1 cell cycle arrest of human breast cancer cells', Carcinogenesis, 32(9), pp. 1315–1323. doi: 10.1093/carcin/bgr116.

Marcotte, R., Lacelle, C. and Wang, E. (2004) 'Senescent fibroblasts resist apoptosis by downregulating caspase-3', Mechanisms of ageing and development, 125(10–11), pp. 777–783. doi: 10.1016/J.MAD.2004.07.007.

Masaldan, S. et al. (2018) 'Copper accumulation in senescent cells: Interplay between copper transporters and impaired autophagy', Redox biology, 16, pp. 322–331. doi: 10.1016/J.REDOX.2018.03.007.

Matsumura, Y. and Maeda, H. (1986) 'A new concept for macromolecular therapeutics in cancer chemotherapy: mechanism of tumoritropic accumulation of proteins and the antitumor agent smancs.', Cancer research, 46(12 Pt 1), pp. 6387–92. Available at: http://www.ncbi.nlm.nih.gov/pubmed/2946403 (Accessed: 9 September 2019).

McCartney, A. et al. (2020) 'Plasma Thymidine Kinase Activity as a Biomarker in Patients with Luminal Metastatic Breast Cancer Treated with Palbociclib within the TREnd Trial', Clinical Cancer Research, 26(9), pp. 2131–2139. doi: 10.1158/1078-0432.CCR-19-3271/75882/AM/PLASMA-THYMIDINE-KINASE-ACTIVITY-AS-A-BIOMARKER-IN.

McHugh, D. and Gil, J. (2018) 'Senescence and aging: Causes, consequences, and therapeutic avenues', Journal of Cell Biology, 217(1), pp. 65–77. doi: 10.1083/JCB.201708092.

Meola, T. R. et al. (2021) 'A safety, tolerability, and pharmacokinetic study of a novel simvastatin silica-lipid hybrid formulation in healthy male participants', Drug delivery and translational research, 11(3), pp. 1261–1272. doi: 10.1007/S13346-020-00853-X.

Michaloglou, C. et al. (2005) 'BRAFE600-associated senescence-like cell cycle arrest of human naevi', Nature, 436(7051), pp. 720–724. doi: 10.1038/nature03890.

Milanovic, M. et al. (2018) 'Senescence-associated reprogramming promotes cancer stemness', Nature, 553(7686), pp. 96–100. doi: 10.1038/nature25167.

Milanovic, M., Yu, Y. and Schmitt, C. A. (2018) 'The Senescence–Stemness Alliance – A

Cancer-Hijacked Regeneration Principle', Trends in Cell Biology, 28(12), pp. 1049–1061. doi: 10.1016/j.tcb.2018.09.001.

Di Mitri, D. and Alimonti, A. (2016) 'Non-Cell-Autonomous Regulation of Cellular Senescence in Cancer', Trends in Cell Biology, 26(3), pp. 215–226. doi: 10.1016/j.tcb.2015.10.005.

Mole, R. H. (1953) 'Whole body irradiation; radiobiology or medicine?', The British journal of radiology, 26(305), pp. 234–241. doi: 10.1259/0007-1285-26-305-234.

Morsli, S., Doherty, G. J. and Muñoz-Espín, D. (2022) 'Activatable senoprobes and senolytics: Novel strategies to detect and target senescent cells', Mechanisms of Ageing and Development, 202(October 2021), p. 111618. doi: 10.1016/j.mad.2021.111618.

Müller, S. et al. (2012) 'Pyridostatin analogues promote telomere dysfunction and long-term growth inhibition in human cancer cells', Organic & Biomolecular Chemistry, 10(32), p. 6537. doi: 10.1039/c2ob25830g.

Muñoz-Espín, D. et al. (2013) 'Programmed Cell Senescence during Mammalian Embryonic Development', Cell, 155(5), pp. 1104–1118. doi: 10.1016/j.cell.2013.10.019.

Muñoz-Espín, D. and Serrano, M. (2014) 'Cellular senescence: From physiology to pathology', Nature Reviews Molecular Cell Biology, 15(7), pp. 482–496. doi: 10.1038/nrm3823.

Muñoz-Espín, D. et al. (2018) 'A versatile drug delivery system targeting senescent cells', EMBO Molecular Medicine, 10(9). doi: 10.15252/emmm.201809355.

Narita, Masashi et al. (2003) 'Rb-Mediated Heterochromatin Formation and Silencing of E2F Target Genes during Cellular Senescence', Cell, 113(6), pp. 703–716. doi: 10.1016/S0092-8674(03)00401-X.

Navya, P. N., Kaphle, A. and Daima, H. K. (2018) 'Nanomedicine in sensing, delivery, imaging and tissue engineering: advances, opportunities and challenges', SPR Nanoscience, 5, pp. 30–56. doi: 10.1039/9781788013871-00030.

Nehme, J. et al. (2020) 'Cellular senescence as a potential mediator of COVID-19 severity in the elderly', Aging cell, 19(10). doi: 10.1111/ACEL.13237.

Nelson, G. et al. (2012) 'A senescent cell bystander effect: Senescence-induced senescence', Aging Cell, 11(2), pp. 345–349. doi: 10.1111/j.1474-9726.2012.00795.x.

Nguyen, H. T. et al. (2017) 'CD9 monoclonal antibody-conjugated PEGylated liposomes for targeted delivery of rapamycin in the treatment of cellular senescence', Nanotechnology, 28(9), p. 095101. doi: 10.1088/1361-6528/aa57b3.

Ohtani, N. et al. (2012) 'Cellular senescence: A double-edged sword in the fight against cancer', Experimental Dermatology, 21(SUPPL.1), pp. 1–4. doi: 10.1111/j.1600-0625.2012.01493.x.

Olovnikov, A. M. (1996) 'Telomeres, telomerase, and aging: Origin of the theory', Experimental Gerontology, 31(4), pp. 443–448. doi: 10.1016/0531-5565(96)00005-8.

Paez-Ribes, M. et al. (2019) 'Targeting senescent cells in translational medicine', EMBO

Molecular Medicine, 11(12), pp. 1–19. doi: 10.15252/emmm.201810234.

Parrinello, S. et al. (2005) 'Stromal-epithelial interactions in aging and cancer: senescent fibroblasts alter epithelial cell differentiation', 118, pp. 485–496. Available at: https://pubmed.ncbi.nlm.nih.gov/15657080/ (Accessed: 22 February 2022).

Passos, J. F. et al. (2007) 'Mitochondrial dysfunction accounts for the stochastic heterogeneity in telomere-dependent senescence', PLoS Biology, 5(5), pp. 1138–1151. doi: 10.1371/JOURNAL.PBIO.0050110.

Passos, J. F. et al. (2010) 'Feedback between p21 and reactive oxygen production is necessary for cell senescence', Molecular Systems Biology, 6, p. 347. doi: 10.1038/MSB.2010.5.

Peeper, D. S. et al. (1993) 'A- and B-type cyclins differentially modulate substrate specificity of cyclin-cdk complexes.', The EMBO journal, 12(5), pp. 1947–54.

Peer, D. et al. (2007) 'Nanocarriers as an emerging platform for cancer therapy', Nature Nanotechnology. Nature Publishing Group, pp. 751–760. doi: 10.1038/nnano.2007.387.

Pernas, S. et al. (2018) CDK4/6 inhibition in breast cancer: current practice and future directions, Therapeutic Advances in Medical Oncology. SAGE Publications Inc. doi: 10.1177/1758835918786451.

Pham, L. M. et al. (2021) 'Targeting and clearance of senescent foamy macrophages and senescent endothelial cells by antibody-functionalized mesoporous silica nanoparticles for alleviating aorta atherosclerosis', Biomaterials, 269. doi: 10.1016/J.BIOMATERIALS.2021.120677.

Phillips, E. et al. (2014) 'Clinical translation of an ultrasmall inorganic optical-PET imaging nanoparticle probe', 6(260). doi: 10.1126/scitranslmed.3009524.

te Poele, R. H. et al. (2002) 'DNA damage is able to induce senescence in tumor cells in vitro and in vivo.', Cancer research, 62(6), pp. 1876–83.

Poleszczuk, J. T. et al. (2016) 'Abscopal Benefits of Localized Radiotherapy Depend on Activated T-cell Trafficking and Distribution between Metastatic Lesions', Cancer research, 76(5), pp. 1009–1018. doi: 10.1158/0008-5472.CAN-15-1423.

Pu, X. et al. (2019) 'Mesoporous Silica Nanoparticles as a Prospective and Promising Approach for Drug Delivery and Biomedical Applications', Current Cancer Drug Targets, 19(4), pp. 285–295. doi: 10.2174/1568009619666181206114904.

Qu, A. et al. (2020) 'An NIR-Responsive DNA-Mediated Nanotetrahedron Enhances the Clearance of Senescent Cells', Advanced Materials, 32(14), p. 2000184. doi: 10.1002/adma.202000184.

Rader, J. et al. (2013) 'Dual CDK4/CDK6 inhibition induces cell-cycle arrest and senescence in neuroblastoma', Clinical Cancer Research, 19(22), pp. 6173–6182. doi: 10.1158/1078-0432.CCR-13-1675.

Radu, D. R. et al. (2004) 'A polyamidoamine dendrimer-capped mesoporous silica nanosphere-based gene transfection reagent', Journal of the American Chemical Society, 126(41), pp. 13216–13217. doi: 10.1021/JA046275M/SUPPL_FILE/JA046275MSI20040825_074858.PDF.

Ramakrishna, G. et al. (2012) 'Role of cellular senescence in hepatic wound healing and

carcinogenesis', European journal of cell biology, 91(10), pp. 739–747. doi: 10.1016/J.EJCB.2012.08.002.

Raman, N. K., Anderson, M. T. and Brinker, C. J. (1996) 'Template-based approaches to the preparation of amorphous, nanoporous silicas', Chemistry of Materials, pp. 1682–1701. doi: 10.1021/cm960138+.

Rao, S. G. and Jackson, J. G. (2016) 'SASP: Tumor Suppressor or Promoter? Yes!', Trends in cancer, 2(11), pp. 676–687. doi: 10.1016/j.trecan.2016.10.001.

Rascol, E. et al. (2017) 'Biological fate of Fe3O4 core-shell mesoporous silica nanoparticles depending on particle surface chemistry', Nanomaterials, 7(7), pp. 1–15. doi: 10.3390/nano7070162.

Rastinehad, A. R. et al. (2019) 'Gold nanoshell-localized photothermal ablation of prostate tumors in a clinical pilot device study', Proceedings of the National Academy of Sciences of the United States of America, 116(37), pp. 18590–18596. doi: 10.1073/pnas.1906929116.

Reymond, N., D'Água, B. B. and Ridley, A. J. (2013) 'Crossing the endothelial barrier during metastasis', Nature Reviews Cancer, 13(12), pp. 858–870. doi: 10.1038/nrc3628.

Reynders, K. et al. (2015) 'The abscopal effect of local radiotherapy: using immunotherapy to make a rare event clinically relevant', Cancer treatment reviews, 41(6), pp. 503–510. doi: 10.1016/J.CTRV.2015.03.011.

Ritschka, B. et al. (2017) 'The senescence-associated secretory phenotype induces cellular plasticity and tissue regeneration', Genes & Development, 31(2), pp. 172–183. doi: 10.1101/gad.290635.116.

Rivadeneira, D. B. et al. (2010) 'Proliferative Suppression by CDK4/6 Inhibition: Complex Function of the Retinoblastoma Pathway in Liver Tissue and Hepatoma Cells', Gastroenterology, 138(5). doi: 10.1053/j.gastro.2010.01.007.

Roberson, R. S. et al. (2005) 'Escape from therapy-induced accelerated cellular senescence in p53-null lung cancer cells and in human lung cancers', Cancer research, 65(7), pp. 2795–2803. doi: 10.1158/0008-5472.CAN-04-1270.

Robles, S. J. and Adami, G. R. (1998) 'Agents that cause DNA double strand breaks lead to p16INK4a enrichment and the premature senescence of normal fibroblasts', Oncogene, 16(9), pp. 1113–1123. doi: 10.1038/sj.onc.1201862.

Rodriguez-Ruiz, M. E. et al. (2019) 'Immunological impact of cell death signaling driven by radiation on the tumor microenvironment', Nature Immunology 2019 21:2, 21(2), pp. 120–134. doi: 10.1038/s41590-019-0561-4.

Rojas, S. et al. (2015) 'Novel methodology for labelling mesoporous silica nanoparticles using the 18F isotope and their in vivo biodistribution by positron emission tomography', Journal of Nanoparticle Research, 17(3). doi: 10.1007/s11051-015-2938-0.

Roninson, I. B. (2003) 'Tumor Cell Senescence in Cancer Treatment 1', CANCER RESEARCH, 63, pp. 2705–2715.

Ruscetti, M. et al. (2020) 'Senescence-Induced Vascular Remodeling Creates Therapeutic Vulnerabilities in Pancreas Cancer', Cell, 181(2), pp. 424-441.e21. doi: 10.1016/j.cell.2020.03.008.

Ryu, S. J., Oh, Y. S. and Park, S. C. (2007) 'Failure of stress-induced downregulation of Bcl-2 contributes to apoptosis resistance in senescent human diploid fibroblasts', Cell death and differentiation, 14(5), pp. 1020–1028. doi: 10.1038/SJ.CDD.4402091.

Sager, R. (1991) 'Senescence as a mode of tumor suppression.', Environmental Health Perspectives, 93, p. 59. doi: 10.1289/EHP.919359.

Sagiv, A. et al. (2016) 'NKG2D ligands mediate immunosurveillance of senescent cells', Aging, 8(2), pp. 328–344. doi: 10.18632/aging.100897.

Saha, A. K. et al. (2020) 'Design Considerations and Assays for Hemocompatibility of FDA-Approved Nanoparticles', Seminars in thrombosis and hemostasis, 46(5), pp. 637–652. doi: 10.1055/S-0039-1688491.

Salama, R. et al. (2014) 'Cellular senescence and its effector programs', Genes and Development, 28(2), pp. 99–114. doi: 10.1101/GAD.235184.113.

Saleh, T. et al. (2018) 'Non-Cell Autonomous Effects of the Senescence-Associated Secretory Phenotype in Cancer Therapy', Frontiers in Oncology, 0(MAY), p. 164. doi: 10.3389/FONC.2018.00164.

Saleh, T. et al. (2019) 'Tumor cell escape from therapy-induced senescence', Biochemical Pharmacology, 162, pp. 202–212. doi: 10.1016/j.bcp.2018.12.013.

Saleh, T. et al. (2020) 'Clearance of therapy-induced senescent tumor cells by the senolytic ABT-263 via interference with BCL-XL–BAX interaction', Molecular Oncology, 14(10), pp. 2504–2519. doi: 10.1002/1878-0261.12761.

Salminen, A., Kauppinen, A. and Kaarniranta, K. (2012) 'Emerging role of NF-κB signaling in the induction of senescence-associated secretory phenotype (SASP)', Cellular Signalling, 24(4), pp. 835–845. doi: 10.1016/J.CELLSIG.2011.12.006.

Sanders, Y. Y. et al. (2013) 'Histone modifications in senescence-associated resistance to apoptosis by oxidative stress', Redox biology, 1(1), pp. 8–16. doi: 10.1016/J.REDOX.2012.11.004.

Sapega, O. et al. (2018) 'Distinct phenotypes and "bystander" effects of senescent tumor cells induced by docetaxel or immunomodulatory cytokines', International Journal of Oncology, 53(5), pp. 1997–2009. doi: 10.3892/IJO.2018.4553/HTML.

Savoca, K. V. et al. (1979) 'Preparation of a non-immunogenic arginase by the covalent attachment of polyethylene glycol', BBA - Protein Structure, 578(1), pp. 47–53. doi: 10.1016/0005-2795(79)90111-9.

Schafer, M. J. et al. (2017) 'Cellular senescence mediates fibrotic pulmonary disease', Nature Communications, 8. doi: 10.1038/ncomms14532.

Schosserer, M., Grillari, J. and Breitenbach, M. (2017) 'The Dual Role of Cellular Senescence in Developing Tumors and Their Response to Cancer Therapy.', Frontiers in oncology, 7(NOV), p. 278. doi: 10.3389/fonc.2017.00278.

Shahbandi, A. et al. (2020) 'BH3 mimetics selectively eliminate chemotherapy-induced senescent cells and improve response in TP53 wild-type breast cancer', Cell Death and Differentiation, 27(11), pp. 3097–3116. doi: 10.1038/s41418-020-0564-6.

Shao, L. et al. (2014) 'Total body irradiation causes long-term mouse BM injury via induction of HSC premature senescence in an Ink4a- and Arf-independent manner', Blood, 123(20), pp. 3105–3115. doi: 10.1182/BLOOD-2013-07-515619.

Shenoy, A. K. and Lu, J. (2016) 'Cancer cells remodel themselves and vasculature to overcome the endothelial barrier', Cancer Letters. Elsevier Ireland Ltd, pp. 534–544. doi: 10.1016/j.canlet.2014.10.031.

Shimabukuro-Vornhagen, A. et al. (2018) 'Cytokine release syndrome', Journal for ImmunoTherapy of Cancer, 6(1), p. 56. doi: 10.1186/S40425-018-0343-9.

Shin, M. D. et al. (2020) 'COVID-19 vaccine development and a potential nanomaterial path forward', Nature Nanotechnology, 15(8), pp. 646–655. doi: 10.1038/S41565-020-0737-Y.

Siva, S. et al. (2016) 'Radiotherapy for non-small cell lung cancer induces DNA damage response in both irradiated and out-of-field normal tissues', Clinical Cancer Research, 22(19), pp. 4817–4826. doi: 10.1158/1078-0432.CCR-16-0138.

Sledge, G. G. W. et al. (2017) 'MONARCH 2: Abemaciclib in combination with fulvestrant in women with HR+/HER2-advanced breast cancer who had progressed while receiving endocrine therapy', 35(25), pp. 2875–2884. doi: 10.1200/JCO.2017.73.7585.

Slowing, I. I., Trewyn, B. G. and Lin, V. S. Y. (2007) 'Mesoporous silica nanoparticles for intracellular delivery of membrane-impermeable proteins', Journal of the American Chemical Society, 129(28), pp. 8845–8849. doi: 10.1021/JA0719780.

Slowing, I., Trewyn, B. G. and Lin, V. S. Y. (2006) 'Effect of surface functionalization of MCM-41-type mesoporous silica nanoparticles on the endocytosis by human cancer cells', Journal of the American Chemical Society, 128(46), pp. 14792–14793. doi: 10.1021/JA0645943/SUPPL_FILE/JA0645943SI20060928_100428.PDF.

Sobhani, N. et al. (2019) 'Combinations in Breast Cancer', Cells, 8(4), pp. 1–24.

Soto-Gamez, A. and Demaria, M. (2017) 'Therapeutic interventions for aging: the case of cellular senescence', Drug Discovery Today, 22(5), pp. 786–795. doi: 10.1016/j.drudis.2017.01.004.

Stein, A., Melde, B. J. and Schroden, R. C. (2000) 'Hybrid Inorganic–Organic Mesoporous Silicates—Nanoscopic Reactors Coming of Age', Advanced Materials, 12(19), pp. 1403–1419. doi: https://doi.org/10.1002/1521-4095(200010)12:19<1403::AID-ADMA1403>3.0.CO;2-X.

Stöber, W., Fink, A. and Bohn, E. (1968) 'Controlled growth of monodisperse silica spheres in the micron size range', Journal of Colloid and Interface Science, 26(1), pp. 62–69. doi: 10.1016/0021-9797(68)90272-5.

Storer, M. et al. (2013) 'Senescence Is a Developmental Mechanism that Contributes to Embryonic Growth and Patterning', Cell, 155(5), pp. 1119–1130. doi: 10.1016/j.cell.2013.10.041.

Suk, J. S. et al. (2016) 'PEGylation as a strategy for improving nanoparticle-based drug and gene delivery', Advanced drug delivery reviews, 99(Pt A), p. 28. doi: 10.1016/J.ADDR.2015.09.012.

Sultana, Z. et al. (2018) 'Is there a role for placental senescence in the genesis of obstetric complications and fetal growth restriction?', American Journal of Obstetrics and Gynecology, 218(2), pp. S762–S773. doi: 10.1016/j.ajog.2017.11.567.

Sun, R. et al. (2017) 'Senescence as a novel mechanism involved in β-adrenergic receptor

mediated cardiac hypertrophy', PLOS ONE. Edited by S. Gupta, 12(8), p. e0182668. doi: 10.1371/journal.pone.0182668.

Sutherland, R. L. and Musgrove, E. A. (2009) 'CDK inhibitors as potential breast cancer therapeutics: new evidence for enhanced efficacy in ER+disease', Breast Cancer Research, 11(6), p. 112. doi: 10.1186/bcr2454.

Syahidah, N. et al. (2021) 'Combination Therapy of Navitoclax with Chemotherapeutic Agents in Solid Tumors and Blood Cancer: A Review of Current Evidence', Pharmaceutics 2021, Vol. 13, Page 1353, 13(9), p. 1353. doi: 10.3390/PHARMACEUTICS13091353.

Takahashi, A., Ohtani, N. and Hara, E. (2007) 'Irreversibility of cellular senescence: dual roles of p16INK4a/Rb-pathway in cell cycle control', Cell Division, 2, p. 10. doi: 10.1186/1747-1028-2-10.

Takai, H., Smogorzewska, A. and De Lange, T. (2003) 'DNA damage foci at dysfunctional telomeres', Current biology : CB, 13(17), pp. 1549–1556. doi: 10.1016/S0960-9822(03)00542-6.

Tan, A. et al. (2014) 'First in man bioavailability and tolerability studies of a silica-lipid hybrid (Lipoceramic) formulation: a Phase I study with ibuprofen', Drug delivery and translational research, 4(3), pp. 212–221. doi: 10.1007/S13346-013-0172-9.

Tchkonia, T. et al. (2013) 'Cellular senescence and the senescent secretory phenotype: therapeutic opportunities', The Journal of Clinical Investigation, 123(3), pp. 966–972. doi: 10.1172/JCI64098.

Tesei, A. et al. (2021) 'TP53 drives abscopal effect by secretion of senescence-associated molecular signals in non-small cell lung cancer', Journal of Experimental and Clinical Cancer Research, 40(1), pp. 1–15. doi: 10.1186/S13046-021-01883-0/FIGURES/8.

Thapa, R. K. et al. (2017) 'Progressive slowdown/prevention of cellular senescence by CD9-targeted delivery of rapamycin using lactose-wrapped calcium carbonate nanoparticles', Scientific Reports, 7(1), p. 43299. Available at: /pmc/articles/PMC5385881/ (Accessed: 13 December 2021).

Toogood, P. L. et al. (2005) 'Discovery of a potent and selective inhibitor of cyclin-dependent kinase 4/6', Journal of Medicinal Chemistry, 48(7), pp. 2388–2406. doi: 10.1021/JM049354H/SUPPL_FILE/JM049354HSI20050107_011813.PDF.

Torres-Guzmán, R. et al. (2017) 'Preclinical characterization of abemaciclib in hormone receptor positive breast cancer', Oncotarget, 8(41), pp. 69493–69507. doi: 10.18632/ONCOTARGET.17778.

Triana-Martínez, F. et al. (2019) 'Identification and characterization of Cardiac Glycosides as senolytic compounds', Nature Communications, 10(1), pp. 1–12. doi: 10.1038/s41467-019-12888-x.

Triana-Martínez, F., Loza, M. I. and Domínguez, E. (2020) 'Beyond Tumor Suppression: Senescence in Cancer Stemness and Tumor Dormancy', Cells, 9(2). doi: 10.3390/cells9020346.

Turner, N. et al. (2018) 'Overall survival with palbociclib and fulvestrant in advanced breast cancer', N Engl J Med, 379, pp. 1926–1936.

Turner, N. C. et al. (2015) 'Palbociclib in Hormone-Receptor–Positive Advanced Breast Cancer', New England Journal of Medicine, 373(3), pp. 209–219. doi: 10.1056/NEJMoa1505270.

Vallet-Regi, M. et al. (2001) 'A new property of MCM-41: Drug delivery system', Chemistry of Materials, 13(2), pp. 308–311. doi: 10.1021/cm0011559.

Verdoorn, B. P. et al. (2021) 'Fisetin for COVID-19 in skilled nursing facilities: Senolytic trials in the COVID era', Journal of the American Geriatrics Society, 69(11), pp. 3023–3033. doi: 10.1111/JGS.17416.

Vicencio, J. M. et al. (2008) 'Senescence, Apoptosis or Autophagy? When a Damaged Cell Must Decide Its Path – A Mini-Review', Gerontology, 54(2), pp. 92–99. doi: 10.1159/000129697.

Walker, A. J. et al. (2016) 'FDA Approval of Palbociclib in Combination with Fulvestrant for the Treatment of Hormone Receptor-Positive, HER2-Negative Metastatic Breast Cancer', Clinical Cancer Research, 22(20), pp. 4968–4972. doi: 10.1158/1078-0432.CCR-16-0493.

Wandrer, F. et al. (2018) 'Senescence mirrors the extent of liver fibrosis in chronic hepatitis C virus infection', Alimentary Pharmacology & Therapeutics, 48(3), pp. 270–280. doi: 10.1111/apt.14802.

Wang, B., Kohli, J. and Demaria, M. (2020) 'Senescent Cells in Cancer Therapy: Friends or Foes?', Trends in Cancer, 6(10), pp. 838–857. doi: 10.1016/j.trecan.2020.05.004.

Wang, C. et al. (2019) 'Inducing and exploiting vulnerabilities for the treatment of liver cancer', Nature, 574(7777), pp. 268–272. doi: 10.1038/S41586-019-1607-3.

Wang, E. (1995) 'Senescent Human Fibroblasts Resist Programmed Cell Death, and Failure to Suppress bcl2 Is Involved', Cancer Research, 55(11).

Wang, X. et al. (1998) 'Evidence of cisplatin-induced senescent-like growth arrest in nasopharyngeal carcinoma cells.', Cancer research, 58(22), pp. 5019–22.

Wen, J. et al. (2017) 'Diverse gatekeepers for mesoporous silica nanoparticle based drug delivery systems', Chemical Society Reviews, 46(19), pp. 6024–6045. doi: 10.1039/C7CS00219J.

Westmeier, D., Stauber, R. H. and Docter, D. (2016) 'The concept of bio-corona in modulating the toxicity of engineered nanomaterials (ENM)', Toxicology and Applied Pharmacology, 299, pp. 53–57. doi: 10.1016/j.taap.2015.11.008.

Wieland, E. et al. (2017) 'Endothelial Notch1 Activity Facilitates Metastasis', Cancer Cell, 31(3), pp. 355–367. doi: 10.1016/j.ccell.2017.01.007.

Wiley, C. D. et al. (2016) 'Mitochondrial Dysfunction Induces Senescence with a Distinct Secretory Phenotype', Cell metabolism, 23(2), pp. 303–314. doi: 10.1016/J.CMET.2015.11.011.

Wiley, C. D. and Campisi, J. (2021) 'The metabolic roots of senescence: mechanisms and opportunities for intervention', Nature Metabolism, 3(10), pp. 1290–1301. doi: 10.1038/s42255-021-00483-8.

Wu, T. and Dai, Y. (2017) 'Tumor microenvironment and therapeutic response', Cancer Letters. Elsevier, pp. 61–68. doi: 10.1016/j.canlet.2016.01.043.

Wu, T. and Tang, M. (2018) 'Review of the effects of manufactured nanoparticles on

mammalian target organs', Journal of Applied Toxicology, 38(1), pp. 25–40. doi: 10.1002/jat.3499.

Wyld, L. et al. (2020) 'Senescence and cancer: A review of clinical implications of senescence and senotherapies', Cancers, 12(8), pp. 1–20. doi: 10.3390/cancers12082134.

Xu, M. et al. (2015) 'JAK inhibition alleviates the cellular senescence-associated secretory phenotype and frailty in old age.', Proceedings of the National Academy of Sciences of the United States of America, 112(46), pp. E6301-10. doi: 10.1073/pnas.1515386112.

Xu, M. et al. (2018) 'Senolytics Improve Physical Function and Increase Lifespan in Old Age', Nature medicine, 24(8), p. 1246. doi: 10.1038/S41591-018-0092-9.

Yanagisawa, T. et al. (1990) 'The preparation of alkyltrimethylammonium-kanemite complexes and their conversion to microporous materials', Bulletin of the Chemical Society of Japan, 63(4), pp. 988–992. doi: 10.1246/bcsj.63.988.

Yang, H. and Fogo, A. B. (2010) 'Cell Senescence in the Aging Kidney', Journal of the American Society of Nephrology, 21(9), pp. 1436–1439. doi: 10.1681/ASN.2010020205.

Yang, N. C. and Hu, M. L. (2005) 'The limitations and validities of senescence associated-β- galactosidase activity as an aging marker for human foreskin fibroblast Hs68 cells', Experimental Gerontology, 40(10), pp. 813–819. doi: 10.1016/j.exger.2005.07.011.

Yang, Y. et al. (2020) 'Silica-Based Nanoparticles for Biomedical Applications: From Nanocarriers to Biomodulators', Accounts of Chemical Research, 53(8), pp. 1545–1556. doi: 10.1021/ACS.ACCOUNTS.0C00280.

Yao, Z. et al. (2020) 'Therapy-Induced Senescence Drives Bone Loss', Cancer research, 80(5), pp. 1171–1182. doi: 10.1158/0008-5472.CAN-19-2348.

Yin, P. T. et al. (2018) 'Overcoming Chemoresistance in Cancer via Combined MicroRNA Therapeutics with Anticancer Drugs Using Multifunctional Magnetic Core–Shell Nanoparticles', ACS Applied Materials & Interfaces, 10(32), pp. 26954–26963. doi: 10.1021/acsami.8b09086.

Young, A. R. J. et al. (2009) 'Autophagy mediates the mitotic senescence transition', Genes & development, 23(7), pp. 798–803. doi: 10.1101/GAD.519709.

Yousefzadeh, M. J. et al. (2018) 'Fisetin is a senotherapeutic that extends health and lifespan', EBioMedicine, 36, pp. 18–28. doi: 10.1016/J.EBIOM.2018.09.015.

Yu, G.-L. et al. (1990) 'In vivo alteration of telomere sequences and senescence caused by mutated Tetrahymena telomerase RNAs', Nature, 344(6262), pp. 126–132. doi: 10.1038/344126a0.

Yu, L. et al. (2016) 'Manganese Extraction" Strategy Enables Tumor-Sensitive Biodegradability and Theranostics of Nanoparticles', Journal of the American Chemical Society, 138(31), pp. 9881–9894. doi: 10.1021/jacs.6b04299.

Yu, M. and Zheng, J. (2015) 'Clearance Pathways and Tumor Targeting of Imaging Nanoparticles', ACS Nano, 9(7), pp. 6655–6674. doi: 10.1021/acsnano.5b01320.

Yu, Q. et al. (2006) 'Requirement for CDK4 kinase function in breast cancer', Cancer Cell,

9(1), pp. 23–32. doi: 10.1016/J.CCR.2005.12.012.

Yu, Q., Geng, Y. and Sicinski, P. (2001) 'Specific protection against breast cancers by cyclin D1 ablation', Nature, 411(6841), pp. 1017–1021. doi: 10.1038/35082500.

Yu, Y. et al. (2020) 'Overexpression of miRNA-3613-3p Enhances the Sensitivity of Triple Negative Breast Cancer to CDK4/6 Inhibitor Palbociclib', Frontiers in Oncology, 10(November), pp. 1–14. doi: 10.3389/fonc.2020.590813.

Yuan, D., Ellis, C. M. and Davis, J. J. (2020) 'Mesoporous Silica Nanoparticles in Bioimaging', Materials (Basel, Switzerland), 13(17). doi: 10.3390/MA13173795.

Yun, M. H., Davaapil, H. and Brockes, J. P. (2015) 'Recurrent turnover of senescent cells during regeneration of a complex structure.', eLife, 4. doi: 10.7554/eLife.05505.

Zhang, L. et al. (2016) 'Tailored Synthesis of Octopus-type Janus Nanoparticles for Synergistic Actively-Targeted and Chemo-Photothermal Therapy', Angewandte Chemie International Edition, 55(6), pp. 2118–2121. doi: 10.1002/anie.201510409.

Zhang, X. et al. (2020) 'Promotion of cellular senescence by THG-1/TSC22D4 knockout through activation of JUNB', Biochemical and biophysical research communications, 522(4), pp. 897–902. doi: 10.1016/J.BBRC.2019.11.145.

Zhang, Y. et al. (2016) 'Mechanical Force-Triggered Drug Delivery', Chemical Reviews, 116(19), pp. 12536–12563. doi: 10.1021/ACS.CHEMREV.6B00369.

Zhao, L. and Wink, M. (2013) 'The β-carboline alkaloid harmine inhibits telomerase activity of MCF-7 cells by down-regulating hTERT mRNA expression accompanied by an accelerated senescent phenotype', PeerJ, 1, p. e174. doi: 10.7717/peerj.174.

Zhao, T. et al. (2018) 'Near-infrared light triggered drug release from mesoporous silica nanoparticles', Journal of Materials Chemistry B, 6(44), pp. 7112–7121. doi: 10.1039/C8TB01548A.

Zhao, Y. et al. (2009) 'Mesoporous silica nanoparticle-based double drug delivery system for glucose-responsive controlled release of insulin and cyclic AMP', Journal of the American Chemical Society, 131(24), pp. 8398–8400. doi: 10.1021/JA901831U/SUPPL_FILE/JA901831U_SI_001.PDF.

Zhao, Y. et al. (2018) 'Naked mole rats can undergo developmental, oncogene-induced and DNA damage-induced cellular senescence', Proceedings of the National Academy of Sciences of the United States of America, 115(8), pp. 1801–1806. doi: 10.1073/PNAS.1721160115.

Zhou, J.-M. et al. (2006) 'Senescence and telomere shortening induced by novel potent G-quadruplex interactive agents, quindoline derivatives, in human cancer cell lines', Oncogene, 25(4), pp. 503–511. doi: 10.1038/sj.onc.1209067.

Zhou, Y. et al. (2018) 'Mesoporous silica nanoparticles for drug and gene delivery', Acta Pharmaceutica Sinica B, 8(2), pp. 165–177. doi: 10.1016/j.apsb.2018.01.007.

Zhu, Y. et al. (2015) 'The Achilles' heel of senescent cells: from transcriptome to senolytic drugs', Aging cell, 14(4), pp. 644–658. doi: 10.1111/acel.12344.

Zhu, Y. et al. (2016) 'Identification of a novel senolytic agent, navitoclax, targeting the Bcl-2 family of anti-apoptotic factors', Aging Cell, 15(3), pp. 428–435. doi: 10.1111/acel.12445.

Zhu, Y. et al. (2017) ‘New agents that target senescent cells: The flavone, fisetin, and the BCL-XL inhibitors, A1331852 and A1155463’, Aging, 9(3), pp. 1–9. doi: 10.18632/aging.101202.